



ELSEVIER

Catalysis Today 52 (1999) 381–495



www.elsevier.com/locate/cattod

Deactivation of hydroprocessing catalysts

Edward Furimsky^{a,*}, Franklin E. Massoth^b

^aIMAF Group 184 Marlborough Avenue, Ottawa, Ont., Canada K1N 8G4

^bDepartment of Fuels Engineering, University of Utah, Salt Lake City 84112, UT, USA

1. Introduction

Hydroprocessing of commercial feeds is extensively practised in the petroleum industry, and to some extent in coal liquefaction and in upgrading of synthetic fuels. The process, employing a molybdenum catalyst supported on a high surface area transition alumina and promoted by cobalt or nickel, is carried out in a trickle-bed reactor or ebullating-bed reactor at elevated temperature and hydrogen pressure.

Hydroprocessing catalysts are quite versatile, exhibiting activity for a number of important reactions. Those of major interest in hydroprocessing are removal of heteroatoms, viz hydrosulfurization (HDS), hydrodenitrogenation (HDN), hydrodemetalation (HDM), and for coal-derived liquids, hydrodeoxygenation (HDO). These reactions involve hydrogenolysis of C-heteroatom bonds. An important attendant reaction is hydrogenation of aromatics (HYD). Typical classes of these reactants are shown in Fig. 1. Hydrogenolysis of C–C bonds is generally minor, except when hydrocracking catalysts are employed.

For relatively light feeds, deactivation of the catalyst is minimal and the process can operate for long periods of time before replacement of the catalyst. However, in hydroprocessing heavy residues, catalyst deactivation can be severe, having an important com-

mercial economic consideration with respect to catalyst lifetime. Similar deactivation is experienced in hydroprocessing coal liquids.

Hydroprocessing reactions occur on the active sites of the catalysts. Also, a suitable pore size distribution is required to ensure the access of reactant molecules to the active sites. A main reason for deactivation of the catalysts involves loss of active sites. A number of basic causes for this loss are listed in Table 1. Blocking of pore mouths, of course, render still active sites unavailable to reactants, while pore mouth restriction could accentuate diffusional limitations on reaction rates. Irreversible site poisoning would reduce the number of sites available for reaction, and may be more severe on promotional sites. Sintering of the active slabs, comprising a plane of Mo(W) atoms sandwiched between the two hexagonal planes of sulphur atoms, would reduce the total number of surface vacancies. Also, rearrangement of the structure might disproportionately reduce certain site center configurations more than others, affecting catalyst selectivity as well as activity.

In commercial operation, hydroprocessing catalysts invariably experience some degree of deactivation, depending on the feed source. Under commercial operating conditions, catalyst activity, for example HDS conversion, is maintained by constantly raising the temperature. Deactivation is then manifested by the temperature-rise profile as a function of time on stream, as illustrated by the typical S-curve of Fig. 2 for a resid feed [1]. Initial deactivation is caused by coke, which appears to rapidly reach a pseudo steady-

*Corresponding author. Tel.: +1-613-565-5604; fax: +1-613-565-5618

E-mail address: efurimsk@netcom.ca (E. Furimsky)


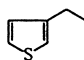
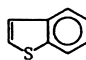
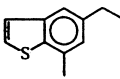
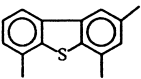

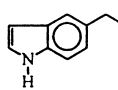
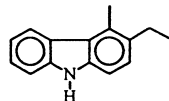

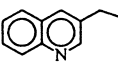
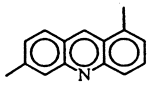

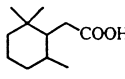
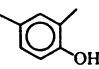

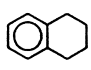
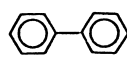
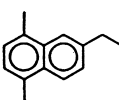
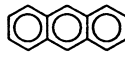
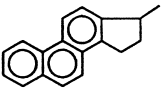

Sulfur compounds			
Thiols (mercaptans), sulfides and disulfides	R-SH	R-S-R'	R-S-S-R'
Thiophenes, benzothiophenes and dibenzothiophenes			
			
Nitrogen compounds			
Pyrrole, indoles and carbazoles			
Pyridine, quinolines and acridines			
Oxygen compounds			
Furan, carboxylic acids and phenols			
Aromatics			
Benzene, tetralin and biphenyl			
Naphthalenes and anthracene			
Phenanthrenes and pyrene			

Fig. 1. Typical heteroatom and aromatic compounds found in petroleum.

state level. Continued deactivation over a longer time period is due to metal deposits, whose rate of deactivation depends on the metals level in the feed. The final, catastrophic loss in activity is attributed to pore constriction and ultimate pore blockage. At this stage,

Table 1

Basic deactivation factors

Active site poisoning by strongly adsorbed species
 Active site coverage by deposits (coke, metals)
 Pore mouth constriction/blockage
 Sintering of active phase

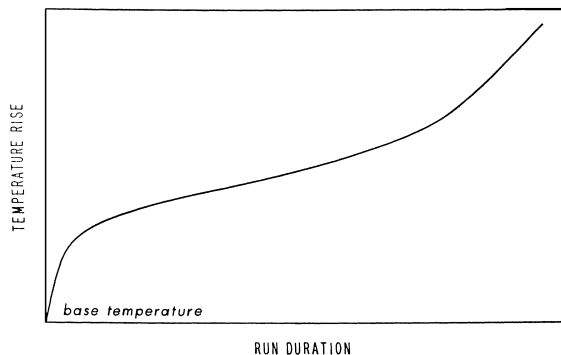


Fig. 2. Typical S-shaped deactivation curve [1].

Table 2
Effect of indole on HDS and HYD conversion

	% Conversion	
	HDS	HYD
Before indole	87	69
After indole	64	21
After 2 days with DBT	80	39

the temperature cannot be raised sufficiently to keep up with deactivation, and the run has to be terminated.

The molecular structure of reactants in the feed has an indirect bearing on catalyst deactivation. Since rates are affected by adsorbed species, strongly adsorbed species can lower reaction rates considerably. This requires increase in temperature to maintain catalyst activity, which is usually accompanied by increased deactivation rates. Adsorbed species reduce the number of active sites via competition with the reactant. Even a simple molecule as indole has been found to have a long-time adsorption effect on HDS and HYD. Table 2 shows that even after two days after its removal, the HDS of dibenzothiophene has not been entirely recovered, and HYD of naphthalene was still appreciably lower than before the addition of indole. This may be explained on the basis of relative reaction rates to desorption rates. A strongly adsorbed compound, having a slow rate of desorption compared to the given reaction, will experience only very slow recovery. This is especially marked in the case of polyaromatic nitrogen compounds, whose rates of desorption are exceedingly slow.

Many studies have been performed to understand the underlying phenomena leading to deactivation in order to develop longer life catalysts [1–10]. Most of these studies have been of a semi-empirical nature, in which various deactivating factors have been compounded, making difficult assessment of the individual factors responsible. There have been few attempts to comprehensively review published information relevant to deactivation of hydroprocessing catalysts. Deactivation of HDS catalysts was part of a review by Bartholomew [2] on deactivation occurring during various reactions. The information on deactivation during direct coal liquefaction was reviewed by Thomas and Thakur [3]. Subsequently, the same authors have published a summary of more than 250 published

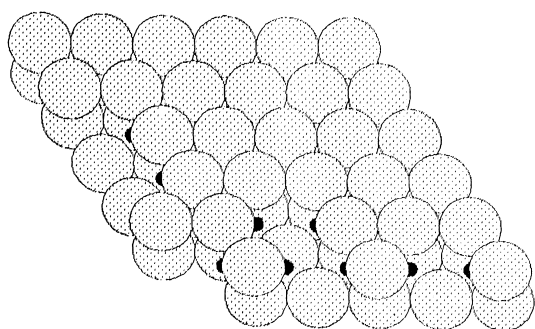
works on deactivation during hydroprocessing of heavy feeds and synthetic crudes [4]. Deactivation by coke was reviewed by Menon [5] and Absi-Halabi et al. [6]. It is to be noted that the latter two reviews dealt mainly with the chemical aspects of coke formation. Thus, little attention was paid to catalyst porosity and associated restrictive diffusion phenomena. These aspects of deactivation were discussed in the review published by Gualda and Toulhoat [7]. Tamm et al. [1] discussed in detail phenomena occurring during deactivation by metals. Various models applied to HDM and deactivation were reviewed by Dautzenberg et al. [8] and Wei [9]. The catalyst deactivation during hydroprocessing of residues was the primary focus of another review published recently by Bartholomew [10].

In this review, we draw upon material from the literature in an attempt to elucidate various basic factors responsible for catalyst deactivation. After a brief background discussion of catalyst structure and active sites, we concentrate on deactivation phenomena with poisons, coke, metals deposits and changes in catalyst active phase structure. A number of remedies relevant to practical situations are also presented.

2. Hydroprocessing catalysts

The catalysts of concern in hydroprocessing consist of molybdenum supported on a high surface area carrier, most commonly alumina, promoted by cobalt or nickel. These catalysts are active in the sulfided state, being either presulfided or sulfided on stream with a sulfur containing feed. CoMo/Al₂O₃ catalysts are usually employed for HDS, HDM catalysts generally have large pores and lower metal contents. Extensive characterization studies of these catalysts have been reviewed by a number of authors [11–15], and we will only summarize here current opinion relative to structure and catalytic sites, without reference to original papers on the subject.

The supports employed usually consist of high surface area (~200 m²/g) transition-aluminas (or silica-alumina or zeolite for hydrocracking). The average pore size is generally between 75 and 300 Å, although a distribution of pore sizes is prevalent. Some supports, especially those used for demetallation, may also sustain macropores, i.e., a bimodal pore structure.

Fig. 3. Model of MoS₂ slab.

The micropore dimensions can have a significant bearing on diffusion of reactants to the active sites, particularly for heavy feeds. The literature on preparation of the hydroprocessing catalysts is quite extensive [16–19]. For the purpose of this review, a brief summary of the key issues on the subject will only be given, without reference to the original works.

Research has shown that sulfided catalysts containing Mo consist of essentially monolayer slabs or clusters of slabs of MoS₂ partially covering the alumina surface. Fig. 3 shows a model representation of a slab, which is believed to be roughly hexagonal in shape. The relative lateral size of the slabs, and the

amount of monolayer slabs and clusters of slabs will depend on the Mo loading relative to the alumina surface area. At high levels of Mo (greater than about 5% Mo per 100 m²/g of alumina surface), bulk MoS₂ can also be present. Because of the relatively small size of the slabs, e.g., 10–50 Mo/slab, a considerable fraction of the terminal sulfur ions will be absent in order to maintain an approximate MoS₂ stoichiometry.

These are shown by the absence of S atoms in Fig. 4. These coordinatively unsaturated sites (CUS) or sulfur anion vacancies are located at the edges of the slabs and have Lewis acid character. Thus, they can adsorb molecules with unpaired electrons, e.g., NO, pyridine, and are believed to be the sites for catalytic reactions. The vacancies can consist of a significant fraction of the edge sulfur atoms. Because of the high concentration of vacancies (about 1 vacancy/edge Mo atom), double and even multiple vacancy centers can be present.

Studies have shown that the presence of Co or Ni does not affect the basic slab size of the MoS₂, being located at the edge sites of the slabs. The Co or Ni does not appear to appreciably increase the number of vacancies, but the vacancies associated with the Co or Ni are considerably more active than those associated with the Mo, leading to the increased ‘promo-

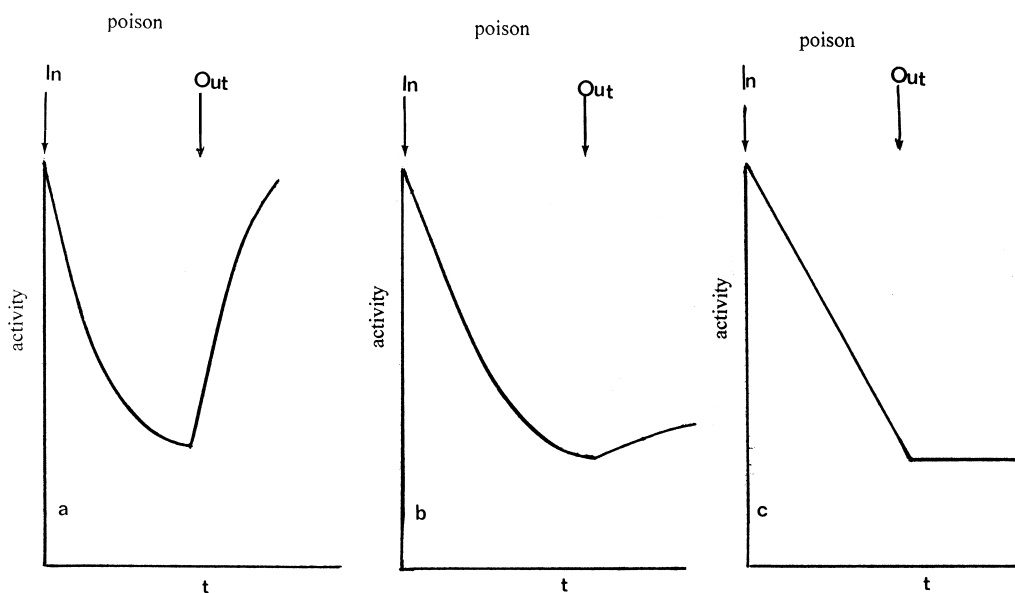


Fig. 4. Activity–time profiles for (a) reversible; (b) quasi-irreversible and (c) irreversible poisoning.

tional' activity of the catalyst. The vacancy concentration under hydroprocessing conditions is thought to be a function of the H_2 and H_2S concentrations. Considerable evidence exists for the presence of $-SH$ groups on the catalyst, and weak Brønsted activity has been shown to be present under typical hydroprocessing conditions.

The relevance of this to deactivation is obvious — any strongly adsorbed species, for example, N-compound, coke molecule, metal deposit, which occupies (poisons) an active vacancy site will cause a loss in catalytic activity. This could affect the Mo vacancies, and more importantly the more active Co or Ni sites. Since most reactants will most likely require multi-vacancy site centers for adsorption, it may not even be necessary to poison all the sites of the active centers to cause deactivation, i.e., one poison molecule could conceivably poison the entire center for reaction.

It is evident from the literature that the different reactions occurring on hydroprocessing catalysts do not take place on the same sites. It may seem difficult at first to reconcile a number of different sites with the idea that vacancies are the active sites. However, one may certainly envision a number of different site ensembles of vacancies to be present, which having different configurational and/or energetic properties, would be more suitable for bonding a particular reactant in an activated state. The consequence of this is that some reactions may be more affected by catalyst deactivation than others.

3. Deactivation by poisons

A poison is a substance which adsorbs on active catalyst sites, resulting in either incapacitating the site or competition with the reactants of a given reaction. The poison may be due to the reactant, reaction intermediates or products, as well as the extraneous compounds present in the feed. The net result is a lowering in the catalyst activity. It is assumed that during poisoning, the basic structure of the active sites is not changed.

A poison may be adsorbed reversibly, irreversibly or quasi-irreversibly. The effects in these cases on the rate or conversion of a given reaction are illustrated in Fig. 4. In the case of a reversible poison, the catalyst activity is restored when the poison is removed from

the feed. Thus, its effect is transitory and is manifested in an inhibition (denominator) term in the usual Langmuir–Hinshelwood rate expression for reactant A, r_A ,

$$r_A = \frac{k_A f(C_A)}{(1 + K_p C_p + \sum K_i C_i)^n} \quad (3.1)$$

where k_A is the rate constant, C_A the concentration of A and $f(C_A)$ its particular rate form, K_p the adsorption constant of the poison and C_p its concentration, K_i the adsorption constant of all other adsorbed species associated with the main reaction and C_i their concentrations, and n the power on the inhibition term. Thus, the rate of the main reaction in the lined-out catalyst will be affected by the strength of adsorption of all species under the given conditions. Since the effect of the $\sum K_i C_i$ term is indigenous to the reaction, it is always present (although some or all of the K_i 's may be sufficiently small that their effect is negligible). The presence of an extraneous reversible poison will further lower the main reaction rate by virtue of its appearance in the inhibition term. Its effect will depend upon its concentration and strength of adsorption. Since the catalyst regains its original activity when the poison is removed, the reversible poison is not a true poison in the sense that it only temporarily competes for active sites. It is thus better described as an 'inhibition' to the main reaction instead of a poison.

An irreversible poison is one that is not desorbed, i.e., its bonding to the active site is so strong that its desorption rate is negligible under reaction conditions. Deactivation by irreversible poisoning does not depend on the concentration of poison (although the rate of deactivation does). Upon its removal from the feed, the catalyst activity remains permanently depressed at its value prior to removal. An essentially irreversible poison at one temperature may become a reversible poison at a higher temperature, although raising temperature sometimes results in decomposition rather than simple desorption. The rate constant in Eq. (3.1) includes the total number of active sites on the catalyst for reaction of A. The irreversible poison will permanently poison some active sites, resulting in a lowering of the number of active sites available. Thus, the irreversible poison will effectively lower the rate constant rather than appear in the inhibition term. However, not all active sites may be covered by a particular poison, only some very active sites. Con-

sequently, the main reaction may not be completely deactivated by this poison, despite its continued presence in the feed. When the adsorbed species polymerize or condense into larger units on the catalyst surface, poisoning loses its meaning; these processes are better described, for example, as deactivation by coke or metal deposition (see subsequent chapters).

A quasi-permanent poison has the characteristics of both reversible and irreversible poisons. Hence, it will lower catalytic activity by virtue of adsorption on active sites, but appear as a permanent due to its very slow desorption rate with respect to the rate of the reaction at hand. As a consequence, adsorption equilibrium is only slowly established, and the reversible poison component will appear in the inhibition term, while the irreversible component will be included in the rate constant. When the poison is removed, the catalyst activity will only be partially restored, the resulting activity loss being due to the permanent poison still residing on the more active sites.

Investigations of the kinetics of inhibition via Eq. (3.1) or other comparable equations are extensive in the literature. In this regard, the review published by Girgis and Gates [20] focuses on inhibition of all reactions occurring during hydroprocessing. Since these studies involve predominantly reversible ‘poison’, in the following literature review, we will mostly be concerned with irreversible and quasi-irreversible poisoning.

3.1. Poisoning by nitrogen compounds

In the case of hydroprocessing, nitrogen-containing compounds are the most common poisons by virtue of their strong adsorption on catalyst sites. Because of their basic nature, they adsorb on catalyst acidic sites, viz. Lewis and Brønsted sites, and may adsorb reversibly or irreversibly, depending on reaction conditions. Most of the nitrogen in petroleum is in the form of 5- and 6-membered heteroatom rings and anilines. The 6-membered rings and anilines are the most basic, accounting for about one third of the total nitrogen. A small amount of porphyrin type nitrogen (in the asphaltenes) is also present in heavy feeds; these will be discussed in the next chapter.

The HDN of N-containing heterorings requires more severe conditions than that of other heteroring-compounds, especially high H_2 pressure. For this

Table 3

Heat of hydrogenation and resonance energies of rings [21]

Equilibrium	$-\Delta H$ (kcal/mol)	E_{res} (kcal/mol)
Pyrrole \rightleftharpoons Pyrrolidine	30	30
Pyridine \rightleftharpoons Piperidine	48	42
Indole \rightleftharpoons Indoline	13	17
Quinoline \rightleftharpoons 1-,2-,3-,4-Tetrahydroquinoline	30	30

reason, N-compounds are often used to study poisoning reactions under mild conditions, e.g., HDS. It is generally accepted that 5-membered N-ring compounds are less basic (less aromatic character) than 6-membered ring compounds. This is supported by the resonance energies shown in Table 3 [21]. These values were estimated from the heat of ring hydrogenation (ΔH) according to the formula: $E_{\text{res}} = 30n - \Delta H$, where n is the number of hydrogenated double bonds. It is evident that the 5-membered rings are less resistant to hydrogenation, suggesting that they will be removed from the feed at a greater rate, as supported by experimental results. Consequently, relative contribution of 5-membered N-rings to poisoning is expected to be less important than of 6-membered N-rings. For this reason, many authors have used pyridine as a poison in HDS studies [22–28], in which the poisoning effect was usually treated as a reversible inhibition.

Besides strongly adsorbing on Lewis sites via the N-electron pair or via the aromatic π -system, N-compounds can also interact with protons from Brønsted sites, forming positively charged species [29,30]. LaVopa and Satterfield [31] related equilibrium adsorption parameters with proton affinities for a number of N-compounds. Fig. 5 shows a good correlation, except for sterically hindered compounds. A similar correlation was presented by Nagai et al. [32], which again failed to correlate sterically hindered compounds. The basic strength and extent of adsorption of several N-compounds on a sulfided CoMo catalyst were compared by Miciukiewicz et al. [33] and are listed in Table 4. The adsorption values given were obtained by microbalance experiments under reaction conditions in which the N-compounds were stable towards HDN, and include adsorption on active as well as on inactive sites (support). The pK_a values are from the literature and represent the basic strength

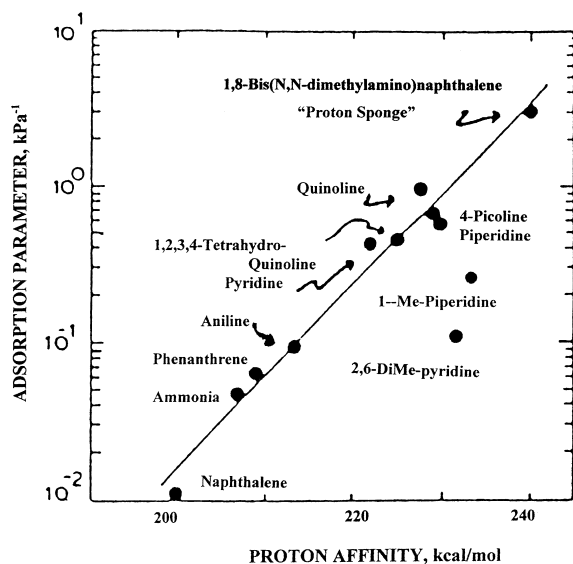


Fig. 5. Correlation between adsorption parameter and proton affinity [31].

Table 4
Nitrogen-compound poisons [33]

Name	Structure	pK ^a	Adsorption ^c (μmol/g)
Piperidine (PIP)		11.1	0.15
Pyridine (PY)		5.3	0.16
2,6-Lutidine (26L)		7 ^b	0.045
3,5-Lutidine (35L)		6.2	0.215
Aniline (AN)		4.6	0.13
<i>N,N</i> -dimethylaniline (NAN)		5.2	0.085
Quinoline (Q)		4.9	0.25
Quinaldine (MQ)		5.8	0.08

^a Handbook of Chemistry and Physics, 60th ed., p. D-161.

^b Estimated from data of substituted puridines.

^c Amount adsorbed on catalyst at 0.25 kPa pressure of N-compound at 623 K, in presence of 1.06 kPa thiophene, 1.73 kPa H₂S and 83.3 kPa H₂.

in water, which is related to the protonation of the base, e.g. $B + H_2O = BH^+ + OH^-$. The basic strength is not necessarily the same as the adsorption strength on catalyst sites. Thus, according to pK_a values in Table 4, piperidine is much more basic than pyridine, yet their overall adsorption on the catalyst is the same, implying that the degree of protonation of the adsorbed base is not directly related to its adsorption on the catalyst. Significant differences between the adsorption of 2,6-lutidine and 3,5-lutidine, as well as quinoline and 2-methylquinoline (quinaldine), indicate the importance of steric hindrance to adsorption. Steric hindrance is not accounted for in the pK_a values or proton affinities. Because adsorption is appreciably diminished by methyl substitution at carbons adjacent to the nitrogen, the interaction of N-bases with catalyst sites occurs predominantly via the N-heteroatom, either by donating its unpaired electron to the Lewis site or by interaction with the proton of a Brønsted site.

The effect of molecular structure of adsorbed N-compounds on the HDS of thiophene and the HYD of hexene was also determined by Miciukiewicz et al. [33]. In these experiments, desorption of the N-compound was extremely slow, indicative of quasi-irreversible adsorption. Deactivation curves are presented in Fig. 6. It is evident that the curves are tailing off with increasing amount of poison, implying that some

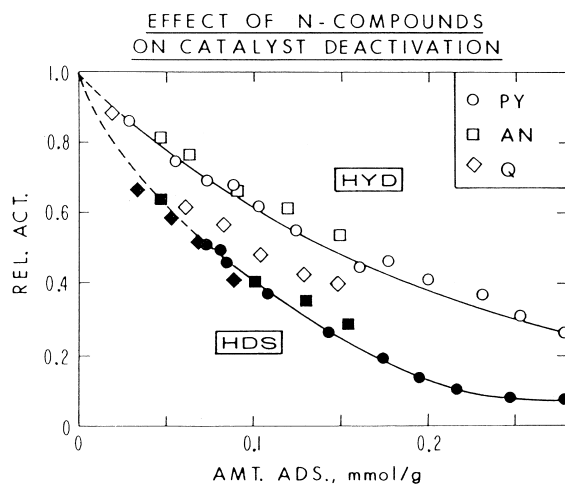


Fig. 6. Effect of N-compounds on relative activities of HDS and HYD; PY – pyridine, AN – aniline, Q – quinoline (CoMo/Al₂O₃, 623 K, near atm. H₂) [33].

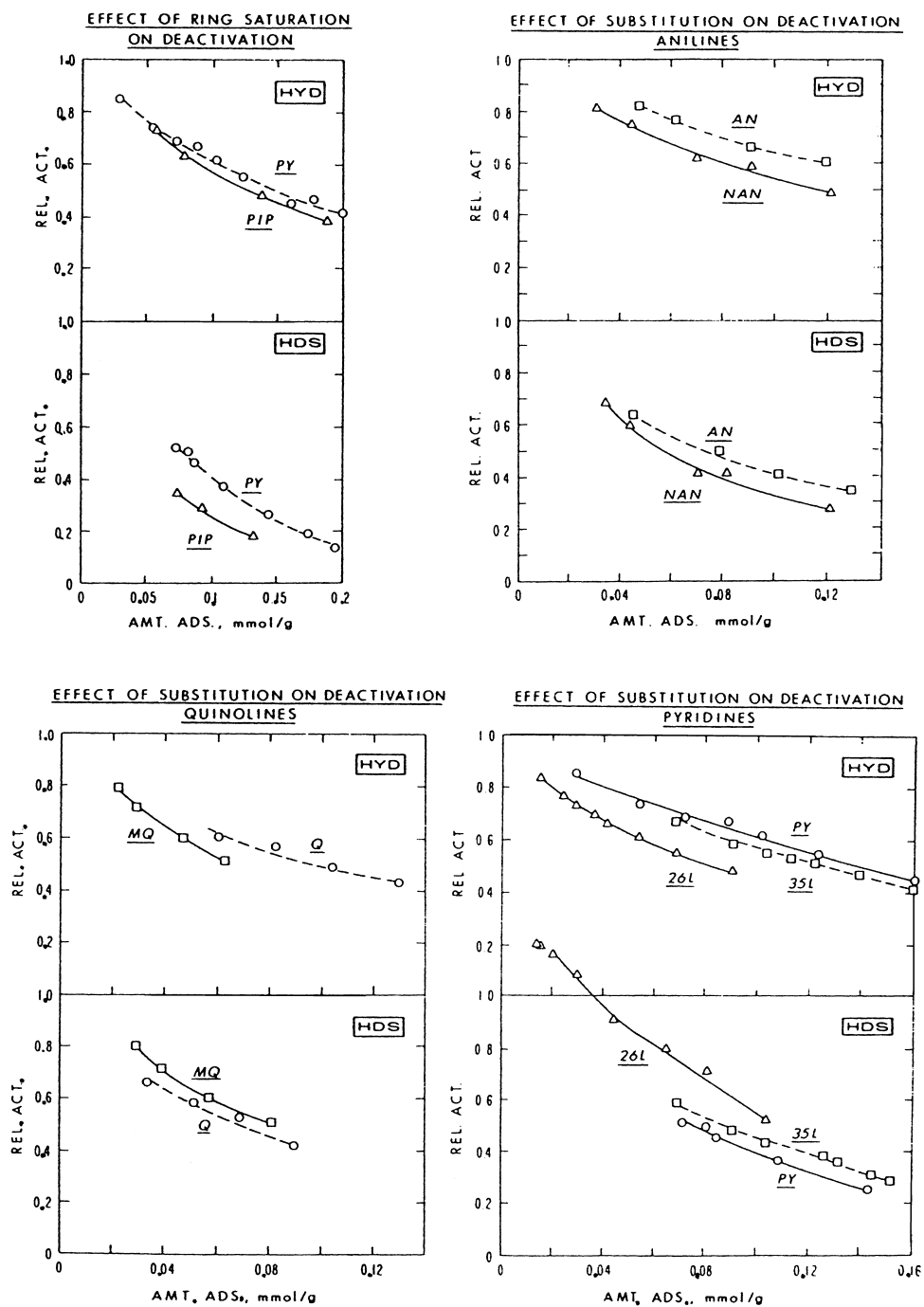


Fig. 7. Effect of the structure of N-compounds on relative activities of HDS and HYD; PY – pyridine, PIP – piperidine, AN – aniline, NAN – *N,N*-dimethylaniline, Q – quinoline, MQ – quinaldine, 26L-2,6-lutidine, 35L-3,5-lutidine (conditions as in Fig. 6) [33].

HDS sites are immune to poisoning. Also, HDS activity is more greatly deactivated compared with HYD for the same amount of poison. The effect of molecular structure on relative activities is shown in Fig. 7. Piperidine, the hydrogenated analog of pyridine, deactivated HDS to a greater extent than HYD. Similarly, HDS was more deactivated than HYD for aniline and its N-substituted analog. Different results were obtained for quinoline and its 2-methyl analog quinaldine. The latter showed a reverse effect, deactivating HYD more than HDS. This effect was even more pronounced for 2,6-dimethylpyridine (2,6-lutidine). Not only was HDS less deactivated than HYD, but a positive promotion of HDS was obtained at low adsorption. In contrast, deactivation by 3,5-dimethylpyridine (3,5-lutidine) was comparable to that of pyridine. A strong poisoning effect of 2,4-lutidine on the HYD of 2-methylnaphthalene was also reported by Ho et al. [34]. It appears that, except for sterically hindered compounds, HDS is more deactivated than HYD. This suggests a greater adsorption of poison on HDS sites compared with that on HYD sites.

The studies of Miciukiewicz et al. [33] were later extended by Yang and Massoth [35] to poisoning of the HDS of 2-methylthiophene and the HDO of 2-methylfuran by piperidine and 2,6-lutidine. Fig. 8 shows the effect of the adsorbed piperidine on the HDS and HDO activities. While the HDS activity decreased gradually and then tailed off with increasing amount of poison, a drastic decrease in the HDO activity was observed in the presence of small amounts

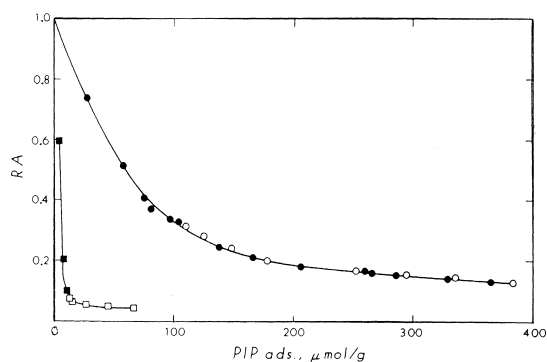


Fig. 8. Effect of piperidine on relative activities; ○● – HDS of methylthiophene, □■ – HDO of methylfuran ($\text{CoMo}/\text{Al}_2\text{O}_3$, 623 K, near atm. H_2) [35].

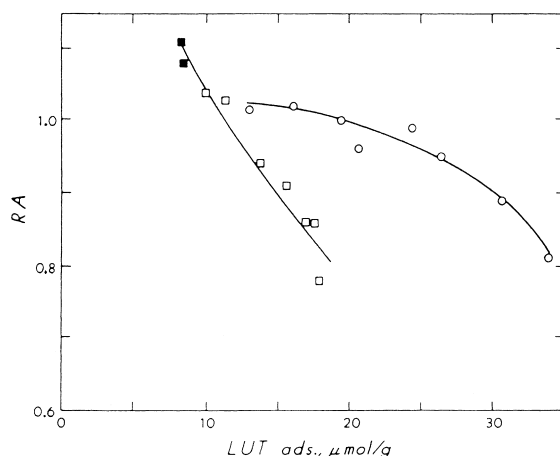


Fig. 9. Effect of lutidine on relative activities (symbols and conditions as in Fig. 8) [35].

of poison. With further addition of poison, the HDO activity remained unchanged. The results for deactivation by 2,6-lutidine, shown in Fig. 9, are much different than those in Fig. 8. This indicates that the reaction sites for HDO are sterically hindered, as was found for HDS sites [33]. Because of the similarity of these results with those for thiophene, the same type of site may be involved in the hydrogenolysis of C–O and C–S bonds.

Strong inhibition by carbazole was observed by Nagai and Kabe [36] during the HDS of benzothio-*phene*. This was attributed to a partial hydrogenation of carbazole to more basic intermediates. A similar reason was given for the inhibition of HDO of *m*-cresol with indole by Odebunmi and Ollis [37]. The inhibition was greater at lower temperatures due to higher ratio of more basic indoline to indole. Besides lowering the activity, often a poison will affect the selectivity of a reaction if its effect is different on different pathways. For example, as shown in Fig. 10 [32], the addition of acridine radically changed the product distribution for HDS of dibenzothiophene at 260°C. Thus, biphenyl became the major product, whereas the yields of hydrogenated products decreased significantly with increasing amounts of acridine. Fig. 11 [36] shows results for the same experiments performed at 300°C. It is evident that the temperature increase from 260 to 300°C decreased the HDS conversion as indicated by the concentration

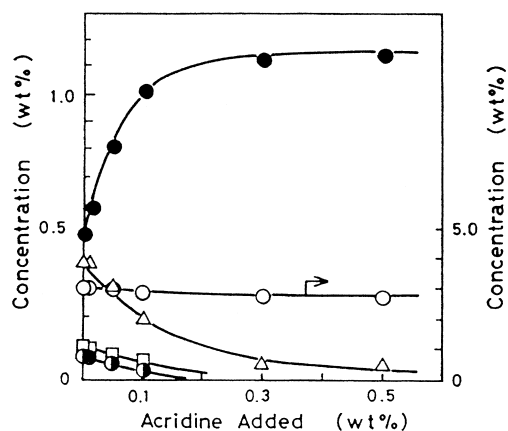


Fig. 10. Effect of added acridine on the products of dibenzothiophene (DBT) HDS; ● – biphenyl, △ – cyclohexylbenzene, ○ – DBT, □ – tetrahydroDBT, ◇ – hexahydroDBT, ○ – bicyclohexyl, ○ – Cyclohexylhexane (NiMo/Al₂O₃; 533 K; 10.1 MPa) [32].

of the reactant dibenzothiophene and that of biphenyl which is the major HDS product.

Ramachandran and Massoth [38] studied the poisoning effect of pyridine on the HDS of benzothiophene. Under the conditions employed, pyridine can

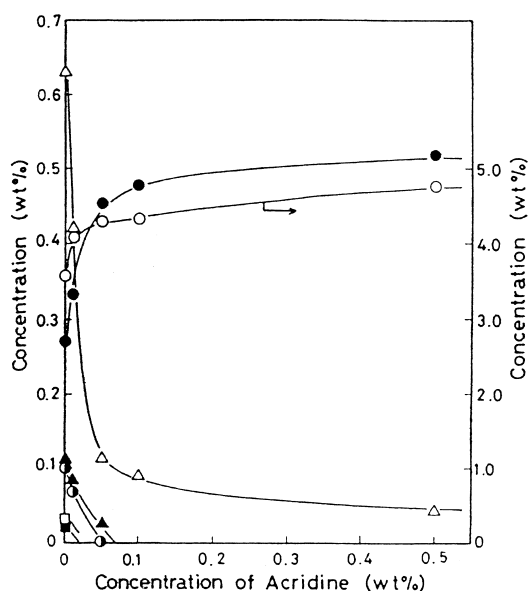


Fig. 11. Effect of added acridine on the products of DBT HDS; ▲ – hexahydroDBT, other symbols the same as in Fig. 10 (NiMo/Al₂O₃; 573 K, 10.1 MPa) [36].

be considered an irreversible poison, as its desorption rate is very slow, and it does not undergo reaction. The catalyst activity initially decreased linearly with increasing amounts of pyridine on the catalyst. However, at about 40% of residual activity, a tailing out occurred, suggesting that some HDS sites are immune to pyridine poisoning, the excess pyridine being adsorbed on non-active sites. Kinetic analysis revealed that the inhibition term was essentially the same without or with pyridine present, whereas the HDS rate constant was smaller for the latter, indicative of quasi-reversible poisoning.

It is not clear whether strongly adsorbed N-compounds actually remain intact, or undergo simple polymerization to larger units, which could account for their 'irreversibility'; once a polymer is formed, it is difficult to reverse the reaction to desorb the parent poison. Dong and Massoth [39] investigated coking of a CoMo/Al₂O₃ catalyst at several coking conditions with a vacuum gas oil containing very little nitrogen both in the absence and presence of acridine and carbazole in the feed. The coked catalysts were Soxhlet extracted with xylene to remove any weakly adsorbed species. By comparing chemical analysis of pairs of coked catalysts at the same coking conditions, they were able to establish that the strongly retained N-compound had the same N/C ratio as that of the parent N-compound suggesting that the latter adsorbed in molecular form, or as a simple polymer of the parent. A similar result was obtained for poisoning by N-phenylcarbazole [40]. In this case, the catalyst was first exposed to the poison, and then tested for HDS and HYD. All activities were about one-half of those of the unpoisoned catalyst. Chemical analysis showed the poisoned catalyst to have an N/C ratio close to N-phenylcarbazole. Yang and Satterfield [41] reported 10% loss in material balance during studies of quinoline HDN. They attributed this to a trimer of hydroquinoline. Similar results were obtained during studies of indole HDN [42]. Depending on reaction conditions, material losses of 5–25% were obtained, and chemical analysis of the catalyst after a run gave N/C ratio close to that of indole.

As mentioned earlier, if the poison adsorption-desorption rates are considerable slower than the reaction rate under the study, the poison must be looked at in terms of a quasi-reversible state at a given concentration of poison. Based on this rational,

Massoth and Miciukiewicz [43] treated a set of experimental data for the effect of pyridine on the HDS of thiophene. A special stirred-flow microbalance provided simultaneous measurements of thiophene conversion and adsorbed pyridine. The thiophene reaction data did not fit the common Langmuir–Hinshelwood kinetic treatment, which assumes fast, reversible adsorption of pyridine. Also, the adsorption data did not adequately fit a Langmuir isotherm, whereas the modified Temkin isotherm showed a good fit. In this isotherm, the coverage by pyridine is given by

$$\theta_N = \frac{W_N}{W_{N,\max}} = b \ln \left(\frac{1 + a_0 p_N}{1 + a_0 p_N \exp(-1/b)} \right)$$

where W_N and p_N are adsorbed weight and partial pressure of pyridine, respectively. This isotherm invokes a distribution of strengths of adsorption sites on the catalyst [43]. The HDS rate constant, k_T will depend on the semi-permanent coverage of active sites by pyridine, viz.

$$k_T = k_T^0 (1 - \theta_N)^n$$

For the relative activity, A_T , the following equation was derived:

$$A_T = \frac{k_T}{k_T^0} \left(\frac{D^0}{D} \right)^n$$

where k_T and k_T^0 are the HDS rate constants and D and D^0 the inhibition terms for the poisoned and unpoisoned catalyst, respectively. As D and D^0 varied less than 5% over the conversion range tested, then

As D and D^0 varied less than 5% over the conversion range tested, then

$$A_T = (1 - \theta_N)^n$$

This equation was combined with the modified Temkin isotherm and solved for the various parameters by nonlinear regression analysis for $n = 1$ and $n = 2$, i.e., both a single and dual site mechanism was tested. Tests of the data fit are given in Fig. 12 [43], showing the dual-site mechanism to be somewhat better.

During HDN, ammonia is produced, most of which will leave the reactor zone with the products. However, a part of NH_3 will be strongly adsorbed on the catalyst. Adsorption of NH_3 is weaker than N-heterocyclic compounds, and is generally treated as a reversible inhibition [31]. Gültekin et al. [44] showed severe poisoning of the hydrogenation of propylbenzene by NH_3 via addition of propylamine to a naphtha feed. Gutberlet and Bertolacini [22] reported a poisoning of the HDS activity, but little effect on HYD of olefins.

It is generally accepted that the cracking functionality has an acidic nature. It is quite obvious that the N-compounds, especially those of a high basicity, will poison cracking sites. Yet, for the hydroprocessing catalysts, the information confirming the poisoning effect is very limited. While studying HDS and HYD of model compounds, Girgis and Gates [20] observed significant poisoning by quinoline, especially that of cracking of model compounds to lighter products.

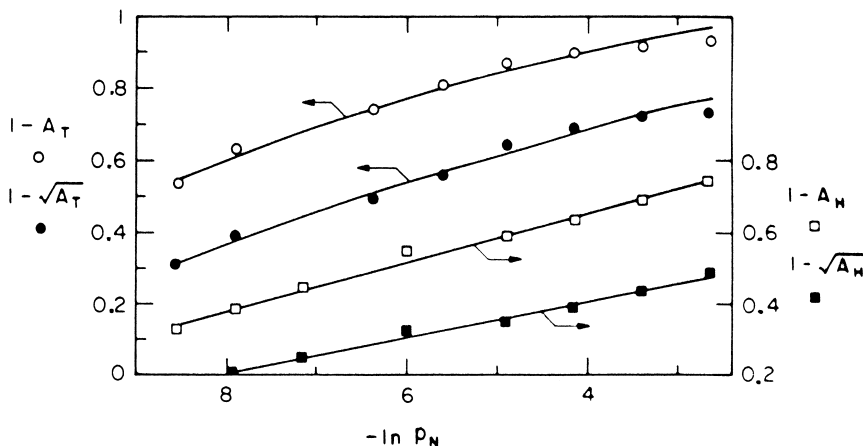


Fig. 12. Test of deactivation with modified Temkin isotherm for single and dual site mechanism (lines represent best fits) [43].

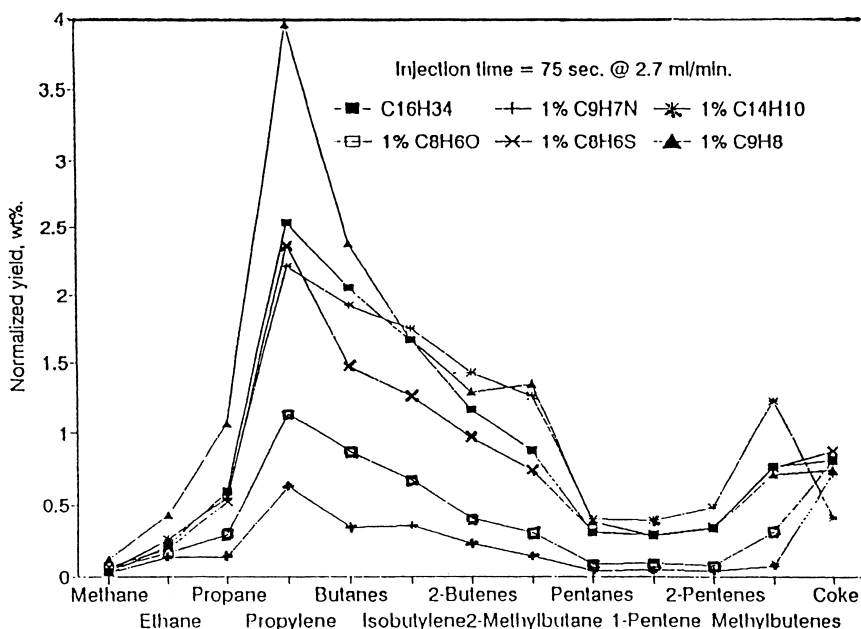


Fig. 13. Effect of poisons (1%) on cracking conversion of hexadecane; ■ – hexadecane, + – quinoline, * – phenanthrene, □ – benzofuran, x – benzoanthropene, ▲ – indene [47].

Hughes et al. [46,47] have used typical cracking catalysts to study cracking of hexadecane in the presence of a number of poisons. As the results in Fig. 13 show, the most severe poisoning of the cracking sites was caused by quinoline. It is believed that among these compounds, quinoline and its partially hydrogenated intermediates will cause the most extensive poisoning also in the case of hydroprocessing catalysts.

HDM is an important functionality of the hydroprocessing catalysts for heavy feeds. Ware and Wei [48] observed significant poisoning by pyridine during the HDM of a Ni-porphyrin using a CoMo/Al₂O₃ catalyst. Each of the reaction steps in the HDM mechanism was suppressed by pyridine. The details of the HDM mechanism proposed by these authors will be discussed in a subsequent chapter.

Information on N-compounds poisoning during the hydroprocessing of real feeds is scarce. Gutberlet and Bertolacini [22] studied the HDS of naphtha spiked by substituted pyridines. With the exception of the 2,6-methylpyridine, all others substituted pyridines inhibited HDS in agreement with results of Miciukiewicz et al. [33]. In a similar study, Jones et al. [49] spiked

a gas oil feed with quinoline and observed a decrease in the sulfur removal.

3.2. Effect of H₂O

Sulfur compounds are more reactive than oxygen compounds, and both are considerably more reactive than nitrogen compounds. Sulfur compounds in conventional and heavy feeds are predominantly as 5-membered thiophenic heterocyclics. They adsorb essentially reversibly, as does H₂S, and have been kinetically treated as an inhibition. Although the oxygen content in conventional feeds is low, in the case of coal-derived liquids and biomass-derived feeds, oxygenated compounds and water derived therefrom may have an inhibiting effect on HDO reactions. It is believed that the inhibiting effect of water can be diminished by maintaining a desirable pressure of H₂S in order to maintain the catalyst in its sulfided state. In the case of the high oxygen content feeds, this may require an addition of an H₂S generating species to the feed. Otherwise, H₂O may modify the catalyst surface during the period of operation, and as such contribute to loss in catalyst

Table 5

Effect of H₂O on HDO of 4-methylphenol and BET surface area of catalyst [57]

Run	Duration (h)	Rate constant (cm ³ min ⁻¹ g cat ⁻¹)	Selectivity (MCH/TOL)	BET surface area (m ² /g)
Fresh catalyst		2.65	20.0	181
Blank	5	2.30	20.5	172
H ₂ O	5	0.90	19.0	133
H ₂ O–H ₂ S	1	1.43	23.3	170
H ₂ O–H ₂ S	2	0.82	19.5	156
H ₂ O–H ₂ S	5	0.92	23.0	150

activity [50]. Although this effect may be reversible, some attention may be paid to the potential activity loss due to the presence of H₂O.

Krishnamurthy and Shah [51] reported that the addition of 0.75 wt.% of dibenzofuran (DBF) to 1 wt.% of dibenzothiophene (DBT) reduced the HDS rate by 25%. However, addition of 1 wt.% of cyclohexylphenol resulted in a two-fold reduction in HDS. This was attributed to inhibition by water, which was rapidly formed from the cyclohexylphenol, although polymer formation on the catalyst surface cannot be ruled out. Girgis and Gates [45] found that the inhibition by 5,6,7,8-tetrahydro-1-naphthol and/or water from it, on the hydrogenation of aromatics and HDO and HDS of DBF and DBT, respectively, was rather weak; however, because of the low reactant concentrations, these authors cautioned that this observation may not be representative of high oxygen content feeds. Odebunmi and Ollis [37,52] reported a gradual loss in catalytic activity during the HDO of *m*-cresol, which could only be recovered by resulfiding the catalyst. When indole was added, catalytic activity was only one-half restored even by resulfiding. These results are indicative of quasi-reversible adsorption. Satterfield and Yang [53] reported that the addition of *m*-ethylphenol to a quinoline feed increased the HDN. The original HDN activity was not fully restored when the phenol was removed. This may be due to formation of a polymer on the catalyst, as benzylether and benzodioxane caused catalyst bed plugging.

Some contrary results are found in the literature on the effect of water. Thus, Lipsch and Schuit [25] observed a poisoning effect of water on HDS of thiophene, and Krishnamurthy and Shah [51] found that the pseudo-first-order rate constant for hydrogenation of biphenyl to cyclohexylbenzene decreased by

an order of magnitude when 1 wt.% water was added to the feed. Vogelzang et al. [50] observed a weak inhibition of naphthol HDO by water. On the other hand, Satterfield et al. [54] reported a promoting effect of water on the HDN of quinoline. The enhancing effect of water was increased in the presence of H₂S.

Laurent and Delmon [55,56] reported that water caused only very weak inhibition in the HDO of phenols, ketones and carboxylic compounds, compared to H₂S and NH₃. These authors expanded their studies [57] to include the HDO of bio-oils under high water pressure in a batch reactor with a sulfided NiMo catalyst. The results from this study for 4-methylphenol are given in Table 5. For the blank run (dodecane solvent), little change in the catalyst activity was noted. However, on the addition of water, about two-thirds of the activity was lost. The poisoning effect of water was evident also with H₂S present, whereas the selectivity of methylcyclohexanol and toluene (MCH/TOL) was hardly affected. The surface changes signify a modification of the catalyst structure by water. In summary, it is apparent that the effect of water gains on importance with increasing concentration in the feed, and after certain level is exceeded, the poisoning effect of water may be quite significant. Almost certainly, poisoning by water will be present during hydroprocessing of the biomass derived feeds.

4. Deactivation by coke

Catalyst deactivation by coke and metal deposits occurs simultaneously if metals are present in the feed. As indicated previously, species which poison active sites on the catalyst contribute to the overall deactivation, as well as changes in the catalyst structure which

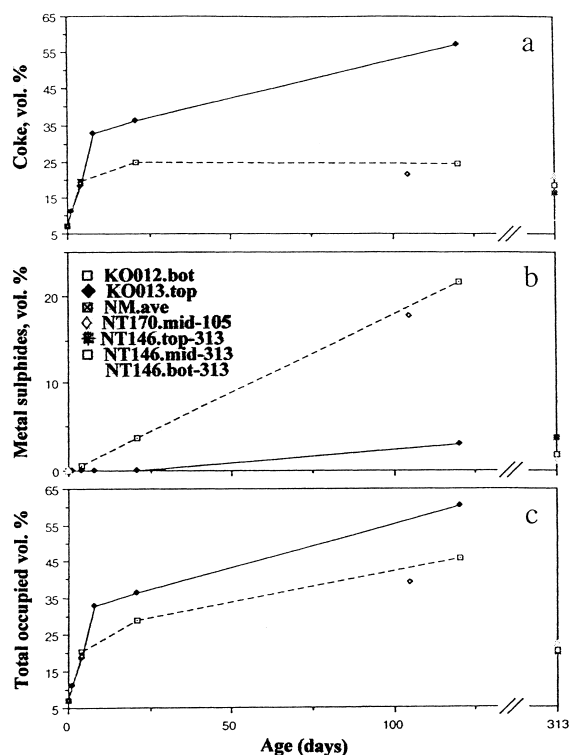


Fig. 14. Evolution of (a) coke, (b) metals and (c) total occupied volume as a function of time on stream [58].

may occur during the operation. It is not easy to distinguish quantitatively between the contribution of all these causes to deactivation. As shown in Fig. 14, there is a difference between the deposition patterns of coke and metals [58]. The symbols for Fig. 14 are identified in Fig. 14b. The former deposits rapidly during the initial stages before attaining a steady-state. About one third of the pore volume of the fresh catalyst is filled during the initial stage on stream. At the same time, metals exhibit more or less linear deposition patterns with time. A similar observation was made by Marafi and Stanislaus [59] using a gas oil feed. Coke deposition was the main cause of the initial pore volume loss. The coke and metal build-up depend on the properties of the feed and hydroprocessing conditions. Netzel et al. [60] have shown that the structure of the catalyst can have a significant effect on the amount of deposited coke. Also, in the case of coke and metals, only a relative extent of deactivation could be estimated, as shown in the results of Table 6 published by Cable et al. [61]. These

Table 6

Relative deactivation by metals and coke [61]

Catalyst function	Relative effect	
	Metals	Coke
HDS	m	m
Hydrogenation	w	s
Cracking	w	vs

m: moderate; w: weak; s: strong; vs: very strong.

results suggest that when the fresh catalyst is compared with the aged-regenerated catalyst, metals appear to have a moderate effect on HDS activity, a very weak effect on hydrogenation activity and a weak effect on cracking activity. Comparing the aged catalyst with the aged-regenerated catalyst shows an additional effect on the HDS activity due to coke. Coke seems to have a strong effect on the hydrogenation, since metals have almost no effect, and coke has a much stronger effect than metals on the cracking activity.

4.1. Origin of catalyst coke

Coke on hydroprocessing catalysts is ubiquitous, i.e., coke is formed from virtually all hydroprocessing feeds employed. General trends which can be established from many studies on realistic feeds indicate that the coke build-up increases with the molecular weight and/or boiling range of the processed feed. However, among feeds having similar boiling range, the one with a high content of coke precursors, e.g., aromatics or heterocyclics, will require the most active catalyst to prevent coke formation. For example, a naphtha fraction from coal liquefaction will require a different catalyst and conditions compared with a similar naphtha fraction derived from a conventional crude.

It is well established that the carbonaceous deposit on spent catalysts at the end of the hydroprocessing operation comprises some carryovers of feed, the asphaltene-like solvent soluble species, and solvent insoluble species. The amount of the carryovers depends on the de-oiling procedure applied during the catalyst withdrawal from the reactor. The average molecular weight of the solvent soluble portion of the deposit is usually significantly greater than the molecular weight of the largest molecules in the feed,

especially in the case of light feeds. In this case, the molecules contained in the carbonaceous deposit on the spent catalyst after the removal of carryovers were not present in the original feed but were formed during the operation [62]. The amount and composition of the soluble portion of the deposit depends on the solvent used for the extraction [63]. Soxhlet extraction of spent hydroprocessing catalysts has been used most frequently before their analysis and/or testing. Alkanes, such as pentane, hexane, cyclohexane and others are suitable for removal of the carryovers and/or non-asphaltenic portion of the deposits. Aromatic solvents, such as benzene, toluene and others appear to be the most suitable for the removal of asphaltene-like species. Other solvents, e.g., methylene chloride, THF, methanol, pyridine, etc. have also been used. However, it is not easy to remove some of these solvents from the catalyst after the extraction. Also, some of the solvents may polymerize during the extraction and as such modify the structure of the organic deposit. A standard extraction procedure, which could be commonly adapted by all researchers involved in the evaluation of the spent hydroprocessing catalysts, would be desirable in order to make comparison of the results obtained by different research groups more meaningful. It was proposed that the insoluble portion of the carbonaceous deposit on the spent catalyst be referred to as 'coke' [64].

4.1.1. Mechanism of coke formation

The significant difference between the average molecular weight of coke molecules and those present in the hydroprocessed feeds indicates that polymerization or polycondensation are the main reactions leading to coke. For example, the extract from the spent catalyst used for hydroprocessing of a naphtha fraction contained molecules as high as coronene [62]. It is obvious that the coke moieties remaining on the catalyst after extraction would be even heavier. Coke forming reactions occur on the catalyst surface; therefore, the structure of the surface is important for controlling the extent of coking. Among hydrocarbon groups, the alkenes, aromatics and heterocyclics are most susceptible to coke formation. Their interaction with the surface is much stronger than that of saturated hydrocarbons. Therefore, they are more likely to convert to higher molecular weight species if sufficient active hydrogen is not available to prevent it.

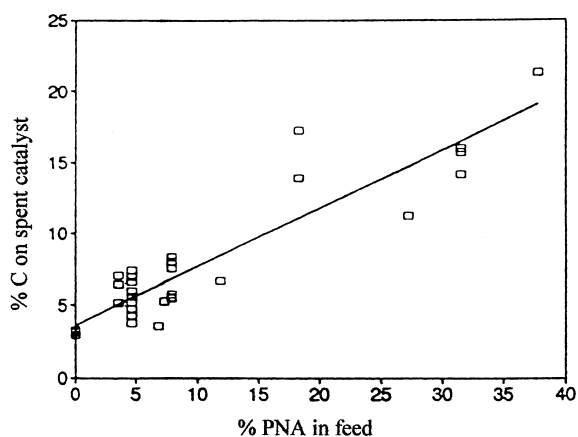


Fig. 15. Effect of the content of PNA in feed on the amount of coke on catalyst [65].

Wiwel et al. [65] obtained a correlation (Fig. 15) between the coke propensity of the feed and the PNA content in the feed. The involvement of heterocyclics in coke formation is supported by the results shown in Table 7 [62]. In this case, the spent catalyst from hydroprocessing of a low sulphur coal-derived naphtha was subjected to sequential extractions by pentane (A), benzene + methanol (B) and pyridine (C). The solvents were then removed to recover the extracts. The significant increase in the heteroatoms content in the extracts compared with the feed is quite evident. The aromaticity and content of phenols in the extracts increased and that of saturated carbon compounds decreased. After every extraction step, the N/C

Table 7
Chemical composition of extracts [62]

	Feed	Extracts		
		A	B	C
Yield, wt. %	—	2.3	3.7	1.3
Carbon	85.3	87.4	81.0	75.3
Hydrogen	9.6	9.4	7.2	5.1
Nitrogen	0.5	0.1	2.2	5.2
Oxygen	4.8	0.3	7.5	5.3
Sulfur	0.0	tr	0.01	0.4
H/C	1.35	1.30	1.06	0.81
N/C	0.005	0.001	0.023	0.059
O/C	0.048	0.003	0.071	0.053
C _{AR}	52.7	56.1	65.0	—
C _S	47.3	43.9	35.0	—
C _{AR-OH}	1.9	tr	2.6	—

ratio of the catalyst gradually increased from 0.001 for the unextracted catalyst, to 0.023 and 0.059 after extractions with A, B and C, respectively. This indicates a significant contribution of the N-containing compounds to coke formation. A similar evaluation of a high sulfur feed confirmed a marked increase of sulfur content in the extracts, as well as that of nitrogen and oxygen compared with the feed [66]. The coke precursors are present in the original feed or can be formed during the operation if sufficient active hydrogen is not supplied. Such a situation may develop during the late stages of the operation, i.e., when the catalyst deactivation reaches an advanced stage. Under such conditions even molecules as small as toluene can act as coke precursors [67].

Zeuthen et al. [68] used pyrene and alkylated pyrenes as well as carbazole and alkylated carbazols in a solution of *n*-heptane for coking a NiMo/Al₂O₃ catalyst under hydroprocessing conditions. In the case of pyrenes, there was little effect of alkyl substitution on the rate of coke formation, indicating a π -interaction of rings with the catalyst surface. However, in the case of carbazoles, the interaction with the surface was significantly reduced by substitution in the first position (neighbor to the nitrogen atom), suggesting that carbazoles interact via the unpaired electrons on the nitrogen.

In the case of heavy feeds, asphaltenes and heavier species can precipitate on the catalyst surface if the colloid stability of the feed cannot be maintained. This requires a proper ratio of oil, resins and asphaltenes in the feed. The resins play a role of stabilizer in preventing precipitation of asphaltenes [69]. Under hydroprocessing conditions, this structure is most likely disrupted and the system may be classified as a pseudo-solution of a random mixture of oil, resins and asphaltenes [70]. It may be important that during hydroprocessing, resins are removed at about the same rate as the asphaltenes. Otherwise, precipitation of asphaltenes from the feed can be a major cause of coke formation [71]. It was established that the coking propensity of asphaltenes is higher than that of resins [72]. After being adsorbed on the surface, both the resins and asphaltenes are gradually converted to lighter fractions; however, a small amount may convert to coke. Nagaishi et al. [73] have shown that the asphaltenes become more aromatic than the original asphaltenes. Condensation of asphaltenes on the cata-

lyst surface may produce coke containing small anisotropic regions consistent with mesophase development [74]. The mechanism shown in Fig. 8 was proposed to explain thermal hydrocracking and pyrolysis of asphaltenes derived from Athabasca bitumen [75]. For this purpose, the model proposed by Suzuki et al. [76] was used. The volatile products are not shown in the mechanism. The partial conversion of asphaltenes shown in Fig. 16 may already occur during preheating the mixture of H₂ and feed prior to contacting catalyst bed. If the catalyst bed is functioning properly, the thermally hydrocracked products will be converted to lighter fractions; otherwise, they will be converted to coke. Thus, the beneficial role of H₂ is evident in the mechanism. Using terminology introduced by Alvarez et al. [77], the products in Fig. 16 formed during hydrocracking of the asphaltene may be viewed as 'mildly aged coke' whereas those formed during pyrolysis as 'aged coke'.

The introduction of bio-feeds raises the problem of potential coke formation from the various O-containing species, among which phenols and furanic rings are predominant. It was indeed confirmed by Laurent et al. [78] that some phenols are important coke precursors in spite of their low molecular weight and size. Thus, the CoMo/Al₂O₃ catalysts used for the HDO of hexadecane solutions containing methoxyphenol, hydroxyphenol, phenol or methylanisol resulted in 7.8, 5.5, 3.5 and 2.8 wt.% of coke, respectively, suggesting that compounds with two oxygens are more efficient coke precursors. These values of coke were rather high considering the short residence time employed. Under hydrogen-deficient conditions, coke can be formed even from THF [79]. In this case, pretreatment of the catalyst is important.

The strength of the interaction of coke precursors with the catalyst depends on the properties of the catalyst surface and the structure of the coke precursor. It was established by Appleby et al. [80] that coking increases with increasing acidity of the surface and/or increasing basicity of the precursor. However, since acidity favors hydrocracking, a balance must be found between the rate of coking and hydrocracking activity. It is believed that both Lewis and Brønsted acid sites may take part during coking, the former by strongly interacting with basic species in the feed, thus prolonging their life on the catalyst, and the latter by supplying protons to form carbonium cations, which

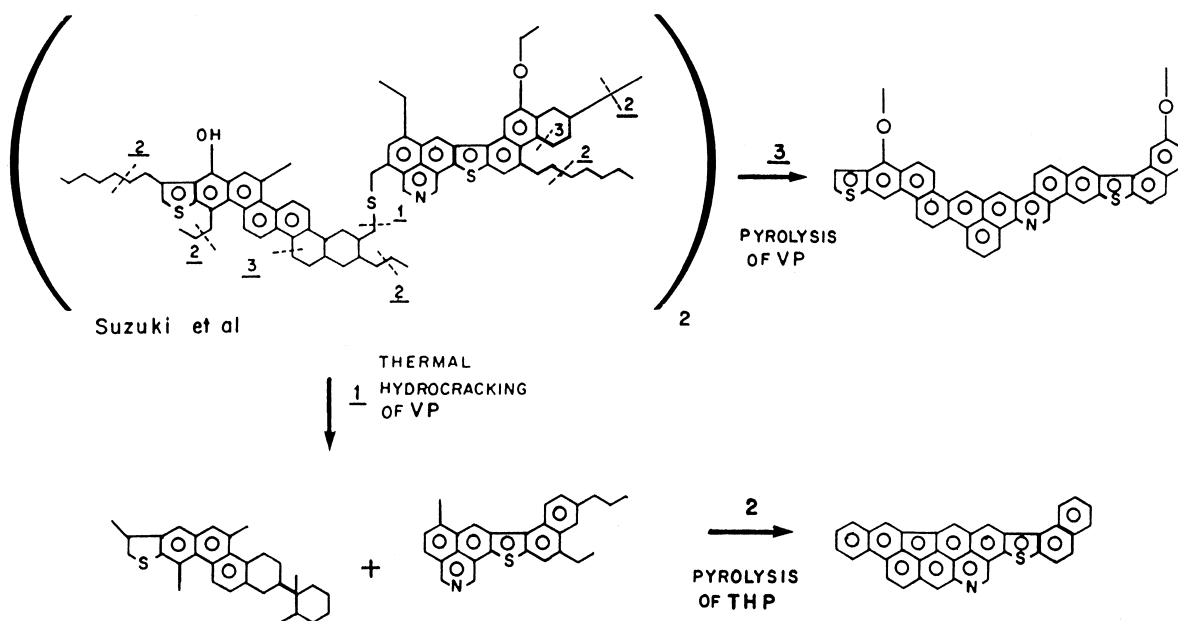
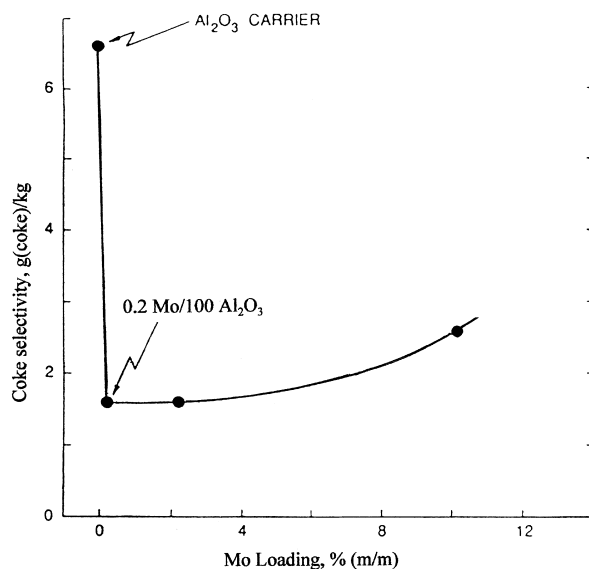


Fig. 16. Tentative mechanism for coke formation from asphaltenes [75].

are assumed to be responsible for coking [81]. However, the contribution of the Lewis and Brønsted acidic sites to coke formation is still controversial [82,83]. Lewis and Brønsted sites are associated with the catalyst active phase, whereas only Lewis sites are present on alumina supports [84]. As shown by Scaroni et al. [85], the HDS catalyst can catalyze coking. Thus, during coking of anthracene under N_2 , the amount of coke on the bare Al_2O_3 support was much smaller than that on a $CoMo/Al_2O_3$ catalyst. The difference may be caused by the presence of the Brønsted acidic sites on the latter and their absence on the bare $\gamma-Al_2O_3$. On the other hand, De Jong et al. [86] showed that during hydroprocessing of a vacuum gas oil, the amount of coke decreased significantly by adding 0.2% of Mo to Al_2O_3 , as the results in Fig. 17 show. Thus, the presence of Mo significantly suppressed coke formation on the alumina support. However, with increasing Mo loading, the amount of coke again increased slightly. The authors assumed that to a certain extent MoS_2 can catalyze coke formation. It is believed that the Brønsted acidic sites on MoS_2/Al_2O_3 aided coke formation via carbonium cations as intermediates.

Besides feed composition and catalyst properties, hydroprocessing conditions are important for control-

ling the extent of coke formation. Of particular importance is the partial pressure of H_2 , temperature and contact time. Hydrogen can convert coke precursors into stable products before they are converted to coke.

Fig. 17. Effect of Mo loading on the coke selectivity and HDS activity (723 K, 30 bar H_2) [86].

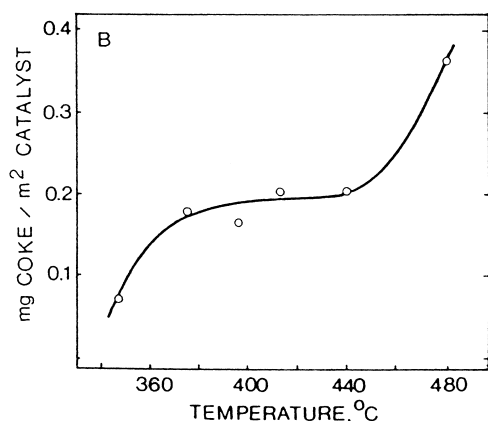


Fig. 18. Effects of temperature on catalyst coke [87].

However, the probability of this conversion decreases with increasing temperature. The results in Fig. 18 suggest that there might be an optimal combination of catalyst properties and processing conditions, which ensures the best performance of the catalyst [87]. These results suggest that at a given partial pressure of H_2 , the coke build-up increases up to about 375°C because the conversion of heavy species to lighter fractions is slow. As a result of the slow conversion, the life of heavy molecules on the catalyst surface is prolonged, which increases the chances of polymerization. A faster conversion of the resins than that of

the asphaltenes, leading to precipitation of the latter may be another reason for this observation. Above 375°C, the hydrogenation of the coke precursors to products competes successfully with their polymerization. Also, an increased conversion of asphaltene-like species (because of the increased temperature), may slow down coking. Stohl and Stephens [88] observed even a slight decrease in the coke formation by increasing temperature from about 360 to 370°C because of the improved conversion of heavy species in the feed and possibly also some of those heavy species which temporarily adsorbed on the catalyst. However, the coke build-up increase above 440°C (Fig. 18) indicates on increasing rate of dehydrogenation followed by polycondensation reactions. Mochida et al. [89] observed little change in coke build-up between 380 and 430°C within the first 10 h on stream. At 430°C, the coke build-up began to increase and the H/C ratio of the coke to decrease afterward, indicating dehydrogenation of the coke. Similar trends were observed by van Dorn et al. [90] who artificially coked Co/NiMo/ Al_2O_3 catalysts at 400 and 500°C. The H/C ratio for the deposited cokes was 1.7 and 0.6, respectively, indicating significant dehydrogenation at 500°C compared with that at 400°C. It is believed that the flat region in Fig. 18 can be expanded by increasing the partial pressure of H_2 . This is supported by results published by Richardson et al. [91], shown

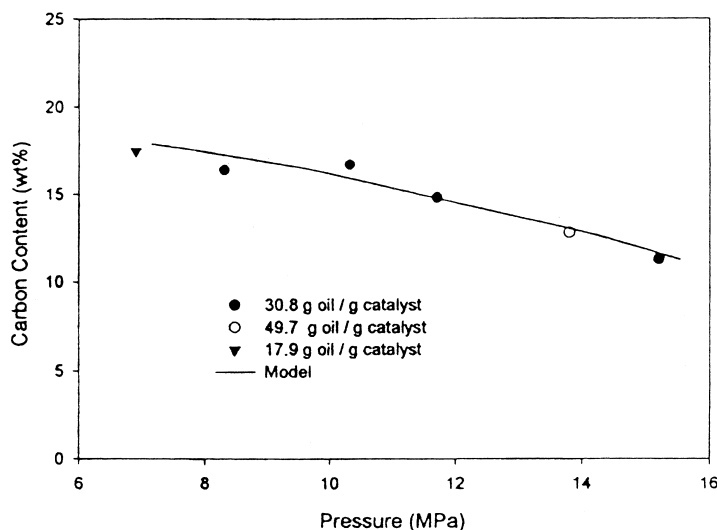


Fig. 19. Carbon content of catalyst as function of H_2 pressure (NiMo/ Al_2O_3 , 703 K) [91].

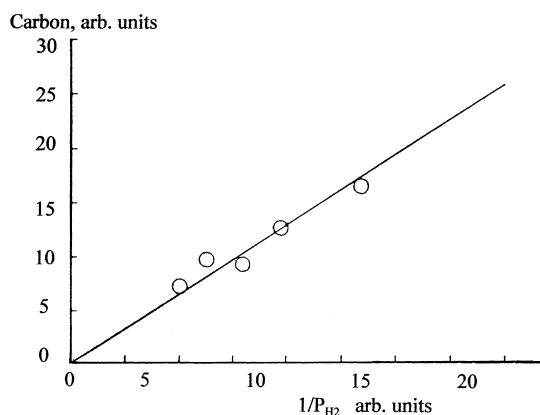


Fig. 20. Steady-state level of carbon on catalyst as function of H_2 pressure [92].

in Fig. 19, obtained at 430°C for the initial coking. As shown in Fig. 20, the effect of the partial pressure of H_2 is even more pronounced on the steady-state level of coke [92]. De Jong et al. [86] showed that H_2 /oil ratio also can influence coke formation. As seen in Fig. 21, a distinct maximum in coke formation is observed at intermediate feed ratios. The model developed by these authors suggested that at low gas rates, the gas oil was mainly in the liquid phase, whereas at high rates, the reactor was operating in the gas phase.

Perhaps, the most detailed study on the effect of processing conditions on deactivation by coke was published by Gualda and Kasztelan [93], who

observed that in a batch system the amount of coke decreased with increasing contact time, temperature and H_2 pressure. This was attributed to a feed 'purification' accompanied by the removal of coke precursors as well as an improved hydrogenation of the coke deposited on the catalyst during the initial stages. More coke was deposited in a continuous flow system because of the uninterrupted supply of coke precursors. As expected, more coke was deposited on $\gamma-Al_2O_3$ than on the $NiMo/Al_2O_3$ catalysts. Also, the H/C ratio of this coke was lower than that deposited on the catalysts, indicating a role of active metals during coke formation. The H/C ratio of the coke seemed to go through a maximum while increasing temperature and contact time. These authors concluded that the behavior of coke on the catalyst is clearly dynamic, as indicated by the effects of conditions as well as differences between the structure of the 'young coke' and the 'aged' coke.

A detailed analysis of the organic deposit on the catalyst is required to elucidate the mechanism of coke formation. The presence of polynuclear aromatics (PNA) shown in Table 8 was confirmed in the extract from the spent catalyst after hydroprocessing a coal-derived naphtha [62]. Yet, according to the boiling range of the naphtha, only lighter PNA's (e.g., alkylated naphthalenes and acridines) are expected in the feed. Similar species were identified as notorious coke makers by Appleby et al. [80] and Bakulin et al. [94]. Nagaishi et al. [73] reported that the apparent first-

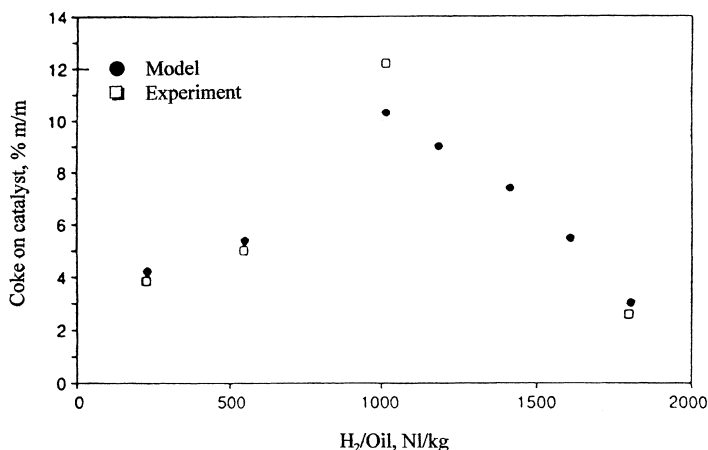


Fig. 21. Effect of H_2 /feed ratio on the coke content of catalyst (NiV/SiO_2 , 723 K, 30 bar H_2) [86].

Table 8
PNA identified in the extract^a [62]

1	Chrysene
2	Benzochrysene
3	Benzophenanthrene
4	Benzofluoranthene
5	Perylene
6	Benzoperylene
7	Benzacridine
8	Benzcarbazole
9	Coronene

^a Decreasing order of abundance.

order rate constant for a residue conversion decreased with increasing content of the aromatic carbon in the residue. The mechanism shown in Fig. 22 is based on the coupling of two naphthalene molecules via route 1b or two alkyl naphthalenes leading to coronene via route 1a. In the latter case, two additional rings can be formed via dehydrocyclization as depicted by dotted lines. Beguin and Setton [95] observed coupling of PNA aided by various metals. Also, coupling was enhanced in the presence of a proton donating medium, such as a Brønsted acid [96]. In this case, the formation of the carbonium cations is predicted. It was established that such carbonium cations can combine with neutral PNA rings to yield larger structures [97]. The coupling capability was significantly diminished after the Brønsted acidity was destroyed by pretreating the support with basic species [98]. The involvement of carbonium cations was assumed in the mechanism proposed by Gates et al. [99] for coking of anthracene. Scaroni and Jenkins [100] assumed the participation

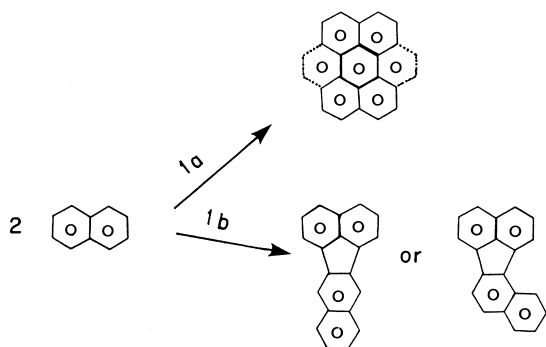


Fig. 22. Tentative mechanism of coupling of naphthalene molecules [62].

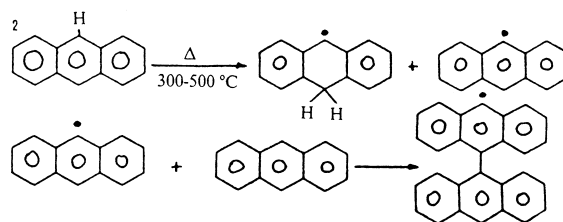


Fig. 23. Free radical mechanism for formation of coke from anthracene [101].

of carbonium cations in a study of several model compounds in the presence of a CoMo/Al₂O₃ catalyst. These authors proposed that the carbonium cations were formed by electron transfer between the aromatic and hetero rings and the catalyst surface.

The involvement of free radicals in coke formation has been proposed by several authors [101–104]. The probability for such a mechanism increases with increasing temperature, which favors the formation of free radicals. An example of this mechanism, proposed by Lewis and Singer [101], is shown in Fig. 23. A similar mechanism may be involved during coke formation from N-containing bases. In this case, two molecules adsorbed at neighboring Lewis acid sites may couple at temperatures favoring dehydrogenation of the heteroring. Once partially dehydrogenated, the heteroring may couple with an aromatic ring according to the mechanism in Fig. 23. Absi-Halabi et al. [6] proposed the polymerization mechanism in Fig. 24 to illustrate coke formation from both light and heavy hydrocarbons. Experimental support for this mechanism was provided by Nohara and Sakai [104] from coking studies of large aromatic structures with small molecules such as butadiene.

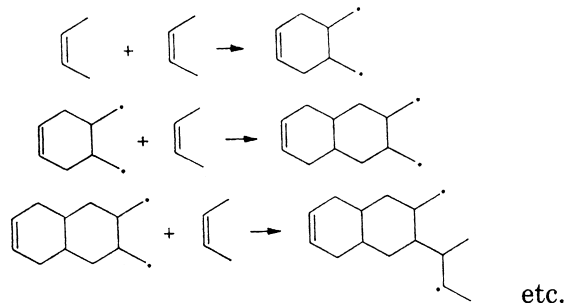


Fig. 24. Mechanism of coke formation by polymerization [6].

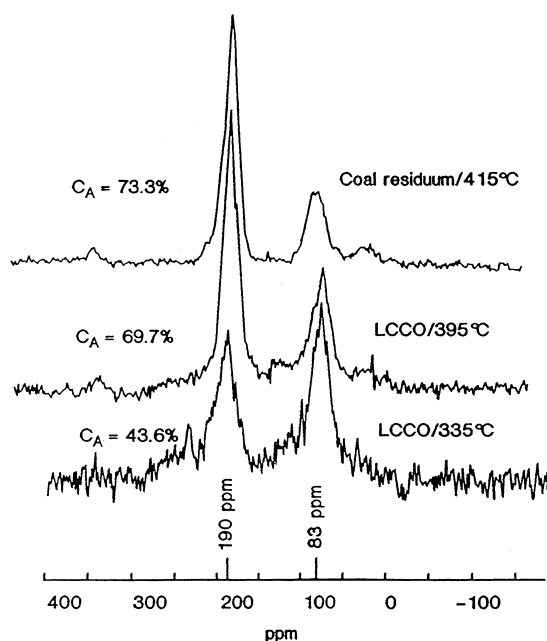


Fig. 25. Effect of temperature on aromaticity of coke (NiMo/Al₂O₃, 12.7 MPa H₂) [105].

Spectroscopic techniques reveal information on chemical structure without destroying the coke on the catalyst. In this regard, ¹³C NMR alone or in combination with other techniques has been used most frequently. It appears that trends established from the chemical analysis of coke and extracts can be confirmed by this technique. For example, the increase in the coke aromaticity with increasing severity of the operation has been confirmed by several studies [105–107]. An example of increasing temperature on coke aromaticity is shown in Fig. 25 [105]. Thus, increasing the temperature from 335 to 395°C increased the content of the aromatic carbon from about 44 to almost 70%. Because some carbon atoms in highly aromatic structures are ‘invisible’ to ¹³CNMR, these values may underestimate the aromaticity [108]. The aromaticity of the coke formed at 335°C was close to that of the feed. Myers et al. [109] have observed increasing aromaticity with the age of the catalyst. Weissman and Edwards [110] used the ¹³C NMR technique to evaluate an aged catalyst after hydroprocessing a high aromatic gas oil and a low aromatic naphtha. The aromaticity of the coke deposit varied from 0.70 to 0.90 and from 0.30 to 0.60 for gas oil and

naphtha, respectively. The naphtha derived deposit had longer aliphatic chain lengths but relatively few aliphatic attachments bridging between the polynuclear aromatic groups. The gas oil derived deposits were highly aromatic and much more condensed, with very short bridging groups or direct phenyl-phenylene bond types. This deposit was described as dense and compact, whereas the naphtha derived deposit as less dense and ‘fluffier’, as the carbons in the deposit had a much higher degree of freedom because of the numerous aliphatic chains present. A fair amount of carbon attached to heteroatoms was also present in the deposits, especially for the naphtha derived coke.

Perhaps the most detailed evaluation of the structure of coke formed on the surface of hydroprocessing catalysts was conducted by Fonseca et al. [58,108] using ¹³C NMR. These authors studied CoMo/Al₂O₃ and NiMo/Al₂O₃ catalysts which were deactivated under different conditions. The catalysts in Fig. 26, identified by NT, are spent NiMo/Al₂O₃ catalysts taken during the hydroprocessing of an atmospheric

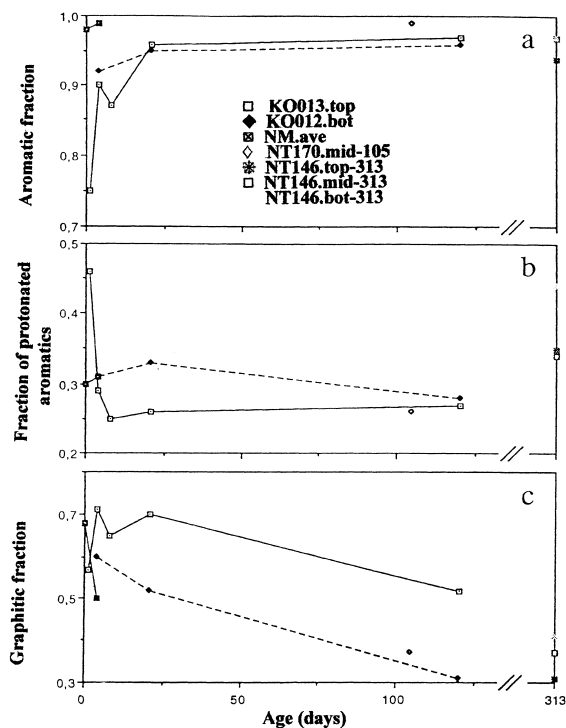


Fig. 26. Evolution of aromaticity (a) protonated aromatics (b) and graphitic fraction (c) as functions of time on-stream [58].

residue, whereas those identified as K are spent CoMo/Al₂O₃ catalysts. The spent catalyst NM was from the treatment of a solution of pyrene in *n*-heptane. The same catalysts are shown in Fig. 14. It is evident that the aromatic fraction of the coke rapidly increased during the first 5 days on stream and then increased only slightly thereafter. The graphitic structure of the coke increased rapidly during the first 4 days on stream and then decreased progressively with aging time. It appears that the graphitic structures are better formed at the beginning of coke deposition when there is more space available for coke rearrangements. More graphitic carbon was formed at the exit of the bed because much less metal deposits were present, i.e., a lower competition with the coke deposition for the space. Marafi and Stanislaus [111] studied hydroprocessing of two very low metal content feeds using a NiMo/Al₂O₃ catalyst. They observed that the aromaticity, determined by ¹³C NMR, of the coke formed during the initial stages was higher than that formed later, indicating that the coke formed initially was undergoing hydrogenation and presumably was converted to lighter fractions.

Magnoux et al. [67] used gas chromatography-mass spectroscopy (GC-MS) for characterizing catalyst coke during pyrolysis of toluene. The main components identified in the methylene chloride extract and the mechanism of coke formation proposed by these authors are shown in Figs. 27 and 28, respectively. It is evident that both ¹³CNMR and GC-MS are excellent tools to confirm participation of the aromatic structures during coke formation.

4.1.2. Effect of restrictive diffusion

It is well known that catalytic hydroprocessing can be influenced by restrictive diffusion in catalysts. This effect becomes critical when the size of reactant molecules approaches the pore diameter. It is important to understand the dependence of the restrictive effects on the nature of the feed and temperature under the reaction conditions, as they may influence the structure and distribution of coke as well as its rate of formation. Although restrictive diffusion phenomena apply equally to metal deposits and coke deposits, information relevant to the former will be discussed in the next chapter.

Diffusivity measurements of solutes from different solutions in the pores of fresh and aged catalysts

provide valuable information on restrictive diffusion. Such information is crucial for the understanding catalyst deactivation. If the solute is relatively small compared with the pore size, its effective diffusivity can be related to bulk diffusivity by the following equation [112]:

$$D_e = \frac{D_b \epsilon}{\tau} \quad (4.1)$$

where D_e is the effective diffusivity, D_b the bulk diffusivity in free solution, and ϵ the porosity and τ the tortuosity of the catalyst. When the solute molecular size approaches that of the pore size, the effective diffusivity becomes less than predicted by Eq. (4.1). To account for this, a restrictive factor, $F(\lambda)$ is added to Eq. (4.1), i.e.,

$$D_e = \frac{D_b \epsilon}{\tau} F(\lambda) \quad (4.2)$$

where λ is the ratio of the solute critical molecular diameter to pore diameter ($=d_s/d_p$). The following empirical correlation was proposed for the restrictive factor [113]:

$$F(\lambda) = \frac{D_e \tau}{D_b \epsilon} e^{-4.6\lambda} \quad (4.3)$$

Studies conducted by Chantong and Massoth [114] with polyaromatic compounds using aluminas of various pore sizes gave a similar relationship, viz.,

$$F(\lambda) = \frac{D_e \tau_0}{D_b} 1.03 e^{-4.5\lambda} \quad (4.4)$$

confirming the general validity of this form for both adsorbing and nonadsorbing solutes. Another form of the restrictive factor, proposed by Beck and Schultz [115] is:

$$F(\lambda) = (1 - \lambda)^z \quad (4.5)$$

This equation can also be approximated by the following empirical expression:

$$F(\lambda) = e^{-b\lambda} \quad (4.6)$$

where b is a constant. Then, a logarithmic plot of $D_e/D_b \epsilon$ versus $\ln(1 - \lambda)$ should yield a straight line with slope equal to z and intercept equal to τ_0 . A nonlinear isothermal adsorption of solute can be related to its bulk concentration C by a Freundlich isotherm, i.e.,

$$q = mC^{1/n} \quad (4.7)$$

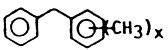
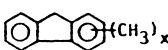
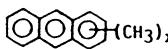
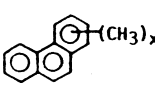
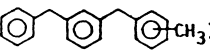
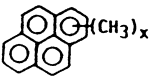
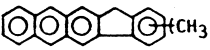
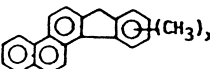
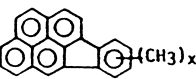
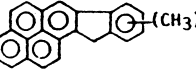
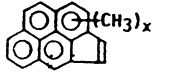
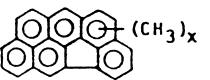
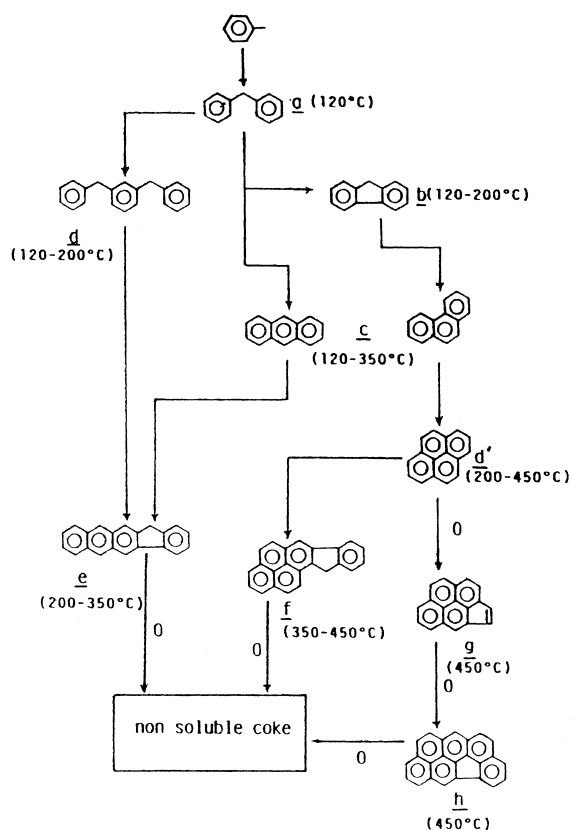
Family	Formulae	Main components			
		T (°C)	x	bp (°C)	Size (Å)
a	 $x=1$	120	1	290	(6x9.5)
b	 $x=1$	120 200	1 1	295	(6x9.5)
c	 $0 \leq x \leq 6$	120	3	360	(6x9.5)
or	 $0 \leq x \leq 6$	200	1	340	(6x8.5)
d	 $0 \leq x \leq 3$	120 200	2 0	> 360 > 360	(6x15.5)
d'	 $0 \leq x \leq 2$	200 350 450	1 0 0	> 395 > 395	(8x8.5)
e	 $0 \leq x \leq 5$	200	1	> 400	(6x15.5)
or	 $0 \leq x \leq 5$	350	0	> 400	(8x14)
f	 $0 \leq x \leq 4$	350	2	> 450	(8x14.5)
or	 $0 \leq x \leq 4$	450	0	> 450	(8x13)
g	 $0 \leq x \leq 1$	450	2	> 450	(8.5x9.5)
h	 $0 \leq x \leq 3$	450	2	450	(8.5x13)

Fig. 27. Components identified in the extract of the spent catalyst used for pyrolysis of toluene [67].

where q is the amount of the adsorbed solute and m and n are constants. This approach was used by Chantong and Massoth [114] to measure restrictive diffusion of naphthalene and coronene solutes in cyclohexane solution in aluminas of varying pore sizes at ambient temperature. The restrictive factor

decreased with increasing λ . The restrictive factor was less than unity even when the molecular diameter was a relatively small fraction of pore diameter.

The work by Chantong and Massoth [114] was later extended by Massoth et al. [116–118] to include three NiMo/Al₂O₃ catalysts whose properties are shown in



• methyl groups are not indicated in the formulae

• 0 = olefins

Fig. 28. Mechanism of thermal formation of coke [67].

Table 9 [118]. Some parameters in this table will be included in a later discussion. A significant difference in the surface area and average micropore diameter among these catalysts is quite evident. To avoid external mass transport, the catalysts were crushed and sieved to 35–65 mesh. The eight solutes studied were naphthalene (NAP), anthracene (ANT), 2,3-benzanthracene (BAN), 1,2,5,6-dibenzanthracene (DBA), coronene (COR), 9-phenylcarbazol (9-PC), tetraphenylporphyrin (TPP) and tetra(4-biphenyl)porphyrin (TBP). The physical properties of the solutes are shown in Table 10. Aliphatic hydrocarbons such as cyclohexane, *n*-heptane and iso-octane were used as solvents. The effective diffusivity, D_e , was determined from the concentration decay time data from the diffusion experiments. In order to calculate D_e , dimensionless time and dimensionless concentration rela-

Table 9

Physical properties of catalysts [118]

	NiMo-125	NiMo-225	NiMo-325
BET S_g (m ² /g)	112	204	291
ρ_p (g/cm ³)	1.28	1.32	1.30
V_p (cm ³ /g)	0.49	0.45	0.45
ϵ	0.627	0.594	0.585
ϵ_μ	0.465	0.451	0.447
ϵ_M	0.162	0.143	0.138
ω_μ (Å)	138	71	54
σ_μ (Å)	1.97	1.76	1.70
d_μ (Å)	174	83	62
ω_M (Å)	10674	6318	9110
σ_M (Å)	1.67	1.71	1.79
d_M (Å)	12174	7296	10793

S_g , ρ , V_p and d are surface area, density, pore volume and pore diameter, respectively.

ϵ , ω and σ porosity, mean value and standard deviation of a log-normal distribution function, respectively.

Subscripts μ and M are for micro and macro pores, respectively.

tionships were developed to back-calculate the ratio of dimensionless time for the nonlinear isotherm case Θ_N , to real time t , viz.,

$$D_e = \frac{\Theta_N}{t} \epsilon r^2 \quad (4.8)$$

where r is the particle radius. Alternatively, D_e can be calculated from the ratio of dimensionless time for the linear isotherm case, Θ_L , to real time and the adsorption constant, K , the ratio of equilibrium uptake to final concentration, viz.,

$$D_e = \frac{\Theta_L}{t} (\epsilon + \rho K) r^2 \quad (4.9)$$

Table 10

Physical properties of solutes [116]

Solute	V_a^a (cm ³ /mol)	d_{cri} (nm)	d_{max} (nm)	d_{aver} (nm)
NAP	157.2	0.74	0.88	0.79
ANT	214	0.74	1.12	0.88
BAN	246	0.74	1.36	0.92
DBA	302.4	0.85	1.57	0.98
COR	294.6	1.11	1.18	0.98
9PC	273.6	1.13	1.15	0.95
TPP	711.4	1.57	1.90	1.31
TBP	1065.8	2.18	2.72	1.50

^a V_a : Molar volume at boiling point.

where ρ is the particle density. For a complete data treatment, the bulk diffusivity, D_b , is also needed. A nonlinear regression analysis of literature data yielded the following equation applicable to aromatic solutes in aliphatic solvents:

$$D_b = 18.7 \times 10^{-8} \frac{M_b^{0.30} T}{\mu_b^{0.84} V_a^{0.55}} \quad (\text{cm}^2/\text{s}) \quad (4.10)$$

where M_b is the solvent molecular weight, V_a is the molar volume of solute at its boiling point and μ_b is the solvent viscosity. To check the D_b values obtained from Eq. (4.10) with the experimental data, Eqs. (4.2) and (4.6) were combined to give

$$\ln \frac{D_e}{\epsilon} = -b d_s \frac{1}{d_p} + \ln \frac{D_b}{\tau} \quad (4.11)$$

Straight line fits of the data plotted as $\ln(D_e/\epsilon)$ versus $1/d_p$ for the solutes in cyclohexane are shown in Fig. 29 [116], where the intercepts are equal to D_b/τ . To calculate D_b , τ has to be determined. This required data from diffusion experiments with a solute having a known value of D_b such as anthracene, i.e., $D_b = 1.2 \times 10^{-5} \text{ cm}^2/\text{s}$. This value of D_b yielded value of τ of 1.37. Eqs. (4.2) and (4.5) can be combined and expressed in logarithmic form to give

$$\ln \delta = Z \ln(1 - \lambda) - \ln \tau \quad (4.12)$$

where δ is the diffusion constrictive factor ($=D_e/\epsilon D_b$). The parameter Z can now be estimated from

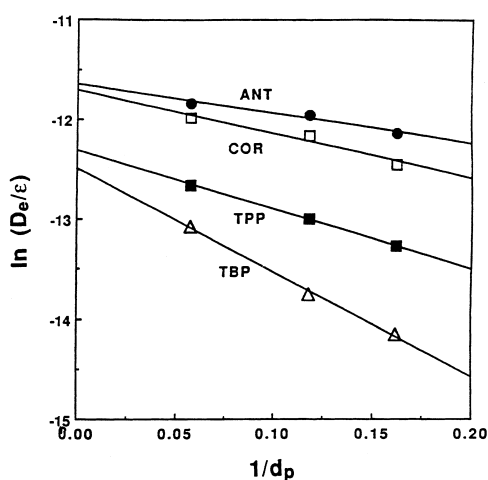


Fig. 29. Determination of tortuosity and bulk diffusivity in cyclohexane [116].

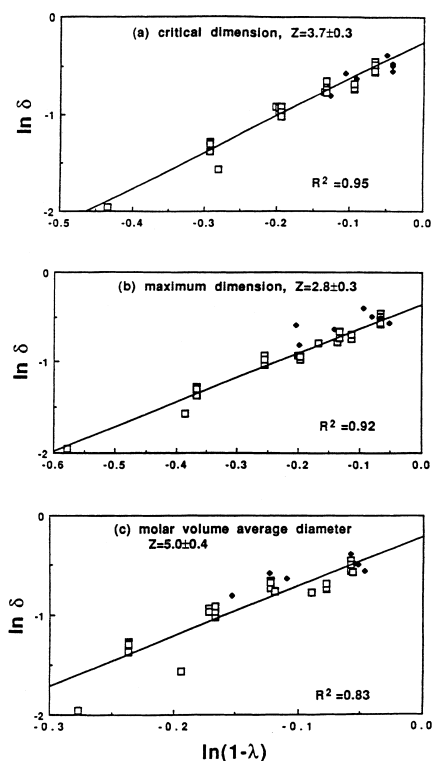


Fig. 30. Comparison of Z factors obtained from different solute molecular dimensions; \square – disk-shaped, \blacklozenge – rod-shaped solutes [116].

Eq. (4.12) from the slopes in Fig. 30 [116]. The best Z value was obtained by using the critical dimension, i.e., in agreement with the value of 4.0 predicted by hydrodynamic theory. The maximum and average dimensions gave unrealistic Z values. Therefore, the use of the critical dimension appears to be the best choice for the solute dimension in computing λ . The nature of the aliphatic solvents had little effect on the diffusivity constriction factor. The average tortuosity factor can be determined using all the measured D_e values by combining Eqs. (4.2) and (4.6) to give

$$\ln \frac{D_e}{\epsilon D_b} = \ln \delta = -b\lambda - \ln \tau \quad (4.13)$$

A semilogarithmic plot of $\ln \delta$ versus λ , using critical dimensions of the solutes Table 10 is given in Fig. 31 [116]. The τ value estimated from the intercept was 1.27 ± 0.03 in a good agreement with the previous estimate. The effect of temperature and

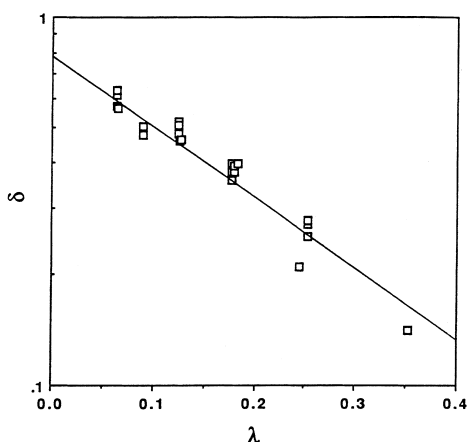


Fig. 31. Determination of tortuosity factor and b constant [116].

H_2 pressure on D_e values was also evaluated [117]. In the latter case, the effect of H_2 pressure was found to be insignificant. The effect of temperature was determined by obtaining the experimental data for COR, TPP and octaethylporphyrin at 298, 313 and 333 K. These results are shown in Fig. 32. The equa-

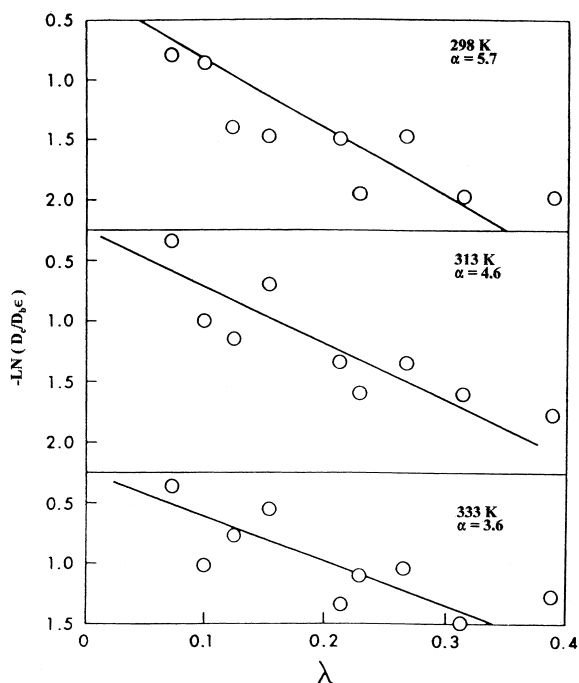


Fig. 32. Variation of $D_b/D_e\epsilon$ with λ [117].

tion relating the restrictive coefficient with temperature is,

$$\ln b = \frac{1.30}{T} - 2.62 \quad (4.14)$$

Then, using Eqs. (4.6) and (4.14), it is possible to estimate the temperature above which restrictive diffusion can be neglected, i.e., $F(\lambda) > 0.9$. For example, at 625 K, a typical hydroprocessing temperature, a restrictive factor of 0.89 is predicted for $\lambda = 0.2$ and a value of 0.75 for $\lambda = 0.5$, confirming that restrictive diffusion is important under hydroprocessing conditions when the molecular size of the reactants is sufficiently large compared to the catalyst pore size.

The concept of restrictive diffusion was used by Lee et al. [118] to test validity of the random pore model using the three NiMo/Al₂O₃ catalysts given in Table 9. The results indicated the catalysts had a bidispersed nature, i.e., the presence of both macro and microporosity. Several monodispersed supports were also tested. The random pore model assumes three types of parallel diffusion passages, i.e., diffusion through macropores, micropores and a series of macropores and micropores. Effective diffusivity is a combination of macropore and micropore diffusivities (D_M and D_μ) and given by Smith [119] as

$$D_e = \epsilon_M^2 D_M + \frac{\epsilon_\mu^2 (1 + 3\epsilon_M)}{1 - \epsilon_M} \eta_i D_\mu \quad (4.15)$$

The effectiveness factor for the entire pellet, η_a , is a function of the Thiele modulus, ϕ_a , viz

$$\eta_a = 3 \frac{\phi_a \coth \phi_a - 1}{\phi_a^2} \quad (4.16)$$

$$\phi_a = R_0 \left(\frac{k_s \rho_p \eta_i}{D_e} \right)^{1/2} \quad (4.17)$$

where R_0 is the radius of catalyst pellet, k_s is the intrinsic rate constant and ρ_p is the catalyst pellet density. It is evident from Eq. (4.17) that the Thiele modulus depends on the effectiveness factor of the microporous particles (η_i). The sorptive data obtained at ambient conditions suggest that macropores in the bidispersed supports did not increase effective diffusivities significantly when compared with the monodispersed supports, suggesting that effective diffusivities were mainly influenced by the average micropore sizes. Then, the general form for expressing

the restrictive diffusion effect becomes

$$F(\lambda) = (1 - \lambda)^z = \frac{D_\mu}{D_b} \quad (4.18)$$

Lee et al. [118] also used their data to test the validity of the globular-structure model proposed Ruckenstein et al. [120]. This model assumes that molecules diffuse through the macropores and then into the micropores, i.e., the molecules can enter the micropores only through the macropores. Thus, it differs considerably from the random-pore model. Very poor correlations were obtained by using this model to fit the diffusion data, suggesting that this model has little validity for hydroprocessing catalysts.

The difficulty in obtaining effective diffusivity data at typical hydroprocessing temperatures can be overcome by obtaining such data in conjunction with catalytic reactions. However, this can be a rather difficult task in the case of realistic feeds compared with model compounds studies. For this purpose, it is necessary to express the effect of temperature on bulk diffusivity (D_b). The Wilke and Chang [121] equation can be expressed as

$$D_b = \frac{B}{V_A^{0.6}} \quad (4.19)$$

where B is a function of temperature and viscosity of solvent, and thus, is a constant; and V_A is the molar volume of reactant at its normal boiling temperature. Substitution of Eq. (4.19) in combined Eqs. (4.2) and (4.5) yields

$$\frac{D_e V_A^{0.6}}{\epsilon} = \frac{B}{\tau} (1 - \lambda)^z \quad (4.20)$$

The logarithmic plot of $D_e V_A^{0.6} / \epsilon$ against $1 - \lambda$ for the catalysts in Table 9 and four solutes gave a z value of 6.9 when λ values of the fresh catalyst were considered [122]. This would indicate significantly larger restrictive effect than expected. However, when a correction was applied to λ values to account for a decrease in the pore mouth size due to coke, a reasonable z value of 4.9 ± 0.5 was obtained. It was indicated by Prasher et al. [123] that the tortuosity factor can also be affected by coke deposits.

Several studies indicate that the effective diffusivity depends upon the equilibrium partition coefficient defined as the ratio of the solute concentration within the porous material to that in the bulk solution [123–

126]. The former depends on the adsorption strength of solute and solvent. Thus, the effective diffusivity is smaller for a solute having a strong adsorption strength than for a non-adsorbing solute. Also, the effective diffusivity of a solute would be higher in the case of strong adsorption of solvent. Adsorption strength affects the radial distribution of solute within the pore. It was shown by Malone and Anderson [127] that if the solute strongly adsorbs on the pore walls, the restrictive effect would be more important because the solute close to the pore wall exhibits a greater drag force than that near the centerline. It is obvious that the adsorption decreases with increasing temperature, resulting in an increase of the effective diffusivity. Lee et al. [128] did not observe a significant temperature effect on the effective diffusivity under typical hydroprocessing conditions. They concluded that the adsorption became unimportant at these temperatures. The additional effect of solvent on the data obtained under reaction conditions would arise from the different solubility of H_2 in different hydrocarbons and different viscosity. Apparently, effective diffusivity and pore size of a catalyst will change with time on stream. This is supported by their values for fresh and spent catalysts shown in Table 11 [129]. The level of decrease of these parameters depends on several factors, e.g., time on stream, properties of feed and catalyst, operating conditions, etc.

4.1.3. Kinetics of coke formation

There is an abundance of information on models for describing the kinetics of coke formation [130,131]. Some of these models were used to study deactivation under conditions which differ markedly from hydroprocessing. Thus, they may not pay adequate attention to the restrictive diffusivity phenomena which are

Table 11
Effective diffusivity and pore diameter of fresh and spent catalysts [129]

		Effective diffusivity ($D_e \times 10^6$ (cm ² /s))	Pore diameter (Å)
NiMo-125	fresh	3.59	175
	spent	2.65	153
NiMo-325	fresh	2.02	62
	spent	1.31	52

occurring during hydroprocessing. Without fully recognizing this fact, such models may only indicate some trends relevant to intrinsic kinetics. The concept of restrictive diffusivity was discussed above in order to put some of the deactivation models in prospective. It is to be noted that there are several models treating the kinetics of coke formation in parallel with the formation of metal deposits. These models will be presented in the subsequent chapter.

Perhaps the most widely used kinetic model was that proposed by Voorhies [132] in 1945 to describe coking of cracking catalysts, i.e.,

$$C_0 = At^n \quad (4.21)$$

where C_0 is the amount of coke on the catalyst at time t . The correlation coefficients (A and n) are usually obtained experimentally for a particular system. This equation may be more applicable to cracking catalysts for which it was proposed. In this case, the size of the catalyst particles is significantly smaller and the contact time shorter than for hydroprocessing catalysts. Also, the coke build-up with time exhibits a different pattern compared with that observed for the latter. Further, in the case of cracking catalysts, the effect of coke on the loss of activity is more linear than in the case of hydroprocessing catalysts. Attempts were made to advance Voorhies' model and/or adapt it to hydroprocessing conditions [133–135]. These investigations were reviewed by Gualda and Toulhoat [7].

It is well established that in the case of hydroprocessing catalysts, at least two regions of coke lay down always exist [6,70]. As shown in Fig. 33 [6], the first region occurs during the initial stages of the operation

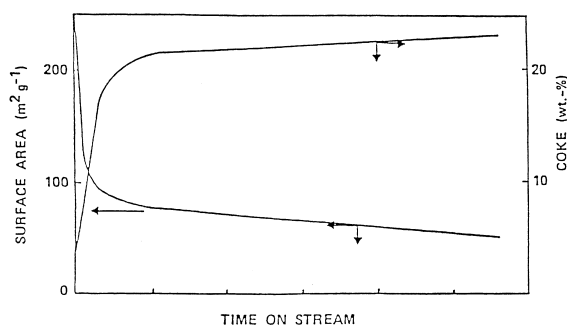


Fig. 33. Typical example of surface area change and coke formation as a function of time on-stream [6].

when coke is rapidly formed before reaching the second, the steady-state region in which the coke lay down is very slow. Near the end of the operation, when the catalyst has lost most of its activity, the coke build-up increases. The catalyst retains a substantial portion of its original activity in spite of the rapid coke deposition during the initial stages. In the steady-state region, the overall coke lay down and the activity loss will follow a different pattern than that during the initial stage. Thus, part of the coke deposited initially will have little effect on the catalyst activity in the steady state. These facts were taken into consideration in the pore-plugging model developed by Newson [136]. According to this author, the 'fast' coke formed initially takes up about one third of the porosity, whereas the 'slow' coke and metals take up the remainder of the porosity. The 'fast' coke is typically formed during the first 50 h on stream. At any time greater than 50 h, the weight fraction of coke on the catalyst, Q , is constant, i.e.,

$$Q = \frac{W_C}{W_f + W_C + W_{MS}} = \text{constant} \quad (4.22)$$

where W_f is weight of catalyst, W_C weight of coke and W_{MS} is weight of metal sulfides. The coke rate in the steady-state (R_C) is expressed in terms of the metal deposition rate, R_{MS} , as follows:

$$R_C = \left(\frac{Q}{1 - Q} \right) R_{MS} \quad (4.23)$$

whereas the coke plugging rate, R_{pl} , is given by

$$R_{pl} = \frac{1}{\rho} \left(\frac{Q}{1 - Q} \right) R_{MS} \quad (4.24)$$

where ρ is the density of the fast coke.

Masamune and Smith [137] have assumed three types of fouling occurring during a main reaction depicted as $A \rightarrow B$, where A and B represent reactant and product, respectively. The fouling results from a partial conversion of A and B as well as that of an impurity in the feed, S , to a solid deposit (presumably coke) on the catalyst, i.e.,

1. $B \rightarrow C$ series fouling,
2. $A \rightarrow C$ parallel fouling,
3. $S \rightarrow C$ independent fouling.

This approach may have some relevance to hydroprocessing if one assumes A to be a mixture of H_2 and

a light feed containing poisons such as nitrogen bases. The formation of coke C may proceed according to the mechanism in Fig. 24 proposed by Absi-Halabi et al. [6]. The first-order rate expressions of the fouling reactions are:

$$\text{Series fouling : } \frac{dq}{dt} = k_{Bf} C_B \left(1 - \frac{q}{q_0}\right) \quad (4.25)$$

$$\text{Parallel fouling : } \frac{dq}{dt} = k_{Af} C_A \left(1 - \frac{q}{q_0}\right) \quad (4.26)$$

$$\text{Independent fouling : } \frac{dq}{dt} = k_{Sf} C_S \left(1 - \frac{q}{q_0}\right) \quad (4.27)$$

where C_A , C_B and C_S are concentrations of A, B and S, k_{Bf} , k_{Af} and k_{Sf} rate constants for the series, parallel and independent fouling, respectively, and q and q_0 the amount of coke at time t and that corresponding to complete deactivation, respectively. A stepwise numerical technique was applied to solve these equations with the aim of obtaining the effectiveness factor. However, parameters such as critical diameter of reactant molecule, pore radius, porosity, etc. or their change with time and/or conditions were not considered. Nevertheless, the results of these calculations indicated several trends regarding deactivation, e.g., for series fouling, the deactivation is least for the catalyst with the lowest diffusion resistance for the main reactant; for parallel fouling, catalysts with some diffusion resistance are more stable for long process times; and for independent fouling, the deactivation is least when the diffusion resistance of the main reactant is a minimum and that of the contaminant is a maximum.

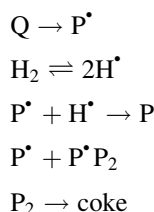
The kinetics of coke formation during hydroprocessing of a vacuum gas oil was investigated by de Jong [138,139]. In this case, a CoMo/Al₂O₃ catalyst was crushed and sieved to obtain a 30–80 mesh size. Both the thermal and catalytic sources of coke were considered. In this case, thermal coke results from condensation of aromatic radicals which can be suppressed by active hydrogen, whereas catalytic coke is produced via dehydrogenation reactions. For the rates of catalytic coke lay-down, the following Langmuir–Hinshelwood type kinetic equation was used:

$$R_c = \frac{k_c K_{ads} C_q}{1 + K_{ads} C_q} \quad (4.28)$$

where C_q is the concentration of coke precursor, Q , and K_{ads} its equilibrium adsorption constant, and k_c is the rate constant dependent on the amount of coke on the catalyst, viz

$$k_c = k_{c,0} \left(1 - \frac{D}{D_{c,max}}\right) \quad (4.29)$$

in which D is the amount of coke deposited. $D_{c,max}$ was estimated by extrapolation of the steady-state coke-time curve to zero time. This would imply that catalytic coke is deposited in the early stages. For the formation of thermal coke, de Jong [138,139] assumed the following mechanism:



In this scheme, the coke precursor generates radical P^* which is either terminated by H^* or converted to coke. The rate of thermal coke formation was expressed as:

$$R_t = k_t C_q^2 / P_{H_2} \quad (4.30)$$

Then, the total rate of coke deposition, R , is

$$R = R_c + R_t \quad (4.31)$$

As the coke in pores reduced the liquid holdup, this was accounted for by the following equations:

$$\epsilon_c = \frac{m_c}{k} \quad (4.32)$$

$$\epsilon_L = 0.15 + V_{P^*} \rho_B - \epsilon_c \quad (4.33)$$

where ϵ_c is the coke holdup, m_c the weight of coke, k the density of the coke, ϵ_L liquid holdup, V_P pore volume of catalyst and ρ_B bulk density of the catalyst. In this case, the coke holdup accounts for coke in the pores, whereas the liquid holdup accounts for volume of the liquid in the reactor. The model was successfully tested for predicting the effects of temperature and H₂/feed ratio on coke formation.

Both active site blocking and pore plugging by coke was considered in the model developed by Haynes and Leung [140,141]. The model was based on the assumption that the catalyst consists of compacted

microparticles, i.e., the porosity inherent within the particles was microporosity and voids due to the space between the compacted particles was macroporosity. The model was developed to simulate properties of two aged catalysts for which a significant loss of microporosity was observed while macroporosity was relatively unaffected during the deactivation period. The microparticle deactivation was assumed to be uniform and the microeffectiveness factor was assumed to be near unity due to the small diffusion paths involved. Thus, the macropores provided the access of the reactant molecules to the active sites within the micropores. These authors derived several mathematical equations. For example:

$$\lambda = \frac{\lambda_0}{(1 - \alpha\psi)^{1/2}} \quad (4.34)$$

where λ and λ_0 are the ratios of molecular radius to effective pore radius for the actual and coke free micropores, respectively, $\alpha = 2W_s/\rho_p r_0$ where W_s is the weight of coke for complete deactivation, ρ_p is the density of coke and r_0 is the effective pore radius; ψ is the reduced coke concentration, e.g., W/W_s . The following equation was used to calculate the rate of coking:

$$R_{\text{obs}} = \rho_x(1 - \epsilon_y)\eta C_{\text{AS}} \quad (4.35)$$

where ρ_x is the microparticle density, ϵ_y the particle porosity, η the effectiveness factor, k the rate constant and C_{AS} the surface reactant concentration. Several conclusions relevant for catalyst design resulted from this study. For example, an optimum macroporosity exists for maintaining acceptable activity and as the intrinsic activity increases, the optimum macroporosity shifts to higher values. Also, the catalyst life can be increased by increasing the micropore size, but this may be accompanied by loss of activity. With respect to initial activity, catalysts possessing a low intrinsic activity are not greatly affected by macroporosity over a wide range of ϵ_y values. For more active catalysts, macroporosity is essential for good initial activity.

Richardson et al. [91] developed a model to predict coke formation during the initial stages of hydroprocessing of heavy feeds. Based on the amount of coke and catalyst properties, a uniform distribution of coke in a monolayer like form was assumed. Thus, the maximum coke which can accumulate on the catalyst is equal to the monolayer coverage. The monolayer

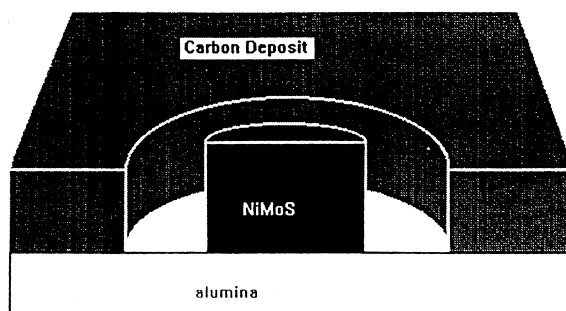


Fig. 34. Schematic representation of catalyst surface, showing a cross section through metal crystallites [91].

calculation assumed that most of the coke originates from the asphaltenes in the feed. In the proximity of the active metal crystallites, a cleared annular zone was assumed (Fig. 34). Inside the cleared zone, no coke is present. Similar assumptions were made by Diez et al. [105] and van Dorn and Moulijn [142]. The alumina surface will remain clear as long as the surface flux of hydrogen is greater than the critical value of the radius of the cleared zone. For the coke buildup, Richardson et al. [91] derived the following first order kinetic equation:

$$C = C_{\text{max}}(1 - e^{-kw}) \quad (4.36)$$

where C is the actual amount of carbon on the catalyst and C_{max} the maximum carbon deposition, i.e., a complete monolayer; w is the cumulative feed to catalyst ratio and k is an adsorption constant. The solid line in Fig. 35 represents the model prediction

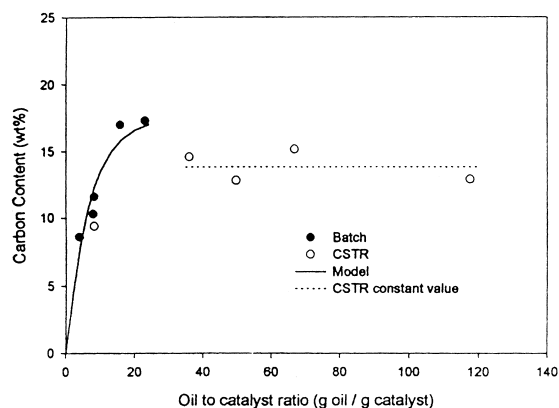


Fig. 35. Carbon content of catalyst as a function of cumulative feed/catalyst ratio ($\text{NiMoAl}_2\text{O}_3$, 703 K, 13.8 MPa) [91].

which agreed well with the experimental data. Another prediction of the model includes a similarity in the structure of the coke deposited on the catalyst during initial stages and asphaltenes in the feed. Thus, a large portion of the former could be extracted. Similar H/C and N/C ratios of the extractable portion of the deposits and that of the bitumen feed was also observed by Chu et al. [143]. However, the density and the average molecular weight of the extract was significantly greater than that of the bitumen. The model presented by Richardson et al. [91] suggests that most of the active sites will survive the initial rapid coke deposition. Yet, it is well known that a relatively large portion of the original catalyst activity is lost during the initial stages. These authors clarified this issue by taking into consideration the change in physical properties of the aged catalyst, i.e., surface area and pore size distribution. The former decreased from 317 to 157 m²/g, whereas pore volume decreased from 0.57 to 0.25 cm³/g. The pore size distribution and reduction in the effective diffusivity are shown in Fig. 36. The latter was estimated from the following equation:

$$\frac{D_{e,c}}{D_{e,f}} = \frac{\epsilon_c}{\epsilon_f} e^{-(\lambda_c - \lambda_f)} \quad (4.37)$$

where the subscripts c and f are for the coked and fresh catalysts, respectively. The predicted ratio of the diffusivity of the coked catalyst compared to the diffusivity of the fresh catalyst decreases rapidly below a pore radius of approximately 8 nm, reaching

0.06 at 2 nm. It is interesting that the peak in the pore size distribution of the aged catalyst in Fig. 36 occurs at about 2 nm as well. This suggests that the feed molecules may be excluded from pores with radius smaller than 2 nm.

4.1.4. Structure and distribution of coke

Advancements in analytical techniques such as temperature programmed oxidation (TPO) and reduction (TPR), X-ray photoelectron spectroscopy (XPS), high resolution electron microscopy (HREM), Fourier transform infra-red (FTIR), Laser Raman spectroscopy (LAS) and others can provide information on the distribution and physical structure (topology) of coke on the catalyst. Researchers could only speculate on these aspects of coke before some of these techniques became available.

One of the first studies on the nature of coke on catalysts was conducted by Haldeman and Botty [144] using an X-ray diffraction technique. It was concluded that coke was a finely divided, highly dispersed phase, present within the pore structure of the catalyst. Both pseudo-graphitic and amorphous structures were present. Using a similar technique, Appleby et al. [80] observed spherical particles of less than 100 Å diameter for coke formed from various model compounds. In both these studies, cracking catalysts were investigated. Nevertheless, because they represent the first attempts to characterize coke on catalysts, it is felt appropriate to mention these studies in this review.

The HREM technique revealed the presence of curved and buckled structures of coke with occasional concentric circles on a spent CoMo/Al₂O₃ catalyst [145]. The coke resembled heat treated carbon, although a little less developed [146]. Also, the part of the catalyst covered with coke had a homogeneous appearance. The coke, consisting of small irregular structures covering most of the surface but not in the proximity of active sites, was observed by van Dorn et al. [142,147]. These results are consistent with the work published by Fleisch et al. [148], who observed an increase in the Mo/Al ratio by XPS with increase in the coke level on the catalyst, confirming that coke is preferentially deposited on the bare support. Dorn et al. [142,147] proposed that at larger distances from the catalytic sites, the coke consists of a three dimensional network. Thus, the major part of the coke is

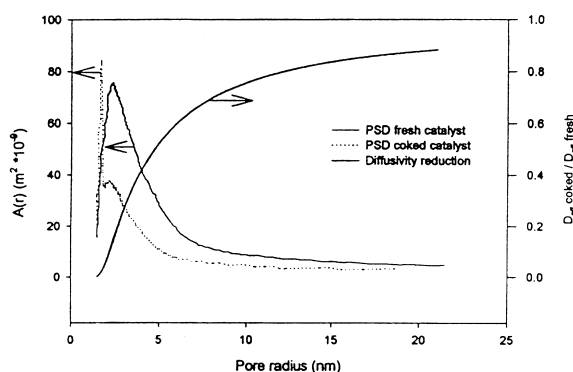


Fig. 36. Pore size distribution based on surface area and reduction of adsorptive diffusivity as a function of pore radius (conditions as in Fig. 35) [91].

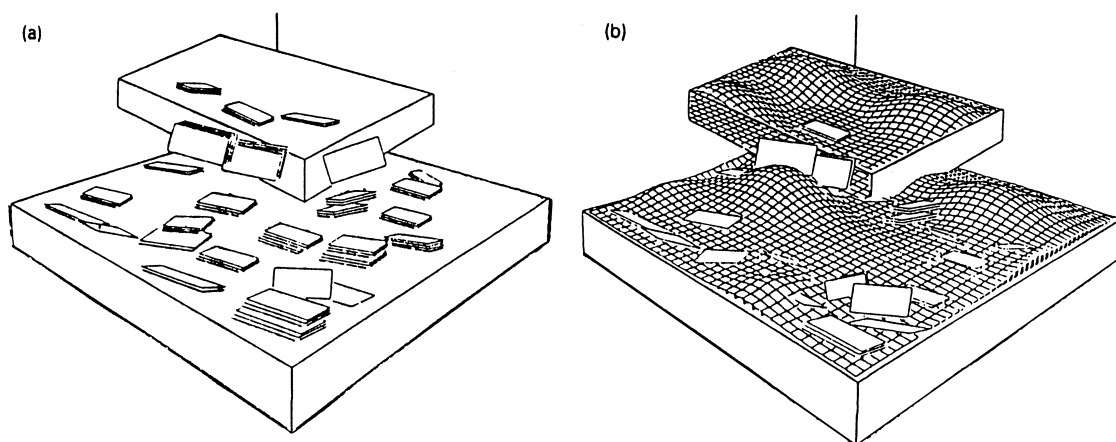


Fig. 37. Model of fresh (a) and deactivated (b) catalyst [147].

covering the support rather than the active phase, suggesting that there may not be any correlation between the amount of coke on the catalyst and catalytic activity. However, it was shown by Chu et al. [143] that a correlation may be obtained after the extractable portion of the deposit blocking the micropores, is removed. The coke, which was in proximity of active sites, could be catalytically hydrolyzed during TPR experiments [149]. The ease of removing the coke during hydrogen gasification was confirmed by Hughes et al. [150]. The model of a hydroprocessing catalyst under reaction conditions proposed by van Dorn et al. [147] is shown in Fig. 37. The model suggests that the support is almost entirely covered with coke, whereas the slabs of active phase are not covered. It is believed that coke on the support consists of several layers, i.e., three-dimensional network.

The slabs of active phase may participate in coke-removing reactions during hydrogen gasification.

It was indicated earlier that properties of the feed influence the structure of the coke on the catalyst. Massoth et al. [40,151,152] studied $\text{NiMo}/\text{Al}_2\text{O}_3$ catalyst having an average pore diameter of 182 Å, used for hydroprocessing of anthracene, a high aromatic gas oil and bitumen feeds. Little pore plugging occurred because of the large pore size of the catalyst. However, there was a difference in the surface area as the result of the different feeds. Thus, for anthracene and gas oil, a rather small decrease in surface area was observed, whereas for coke produced from bitumen, the surface area actually increased. The authors [151]

attributed these observations to the porosity of the coke contributing to the overall surface area. In the case of anthracene and high aromatic gas oil, a compact aromatic, graphitic type of coke is formed. On the other hand, aromatics (two or three rings) in the bitumen contain large aliphatic groups attached to them, which may prevent condensation into fused rings in the pores [153]. Then, the coke from bitumen is expected to possess a higher porosity than that from anthracene and gas oil. Pores of 200 Å and higher were observed in the deposit on the catalyst after the bitumen treatment [143]. A significant effect of the origin of the feed on the textural properties of coke was demonstrated by Aldag [154]. In this case, coke on the catalyst after hydroprocessing the residue derived from a Maya crude approached the structure of a thermal coke, whereas that after hydroprocessing the residue derived from a Honda crude showed the presence of a catalytic coke with filaments on the order of 100–200 nm in diameter.

The topology of the coke deposits on aged catalysts was investigated by de Jong et al. [86,138,139,155], using XPS. The catalysts ($\text{CoMo}/\text{Al}_2\text{O}_3$ and $\text{Mo}/\text{Al}_2\text{O}_3$) were crushed to 30–80 mesh and presulfided prior to the aging tests using a gas oil feed. For both catalysts, about 25% coke was deposited. Two types of coke were assumed, i.e., thermal and catalytic. The former tends to agglomerate, whereas the catalytic coke tends to spread on the catalyst surface. In the case of the $\text{CoMo}/\text{Al}_2\text{O}_3$ catalyst, almost 96% of the surface was covered by the coke. The calculated layer

Table 12
Carbon distribution (wt.%) [88]

Catalyst	A	B	C	D	E
242-PS	5	5	3	2	2
242-43	5	3	3	2	2
242-527	7	6	6	7	7

thickness corresponded to three to four layers of coke. On the $\text{Mo}/\text{Al}_2\text{O}_3$ catalyst, only about 50% of the surface was covered with the coke. Apparently, with this catalyst, the coke tends to agglomerate near the active phase. The use of small particle sizes ensured that no coke gradient was present.

Using LRS, Van Langeveld et al. [156] observed differences in the amount of carbon deposited in various positions in the cross section of a quadrolobe extrudate. The different carbon distribution was attributed to several factors, i.e., the variations in the local amount of active phase metal, the occurrence of local hot spots and the orientation of the particle in the reactor bed. Other studies were conducted to determine the radial distribution of the coke in the catalyst particle. For example, Stohl and Stephens [88] have determined the radial distribution of carbon during the hydroprocessing a coal-derived feed. The results of these analyses are shown in Table 12. Symbols A, B, C, D and E are the radial position in the extrudate, i.e., E is in the center of the extrudate and A on its surface; B is slightly below the surface, whereas C and D are at one third and two thirds of the radius, respectively. The catalyst identified as 242-PS was from the very early stages of the operation, whereas 242-43 and 242-527 were after processing of 43 lb of the feed/lb of catalyst and 527 lb of the feed/lb of catalyst, respectively. It is evident that during the early stages, carbon deposited predominantly on the external surface of the extrudate; however, in the course of the operation, carbon gradually penetrated into the interior of the extrudates.

The effect of mesoporosity on coke deposition profiles was investigated by Yoshimura et al. [157] using three monomodal $\text{NiMo}/\text{Al}_2\text{O}_3$ catalysts. The catalysts had similar chemical composition and shape (0.79 mm extrudate) but had different average mesopore diameters. Thus, the catalysts B and C in Fig. 38 had average mesopore diameters of 10.8 and 22.4 nm, respectively, whereas that of the catalyst A was

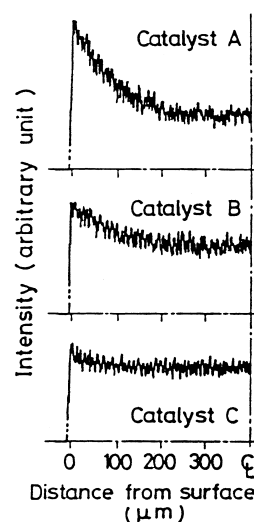


Fig. 38. Radial concentration profiles of carbon on spent catalysts by EPMA [157].

8.8 nm. It is evident that the mesopore diameter of at least 10.8 nm is required to ensure diffusion of large molecules into the catalyst interior; otherwise, large molecules will deposit near the outer surface. Moreover, these authors suggested that deposits on the catalyst exterior may hinder diffusion of the product molecules from the catalyst interior. In the case of fixed bed operation, the coke distribution profiles depend on the time on stream and the position in the reactor. These effects were investigated in detail by Tamm et al. [1]. Some interesting changes in the profiles are evident in Fig. 39. In the interior of the particles, the level of coke increases linearly with time. But at some point in the reactor, the coke level on the exterior of the particles passes through a maximum early on and then declines with time. The coke level is the lowest at the reactor inlet and the highest at the reactor exit at all times during the run.

Using an $\text{NiMo}/\text{Al}_2\text{O}_3$ catalyst and coronene in cyclohexane solution as the solute, Massoth and co-workers [40,114,151] observed that coronene adsorbs on both the alumina and active phase, whereas its adsorption on the coke is nil. Then, the lowering in adsorption with increasing coke is proportional to the loss in surface area due to coke. The results in Fig. 40 [40] show the effect of coke on relative uptake of

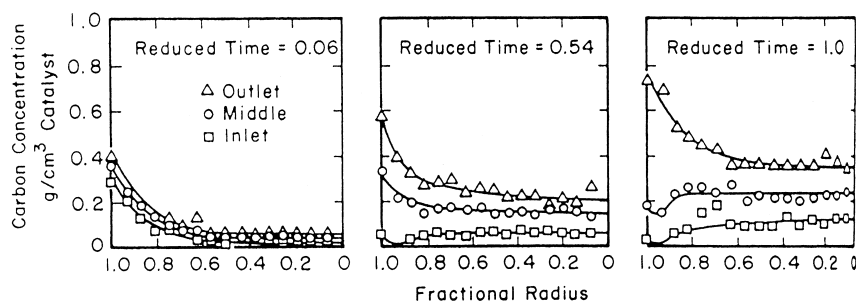


Fig. 39. Carbon distribution as function of reactor position and time [1].

coronene and relative diffusivity for the catalyst coked with anthracene and a vacuum gas oil. These results show that for the gas oil coke, the coronene adsorption drops at 2 wt.% coke but exhibits little change thereafter. This implies that the coke is concentrated near the mouth of the pores. On the other hand, catalyst diffusivity measurements show a continual decrease with the coke content. This suggests that the additional coke builds on the original coke, without further penetration into the pores, resulting in lowered diffusivity due to pore mouth constriction. The anthracene coked catalysts show a continuous decrease in coronene uptake with coke content and a sharper decline in diffusivities. These results show that for the same amount of coke, the shape of the coke deposits should be shallower than that from the gas oil coke. Thus, the gas oil coke seems to deposit on the original coke,

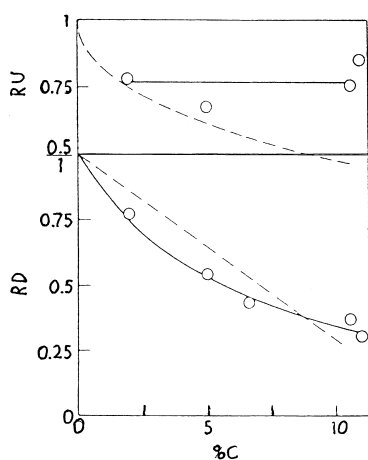


Fig. 40. Effect of carbon on relative coronene uptake (RU) and relative diffusivity (RD) [40].

whereas the anthracene coke penetrates further into the catalyst pores. Based on these observations, the two models shown in Fig. 41 [40] were proposed, i.e., one for the gas oil coke and the other for the anthracene coke. In any case, as shown in Fig. 42, pore diameter is a key parameter in determining the distribution of coke [158]. These effects become more evident with increasing size of reactant molecules and/or decreasing pore diameter.

Yang and Guin [159] developed a model which assumes that porosity, pore size and effective diffusivity are all a function of radial position in the catalyst particle. The diffusion parameters were determined by fitting a mathematical model to the experimentally observed solute uptake. One unimodal (A) and one bimodal (B) NiMo/Al₂O₃ catalyst in four different particle sizes were examined. For this purpose, a solution of quinoline in cyclohexane was used. The results in Fig. 43 show that coke is the main contributor to loss of porosity. Both a uniform and non-uniform coke distribution was considered. For the local degree of restrictive diffusion due to pore plugging by coke, Yang and Guin [159] derived dimensionless functions for the nonuniform porosity model

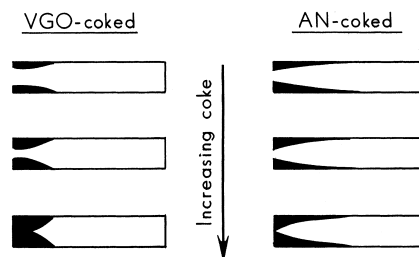


Fig. 41. Idealized model of coke pores [40].

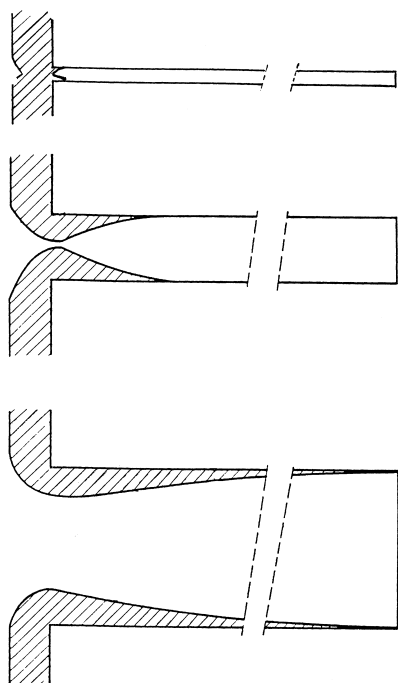


Fig. 42. Effect of pore mouth diameter on catalyst deactivation [158].

via the following equations:

$$g_1 = \frac{K_p \epsilon}{K_{p0} \epsilon_0} \quad g_2 = \frac{K_p K_r \epsilon}{K_{p0} K_{r0} \epsilon_0} \quad (4.38)$$

For the fresh catalysts, $g_1 = g_2 = 1$. For spent uniform particles, g_1 and g_2 are constant but less than 1.

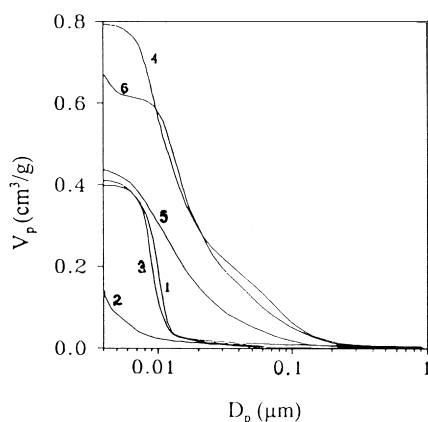


Fig. 43. Cumulative pore size distribution by mercury porosimetry: (1) fresh A; (2) spent A; (3) regenerated A; (4) fresh B; (5) spent B; (6) regenerated B [159].

For nonuniform catalyst particles, g_1 and g_2 are functions of radial position inside the particle. In these equations, ϵ and ϵ_0 are porosities for spent and fresh catalysts, respectively, and $K_p(K_{p0})$ and $K_r(K_{r0})$ are partition and restrictive factors for spent and fresh particles, respectively. In the case of nonuniform particles, the local pore diffusivity at any radial position in the particle is given by

$$D_e = \frac{g_2 \tau_0}{\tau} D_\infty \quad (4.39)$$

Thus, the local diffusivity D_e can be significantly reduced from the fresh catalyst value D_4 by the local value of g_2 , which reflects the hinderance effects due to the local reduction in pore diameter caused by coke deposit. The numerical solution of the diffusion model for both uniform and nonuniform distribution gave the parameters shown in Table 13 [159]. In the former case, extremely low values of diffusivities, or correspondingly high values of tortuosities were obtained for spent catalysts. For the crushed spent catalyst, higher diffusivities and more reasonable tortuosities were obtained. This indicates a nonuniform distribution of coke. Indeed, better values of the parameters were obtained when a nonuniform model was applied.

4.2. Effect of coke on catalyst activity

Rapid coke formation during the initial stages of hydroprocessing is an established fact. For some feeds, the initial coke build-up has little effect on catalyst activity [65]. As it was shown earlier, coke is formed even during hydroprocessing of light feeds such as naphtha. In this case, the size of the coke molecules increases because of a gradual polymerization until they begin to cover active sites. Then, the average molecular weight of the coke as well as its molecular diameter will be significantly greater than that of the largest molecules in the light feed. For heavy feeds, physical deposition of the large asphaltenic molecules will speed up the rate of coke formation. This is supported by the results published by Stohl and Stephens [160] who showed that boiling point cut of the feed has a significant effect on the activity. Thus, processing a -290°C feed using an extrudate $\text{NiMo}/\text{Al}_2\text{O}_3$ catalyst caused a 23% loss of hydrogenation activity compared to the fresh catalyst but had no effect on HDS activity. At the same time,

Table 13
Diffusional parameters for uniform and nonuniform particles [159]

Catalyat	ϵ	λ	K_p	K_r	τ	$D_c \times 10^6$ (cm ² /s)
<i>Uniform model</i>						
Catalyst A						
Fresh		0.055	0.89	0.88	2.1	100
Spent (extrudate)		0.094	0.82	0.80	1080	0.07
Spent (crushed)		0.094	0.82	0.80	10.5	7.1
Regenerated		0.054	0.90	0.89	11.5	17.1
Catalyst B						
Fresh		0.050	0.90	0.90	1.1	100
Spent (extrudated)		0.084	0.84	0.83	116	0.44
Spent (crushed)		0.084	0.84	0.83	4.3	12.0
Regenerated		0.045	0.81	0.91	3.1	34.9
<i>Nonuniform model^a</i>						
Catalyst A	0.009	0.47	0.28	0.21	4.1	0.0015
Catalyst B	0.029	0.26	0.55	0.49	3.7	0.024

^a Spent extrudates.

processing -454°C feed resulted in the 82 and 70% loss of hydrogenation and HDS activity, respectively. For feeds of a similar boiling point cut, the rate of coke formation will be greater for the more aromatic feeds. It is noted that the effect of coke on the catalyst activity can be elucidated only for feeds containing no metals. Otherwise, the effects of both coke and metals on activity are compounded. However, some information suggests that the deactivating effect of metals becomes evident only after a certain metal loading on the catalyst is attained [161]. Nevertheless, in this part of the review, studies will be included which deal mainly with the effect of coke on the activity while paying little attention to metals.

Massoth and coworkers [152,162] used a Co/NiMo/ Al_2O_3 catalyst to study deactivation by coke. The catalyst was crushed and sieved to 20–40 mesh and subsequently coked in a high pressure autoclave to varying levels of coke. For this purpose, a coal-derived middle distillate was used. The effect of carbon content on the fraction of pore coverage determined by coronene adsorption is shown in Fig. 44 [162]. The activities of these catalysts were determined using model compounds- dibenzothiophene for HDS, dibenzofuran for HDO and indole for CNH. The effect of carbon content on the relative activities (RA) is shown in Fig. 45. The extrapolation of the results in Fig. 44 and 2 indicates a complete deactivation at about 20%

carbon on the catalyst. A simple model of coke deactivation was developed to relate catalyst activity to carbon content. In this model, the rate constant of the deactivated catalyst (k) was given as

$$k = k_0(1 - \Theta_c) \quad (4.40)$$

where k_0 is the rate constant for the fresh catalyst and Θ_c is the fraction of active sites covered by coke. Thus,

$$\Theta_c = 1 - \frac{k}{k_0} = 1 - \text{RA} \quad (4.41)$$

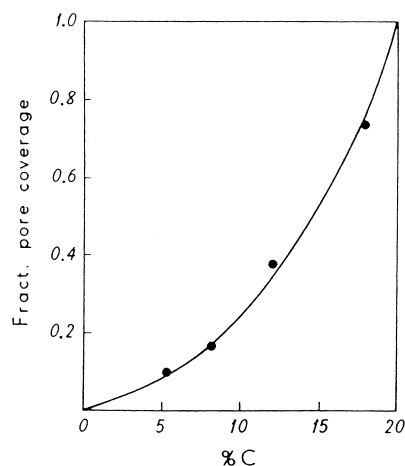


Fig. 44. Fraction pore coverage vs. carbon [162].

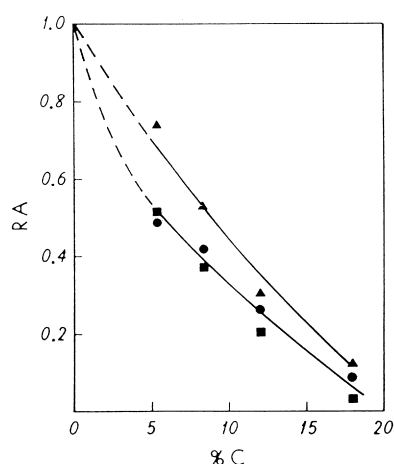


Fig. 45. Relative catalyst activity vs. carbon content; ● – HDS, ■ – HDO, ▲ – CNH [162].

The fraction of poisoned sites can also be given by

$$\Theta_c = \frac{N_p}{N_c} \quad (4.42)$$

where N_p is the number of coke covered sites and N_s is the total number of active sites. The average number of carbon atoms on a poisoned site at a given carbon content is given as

$$\gamma_C = \frac{N_{c,a}}{N_p} \quad (4.43)$$

where $N_{c,a}$ is the total number of carbon atoms on the poisoned sites. The ratio of carbon deposited on the inactive support as well as on the active sites is defined as

$$a = \frac{N_{c,i}}{N_{c,a}} \quad (4.44)$$

Combining Eq. (4.42) to Eq. (4.44) gives

$$\Theta_c = \frac{N_c}{N_s(1+a)\gamma_C} \quad (4.45)$$

where N_c is the total number of carbon atoms. Equation Eq. (4.45) can be rewritten in terms of carbon content,

$$\Theta_c = \frac{12C}{n_s(1+a)\gamma_C} \quad (4.46)$$

where C is the amount of carbon per gram of catalyst

(g C/g cat) and n_s is the number of active sites/g cat in mols. Finally, variation of γ_C with carbon content takes the form

$$\gamma_C = \alpha C_m \quad (4.47)$$

where α is a proportionality constant and m is a constant. Then Eq. (4.46) becomes

$$\Theta_c = \beta C^n \quad (4.48)$$

where $\beta = 1/12n_s(1+a)\alpha$ and $n = 1 - m$. Combination of Eqs. (4.41) and (4.48) yields

$$1 - RA = \beta C^n \quad (4.49)$$

$$\ln(1 - RA) = \ln \beta + n \ln C \quad (4.50)$$

The data fit based on Eq. (4.50) is shown in Fig. 46 [162]. From this correlation, the parameters n , m and β can be estimated. The relationship between the catalytically poisoned sites and the coke covered sites (fraction pore coverage) is shown in Fig. 47. It is evident that catalytic sites are deactivated to a much greater extent compared to coked sites.

The conventional methodology proposed by Froment [163] has been widely used by other researchers for the development of models predicting deactivation by coke. In general terms, the mechanism includes the following steps:

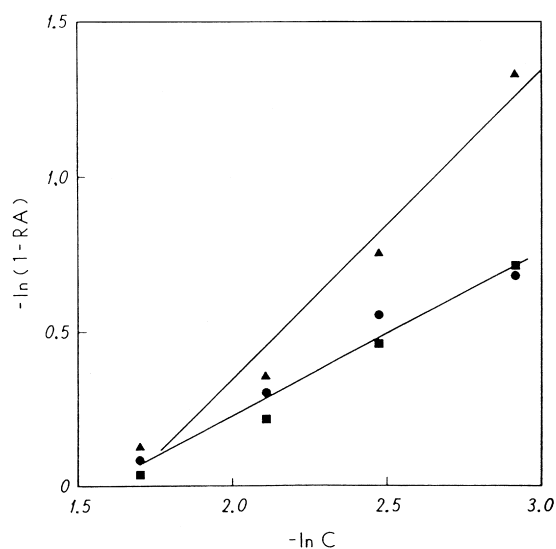


Fig. 46. Activity correlation according to Eq. (4.50); ● – HDS, ■ – HDO, ▲ – CNH [162].

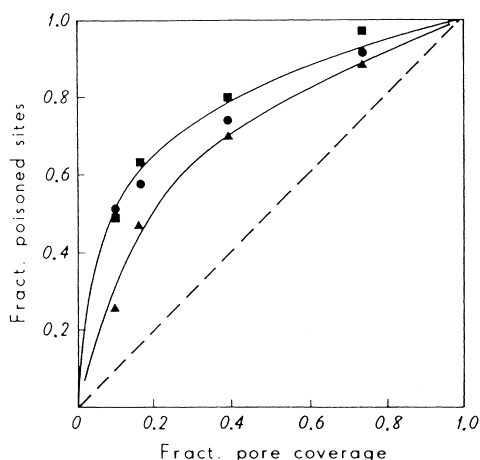


Fig. 47. Fraction poisoned active sites vs. fraction pore coverage; ● – HDS, ■ – HDO, ▲ – CNH [162].

- Step 1 $A + S = AS$
 Step 2 $AS = RS$
 Step 3 $RS = R + S$
 Step 4 $A + S = A * S$
 Step 5 $A * S = \text{Coke}$

In this set of reactions, the reactant A adsorbs at active site S to form AS, which is subsequently converted to a product still adsorbed at the same site, i.e., RS. The product R then desorbs and the active site S is recovered. In parallel with these reactions, the reactant forms a coke precursor A*S, which is converted to coke. This approach was used by Kittrell et al. [164–166] to derive the following equation:

$$\ln a = - \frac{k_d K_A^* C_A}{1 + K_A K_C + K_A^* C_A + K_R C_R} t \quad (4.51)$$

where a is the catalyst activity at time t ; K_A , K_A^* , K_C and K_R are equilibrium adsorption constants of the reactant, coke precursor and product, respectively, C_A and C_R are concentrations of reactant and product, respectively, and k_d is the deactivation constant. These authors assumed that the deactivation reactions were significantly slower than the hydroprocessing reactions. In the case of hydroprocessing, a similar situation may be approached after the steady-state level of coke is attained. Thus, the model may be applicable to a catalyst which was precoked to a steady-state level. Because a uniform coke lay down was assumed and

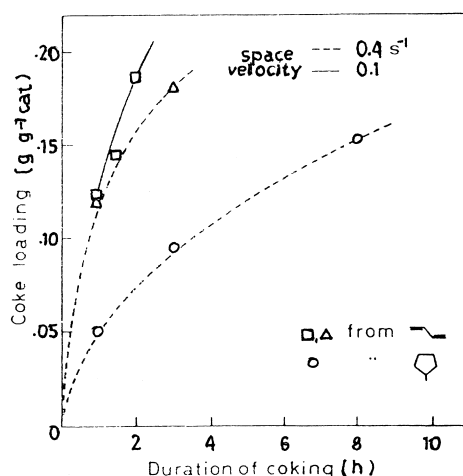


Fig. 48. Kinetics of coke deposition; ○ – methylcyclopentane, □△ – 1,3-butadiene [167].

physical properties such as pore size distribution were not considered, in the case of hydroprocessing catalysts, this model can be applied only to the intrinsic rate of coke deactivation.

Arteaga et al. [167,168] coked a CoMo/Al₂O₃ catalyst with gas mixtures containing Ar and either 1,3-butadiene or methylcyclopentane at 450°C. As shown in Fig. 48 [167], the rate of coke formation was higher from butadiene than from methylcyclopentane. Fig. 49 [168] shows that the HDS and HYD activities, defined as the conversion of thiophene and cyclohexene respectively, decreased with coke loading and reached almost zero above 16% of coke.

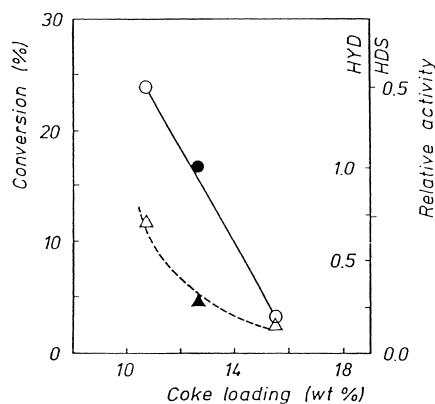


Fig. 49. Effect of coke loading on HDS and hydrogenation (HYD) activity; (○●) – HDS, (△▲) – HYD [168].

The effect of the chemical composition of the feed on catalyst deactivation was studied in detail by Stohl and Stephens [169]. Using adsorption column chromatography, these authors isolated four different groups of hydrocarbons from the feed (V-178), viz, aliphatic hydrocarbons, neutral polycyclic aromatic compounds (PAC), nitrogen polycyclic aromatic compounds (N-PAC) and hydroxy polycyclic aromatic hydrocarbons (HPAH). Subsequently, these fractions were hydroprocessed in the presence of a NiMo/Al₂O₃ catalyst, both in powder form and extrudate form. The activities of the fresh and aged catalysts were determined using the hydrogenation of perylene. The measured intrinsic activity losses of the powder catalysts (α) and the measured remaining activities of the extrudate catalysts (F) are correlated in Fig. 50. A quantitative mathematical expression related these parameters with the effective diffusivity [170]. Since the intrinsic activity loss increased more rapidly than the remaining extrudate activity, the dominant mode of deactivation was homogeneous poisoning of active sites. The aliphatic hydrocarbons and PAC fraction caused less deactivation than the feed, while the N-PAC and HPAH fractions caused more deactivation. This trend in deactivation was inversely correlated with the carbon content of the aged catalysts, i.e., deactivation was highest for the HPAH and lowest for aliphatic hydrocarbons.

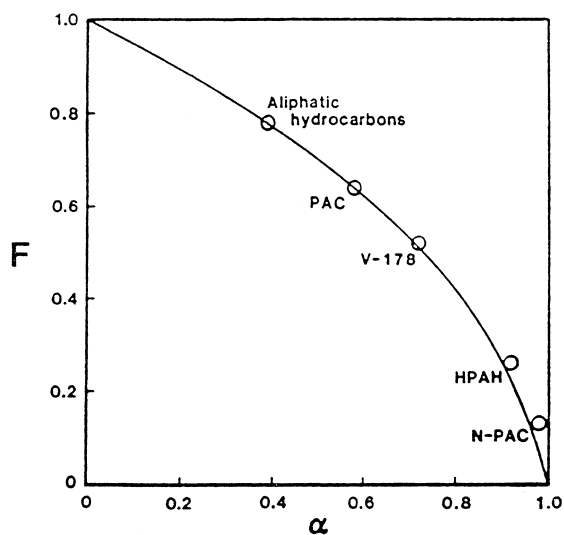


Fig. 50. Effect of feed composition of intrinsic activity losses (α) and remaining activities (F) [169].

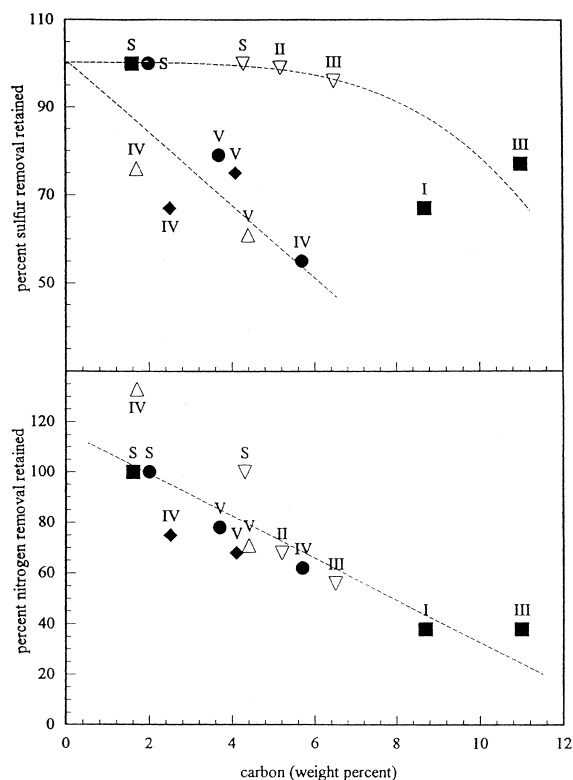


Fig. 51. Effect of total carbon deposited on HDS (top) and HDN (bottom) (623 K, 5.5 MPa) [110].

Weissman and Edwards [110] used two light gas oils and two naphthas to study deactivation of several NiMo/Al₂O₃ and CoMo/Al₂O₃ catalysts. The results of this study are summarized in Fig. 51. The symbols represent different catalysts, whereas the symbol labels refer to different feeds, i.e., S and I to III are from naphtha tests and IV and V are from gas oil tests. It is evident that HDN follows similar trends with respect to coke content for all feeds and catalysts, whereas HDS of gas oils differs from that of naphthas. In the latter case, it takes almost 6% of carbon before any activity loss is observed. An interesting correlation was obtained between the non-protonated aromatic carbon (determined by ¹³C NMR) and the pore volume and the pore diameter. The authors proposed that the origin of these differences is in the type of carbon originated from the gas oils and from the naphthas, the former being more compact while the latter being less dense. Little effect of the initial coke

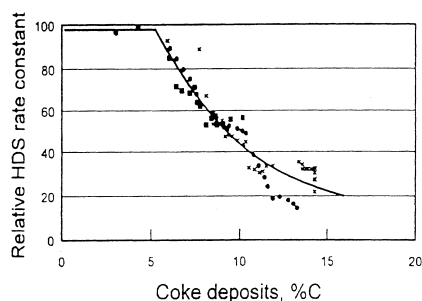


Fig. 52. Effect of coke deposits on relative HDS activity [68].

deposition on HDS activity was observed by Zeuthen et al. [68]. These authors used a solution of pyrene and methylated pyrenes for coking an NiMo/Al₂O₃ catalyst to different levels of coke under typical hydroprocessing conditions. The addition of benzothiophene to feeds had little effect on the rate of coke formation. Therefore, the HDS of benzothiophene in the pyrene solution was an ideal feed to study the effect of coke formation on HDS. As the results in Fig. 52 show, no loss of HDS activity was observed before about 4 wt.% of coke was deposited. Subsequently, the HDS rate declined exponentially.

Diez et al. [105] prepared hydroprocessing catalysts with varying amounts of coke in the absence of metal deposits by using a highly aromatic cycle oil (190–380°C). A second feed, containing 50% deashed coal and 50% of naphtha, containing primarily alkyl-substituted naphthalenes, was used to prepare a coked catalyst with a higher carbon content. Metal contaminants in the deashed residue were low, less than 1 ppm for V, Ni and Ti and about 200 ppm Fe. The results showed a negligible difference in the amount of coke formed between 20 and 70 h with the cycle oil. The catalyst used with the coal residue for 70 h at 415°C contained 10.6% C. There was a slight decrease in surface area from 146 to 130 m²/g after the operation using the cycle oil, whereas that for the coal residue decreased to 113 m²/g. The HDS, HDN and HYD activity of the used catalysts was determined using model compounds. Deposition of 3% coke resulted in about 20% decrease of all functionalities. However, deposition of 10.6% coke resulted in a loss of 75% of HDS and HYD activity. At the same time, the HDN activity decreased to about 5% of the fresh catalyst. Although the heavily coked catalyst still had activity for quinoline hydrogenation, it had little activity to

cleave the C–N bond. Diez et al. [105] assumed edge blocking of the Ni promoted MoS₂ crystallites by coke as a possible cause of deactivation. Because the MoS₂ crystallites are about 0.615 nm thick [171,172], coke deposits with a thickness less than 0.5 nm should be ineffective in blocking catalyst sites. However, as the coke thickness increases beyond about 0.7 nm, the catalyst activity may decrease rapidly [173].

Volume blends of 70/30 of solvent refined coal (SRC) and hydrogenated creosote oil were used by Curtis et al. [174] to investigate deactivation of NiMo/Al₂O₃ extrudate (1/32 in.) catalysts. The SRC was obtained by critical solvent deashing of coal. This ensured very low ash content in the investigated mixtures. Four deactivation cycles were performed with each cycle followed by a separate hydrogenation experiment on a catalyst aliquot using naphthalene in hexadecane to determine catalyst deactivation. The spent catalysts A and B are from hydroprocessing of the 70/30 and 50/50 blends, respectively. Parallel experiments were performed with the solvent and the catalyst with no SRC present. In this case, essentially no catalyst deactivation occurred as measured by naphthalene conversion. However, the aged catalyst exhibited significantly different product distribution, showing an increase in the tetraline yield, relative to that of decaline. It was found that deactivation increased with the SRC loading, as did loss of surface area. An increase in the hydroprocessing temperature from 430 to 500°C increased deactivation, as indicated by the decreased conversion of naphthalene hydrogenation in Table 14 [174]. In this case, the blends contained the same amount of SRC. A similar observation was made by Hertan et al. [175]. These authors used hydrogenation of naphthalene to tetraline and HDO of benzofuran for the activity determinations.

Table 14
Effect of temperature on naphthalene conversion [174]

Temperature (°C)	Naphthalene conversion (%)
SRC/Solvent 70/30	
430	84
460	51
500	17
SRC/Solvent 50/50	
430	84
460	40
500	10

The loss of hydrogenation activity was more pronounced than that of HDO activity.

Two types of coke on the catalyst, each having a different deactivating effect, were reported by Chu et al. [143]. Different amounts of coke were deposited by reacting solutions of either bitumen in *n*-heptane or maltenes in *n*-heptane for different periods of time. Subsequently, the aged catalysts were purged with a heptane/H₂ gaseous mixture prior to (in situ) activity tests. In this case, naphthalene hydrogenation and indole HDN were used as model reactions. Subsequently, a portion of the aged catalyst was Soxhlet extracted with heptane followed by chloroform and resulfided prior to a second (ex situ) activity test. Thus, the main difference between the aged catalyst used during the in situ and ex situ testing was that the former contained the total coke, while the latter contained only that coke which was left after extraction. The relative in situ activities of hydrogenation (HYD) and hydrogenolysis of the first C–N bond (CNH) in indole versus ex situ activities are shown in Fig. 53

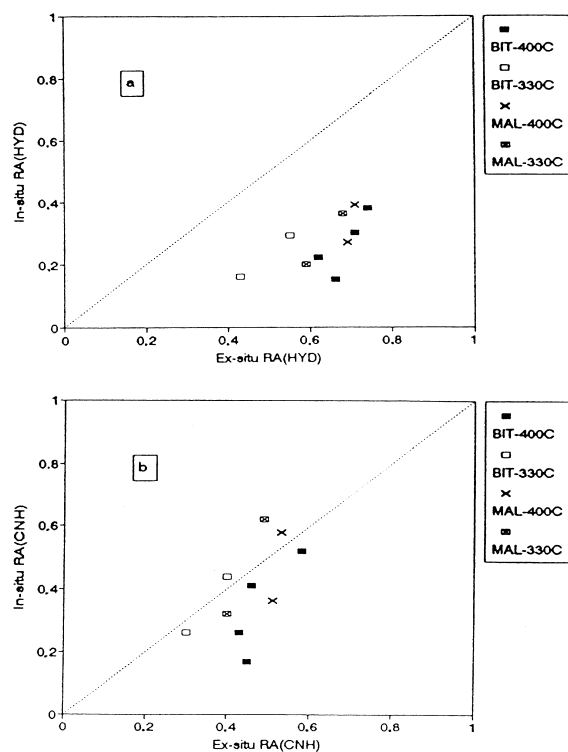


Fig. 53. In situ vs. ex situ relative activities (RA) for (a) HYD and (b) CNH (NiMo/Al₂O₃) [143].

[143]. The in situ relative HYD activity is much lower than ex situ, whereas for HDN both activities are similar. This suggests that part of the deposit which was extracted by chloroform affected HYD activity, but had little effect on the CNH activity.

An NiMo/Al₂O₃ HDM catalyst, having an average pore diameter of 180 Å was artificially coked to various levels of coke using bitumen or anthracene [151]. Another series of aged catalysts was prepared by adding carbazole (AN-CB coked) to the anthracene feed and Ni porphyrin to the bitumen (BIT-Ni coked). Relatively small changes in the surface area, pore volume and pore radius were observed, which were attributed to the large average pore diameter of the fresh catalyst. The activities of the catalysts were determined using conversion of naphthalene to tetraline as a measure of hydrogenation activity (HYD), and conversion of indole for CNH activity. The effect of coke on the relative activities is shown in Fig. 54. Since the analysis showed little plugging of pores by coke, deactivation must be due to covering active sites by coke. Initial deactivation was linear up to about 4% of carbon. Relative activities then dropped slower with increasing carbon. It was proposed that at this stage coke grows more upon itself rather than by deposition on new sites. At high coke levels, HDN activities tended to line out, indicating that some active sites still remain at this stage. These residual sites may have a high HYD activity, thus preventing formation of coke in their proximity. It appears that HYD activity is much less affected than CNH and HDN activities, suggesting that HYD sites are less susceptible to coke formation. The relative activities do not appear to be affected by the nature of the coke precursor. The effect of temperature on deactivation was also measured and the change of activation energies with increasing coke is shown in Fig. 55 [151]. The coked catalysts have lower activation energies than that of the sulfided catalyst. The decrease in HYD and CNH activation energies with coke content suggests that the coke deposits first on high activation energy sites having low HYD activity (high coke propensity sites), while leaving low activation energy sites having high activity (low coke propensity sites).

The concept of activation energy was further expanded by Massoth [176] who has developed a variable site model based on a normal (Gaussian) variable activation energy function. The normal dis-

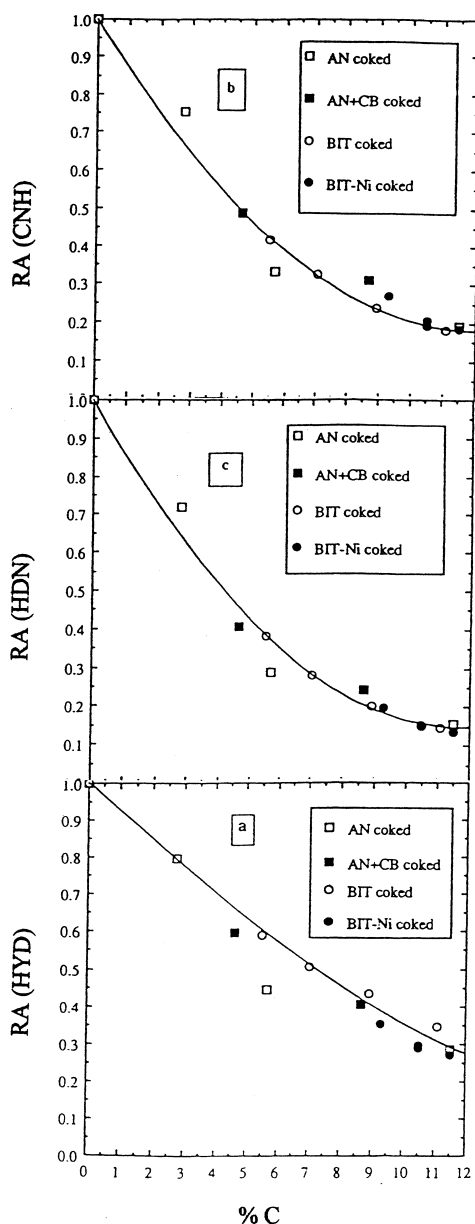


Fig. 54. Effect of coke on relative activities (RA) of (a) HYD, (b) HDN and (c) CNH [151].

tribution of active sites, $n(E)$, of activation energy, E , is given by

$$n(E) = \frac{1}{\sigma\sqrt{2\pi}} \exp\left\{-\frac{(E-E_0)^2}{2\sigma^2}\right\}$$

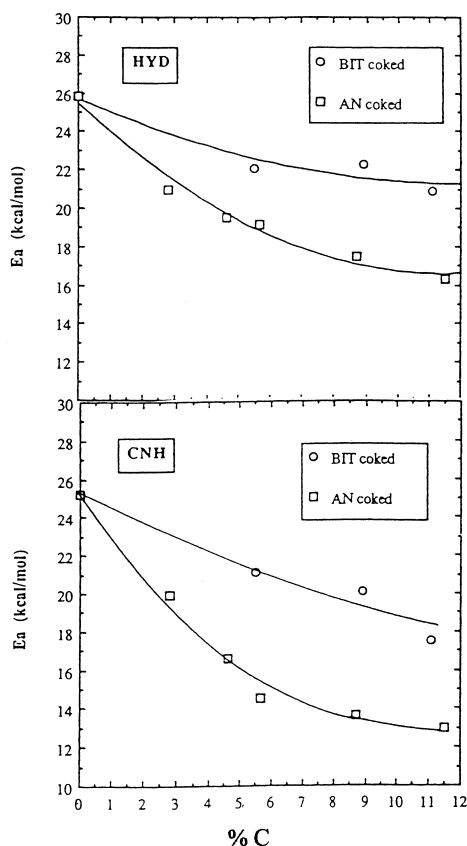


Fig. 55. Apparent activation energies vs. carbon for HYD (top) and CNH (bottom) [151].

where E_0 and σ are the mean activation energy of all sites and distribution parameter, respectively. A series of mathematical integrals was used to define parameters such as total number of active sites, n , mean activation energy, E_m , and finally global rate constants. Two cases were considered for deactivation by coke, i.e., site selective deactivation (SSD) and site preference deactivation (SPD). In the former case, the coking precursor is exclusively adsorbed on the sites of the highest activation energy, whereas for the SPD case, the precursor adsorbs preferentially but not exclusively on the high energy sites. The global rate constants for the two cases were given as

$$k' = \int_{E_L}^{E'} k'(E) dE, \quad k' = \int_{E_L}^{E_H} k'(E) dE$$

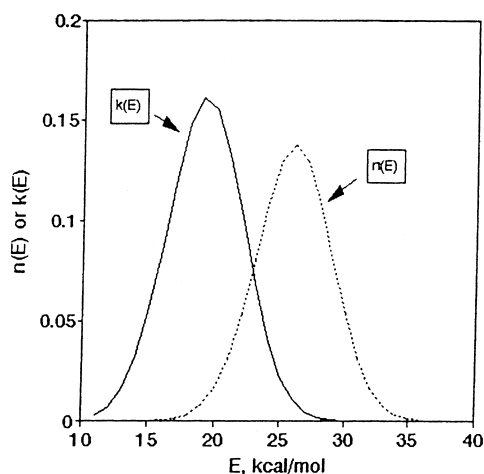


Fig. 56. Distribution of sites and rate constants as a function of site activation energy [176].

for the SSD case and SPD case, respectively. The set of data on activation energies and relative activities determined experimentally was used to obtain distribution parameter σ . The best fit of data was obtained for $\sigma = 2.9$ for the anthracene coked catalyst. The important finding of this study is the relationship between $k(E)$ and $n(E)$ versus E shown in Fig. 56 [176]. It is evident that the lowest E sites, i.e., 18 to 22 kcal/mol contain the highest activities, despite relatively few sites in this region. On the other hand, values above 25 kcal/mol represent a small fraction of the activity despite having the majority of the sites. Relative activities for the bitumen coked catalyst were shifted to higher activation energies suggesting that the SPD mode describes better the deactivation by bitumen.

Besides blocking active sites, coke deposition has an adverse effect on the catalyst porosity. Thus, the mode of catalyst deactivation depends on pore diameter. As shown in Fig. 57 [177], for small pore diameters, catalytic activity will be lost as result of pore mouth plugging, whereas for large pore diameters, because of the core deactivation. The combined effect of the feed properties and pore size on the activity is shown in Fig. 58 [178]. As expected, for the light feed, activity will decline with increasing pore size, whereas an optimal pore size exists for which the activity loss is minimal. Fig. 59 shows the pore size distribution data from the study published by Chu

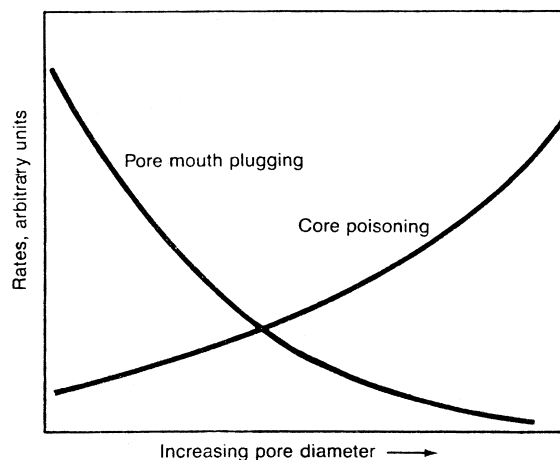


Fig. 57. Effect of pore diameter on deactivation mode [177].

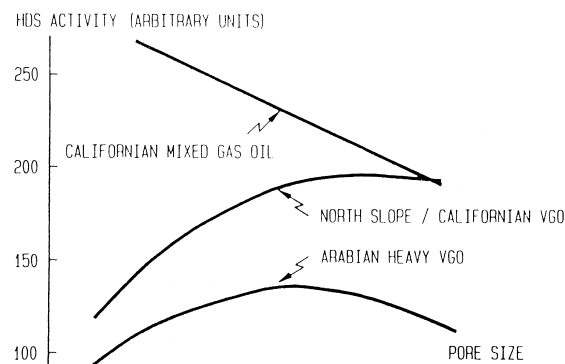


Fig. 58. Effect of pore size and feed properties on deactivation [178].

et al. [143]. A significant loss of porosity for catalyst from the in situ testing (cat. A) compared with that for the ex situ testing (cat. C) is quite evident. For the latter, activities could be related to the coke content, indicating loss of active sites by coke. A reasonable relationship between the in situ relative activities and the fraction of unblocked surface area is shown in Fig. 60. The dashed line represents the activity for HYD and CNH if all free surface contained the same intrinsic activity as the sulfided catalyst. Deviations between the dashed line and the experimental curves represent additional loss of the remaining active sites. A direct correlation between the relative catalytic activity and the unblocked surface area was obtained.

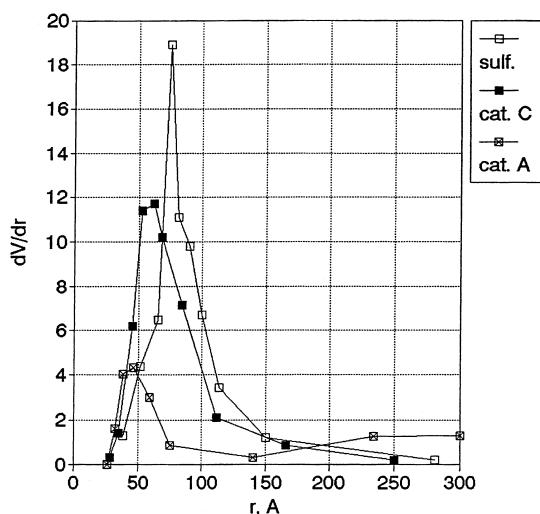


Fig. 59. Plots of pore size distribution for sulfided catalyst, catalyst A and catalyst B (NiMo/Al₂O₃) [143].

Hydroprocessing of an atmospheric residue from coal liquefaction in a mixture with creosote oil was investigated by Yoshimura et al. [157]. The mixture was deashed to less than 0.01% ash to eliminate the interference with metals. Three NiMo/Al₂O₃ catalysts, having similar chemical compositions but different surface characteristics, were used. The effect of the average pore diameter on HDS, HDN and hydrocrack-

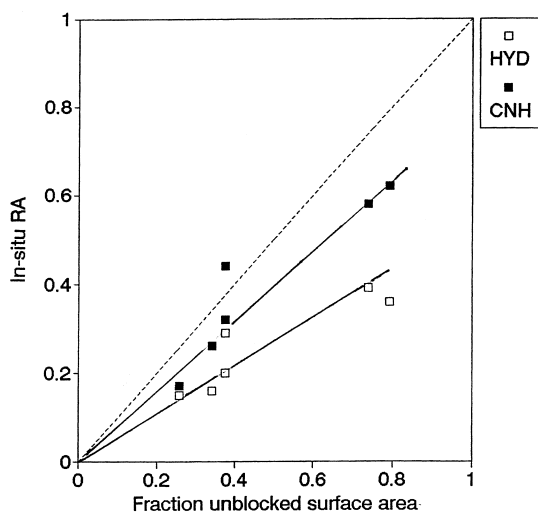


Fig. 60. In situ relative activities (RA) vs. fraction of unblocked surface area for HYD and CNH [143].

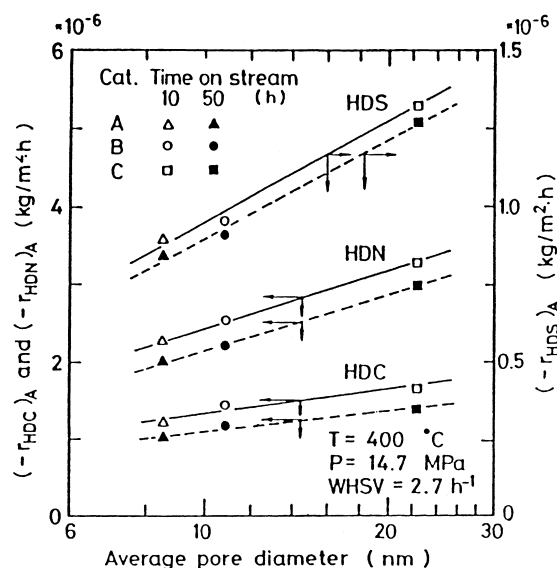


Fig. 61. Effect of average pore diameter on the rates of HDS, HDN and HDC (coal liquid, NiMo/Al₂O₃) [157].

ing (HDC) is shown in Fig. 61. Catalyst A had the smallest pore diameter and the lowest activity. The analysis of spent catalysts after the toluene extraction showed only a small difference in the loss of surface area. As expected, the smallest loss of pore volume was observed for catalyst C, which had the largest pores. As was shown in Fig. 38 [157], the distribution of carbon per unit of catalyst surface, determined by particle micro analysis (EPMA), indicates preferential accumulation on the catalyst external surface with decreasing average pore diameter. In another study, Yoshimura et al. [179] enriched a mixture of coal-derived atmospheric residue and creosote oil with toluene insolubles from de-ashing of coal, i.e., the content of the toluene insolubles was increased from 0.42 to 3.32%, whereas that of ash from 0.01 to 0.04. As the results in Table 15 show, all functionalities were adversely affected by the toluene insolubles. Also, the radial profile of carbon showed accumulation near the catalyst outer surface, causing a significant decrease in pore size and pore volume. Pore size distributions of the spent catalysts after 50 h on stream (Fig. 62) was influenced by the addition of toluene insolubles as well. The results from these studies confirm that coke deposition is a major contributor to catalyst deactivation during hydroprocessing of

Table 15
Conversions of whole feed and +623 K fraction [179]

Reaction	Feed		Feed + TI ^a	
	10 h	50 h	10 h	50 h
<i>Whole feed</i>				
HDS	87.3	86.7	80.6	80.0
HDN	70.7	61.3	51.3	43.6
<i>+623 K fraction</i>				
HDHI ^b	96.2	93.8	84.2	80.7
HDC	42.8	34.7	22.1	15.8
HDS	89.6	87.1	78.6	69.4
HDN	75.5	63.3	51.6	43.1
H ₂ consumption (%)	2.69	2.38	2.28	2.15

^a TI: toluene insolubles.

^b Conversion of hexane insolubles to hexane solubles.

coal-derived feeds. The same was confirmed by Ocampo et al. [180]. Thus, the deactivating effects of a coal slurry and that of the ashless coal slurry were similar, suggesting that mineral matter was less detrimental than coke.

5. Deactivation by metal deposits

During hydroprocessing, part of the metals present in the feed will deposit on the catalyst surface and cause deactivation. The nature of the metals deposited depends on the origin of the feed. V and Ni are the

predominant metals in petroleum crudes, heavy oils and oil shale- derived liquids, while Fe and Ti are the main metals in coal-derived liquids. Heavy oils derived from tar sands may contain V, Ni, Ti, Fe and small amounts of other metals, in addition to clay-like mineral matter. Alkalis can also be present if the feed is not completely dewatered. In some cases, alkalis are introduced during the separation of heavy oil from sands. Biofeeds, usually prepared by a thermal treatment of biomass, are the least contaminated by metals.

In summary of previous discussions, it is again emphasized that the deactivation by metals always occurs simultaneously along with that by coke. Deactivation by metals is irreversible. Kinetic data have shown that the rate of metal deposition varies from metal to metal. For example, in the case of V and Ni, the initial deposition occurs at much higher rate for V than for Ni, and increases with increasing pore diameter [181]. This suggests that the formation of V deposits may have an adverse effect on the rate of Ni deposit formation. While the initial coke deposition is rapid before the pseudo-equilibrium level is reached, metal deposits continually increase with time [182]. The general trends in the formation of coke and metal deposits are shown in Fig. 63 [92]. Then, during the entire period, metals deposition occurs on the catalyst, which has already lost a substantial portion of its original porosity and surface area [58]. This is generally true for petroleum-derived feeds and coal-

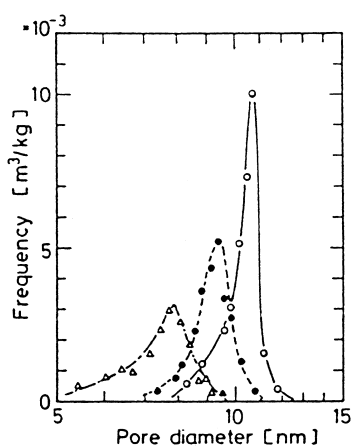


Fig. 62. Pore size distribution; ○ – fresh catalyst, ● – spent catalyst from high TI feed, △ – spent catalyst from low TI feed [179].

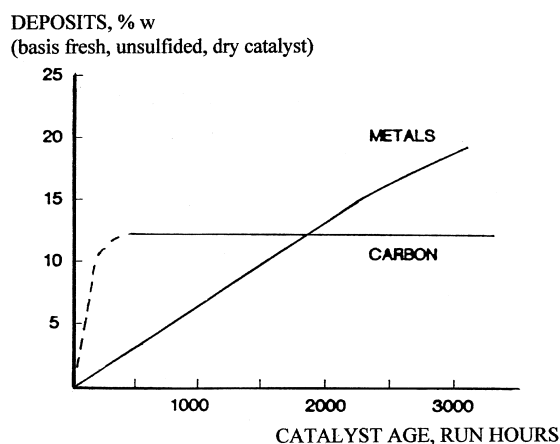


Fig. 63. Metals and carbon deposits as function of catalyst age [92].

derived feeds as well as other feeds. In order to maintain design activity, temperature is raised to offset deactivation. Hence, the deposition of metals affects the lifetime of the catalyst.

Cross-sectional profiles show that some metals tend to deposit on the external surface of the catalyst particles, whereas others are more evenly distributed. This leads to diffusion limitations which affect access to the active sites in the particle interior. It is evident that coke and metals plug the pores and eventually may lead to a complete loss of the activity [136]. Jacobsen et al. [183] have suggested that metal sulfides gradually narrow the pores and thus slow down the diffusion of reactant molecules into the undeactivated interior of the catalyst particles. At the end of the run, the catalyst may still possess some activity. In other words, a complete loss of activity is generally not observed. End run occurs when either the temperature to maintain the activity is too high for reactor design or the loss of active sites by pore plugging is too large to maintain design activity by raising the temperature.

5.1. Formation of and deactivation by V and Ni deposits

The contents of V and Ni in crudes vary between a few parts per million to several 1000 ppm. With few exceptions, the content of V is greater than that of Ni. Several forms of V and Ni porphyrins were isolated from crude oil, i.e., deoxo-phylo-erythro-etio-vanadyl porphyrin (DPEP), etio-vanadyl porphyrin and rhodo porphyrin [183–185]. The typical structures of porphyrins found in the Alberta oil-sand bitumen are shown in Fig. 64. [186]. The frequently investigated tetra-phenyl-substituted porphyrin is much less common in crudes than the other porphyrins, but it may resemble part of the metals present in asphaltenes [187]. Porphyrins account for about one-half of the V and Ni in heavy feeds. The unaccounted part of the metals are in less characterized forms, which may include bonds with nitrogen, oxygen and sulphur in the defect centers of asphaltene sheets [188,189]. The latter structures are more stable than porphyrins suggesting that deposition of the metals during hydro-

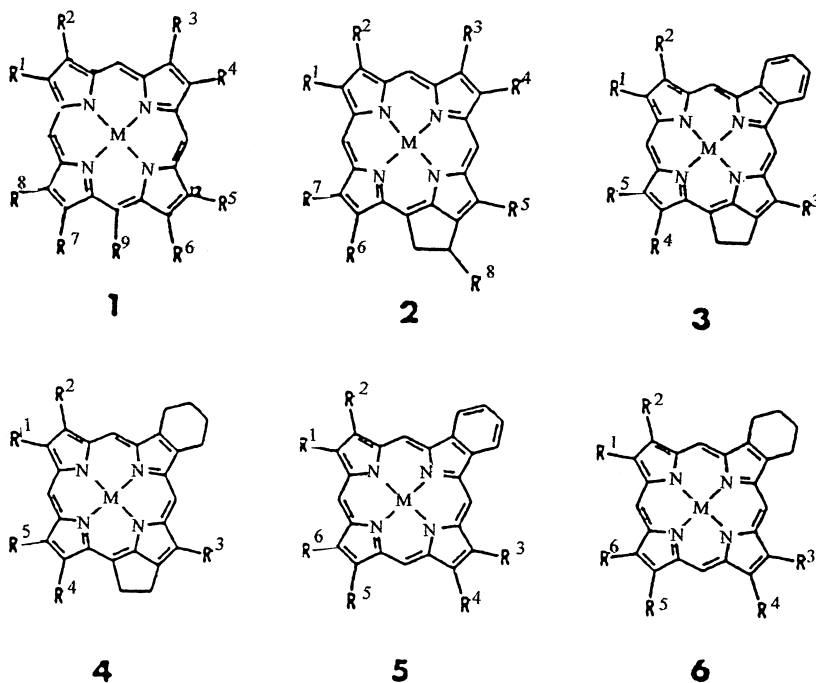


Fig. 64. Major porphyrin types in heavy oils: (1) etio; (2) desoxophylloerythroetioporphyrin (DPEP); (3) benzoDPEP; (4) tetrahydrobenzoDPEP (THBD); (5) benzoetio; (6) tetrahydrobenzoetio (THBE) [186].

processing may be faster from porphyrins. Grigsby and Green [190] pointed out some uncertainty in characterizing V species in crudes. Thus, at least a part of the apparent 'non-porphyrinic V' may be, in fact, porphyrinic. This is supported by the work published by Sakanishi et al. [191]. Using the change in molecular weight on a solvent treatment, these authors assumed that four molecules of the asphaltene units are associated to form aggregates in which porphyrins may be occluded by a strong non-covalent interaction. Porphyrins can be released from the aggregates once the interaction of the asphaltene units is weakened by solvent action. A number of issues need to be addressed to explain deactivation by metals. These include the orientation and interaction of the metal containing compounds with the catalyst surface, as well as their mechanism and kinetics under hydroprocessing conditions.

5.1.1. *Interaction of V and Ni containing compounds with catalyst surface*

In the case of metal porphyrins, some observations can be rationalized by assuming that they lie flat on the catalyst surface with the plane of the molecule parallel with the surface [189]. Loos et al. [192] used the EXAFS technique to explain the form of the interaction of several V porphyrins, including two which were isolated from a crude oil, with an Al_2O_3 and an oxidic form of the $\text{NiMo}/\text{Al}_2\text{O}_3$ catalyst under ambient conditions. The porphyrins were deposited on the catalysts by impregnation. They concluded that the interaction with the bare support (Al_2O_3) was much weaker than with the catalyst. Moreover, a negative axial shift of V back to the plane of the porphyrin was observed. Thus, there was no evidence for a direct interaction of the $\text{V}=\text{O}$ moiety with any specific site of the support. Some of the signals detected were assigned to oxygen atoms of the MoO_3 layer on top of which the porphyrin might be adsorbed. This observation is consistent with the porphyrin molecule lying flat on the oxomolybdenum phase of the catalyst. Loos et al. [193] extended their study to include HDM conditions. The presence of the $\text{V}=\text{O}$ group in the spent catalyst was again confirmed; however, the other part of the V was coordinated with at least four sulfur atoms in a V polyhedron. In this case, the $\text{NiMo}/\text{Al}_2\text{O}_3$ catalyst was presulfided prior to a hydrogenation run, followed by an HDM run. On the bare Al_2O_3 support,

used as a baseline in the HDM run, the $\text{V}=\text{O}$ group coordinated to the additional oxygen and sulfur ligands.

Mitchell and Scott [194] used ESR to study the nature of the interaction between the sulfided catalyst surface and several porphyrins. They concluded that the porphyrins are bound to the catalyst surface by a donor-acceptor or a charge transfer interaction of the π system of the porphyrin ring (the donor), and Brønsted and/or Lewis acid sites of the catalyst (the acceptor). However, such an interaction may be difficult for the tetraphenyl substituted porphyrins because the planes of the phenyl groups are oriented perpendicular to the plane of the porphyrin. The adsorbed porphyrin may be oxidized by the MoO_3 component of the oxidic catalyst or reduced by hydrogenation on the sulphided catalyst. The VO-TPP porphyrin deposited on a bimodal $\gamma\text{-Al}_2\text{O}_3$, $\text{Mo}/\text{Al}_2\text{O}_3$ and $\text{NiMo}/\text{Al}_2\text{O}_3$ was investigated by Knozinger et al. [195,196] using Raman and electron spin resonance techniques. The catalysts were in an oxidic, reduced and sulphided form. The main conclusion from this study was that VO-TPP is bound to the catalyst via a donor-acceptor interaction through the vanadyl group in which V^{4+} interacts with donor (Lewis base) sites by charge transfer from the surface to the porphyrin ring. The acceptor (Lewis acid) sites on the surface are responsible for the reduction of the excess of negative charge in the ring. Thus, VO-TPP adsorbs on the surface not covered with active metals. On the catalyst, thermal decomposition of the porphyrin began at about 200°C . In H_2 , coke formation was observed at about 250°C .

It is believed that the non-porphyrin type of V and presumably also Ni will end-up on the catalyst surface in a sulphided form as well. Because they are associated with the asphaltene molecules [189], the interaction of this part of V and Ni with the catalyst surface will be to a great extent influenced by the form of the adsorption of such molecules on the catalyst. In this regard, little information could be found in the literature. Thus, some research efforts are required to fill this gap.

5.1.2. *Mechanism of HDM*

An ultimate result of the HDM of porphyrins and other metal containing compounds in the feed is the deposition of metals, predominantly as metal sulfides, on the catalyst surface and catalyst deactivation asso-

ciated with it. Most of the efforts have been devoted to metal porphyrins. Because they are less stable than the other metal containing species, their HDM and the ultimate metal deposit formation will be faster. Understanding of the HDM mechanism is essential to explain catalyst deactivation. Also, such knowledge may aid in the preparation of tailor-made catalysts to suit hydroprocessing of a particular feed. All evidence suggests that the presence of H_2 and catalyst is essential for the HDM of porphyrins to occur. Otherwise, their conversion will be very low. The mechanism of HDM has been investigated using model compounds, as well as feedstocks containing metals of interest. Little information is available on the HDM mechanism of the non-porphyrin type of the V- and Ni-containing species, though their contribution to deactivation may be important. If this part of the V and Ni compounds is associated with the asphaltene sheets [92,189], their fate during hydroprocessing will depend on the conversion of the asphaltenes.

Under hydroprocessing conditions, the metal porphyrin (M-P) is hydrogenated in the first step to chlorin, in which hydrogens are introduced into β positions of one of the pyrrole rings. The formation of the intermediate chlorin from V and Ni etiopor-

phyrin was observed by Huang and Wei [197,198] in the presence of an oxidic $CoMo/Al_2O_3$ catalyst and high H_2 pressure. Chlorin was indeed confirmed by isolation in a pure form using column chromatography, followed by its structure confirmation using mass spectroscopy [199]. It was concluded that the formation of other intermediates is also possible, as it was evidenced by shoulders on the UV-Vis peak of the chlorin. Ware and Wei [200] isolated a second intermediate ($Ni-PH_4$) and a third intermediate ($Ni-X$) and included them in the overall HDM mechanism shown in Fig. 65. Detection of the $Ni-X$ intermediate was prompted by the lack of mass balance of Ni in the solution, in which Ni-P, Ni-P2 and Ni-P4 did not account for a large portion of Ni in the solution. In this case, liquid chromatography was used for the isolation. The structure of $Ni-X$ shown in Fig. 65 was assigned after an extensive spectroscopic evaluation. It is evident that this intermediate has lost its porphyrin character. At high Ni-P conversions, this intermediate accounted for as much as 80% of the total metal in the solution; therefore, its role in the overall HDM may be important. The formation of this intermediate was favored by an oxidic catalyst, whereas the sulphided $CoMo/Al_2O_3$ catalyst favored the direct

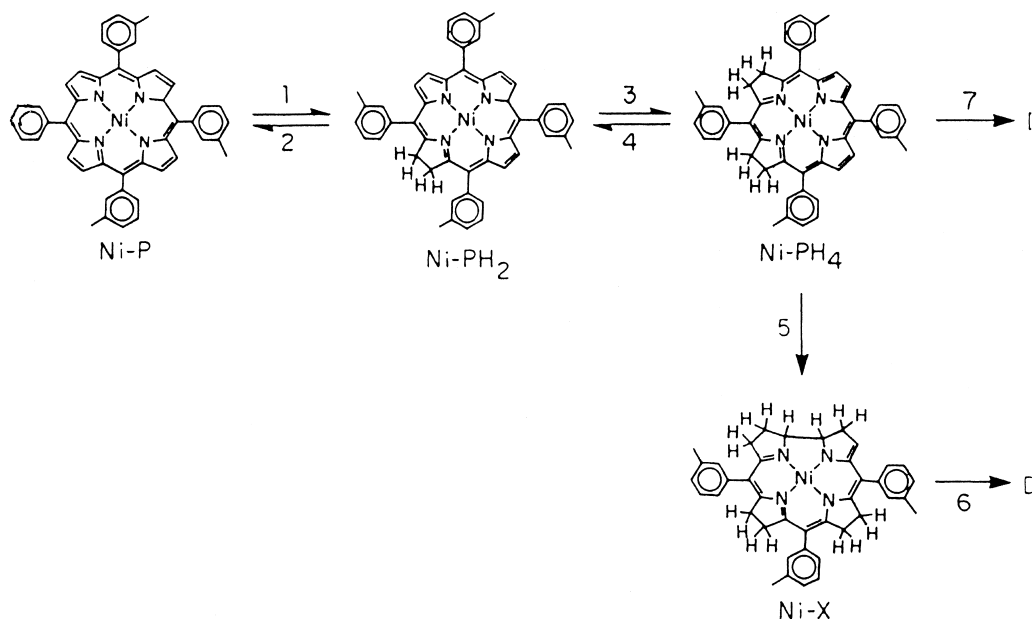


Fig. 65. Tentative mechanism of HDM of Ni-porphyrin [200].

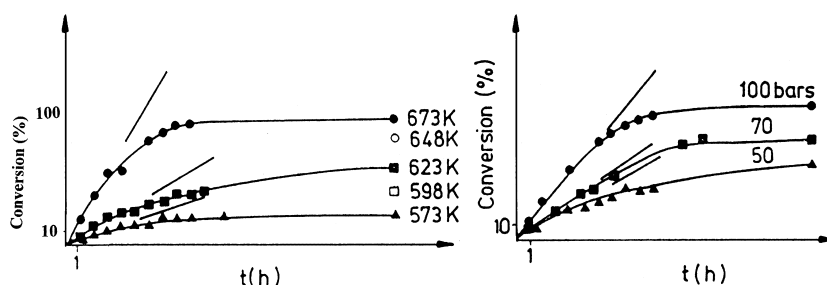


Fig. 66. Percentage of VO-porphyrin hydrogenated vs. time at different pressures and temperatures [201].

release of the metals. This was attributed to an enhanced bond cleavage activity of the sulfided catalyst, promoting ring rupture of the intermediate at the expense of further skeletal rearrangement. Presumably, this was consistent with the increased presence of the Brønsted sites associated with the generation of $-SH$ groups.

Formation of chlorin from porphyrin does not require the presence of a catalyst. While studying vanadyl octaethyl porphyrin, Vandeneekoutte et al. [201] have shown that temperature and H_2 pressure are the main parameters influencing this reaction. The results shown in Fig. 66 were obtained by these authors in the absence of catalyst. At 723 K and 50 atm of H_2 , the equilibrium is practically displaced towards chlorin. When the solution is exposed to air at room temperature, the equilibrium gradually shifts back to the porphyrin. The authors suggested that the aromaticity of chlorin is preserved by an increase in the electron population in the methine bridges. Then, hydrogens in the methine group in the chlorin are more exchangeable, i.e., more acidic than in the porphyrin. This may be a key factor for the increased reactivity of chlorin compared with the corresponding porphyrin.

The formation of the intermediate chlorin was part of the mechanism described by Chen and Massoth [202]. Similarly as in the previous studies, V and Ni porphyrins were dissolved in a Nujol and treated at 320°C and 69 atm of H_2 in a batch stirred reactor. A 35–65 mesh particle size of the sulfided $CoMo/Al_2O_3$ catalyst was used for testing. The UV-Vis spectra of the original solution and the one after 1 h reaction time confirmed the presence of a new peak (at 633 nm) consistent with Ni/V-PH2. As the results in Fig. 67 show, the appearance of the new peak was comple-

mented by the decrease of the porphyrin peak. Fig. 68 shows that as the absorption of the porphyrin peak decreased, that of the intermediate reached a maximum and then also decreased. These trends were similar for both the V and Ni porphyrins and were in general agreement with other studies [129,189,198,201].

Tsai et al. [129] showed that the hydrogenation of porphyrin over sulfided $NiMo/Al_2O_3$ catalyst is influenced by properties of the hydrocarbon medium. The hydrogen transfer ability of the medium was found to be the most important parameter. Among several solvents used, a triple-hydrogenated coal-derived

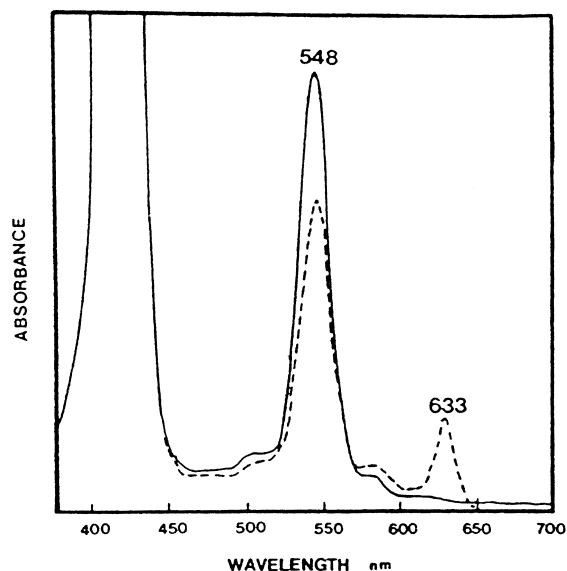


Fig. 67. UV-Vis absorption spectra of pure VO-porphyrin (—) and sample collected during HDM run (---) ($NiMo/Al_2O_3$, 593 K, 69 atm) [202].

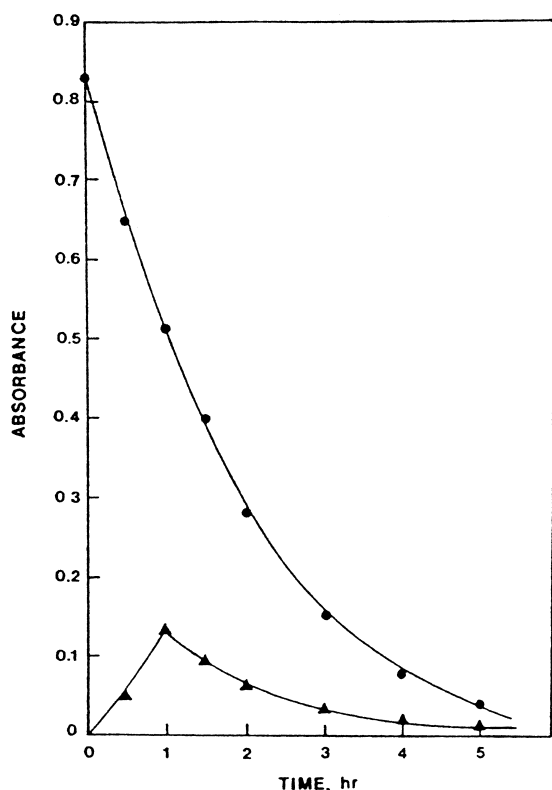


Fig. 68. Absorbance–time profiles for VO-porphyrin (●) and intermediate (▲) during HDM run (conditions as in Fig. 67) [202].

liquid was superior because of the high content of polycyclic hydroaromatic structures, rich in naphthenic hydrogen and attached alkyl groups. Such structures were observed to be much better hydrogen transfer agents compared with tetraline, decaline and other solvents [203,204]. As shown in Fig. 69 [129], during the hydrogenation of the hydrotreated coal-derived liquid, the typical chlorin peak showed up first as an initial intermediate, while another peak showed up later as a secondary hydrogenation product. As reaction proceeded, the UV–Vis absorption intensities of both peaks showed an increase and then decrease, after reaching a maximum, indicative of intermediate products. However, with pure solvents, such as mesitylene, decaline or tetraline, only one intermediate product (chlorin) was observed, even up to 75% conversion of the reactant. The deeper hydrogenation ability of the triple-hydrogenated coal derived liquid was attributed to better hydrogen trans-

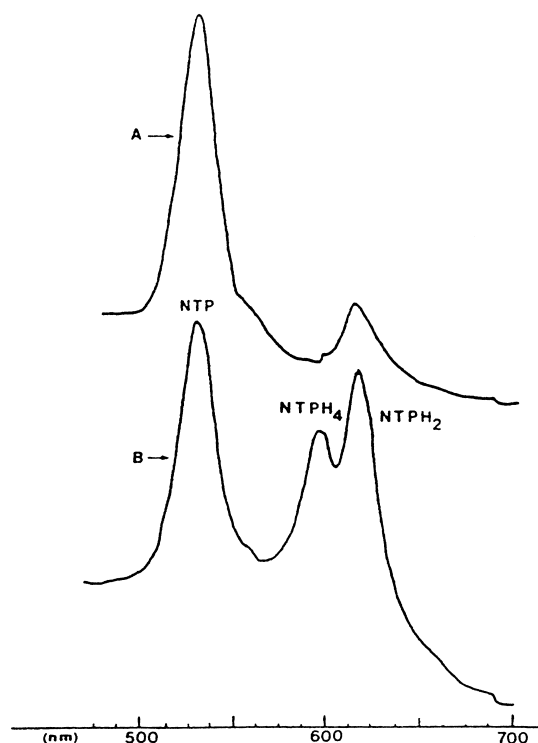


Fig. 69. UV–Vis spectra products of hydrogenation of Ni-porphyrin (A) in mesitylene and (B) hydrogenated CDL [129].

fer rather than hydrogen solubility, since the latter was lower than that in the other solvents. The authors summarized their observations in the overall mechanism shown in Fig. 70 [129]. In this mechanism, NTP depicts Ni porphyrin and NTP2 and NTP4 the first and second intermediates. Formation of NTP4 in hydrogen

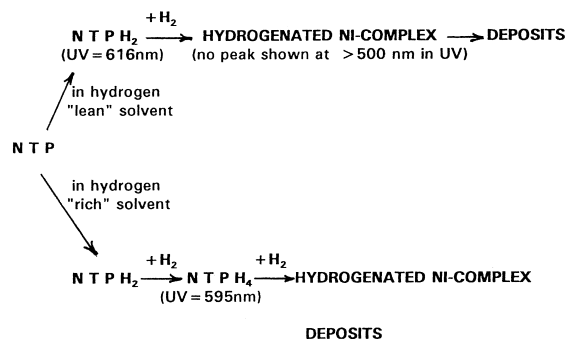


Fig. 70. Proposed reaction scheme for hydrogenation of NTP and NBP [129].

lean solvents cannot be excluded. Thus, this intermediate and possibly others were formed but were removed at the faster rate than the rate of their formation. It was suggested by Mitchell [189] that phlorin is among possible intermediates as well, although it was not detected in the products. It can be formed by hydrogenation of methine or meso carbons. Phlorin is unstable and is easily converted to chlorin. Nevertheless, the hydrogenation activity of the catalyst seems to play an important role in the overall HDM mechanism. This is supported by the observation of the three intermediates noted by Ware and Wei [200].

As it was indicated earlier, the presence of catalyst is crucial for achieving the final fragmentation of the porphyrin molecule, which requires hydrogenolysis of C–N bonds. According to Weitcamp et al. [205], at lower temperatures, the main hydrocarbon products from the HDM of porphyrin would be predominantly dipyrroles, while at higher temperatures, the HDN of dipyrroles would lead to hydrocarbons and ammonia if a sufficient H_2 pressure is maintained. The formation of polypyrroles was confirmed by Rankel [206]. Thus, at least a partial break up of the intermediates is required to release the metal, because the metal free porphyrin could not be detected in the liquid products [207]. Deposited metals will be rapidly sulphided by H_2S from the HDS reactions occurring simultaneously. Perhaps the role of H_2S in the overall HDM deserves more attention in view of observations made by Rankel [206] that H_2S plus H_2 in the absence of catalyst can produce thermally cleaved porphyrin rings or polypyrroles from both V and Ni porphyrins, with the former being more reactive. This would indicate a modification of HDM mechanism by H_2S .

Perhaps the most detailed account of the mechanism of HDM of porphyrins was given by Janssens et al. [187]. From molecular modeling calculations and GC-MS analysis of the HDM products, these authors were able to confirm the presence of the intermediates proposed by other researchers, as well as new intermediates not identified and/or proposed previously. The overall mechanism proposed by these authors is shown in Fig. 71. In this case, M represents either Ni or $V=O$, as it was assumed that the different metal species should have little influence on the mechanism. In the first step, the tetraphenylporphyrin (M-TPP) is

converted to chlorin (M-TPC), in agreement with other researchers [199–204]. In the next step, the M-TPC is converted to tetrahydroporphyrin and/or isobacteriochlorin (M-TPiB). The formation of bacteriochlorin is less probable but cannot be ruled out completely. In the next step, the M-TPiB is hydrogenated to hexahydroporphyrin (M-TPHP). The octahydrogenated species arising from the hydrogenation of M-TPHP was not confirmed, but assumed to be part of the mechanism. In this case, the molecular modeling suggested that the hydrogenation of the meso-bridge positions would yield a more stable intermediate (M-B) than that of the last pyrrole ring. The meso position becomes susceptible to attack leading either to an immediate ring cleavage and metal removal or to a tolyl elimination leading to the new M-Bil structure. Most likely, the next step is metal removal because of the unstable coordination in the M-Bil structure. According to the authors [187], elimination of pyrrole groups before the metal removal is not probable because of the minimum coordination number of four of the metal atom. The metal atom is removed with the aid of H_2S . In this case, the role of H_2S is not fully understood. Further hydrogenation leads to monopyrrole and phenyl-group containing molecules.

The information on the HDM mechanism of non-porphyrin metal-containing species is limited because the structure of these species is much less defined than that of porphyrins. The evaluation of a heavy crude by size exclusion chromatography has shown that both V and Ni are quite evenly distributed in fractions having average molecular weights between 370 and 6680 [208]. Fractions having average molecular weight between 1420 and 6680 accounted for 56 and 72% of V and Ni, respectively. Sughrue et al. [209] used size exclusion chromatography with inductively coupled plasma emission detection to study removal of V from residual oils. The distribution of V shown in Fig. 72 indicates the presence of small and large V-containing molecules. The former were more reactive and could be readily removed under mild hydroprocessing conditions. It is speculated that the structure of the small molecules approaches that of the porphyrin. Nevertheless, there are indications that the non-porphyrin type of the metal containing compounds may account for more metals than the porphyrins. More information on HDM of such structures would be desirable.

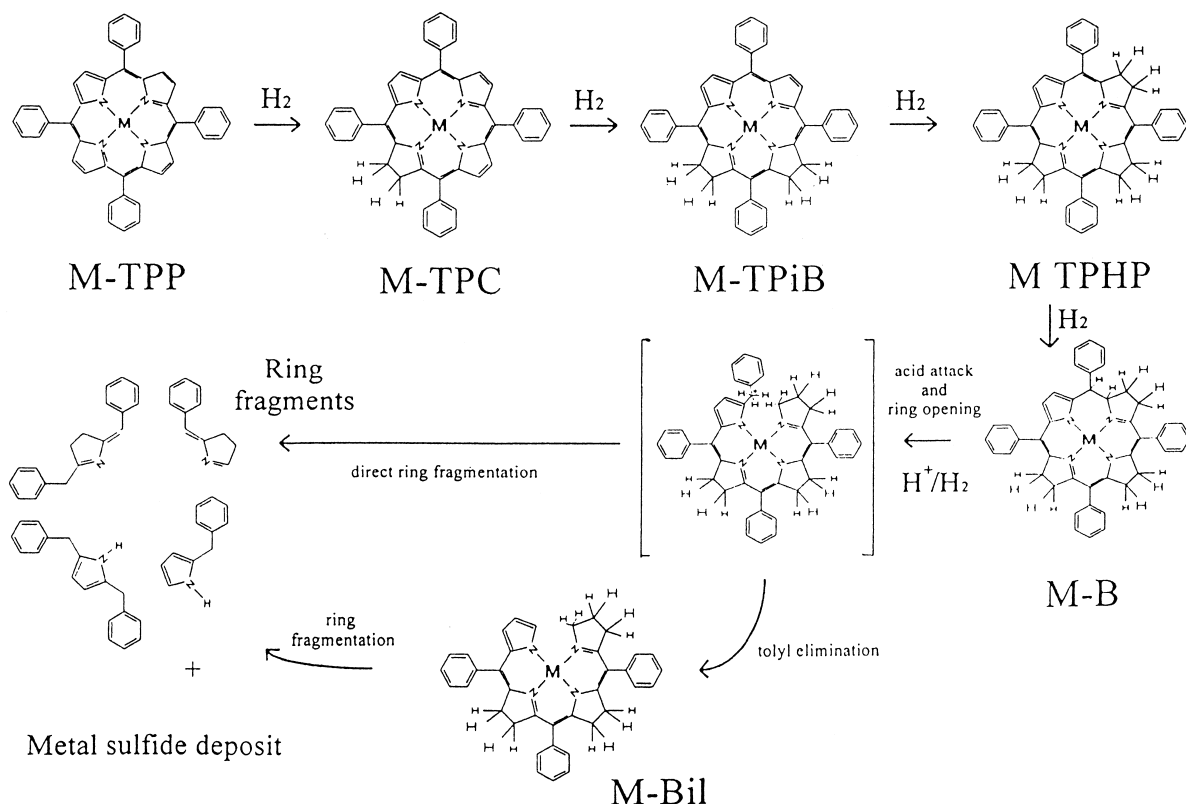


Fig. 71. A complete reaction mechanism for HDM of metallocporphyrins; M = Ni or VO [187].

5.1.3. Kinetics of HDM of V and Ni

It was indicated earlier that physical properties of the catalyst are important because of the size of the

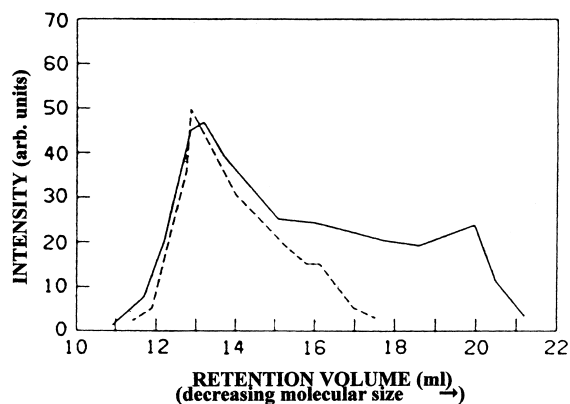


Fig. 72. Size exclusion chromatography for V in feed (—) and product (---) [209].

metal-containing compounds. Of a particular importance is the size of the catalyst particles. As shown in Fig. 73 [210], for particle sizes less than about 1 mm, HDM rate was constant, indicating the absence of diffusional phenomena. The effect of the size of the catalyst particles on the rate of HDM was studied extensively by Kobayashi et al. [181]. To avoid diffusion problems and/or to determine the intrinsic kinetics, many studies were conducted using a powder form of catalyst either in an oxidic or sulphided form. Such information is important for understanding HDM. However, from the practical point of view, the investigation of catalysts in their operating form is crucial because the diffusion phenomena have a significant impact on the performance and lifetime of the catalyst. A number of studies on the kinetics of metal removal from various crudes and residues in the presence of hydroprocessing catalysts have appeared in the scientific literature. The kinetic order of HDM with respect to the metal concentration in the feed has

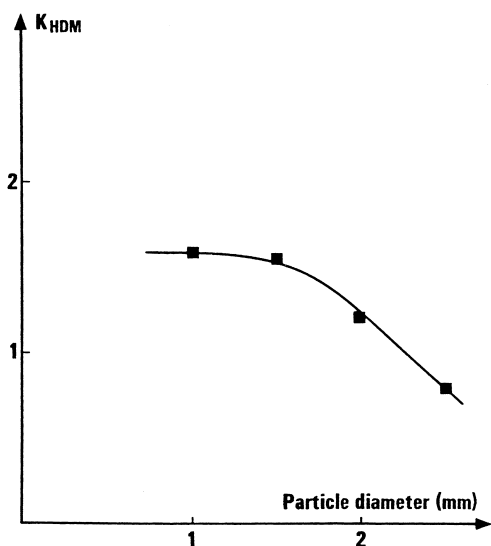


Fig. 73. Effect of particle diameter on HDM activity [210].

been reported as first-order [211–213] and second-order [214,215]. The discrepancies could be attributed to many different sulphur, nitrogen, metal and asphaltenic compounds in crudes and residues. Besides this, the different amounts and reactivity of the various metal-containing (porphyrin and non-porphyrin) compounds may have also contributed. The type of catalyst, its particle size and shape in particular, should also be taken into consideration when different studies are compared. Last but not least, the conditions applied during the hydroprocessing operation are important.

5.1.3.1. Intrinsic kinetics. An extensive database exists on the kinetics of HDM of porphyrins. The kinetics of the non-porphyrin V and Ni are less understood, although they are part of the overall rate during HDM of the metal containing feeds. An oxidic CoMo/Al₂O₃ catalyst, in a powder form (0.075–0.086 mm) was used by Huang and Wei [197,198] to investigate the kinetics of HDM of tetraphenyl- and etio-porphyrins of V and Ni in a batch reactor. After the first contact with the catalyst, a rapid decline in the V concentration from 20 to about 10 ppm was observed, compared with little change for Ni. The etio structures were used to compare the removal of V with Ni. At lower temperature, the Ni-etio was more reactive, but VO-

etio, having a higher activation energy, was more reactive at high temperatures, i.e., activation energy for the VO-etio and Ni-etio porphyrins were 37.1 and 27.6 kcal/mol, respectively. The rates of HDM of V and Ni fitted 0.5 order kinetics well but a temperature dependence on the order was noted. Because of the catalyst particle size chosen, no external diffusion limitations were observed. The results were consistent with other studies [216–218].

The studies performed with the oxidic catalyst [197,198] were later expanded to evaluate the effect of the catalyst presulfiding as well as poisoning by pyridine on the HDM kinetics [48]. It was already noted that sulfidation of the catalyst influenced the HDM mechanism [200]. Comparison of the results in Fig. 74 [200], obtained for the oxidic catalyst with those in Fig. 75 [48] obtained for the sulfided catalyst, confirm a dramatic effect of presulfiding on the rate of HDM. For example, for the sulfided catalyst, about

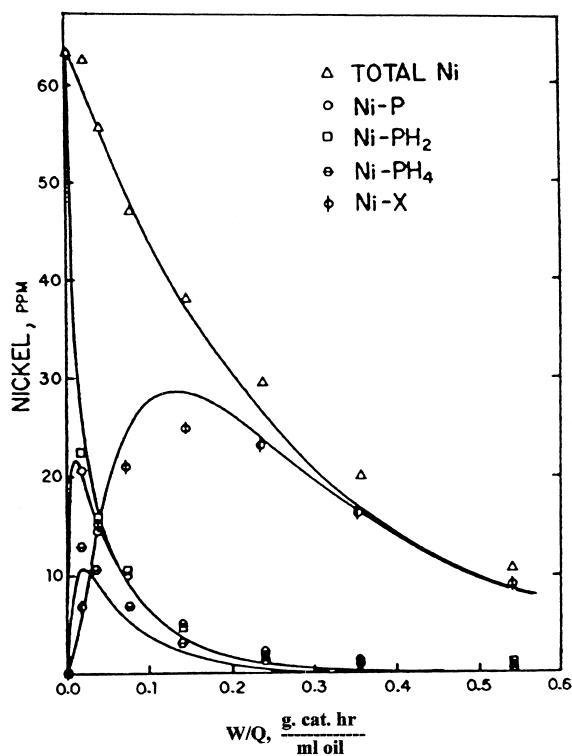


Fig. 74. Concentration vs. contact time during HDM of Ni-porphyrin (63 ppm of Ni in feed, CoMo/Al₂O₃ oxid., 618 K, 6.99 MPa) [200].

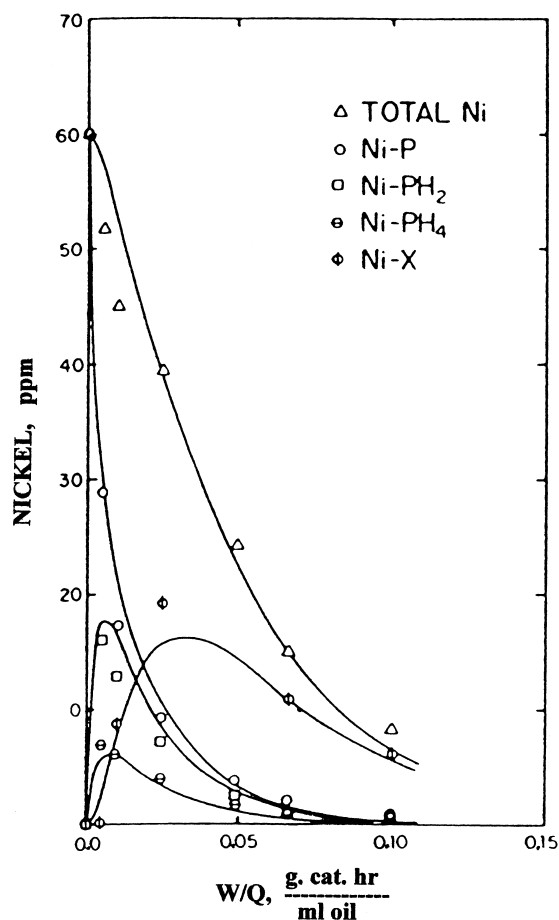


Fig. 75. Concentration vs. time during HDM of Ni-porphyrin (conditions the same as in Fig. 74 except sulfur catalyst) [48].

80% Ni removal was achieved at a contact time of 0.075 g cat h/ml oil compared with about 0.42 g cat h/ml oil for the oxidic catalyst. Results such as shown in Figs. 74 and 75 were used to calculate kinetic parameters using the sequential hydrogenation/hydrogenolysis model of Fig. 65, assuming first order kinetics for each of the reaction steps and constant H_2 pressure. The parameters in Table 16 [48] are the ratios of the rate coefficient of the sulfided catalyst to that of the corresponding rate coefficient of the oxide catalyst. The effect of catalyst prereduction was also evaluated. Poisoning of the catalyst by pyridine was quite evident. As expected, prereduction increased the kinetic parameters. In the case of presulfiding, the metal deposit steps were influenced to a much greater extent than the dynamic equilibria. At all temperatures, the

Table 16
Kinetic parameters for HDM of Ni-T3MPP^a

Reaction step	$k_{\text{pyrid}}/k_{\text{oxid}}$	$k_{\text{red}}/k_{\text{oxid}}$	$k_{\text{sulph}}/k_{\text{oxid}}$
1	0.42	2.5	1.7
2	0.56	2.1	1.7
3	0.35	1.9	2.0
4	0.52	1.4	2.6
5	0.15	2.5	3.5
6	0.61	2.2	7.1
7	0.78	2.2	6.7

^a Experimental conditions: 345°C; 6.99 MPa H_2 ; 65 ppm Ni [48].

selectivity of Ni-PH4 to Ni-X relative to direct metal deposition (k_5/k_7) was smaller on the sulphided catalyst compared to the oxidic catalyst. The kinetic parameters estimated by Ware and Wei [48] for the sulfided catalyst are shown in Table 17. The relative magnitudes of the rate parameters suggest that the metal deposition steps (k_6 , k_7) are rate limiting in the overall mechanism.

The assumption of first-order kinetics for all steps in the mechanism shown in Fig. 65 [200] may affect the validity of kinetic parameters though they may be useful to indicate relative trends. A detailed kinetic analysis performed by Chen and Massoth [202] takes into consideration the effect of temperature, H_2 pressure and concentration of V and Ni porphyrins on the overall kinetics. In this case, sulfided CoMo/ Al_2O_3 extrudates were crushed and sieved to obtain 0.21–0.42 mm (35–65 mesh) size particles in order to obtain intrinsic kinetics. The effect of temperature on the kinetic order is shown in the first-order plot of Fig. 76, in which two temperature regions may be identified. Above 350°C, the kinetics follow first-order, whereas below 350°C, the curvature in the plots is evident. This

Table 17
Kinetic parameters for HDM of Ni-T3MPP^a

Reaction step	k (ml oil/g cat. h)	E (kcal/mol)	H_2 pressure order
1	183	23.0	1
2	164	24.9	0
3	250	19.7	1
4	400	23.1	0
5	171	40.3	2
6	27	29.4	2
7	120	20.0	3

^a Experimental conditions: 345°C; 6.99 MPa; 60 ppm Ni [48].

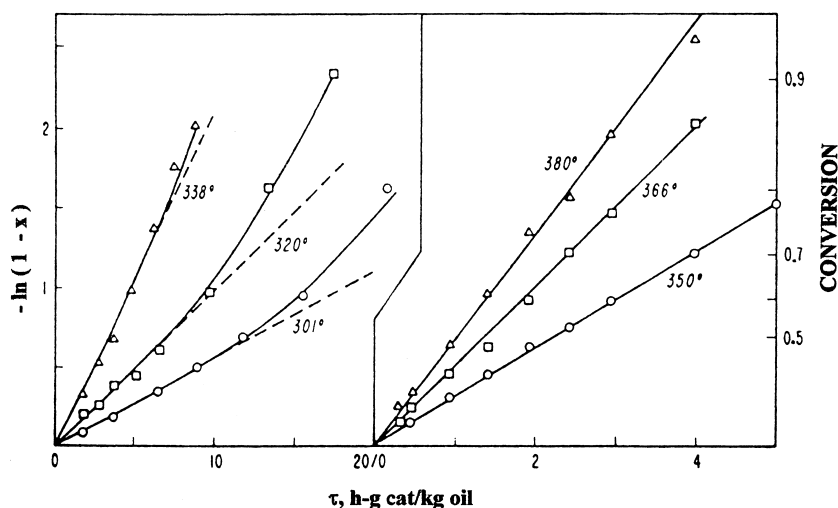


Fig. 76. First order plots of Ni-porphyrin disappearance as function of temperature (35 ppm of Ni in feed, CoMo/Al₂O₃, 6.99 MPa) [202].

curvature was attributed to the adsorption of the reactant being greater than that of the dipyrrole products, indicating inhibition by the reactant. The mechanistic scheme which suited best the kinetic analysis is shown in Fig. 77, i.e., the direct conversion (from A to C) had to be considered as part of the overall mechanism. The direct path is probably not a real path but rather a direct conversion of porphyrin to the hydrogenated intermediates and products in a single adsorption step without desorption of the intermediates, thus avoiding desorption and readsorption. Solution of the appropriate differential equations describing this system yields the following equations:

$$X_B = \frac{\beta_1}{\beta_2 - 1} (X_A - X_A^{\beta_2}) \quad (5.1)$$

$$\beta_1 = \frac{k_1}{k_1 + k_3}, \quad \beta_2 = \frac{k_2}{k_1 + k_3} \quad (5.2)$$

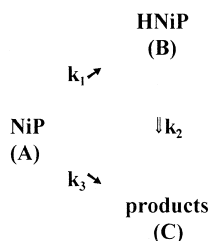


Fig. 77. Reaction network for kinetic analysis [202].

where X_A and X_B are mole fractions for a given run whereas β_1 and β_2 were obtained by non-linear regression analysis. Fig. 78 shows the experimental data and

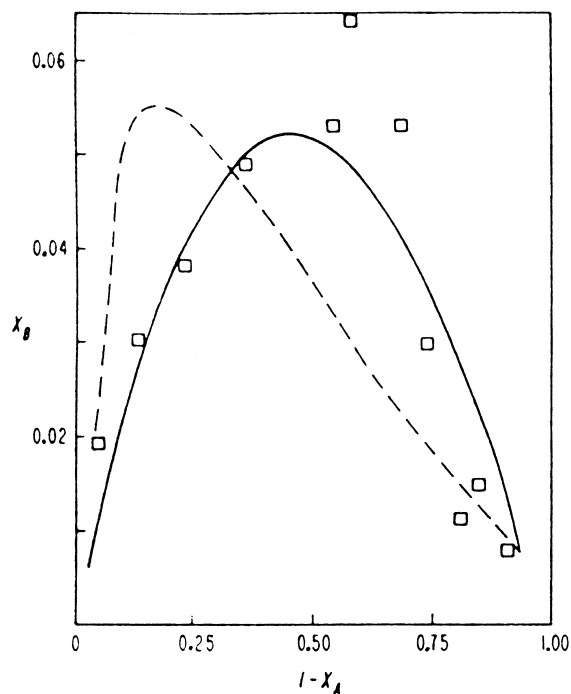


Fig. 78. Selectivity plot of X_B vs. $1 - X_A$; fit of data with k_3 (—) and without k_3 (---) [202].

Table 18
Rate constants for HDM Ni–P [202]

Constant (kg oil/g cat h)	
k_{NP}	16.4
k_1	0.56
k_2	5.91
k_3	1.74

the fit based on the scheme in Fig. 77 (solid line) and the one not including k_3 (broken line). It is obvious that the former gives a much better fit of the kinetic data. The scatter of the data is not surprising considering the limitations of the analytical accuracy by UV–Vis spectroscopy. The estimated rate constants are shown in Table 18 [202]. Increasing H_2 pressure increased the reactant conversion (Fig. 79). From the first-order plot, the following power equation in p_H was obtained:

$$r_{NP} = \frac{3.63c_{NP}}{1 + 0.14c_{NP}^0} p_H^{1.57 \pm 0.15} \quad (5.3)$$

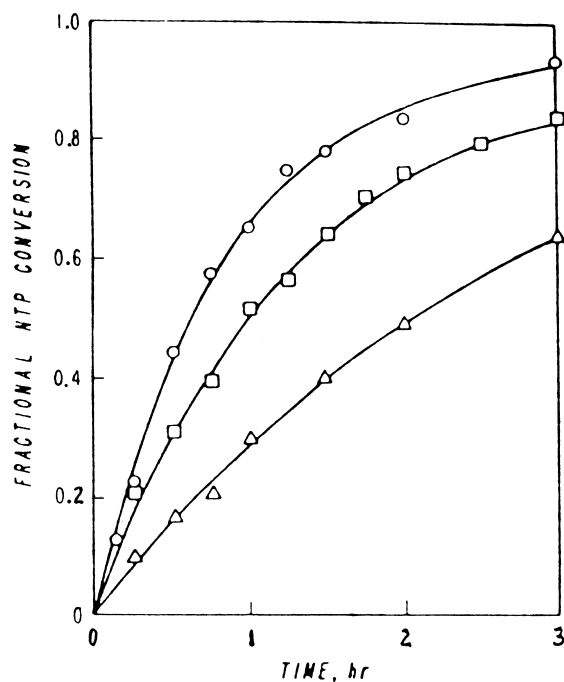


Fig. 79. Effect of H_2 pressure on Ni-porphyrin reaction; (○) 89, (□) 69, (△) 42 atm (other conditions are the same as in Fig. 76) [202].

The noninteger order signifies that the overall rate is not a simple function of H_2 pressure. The 1.57 power in p_H can be rationalized if Path 1 is assumed to be first-order and Path 3 second-order in p_H . The effect of temperature could be best described when two temperature regions were assumed, i.e., between 275–350°C and 350–380°C.

5.1.3.2. Diffusion controlled kinetics. Because of their size, the concept of restrictive diffusion presented earlier is applicable to the metal bearing species present in heavy feeds. In summary, when the molecular diameter of the porphyrins and metal containing asphaltenes approach the size of the pore diameter, their diffusion rate into the liquid filled pores becomes smaller than that in the bulk liquid medium. If the diameter of the molecule equals or is more than that of the pore diameter, diffusion into the pore completely ceases [219]. Therefore, the smallest micropores will not be accessible to large molecules such as porphyrins. The molecular size distribution in Fig. 80

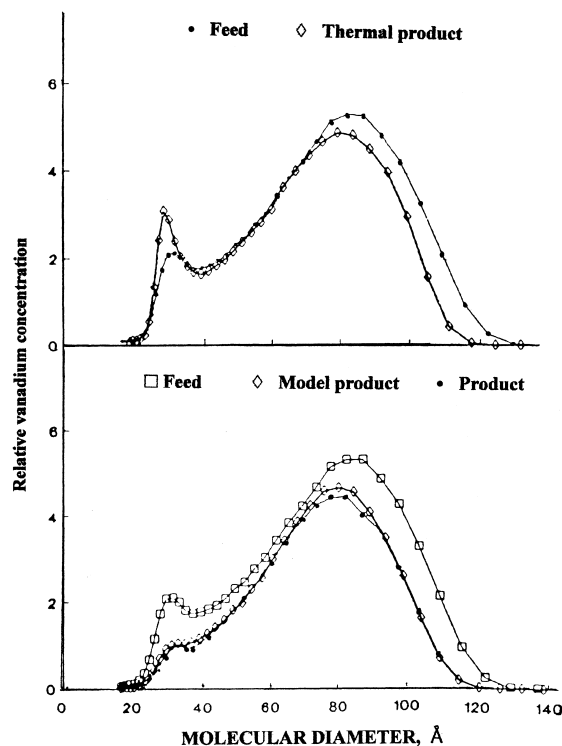


Fig. 80. Distribution of diameter of V molecules in feed and products [220].

shows that the size of the V-containing molecules varies between 15 and 150 Å, indicating that the micropores would be mostly affected by diffusion [220]. If the diffusion rate of a V- or Ni-containing molecule is the slow step compared with its surface reaction, only the outer portion of the catalyst will be utilized. As a result, the conversion versus time on stream will exhibit a nonlinear decrease, compared with a nearly linear decrease for the powdered form of a catalyst [221]. Note that the smallest pores could also be affected in powder catalysts, even though the path is shorter.

Most studies on diffusion controlled HDM kinetics of model compounds involved porphyrins. Lee et al. [118,122,128] investigated the effect of particle and pore size on the HDM kinetics of Ni-tetraphenylporphyrin (Ni-TPP) and Ni-tetra(4-biphenyl)porphyrin (Ni-TBP), having critical molecular diameters of 15.7 and 21.8 Å, respectively. For this purpose, they used three NiMo/Al₂O₃ catalysts whose properties are given in Table 9 [118]. Spheres of 1/8-in. and 60–80 mesh size particles were used. The effect of particle size on reaction rate was estimated, using the measured apparent rate constant and the relationship between the effectiveness factor, η , and the Thiele modulus expressed as

$$\eta = \frac{3}{\phi} \left(\frac{1}{\tanh \phi} - \frac{1}{\phi} \right) \quad (5.4)$$

in which the usual form of the Thiele modulus for spherical particles, ϕ_s , used was:

$$\phi_s = R_0 \left(\frac{k_s \rho_p}{D_e} \right)^{0.5} \quad (5.5)$$

Initial runs with fresh catalysts gave erratic results, presumably due to rapid deactivation. Accordingly, one catalyst was used in a sequence of batch reaction runs to investigate the deactivation phenomena. In these tests, the catalyst was always kept in the reactor and only the feed solution (Ni-TPP in mesitylene) was replaced after each run. As shown in Fig. 81 [122], catalyst deactivation occurred very rapidly, finally reaching a steady state. It was realized that the initial deactivation was caused by a rapid initial buildup of coke. Subsequently, reaction of a concentrated Ni-TPP solution over the catalyst was used to age catalysts. After aging, the data could be fitted to first-order kinetics. First-order plots of the hydrogenation of

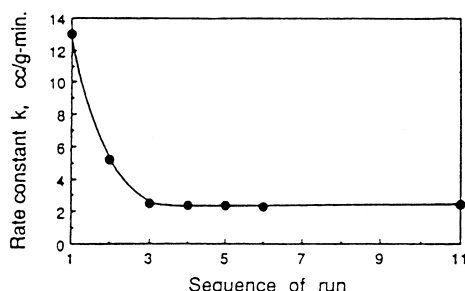


Fig. 81. Deactivation profile of NiMo-125 catalyst for reaction of Ni-porphyrin in mesitylene (623 K, 5.27 MPa H₂) [122].

Ni-TPP and Ni-TBP in decalin are shown in Fig. 82. The rate constants estimated from such plots and effectiveness factors are listed in Table 19. The increase in the rate constant with decreasing particle size is quite evident. Also, when the reactant molecular size was increased or the micropore size was decreased, the effectiveness factor decreased. The effective diffusivities of the fresh and aged catalysts were determined from sorptive diffusion experiments at ambient conditions, using a coronene solution in cyclohexane. The results shown in Table 20 indicate a significant change in physical properties between the aged and fresh catalysts. This fact has to be taken into consideration in order to determine restrictive diffusion in more realistic terms. For this purpose, Lee et al. [118] attempted to obtain a corrected size of the pore mouths of aged catalyst by taking the ratio of D_e (Eq. (4.20)), i.e.,

$$\frac{D'_e}{D_e} = \frac{\lambda^2 (1 - \lambda')^4}{(\lambda')^2 (1 - \lambda)^4} \quad (5.6)$$

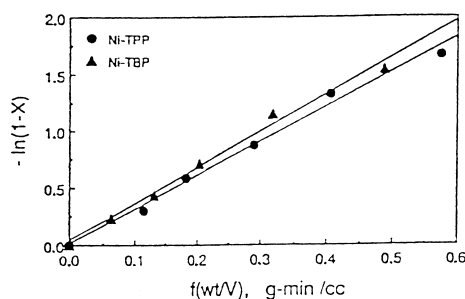


Fig. 82. First-order conversion of Ni-porphyrins in decalin with NiMo-225 catalyst (623 K, 5.27 MPa) [122].

Table 19
Rate constants and effectiveness factors for hydrogenation of Ni-TPP and Ni-TBP [122]

	Catalyst					
	NiMo-125		NiMo-225		NiMo-325	
Hydrogenaton of Ni-TPP						
Particle radius (cm)	0.011	0.184	0.011	0.183	0.011	0.167
Rate constant ^a (cm ³ /g min)	3.366	0.742	3.000	0.476	3.278	0.423
Effectiveness factor ^a	0.96	0.21	0.93	0.15	0.85	0.11
Particle radius (cm)	0.011	0.184	0.011	0.183	0.011	0.167
Rate constant ^b (cm ³ /g min)	1.982	0.603	2.453	0.372	2.030	0.297
Effectiveness factor ^b	0.98	0.30	0.91	0.14	0.88	0.13
Hydrogenation of Ni-TBP						
Particle radius (cm)	0.011	0.184	0.011	0.183	0.011	0.167
Rate const. (cm ³ /g min)	3.812	0.662	3.207	0.371	3.301	0.299
Effectiveness factor	0.94	0.16	0.85	0.10	0.65	0.06

^{a,b} Data for different experimental conditions.

where primed parameters refer to aged catalyst. Two assumptions were made to derive this equation; the tortuosity factor of the aged and fresh catalysts are the same and coke does not completely block the pores, i.e., the number of pores remains the same. Then, $\epsilon'/\epsilon = d_p'^2/d_p^2 = \lambda^2/\lambda'^2$ was incorporated to account for the decrease in the surface fraction of pores for the aged catalysts due to the reduction in pore mouth size by coke. Using the above equation and the D_e values in Table 20[122], the corrected pore diameters of the aged catalysts were calculated to be 116.7, 59.2 and 45.7 Å for NiMo-125, NiMo-225 and NiMo-325, respectively, compared with 174, 83 and 62 for the corresponding fresh catalysts. Consequently, surface porosities were adjusted to estimate effective diffusivities under reaction conditions by using the following equation:

$$D_e' = \frac{D_b \epsilon'}{\tau} (1 - \lambda)^z = \frac{B \epsilon \lambda^2}{V_A^{0.6} \tau (\lambda')^2} (1 - \lambda')^z \tag{5.7}$$

As the results in Fig. 83 show, when the corrected value of λ' was used, a value 4.9 was obtained for the z

Table 20
Effective diffusivity data ($D_e \times 10^6$, cm²/s) for fresh and spent NiMo catalysts [122]

NiMo-125		NiMo-225		NiMo-325	
Fresh	Spent	Fresh	Spent	Fresh	Spent
3.59	1.31	2.52	1.15	1.94	0.71

parameter. Without applying the correction for the pore size, an unrealistic value of 6.9 was obtained. It was felt appropriate to review the approach made by Lee et al. [118,122,128] in more detail as it gives an excellent illustration of the restrictive diffusion phenomena relevant to diffusion controlled HDM kinetics.

Tsai et al. [129] studied the effect of solvent on hydrogenation of Ni-TPP at 335°C and 50 atm of H₂. In this case, a triple-hydrogenated coal-derived liquid (HT-CDL) having a boiling range of 230–350°C was compared with mesitylene, tetralin and decalin. For the reactivity tests, the NiMo 125 and NiMo 325 catalysts shown in Table 9 were used in two particle sizes, i.e., 0.33 cm (1/8 in.) spheres and 0.036 cm

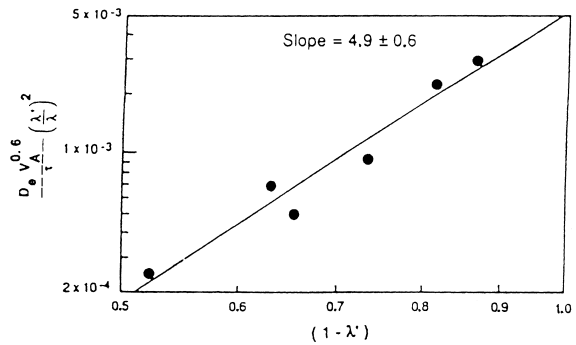


Fig. 83. Determination of Z from experimental data for hydrogenation of Ni-porphyrins [122].

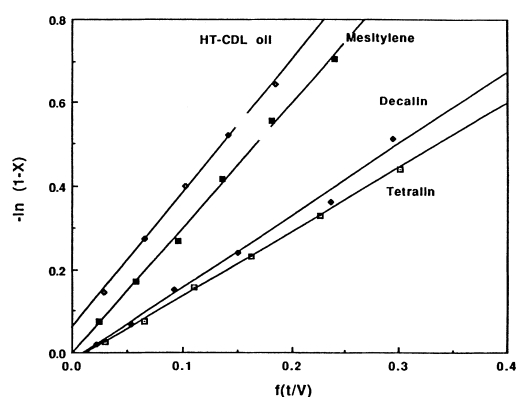


Fig. 84. First-order kinetics plots for hydrogenation of Ni-porphyrin in various solvents [129].

particles. To achieve a stable activity for kinetic measurements, the catalyst was predeactivated by depositing about 1.6 wt.% of coke. First-order kinetic plots in Fig. 84 show that the best performance was obtained with the HT-CDL. The effective diffusivity and uptake in coronene-cyclohexane solution at ambient conditions for the fresh and spent NiMo-125 and NiMo-325 catalysts are shown in Table 21. These results suggest that while the pore diameter reduction was only about 5%, the reduction of the effective diffusivity was considerably more. This implies that the coke deposit in the catalyst is concentrated at the pore mouths. The estimated parameters, such as the rate constants, intrinsic rate constants, effectiveness factor and effective diffusivity are given in Table 22.

Table 21

Effective diffusivity and uptake in coronene-cyclohexane solution [129]

Catalyst	Effectivediffusion ($D_e \times 10^6$ (cm^2/g))	Uptake of coronene (mg/g of cat)	Pore diameter (\AA°)
NiMo 125 fresh	3.59	4.2	175
NiMo 125 spent	2.65	3.8	153
NiMo 325 fresh	2.02	13.4	62
NiMo 325 spent	1.31	11.9	52

In this case, the effectiveness factor is defined as the ratio of the observed rate to the intrinsic rate. These results show that the effectiveness factor decreased as pore size decreased, indicating more diffusion resistance in smaller pores. This confirms that the mobility of the reactants is hindered by pore size, indicative of a restrictive diffusion effect. The Z-value estimated from these measurements was 4.2, which is close to the hydrodynamic theory prediction and only slightly higher than the 3.7 value obtained from ambient diffusion studies [114] and lower than 4.9 obtained for pure solvents during hydrogenation [128]. This suggests that the effect of restrictive diffusion in the HT-CDL was less than in the pure solvents, which was attributed to a superior hydrogen donor ability of the former.

To investigate the cumulative effects of solvent and temperature, as well particle size and pore size upon restrictive diffusion rates, Lee et al. [128] performed

Table 22

Kinetic parameters for hydrogenation at 335°C and 50 atm H_2 [129]

Catalyst	Particulatesize (cm)	Rate constant (cc/g min)		Effectiveness factor	
		NTP	NBP	NTP	NBP
NiMo 125	0.175	2.79	3.68	0.29	0.18
NiMo 125	0.0181	8.99	16.5	0.94	0.83
NiMo 325	0.161	2.07	2.11	0.19	0.09
NiMo 325	0.0181	8.90	13.2	0.84	0.57
		Intrinsic rate constants (cc/g min)		Effective diffusivity ($D_e \times 10^6$ (cm^2/s))	
		NTP	NBP	NTP	NBP
NiMo 125	9.60	19.9	7.63	5.78	
NiMo 325	10.6	23.1	2.41	1.05	

NTP: Ni-tetraphenylporphyrin.

NBP: Ni-tetra(4-biphenyl)porphyrin.

Table 23

Apparent and intrinsic rate constants and effectiveness factors [128]

	Decalin				Mesitylene			
	300°C		350°C		300°C		350°C	
	NiMo-125							
Intrinsic rate constant cm ³ /(g min)	1.08		4.06		1.34		6.28	
Particle radius, cm	0.01	0.18	0.01	0.18	0.01	0.18	0.01	0.18
Rate constant (cm ³ /(g min))	1.04	0.22	3.81	0.66	1.32	0.39	5.99	1.17
Effective factor	0.96	0.20	0.94	0.16	0.98	0.29	0.95	0.19
	NiMo-225							
Intrinsic rate constant (cm ³ /(g min))	0.93		3.78		1.10		7.43	
Particle radius (cm)	0.01	0.18	0.01	0.18	0.01	0.18	0.01	0.18
Rate constant cm ³ /(g min)	0.85	0.13	3.21	0.37	1.06	0.23	6.67	0.92
Effective factor	0.91	0.14	0.85	0.10	0.96	0.21	0.90	0.12
	NiMo-325							
Intrinsic rate constant (cm ³ /(g min))	1.06		5.09		1.17		8.77	
Particle radius (cm)	0.01	0.17	0.01	0.17	0.01	0.17	0.01	0.17
Rate constant (cm ³ /(g min))	0.82	0.09	3.30	0.30	1.04	0.16	6.54	0.67
Effect factor	0.77	0.08	0.65	0.06	0.90	0.13	0.75	0.08

hydrogenation of Ni-TTP and Ni-TBP in mesitylene and decalin at 300 and 350°C, using the NiMo-125, NiMo-225 and NiMo-325 catalysts of Table 9. The results of hydrogenation of Ni-TBP at 5.27 MPa are shown in Table 23. The same set of results was also obtained for Ni-TTP. At higher temperatures, the intraparticle resistance becomes more important, since a larger increase in the reaction rate due to temperature rise occurs compared with that of intraparticle diffusion phenomena. The particle size effect was more significant with the NiMo-325 catalyst, which had considerably lower average micropore diameter than the NiMo-125 and NiMo-225 catalysts. The effective diffusivities were estimated using the relationship between effectiveness factor and Thiele modulus. These results are given in Table 24. It is again apparent that the mobility of both Ni-TTP and Ni-TBP was hindered by pore size. The lower viscosity of mesitylene at the experimental temperatures was one of the reasons for higher effective diffusivities compared with that in decalin. Also, for the former, the critical temperature had been approached. This was supported by the lower z parameter in mesitylene at 350°C compared with that in decalin. Lee et al. [128] concluded that the restrictive effect can be reduced by employing solvents with relatively low critical temperatures.

The results in Table 25, published by Johnson et al. [222] represent an extreme case of the low uptake of coronene caused by the loss of diffusivity due to catalyst deactivation. The three catalysts contained 2% Co and 7% Mo on different alumina supports. The catalysts in extrudate form were used in different hydroprocessing operations and contained coke and metal deposits, with a dense outer crust. A portion of each spent catalyst was crushed, and both extrudates and crushed particles were tested for diffusivity. As can be seen in Table 25, the extrudates had very low

Table 24

Effective diffusivities ($D_e \times 10^6$, cm^2/s) [128]

	Decalin		Mesitylene	
	300°C	350°C	300°C	350°C
	NiMo-125			
Ni-TTP	8.49	17.9	24.4	43.8
Ni-TBP	4.14	9.76	11.2	20.5
	NiMo-225			
Ni-TTP	2.32	6.36	9.10	15.7
Ni-TBP	1.57	3.24	4.88	10.4
	NiMo-325			
Ni-TTP	1.26	3.39	2.78	7.59
Ni-TBP	0.52	1.23	1.57	3.63

Table 25
Effective diffusivities and uptakes of coronene [222]

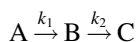
Catalyst	$D_e \times 10^{10} \text{ (m}^2\text{/s)}$			Uptake $\times 10^3 \text{ (kg/kg)}$		
	E	A	F	E	A	F
Crushed						
Support	4.3	5.0	5.9	11.6	8.8	6.9
Fresh	4.0	4.9	5.3	14.6	11.3	7.4
Aged	0.3	0.2	0.1	2.3	1.8	1.5
Regen.	1.3	1.2	0.5	7.2	5.7	5.2
Extrudates						
Fresh	4.1	5.1	5.1	11.6	10.9	8.3
Aged ^a	— ^b	<0.01	<0.01	—	—	—
Regen [*]	0.2	0.1	0.1	—	—	—

^a D_e value based on uptake values for crushed catalysts.

^b Too slow to measure.

diffusivities. However, the crushed catalysts exhibited appreciably larger diffusivities, indicating that the outer crust was extremely impervious. Regeneration improved the parameters but the original values could not be attained, confirming that the metal deposits were a main contributor to deactivation.

Several studies were published on the kinetics of HDM of petroleum residues, in which case diffusional phenomena are almost certainly present. Beaton and Bertolacini [188] used a first-order reaction expression to describe the overall HDM of V and Ni. They found the HDM of V to be faster than that of Ni. Similarly, the work published by Bartholdy and Hannerup [223] used an atmospheric residue to study removal of V. These authors combined the rate constants and diffusional parameters into the same equation, assuming a sequential first-order reaction network for HDM, i.e.,



In this network, the first step involves hydrogenation of the porphyrins, whereas the second step is a reaction between the hydrogenated porphyrins and H_2S , leading to metal sulfide deposits. For the concentration through the reactor, the following kinetic expression was derived:

$$\frac{C_B}{C_A} = \delta(1 - e^{-(k_{2e} - k_{1e})U/Fy}) \quad (5.8)$$

where C_A and C_B are concentrations of A and B in the bulk phase outside the catalyst, respectively, U is volume of catalyst, F flow rate of the feed, y the length of catalyst bed and $\delta = k_1/k_1 + k_2$. It was

assumed that k_1 and k_2 are proportional to partial pressure of H_2 and H_2S , respectively. In these equations, k_2 and k_{2e} , k_1 and k_{1e} are the rate constants for the intrinsic and diffusion limited operations, respectively. While applying this approach to V removal, Bartholdy and Hannerup [223] observed that the simple first-order reaction $A \rightarrow B$ is the rate-controlling step.

The HDM of an atmospheric residue was simulated by Bourseau et al. [224]. The parameters used in the model include the Thiele modulus, minimum and maximum pore diameter (R_m and R_M , respectively), effective diffusivity, ratio of particle length to twice radius (α), and ratio of the radius maximal to minimal (β). As the results in Fig. 85 show (solid line), the

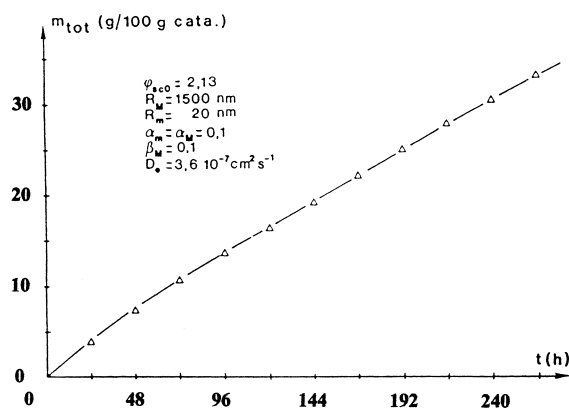


Fig. 85. Experimental (Δ) and computed (—) values of total mass of metal sulfide deposited [224].

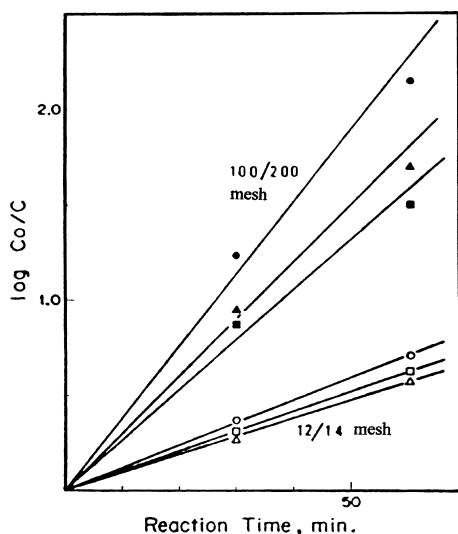


Fig. 86. First-order plot of reactions; (○●) HDV, (△▲) HDNi, (□■) HDasph. [225].

removal of V and Ni could be predicted quite well by the model. Kobayashi et al. [181,225] compared the intrinsic and diffusion controlled HDM using two different particle sizes of 1.3 and 0.11 mm, during hydroprocessing of an atmospheric residue. As the results in Fig. 86 [225] show, the experimental results agreed well with the predicted values (solid lines). The prediction was made using the following first-order equation:

$$\ln \frac{C_0}{C} = \frac{W_e S}{V_r} k t \quad (5.9)$$

where C_0 is the initial concentration, C the concentration after 30 and 60 min, W_e the catalyst weight, S the surface area, V_r the reaction volume, k the rate constant and t the time. Fig. 86 reveals that all reactions can reasonably be expressed by first-order kinetics. The effect of particle size on the overall HDM is quite evident. Based on these results, Kobayashi et al. [225] determined the effect of particle size on the effectiveness factor (k/k_i) for removal of V and Ni (Fig. 87). In a similar study, Reyes et al. [226] made an attempt to predict the effect of the amount of deposited V on the apparent rate constant. As demonstrated in Fig. 88, first-order HDM kinetics were confirmed over a wide H_2 pressure range [227].

The kinetics of removal of V from several atmospheric residues was investigated by Sughrue et al.

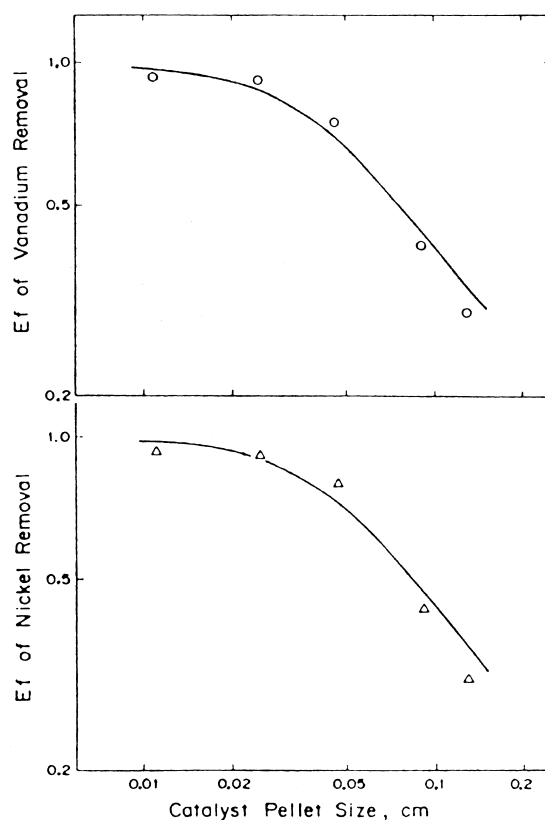


Fig. 87. Relationship between effectiveness factor and pellet size during HDNi [225].

[209]. In Fig. 89, a plot of first-order kinetics in an isothermal, plug flow reactor shows excellent fits of

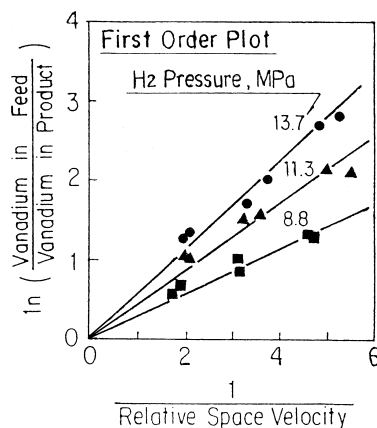


Fig. 88. Effect of H_2 pressure on first-order plot of V removal [227].

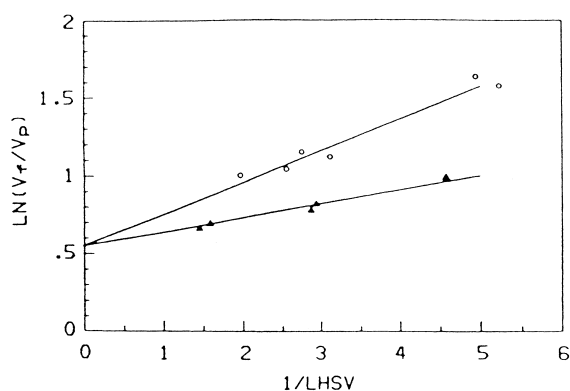


Fig. 89. Effect of temperature on HDV kinetics: (○) 644 K; (▲) 616 K [209].

the data at both 616 and 644 K. However, the intercept for both lines was not zero, (as it should be for true first-order kinetics) and is indicative of adsorption inhibition by V-compounds. Oleck and Sherry [215] reported that their HDM data could be best correlated when they assumed reactive and nonreactive fractions of V. If parallel, first-order kinetics with two types of V, i.e., slow reacting and fast reacting, were assumed, the following equation applies when there is no fast reacting V left:

$$\ln\left(\frac{V_f}{V_p}\right) = \frac{k}{LHSV} + \ln\left(\frac{V_f}{V_{sr}}\right) \quad (5.10)$$

where V_f , V_p and V_{sr} are V in the feed, products and slow reacting V, respectively, and k is the rate constant. Sughrue et al. [209] used Eq. (5.10) to plot $\ln(V_f/V_p)$ versus $\ln(1/LHSV)$ for both parallel first-order and simple first-order reaction models. These results are shown in Fig. 89. For the simple first-order reaction model, where V is the total vanadium in the feed, the value of the slope (order) varied between 0.4 to 0.7, whereas for the parallel first-order kinetics the value of the slope was one, indicating ideal reactor behavior.

Rajagopalan and Luss [219] derived several mathematical models to simulate HDM reactions without comparing their models with the experimental data. They proposed the following equation for the rate of the deposit formation:

$$\frac{dm}{dt} = \alpha 2\pi r_p k C M \quad (5.11)$$

where m is metals removed at time t , α is the number of metal atoms per reactant molecule; r_p is the actual

pore radius; k is rate constant; and C is the concentration and M molecular weight of the metal sulfide. The volume of the metal sulfide can be calculated from its amount and density and can be used for estimating the change in porosity. The above equation was rewritten by Pereira and Beeckman [228] in the following form to test the experimental data from the HDM of a vacuum residue derived from the Boscan crude:

$$\frac{df_m}{dt} = -\frac{2kCM_d u_m}{d_m^0 \rho_d} \quad (5.12)$$

where f_m is the fraction of the initial micropore diameter (d_p^0) that is still available for diffusion, C is the concentration of metals in the feed, M_d is the molecular weight of the deposit, u_m is the dimensionless metal concentration in the feed normalized with respect to the reactor inlet concentration and, ρ_d is the deposit density. The model used by these authors assumes a random distribution of the macropores and that the metal bearing molecules can enter the micropores only through macropores. However, this assumption breaks down when the catalyst has very low macroporosity. In this case, diffusion into the particle through micropores becomes important. The local weight of deposit per unit area of catalyst surface is given by

$$w = \frac{d_i^0(1 - f_i^2)\rho_d}{4} \quad (5.13)$$

where $i = m, M$ subscripts are for micropores and macropores, respectively. Thus, the total weight of deposits is obtained by summing up the deposits in the micropores and macropores. The isothermal HDM reactor was modelled as a series of mixing cells based on the equation of Pereira et al. [229] discussed above. Fig. 90 shows that the model predictions were quite accurate during the first ten days. It is noted that after 6 days on stream, temperature was raised from 644 to 672 K. Interparticle deposits were found at the end of the runs. When this was taken into consideration, the prediction improved significantly. Similar predictions were made for cylinder and minilith catalyst shapes.

Attempts to develop models for predicting the HDM kinetics began several decades ago. A number of important studies appeared in the scientific literature [1,123–125,230–238]. These and other studies have been cited by other researchers and discussed in some previous reviews on catalyst deactivation. New

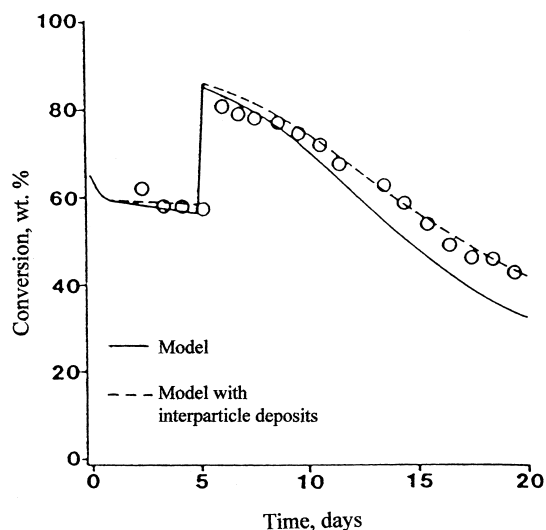


Fig. 90. Experimental (○) and predicted HDM conversion (644 and 672 K, 14.0 MPa) [229].

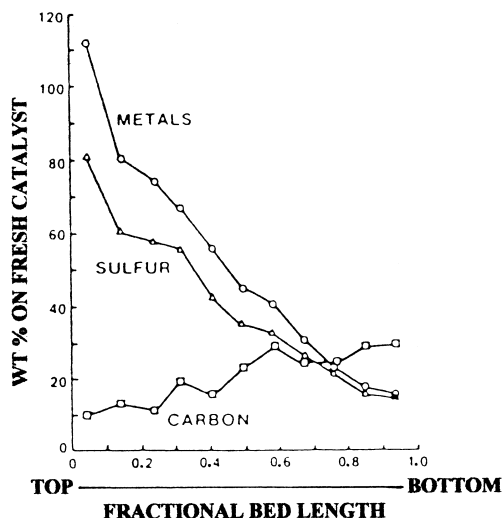


Fig. 91. Distribution of metals (V + Ni), carbon and sulfur through bed length [239].

concepts for explaining HDM reactions have also been introduced. For example, Macé and Wei [237] suggested that it is more realistic to model HDM by assuming the catalyst comprises random spheres and/or needles rather than cylindrical pores. These authors have proposed four models for predicting the catalyst performance, i.e., random sphere model, random needle model, discrete percolation and continuous random walk.

5.1.3.3. Radial profiles of V and Ni. Diffusion controlled kinetics implies that the cross-sectional distribution of V and Ni will change during the HDM reaction. This will result in a nonuniform distribution of metals. Among several parameters, hydroprocessing conditions can influence the distribution of metals. The position of the catalyst in the reactor bed is also important, as shown in Fig. 91 published by Simpson [239]. Thus, the largest deposition of metals occurs at the inlet of the bed and then decreases while approaching the reactor exit. As expected, sulfur exhibits the same trends as metals, whereas carbon deposition exhibits the opposite trend.

It was estimated by Wei [240] that if a uniform distribution is assumed, 20 wt.% of coke and 20 wt.% of a V sulfide deposited on a catalyst having about 200 m²/g of surface area would represent 5–6 ML

(monolayers) equivalent of deposits. This would result in complete covering of the catalyst surface. In spite of such deposit, the catalyst still retains some activity. This can be reconciled by assuming either a nonuniform distribution or the presence of large crystallites of metal sulfides. It was suggested that there is a fixed number of nucleation sites where the depositions can occur and then these crystallites grow in size with time [241,242]. Apparently, the metal species are present as large crystallites several hundreds of Angstroms in length rather than as a uniform layers.

Tamm et al. [1] suggested that the radial profiles of metals can be characterized by a distribution parameter defined as:

$$\Theta_m = \frac{\int_0^1 M(r) r dr}{M_{\max} \int_0^1 r dr} \quad (5.14)$$

In this equation, $M(r)$ is the local radial concentration of metal deposit in the catalyst particle; M_{\max} is the maximum concentration and r is the fractional radius. The Θ_m is the ratio of the average metal concentration to the concentration at the maximum. The validity of this parameter was tested during hydroprocessing of an atmospheric residue. Samples of the catalyst were periodically withdrawn from the inlet, middle and outlet of the reactor for analysis of metals by electron microprobe. Examples of the metal

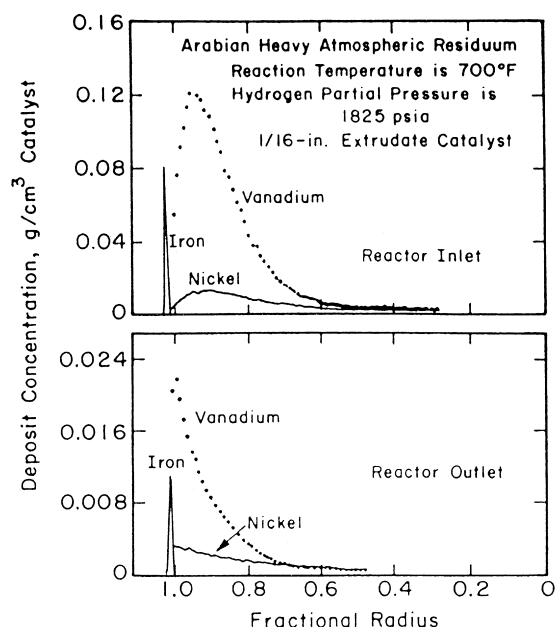


Fig. 92. Typical deposition patterns for Ni, V and Fe [1].

profiles are shown in Fig. 92 [1]. Similar trends were established by Janssens et al. [243]. These results were used for estimating the parameter at different intervals of the run. The change in the parameter with time on stream is shown in Fig. 93. These results show that metals have less access to the interior of the catalyst extrudate with time on stream. Also, Ni penetrates the interior more than V. The results further show that the metal deposition is the largest at the inlet and smallest at the outlet of the catalyst bed, in agreement with the results in Fig. 91 [239]. The operating parameters also

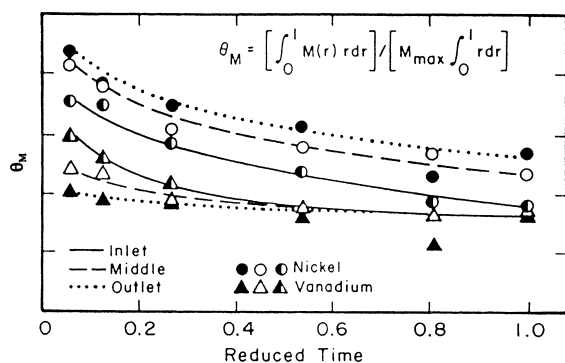
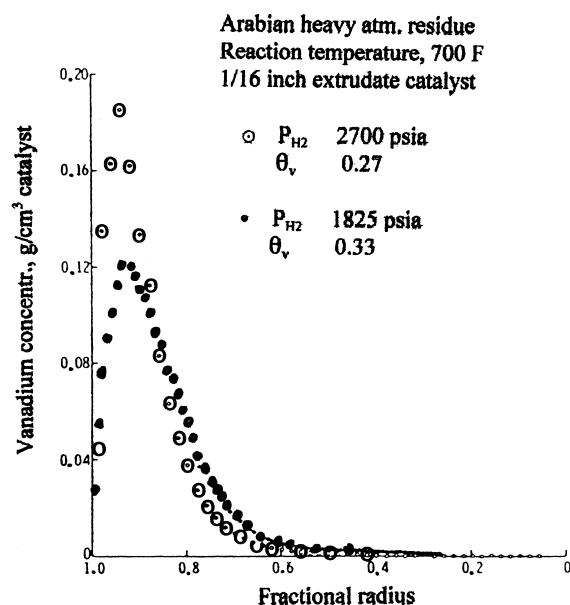
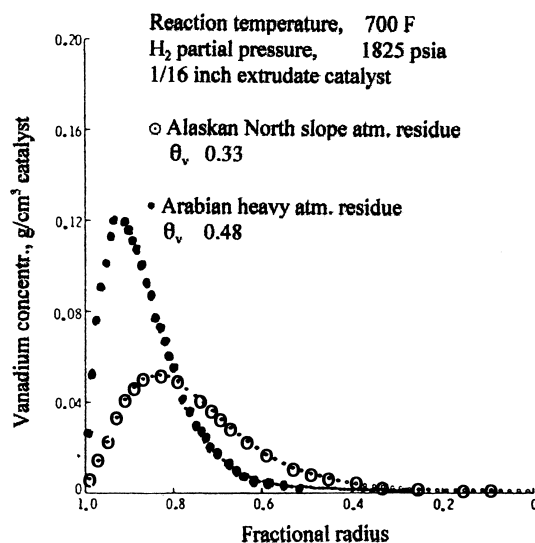


Fig. 93. Ni and V distribution parameters as a function of reactor position and time [1].

Fig. 94. Effect of H₂ partial pressure on V deposition; (○) 19.0 MPa H₂ and Θ_v of 0.27, (●) 12.8 MPa H₂ and Θ_v of 0.33 (Arab. heavy atm., res., 644 K) [1].

influence the metal profiles. Examples of the effect of hydrogen pressure and type of feed are shown in Figs. 94 and 95, respectively.

Fig. 95. Effect of the feed type on V deposition (●) Arab. heavy atm. res. and Θ_v of 0.33, (○) Alask. North Slope atm. res. and Θ_v of 0.48 (644 K, 12.8 MPa H₂) [1].

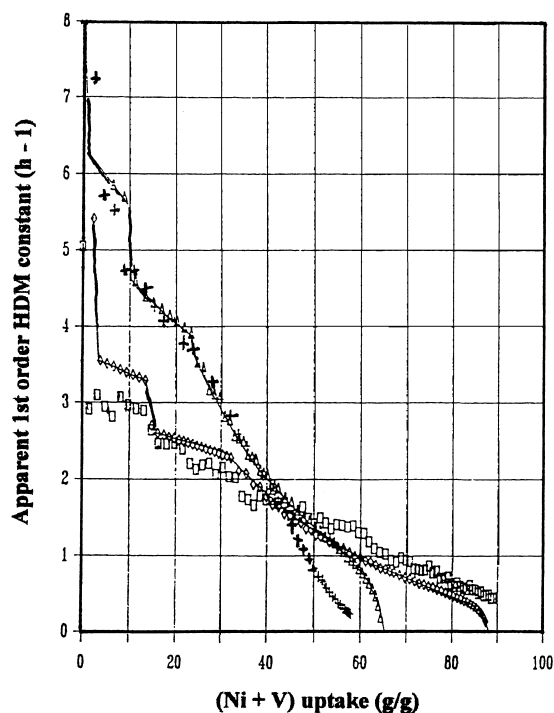


Fig. 96. Comparison of simulated and experimental data for HDM aging test results; (□) 653 K experimental, (◇) 653 K simulated, (+) 673 K experimental, (△) 673 K simulated [245].

The usefulness of the Θ_m parameter has been recognized by many researchers. For example, Toulhoat et al. [244,245] correlated the Θ_m parameter with experimental results, such as the relative first-order rate constant and surface area from simulated aging. As the results in Fig. 96 show, a discontinuity appears in the first derivative of the Θ_m parameter between 30–40% metal loading. This indicates that the ultimate metal storage capacity of the catalyst is being approached. Bartholdy and Hannerup [223] have related the distribution parameter to the rate constants for the sequential reaction network discussed earlier in the form of the following equation:

$$Q_m = p \frac{C_A}{C_B} \frac{k_{1e}}{k_1} + \left(1 - p \frac{C_A}{C_B}\right) \frac{k_{2e}}{k_1} \quad (5.15)$$

where $p = k_1/k_1 + k_{2e}$. When the equilibrium value $C_B/C_A = p$ has been reached, $Q_m = k_{1e}/k_1 = 1$. As the results in Fig. 97 show, the efficiency of the V removal could be correlated with the distribution parameter. Moreover, the results in Fig. 98 indicate a potential for

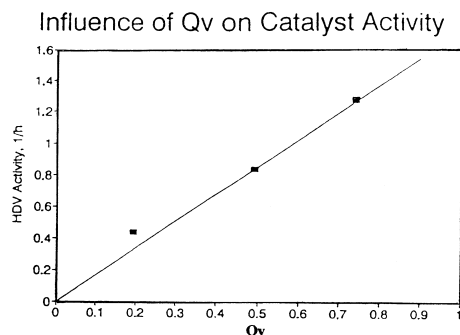


Fig. 97. Effect of distribution parameter on V removal [223].

predicting the Q_m value from the Thiele modulus. Hung et al. [246] showed that the optimum distribution factors for an HDM catalyst is case specific and is determined by feed properties, process conditions and product quality requirements.

Wei et al. [200,247] reported deposition profiles from the HDM of Ni- and V-etio porphyrins using 1/16 in extrudates of a CoMo/Al₂O₃ catalyst in various positions in the catalyst bed. For both porphyrins, so-called M profiles were observed at the entrance of the catalyst bed with a gradual change to the U-shape profile while approaching the end of the bed. In Fig. 99 [48], the internal maximum of the M-shape profile was much sharper in the case of Ni as compared to V. The experimental data was compared with that obtained by a model. The work was later expanded to compare an oxidic form of the CoMoAl₂O₃ catalyst with its sulfided form [48,200]. For this purpose, Ni-etio and -N3TPP porphyrins were used. As the results in Fig. 100 [200] show, the profile of Ni deposits

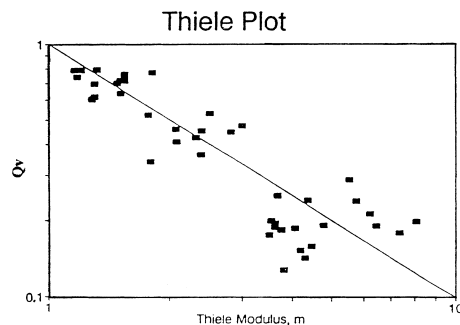


Fig. 98. Correlation between distribution parameter and Thiele modulus [223].

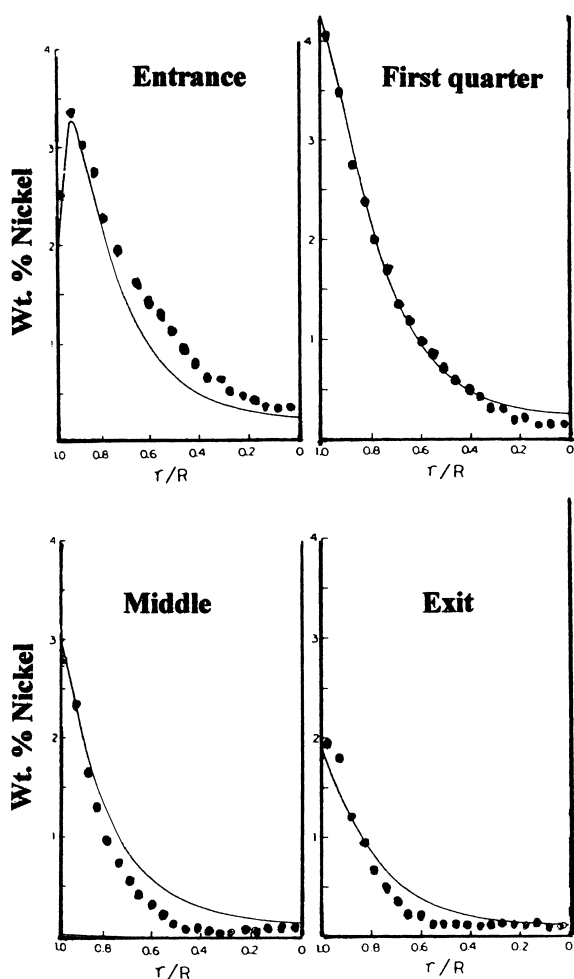


Fig. 99. Ni-deposition profiles in 1.6 mm pellet at various axial positions; solid lines from model calculations (CoMo/Al₂O₃ sulfur, 618 K, 6.99 MPa H₂) [48].

varied across the catalyst bed confirming previous findings. The solid lines represent a prediction based on the model developed by the authors. For sulfided catalyst, the Ni maximum in the M-shape profile shifted towards the outer edge of particles. The M profile at the entrance is explained by the absence of the deposit species in the oil at the entrance. Thus, such species have to be first formed by hydrogenation while reactant molecules diffuse into pores. The shift in the Ni maximum to the exterior is consistent with the higher HDM rate in the presence of the sulfided catalyst. The Ni deposition profile was influenced by

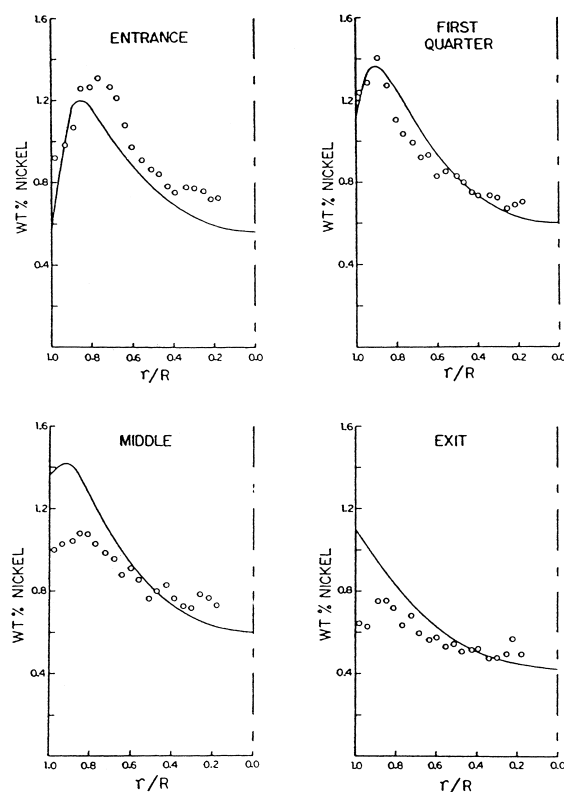


Fig. 100. Ni-deposition profiles in 1.6 mm pellet at various axial positions (all the same as in Fig. 99 except CoMo/Al₂O₃ sulfur) [200].

various catalyst pretreatments, e.g., doping with Na and Cs and halogenation [248]. The observations made by Agarwal and Wei [247] are in general agreement with the results published by Tamm et al. [1]. Internal maxima were also reported by other authors [249–251]. Other studies have shown that V forms a U-shape profile, whereas Ni tends to be more uniformly distributed [252–254]. Considering the number of parameters influencing HDM, i.e., feed and catalyst characteristics as well as experimental conditions, the reported differences in the metal profiles are not surprising.

A simple pore-plugging model developed by Oye-kunle and Hughes [255] was based on second-order HDM kinetics [136,256–259]. Later, this model was modified and used for estimating the effectiveness factor for HDM, metal deposition thickness within the catalyst pores, radial distribution of metals, cata-

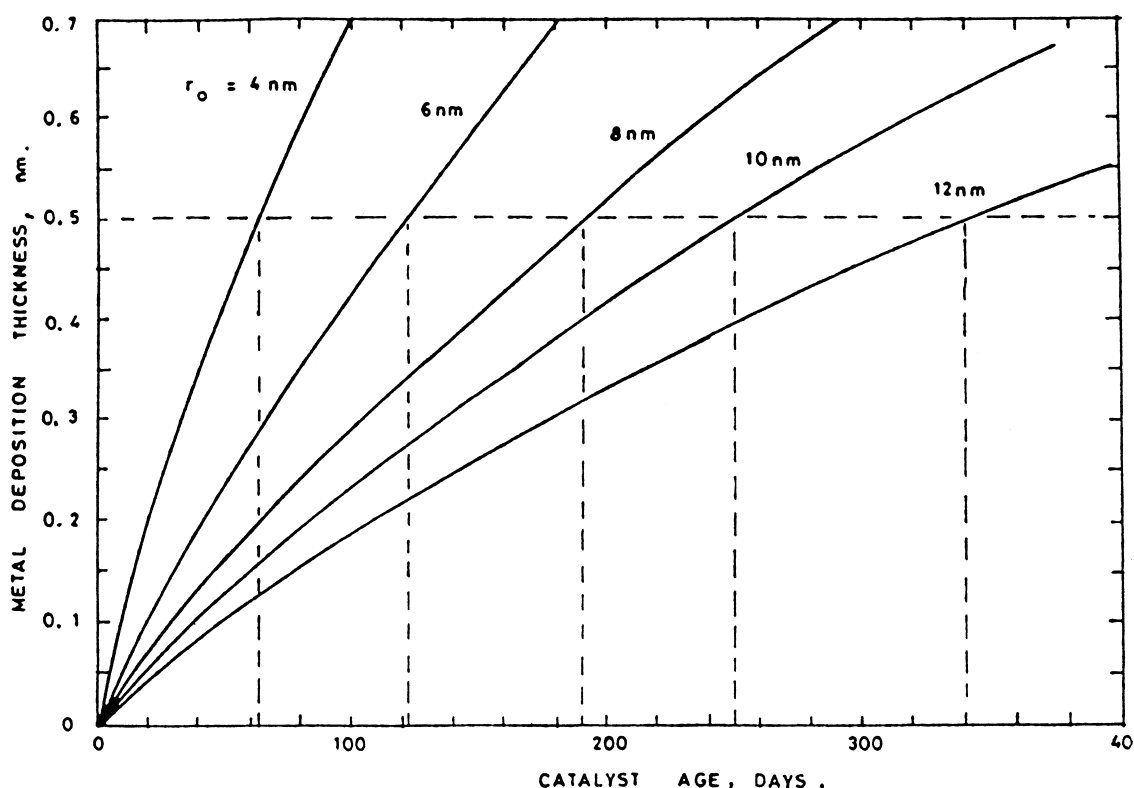


Fig. 101. Metal deposition thickness as a function of catalyst age [255].

lyst age and the rate of HDM. The thickness of the metal deposits m was computed from the following equation:

$$m = r_0 \left(1 - \frac{r}{r_0} \right) \quad (5.16)$$

where r is the instantaneous pore radius and r_0 is the initial pore radius. Fig. 101 [255] shows that the metal deposition thickness increases with time on stream. Also, metal deposition decreases with increasing pore size for catalysts of the same age. These results further indicate that with decreasing average pore diameter of catalysts, the radial profiles of metals will get sharper. Melkote and Jensen [260] used the pore plugging model to study the evolution of topological properties assuming two modes of metal deposition, i.e., uniform and discrete. Apparently, the former would cause a rapid deactivation, contrary to experimental observations. Thus, both site coverage and pore plugging were considered, similar to that by Sahimi and Totsis [258]

and Beeckman and Froment [233,234]. The model can describe the birth and propagation of the pore plugging 'wave' through the particle, and relate this to experimentally measured deposition profiles. Melkote and Jensen [260] used the experimental results published by other authors [1,245,259] to test their models. The best fit was obtained when the discrete deposition mode was applied.

The percolation model, based on the regular discrete Bethe network was used by Janssens et al. [261] and Sahimi et al. [262] to study the effect of the diffusion coefficient on the distribution of V during the HDM of VO-TPP. The maximum in the V profile was shifted to the edge of the particle with decreasing diffusion coefficient (Fig. 102). For bulk diffusion, the deposition occurred at the center of the catalyst pellet indicating that the deposition process is reaction rate determined. With decreasing diffusivity, the metal deposition process becomes more diffusion rate determined.

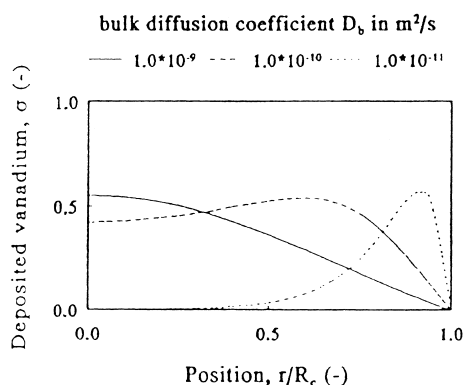


Fig. 102. Influence of bulk diffusion coefficient on metal deposition profiles [261].

5.1.4. Effect of V and Ni Deposits on Activity

This topic of catalyst deactivation is well documented in the scientific literature. Information is available on the activity of the aged catalysts determined during hydroprocessing of model compounds as well as real feeds.

5.1.4.1. Effect on HDM. As the results in Fig. 103 show, the rate of deactivation can be influenced by the catalyst properties [210]. The type of the feed, reaction conditions, and the content of V and Ni in particular are important for the rate of deactivation. The rate of HDM will gradually decline with progressive deposition of V and Ni. At a certain point, the metals will end up in the products. This issue was considered by Toulhoat et al. [245] in a study of a feed

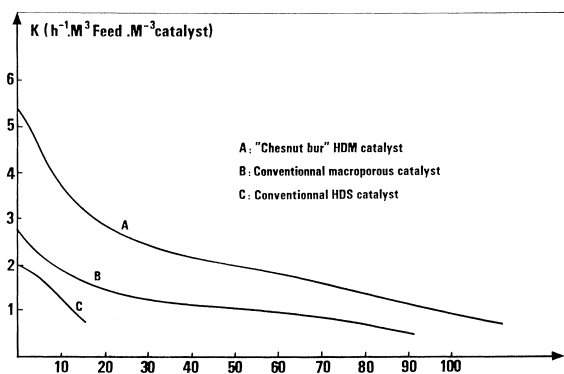


Fig. 103. Relationship between HDM rate and the amount of adsorbed metals for different catalysts [210].

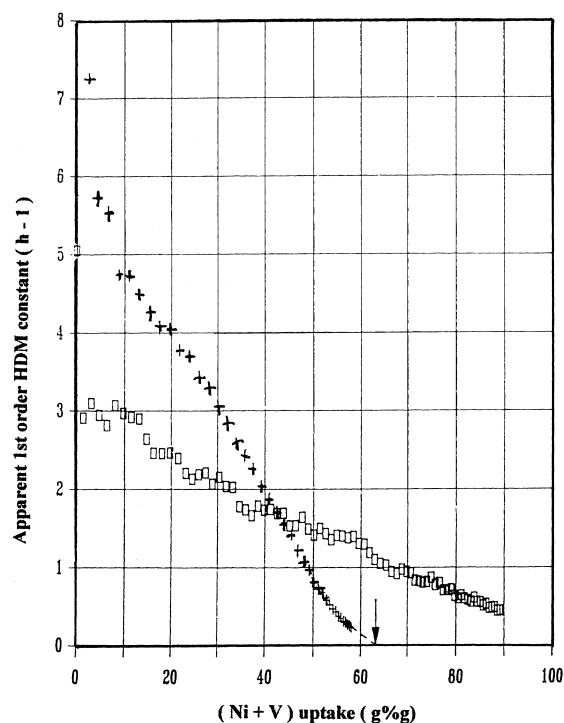


Fig. 104. Apparent first-order constant for HDM (h^{-1}) vs. (Ni + V) uptake (g/g); \square – 380°C , $+$ – 400°C [245].

derived from Boscan crude containing 620 ppm of V + Ni. The results in Fig. 104 indicate significant differences in deactivation at two temperatures. At about 40% metal loading, the deactivation curves crossed and the rate constant approached zero at about 65% loading at 400°C , whereas at 380°C the catalyst did not lose all activity even at 90% metal loading. The authors attempted to simulate the experimental results using a deactivation model, which takes into account the ultimate storage capacity of the catalyst for V + Ni, its textural properties, initial activity and selectivities, the dimensions of the pellets and the reactivity of the feed.

5.1.4.2. Effect on catalyst activity. Ledoux and Hantzer [263] conducted a detailed study of catalyst deactivation using model compounds containing V and Ni. One series of samples was prepared by impregnation of a $\text{NiMo}/\text{Al}_2\text{O}_3$ catalyst with a water solution of ammonium vanadate and nickel

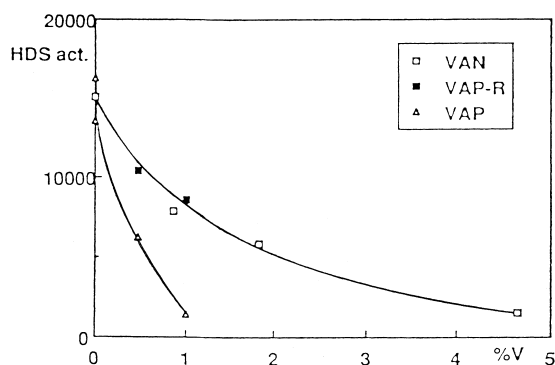


Fig. 105. Effect of vanadium content on HDS activity (NiMo/ Al_2O_3 , 500 K, near atm. H_2) [263].

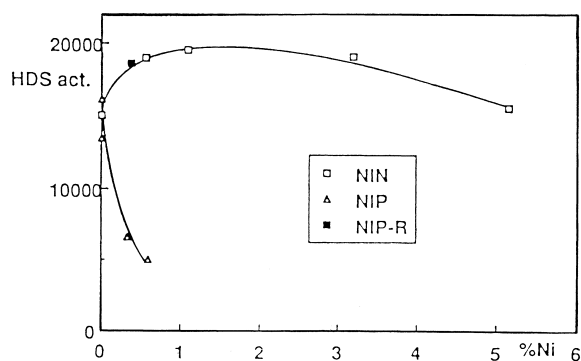


Fig. 106. Effect of nickel content on HDS activity (conditions as in Fig. 105) [263].

nitrate. This series was designated as VAN-X and NIN-X for samples containing V and Ni, respectively. The X in this designation represents the approximate amount of the metals in wt.%. For another series of samples, porphyrin from a toluene solution was deposited on presulfided extrudates of the catalyst. After removing the solvent, the impregnated extrudates were sulfided in the reactor at 450°C in a $\text{H}_2\text{S}/\text{H}_2$ mixture. These samples were designated as VAP-X and NIP-X. Finally, H_2 -porphyrin without metal (VAP-O) was deposited on the catalyst. After determining the HDS activity of thiophene, the VAP and NIP catalysts were regenerated and subsequently resulfided. These samples are designated as VAP-XR and NIP-XR. Fig. 105 shows the effect of the V content on the HDS activity. It is evident that the VAP samples were much more deactivated by the same amount of V than the VAN samples. However, upon regeneration, the activity of the VAP-R approached that of the VAN. These results indicate that V-porphyrin deactivates the catalyst much more than the impregnated V, and that upon oxidative regeneration, the V-porphyrin is converted to V species similar to impregnated V. As shown in Fig. 106, very different behavior is observed for the Ni-containing samples. In this case, the NIN samples were more active than the original catalyst, whereas the NIP samples followed similar trends as the VAP samples. The beneficial effect of the additional Ni was attributed to its association with the active phase of the catalyst. The HDS activity of the VAP-0 and H_2 -porphyrin, i.e., species containing no metals, decreased only slightly compared with the

catalysts impregnated with a similar amount of the metal containing porphyrins.

Dejonghe et al. [264] studied the effect of V on the HYD activity of toluene. Rather than impregnate the catalysts, these authors deposited V during the HDM of VO(OEP) under typical hydroprocessing conditions. Thus, the HYD activity was determined at the end of the HDM experiments of different durations. The results of these tests are shown in Fig. 107. For the NiMo/ Al_2O_3 catalyst, the HYD activity is almost constant up to 2% V, and then begins to decline slowly. For the Mo/ Al_2O_3 catalyst, the activity increased, but never reached that of the NiMo/ Al_2O_3 catalyst. This is consistent with the results published by Guillard et al. [265], who observed some catalytic activity of the V sulfides for several hydroprocessing reactions. Little activity was observed on the bare Al_2O_3 .

Kim and Massoth [266] studied the effect of V on a CoMo/ Al_2O_3 catalyst activity. One series of V deposited catalysts (V-IMP) was prepared by impregnation using ammonium metavanadate dissolved in an aqueous oxalic acid solution, and the other series by reaction of VO-TPP with the catalyst under hydroprocessing conditions. As seen in Fig. 108, a relatively small amount of V introduced by impregnation drastically deactivated all catalyst functionalities. The V-TPP deactivation data do not exhibit a smooth decay, but an apparent line out in activity above about 2% V. The temperature increase required to compensate for deactivation is shown in Fig. 109. Again, the difference between the V-IMP and V-TPP series is quite evident. It is obvious that the impregnation ensures more uniform distribution of V in the particle. The

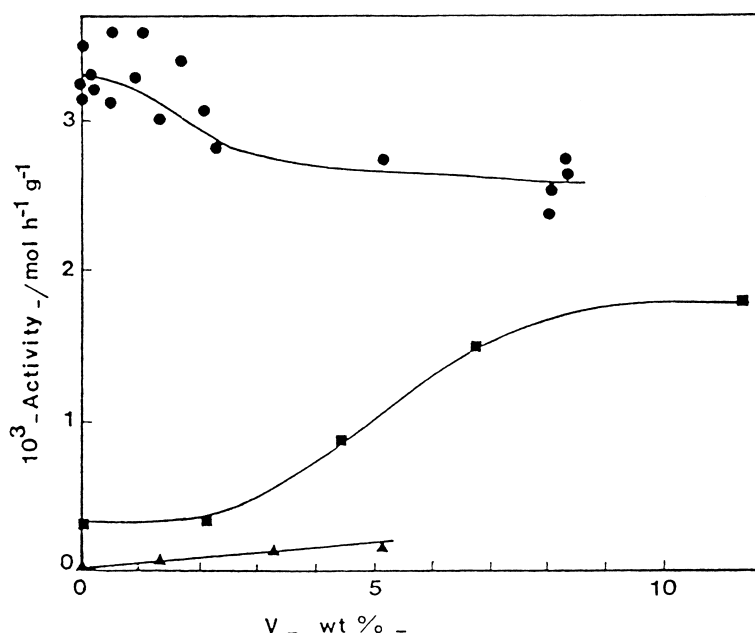


Fig. 107. Effect of vanadium on toluene hydrogenation activity (● – NiMo/Al₂O₃, ■ – Mo/Al₂O₃, ▲ – Al₂O₃, 623 K, 10 MPa) [264].

HYD and CNH activities increased, while the HDS activity was maintained at 48% by the temperature increase. This was attributed to higher activation energies of the HYD and CNH functionalities. Moreover, as the results in Fig. 110 show, the activation energy for CNH goes through a maximum, while that of HYD shows little change, and that of HDS shows a small increase with increasing V content.

The effect of V and Ni sulfides on the activity of a NiMo/Al₂O₃ catalyst was investigated by Diez et al. [105]. The catalysts were impregnated with Ni and V naphthenates from a toluene solution. Subsequently, the catalysts were dried and calcined under controlled conditions. Electron microprobe analysis showed that both the V and Ni were uniformly distributed throughout the particle. After sulfidation, the fresh and metal-deposited catalysts were used to determine the activity for HDS, HDN and HYD of dibenzothiophene, quinoline and naphthalene, respectively. In every case, V and Ni had little effect on the reaction network, but affected the individual rate constants. Thus, the added Ni had little effect on hydrogenation of naphthalene and hydrogenolysis of dibenzothiophene, while the added V decreased the rate constants in the former and increased those in the hydrogenation network of

dibenzothiophene. The added V enhanced cracking activity, whereas the added Ni had little effect. The authors attempted to predict deactivation by using a process model. They concluded that Ni and V deposits have to be considered separately in the model.

Ammus et al. [161] compared three different particle sizes of a commercial CoMo/Al₂O₃ catalyst, i.e., 1/8-in., 1/16-in. and pulverized with a mean particle diameter of 0.34 mm, during the hydroprocessing of an atmospheric residue containing 9 and 11 ppm V and Ni, respectively. Another CoMo/Al₂O₃ catalyst was used in two different particle sizes. The effect of coke and metals on catalyst properties are given in Table 26 for the pulverized sample. After 70 h on stream, almost all surface area and pore volume could be recovered on regeneration, indicating that coke was mainly responsible for the decrease of these parameters. At the same time, the mean pore diameter decreased by about 25%, suggesting that metals were depositing near the pore mouth. However, the recovery of surface area and pore volume decreased significantly after 200 h on stream. These results suggest that up to a certain level of metal deposits, the surface area and pore volume of the catalysts are unaffected. These effects were less pronounced for larger particles,

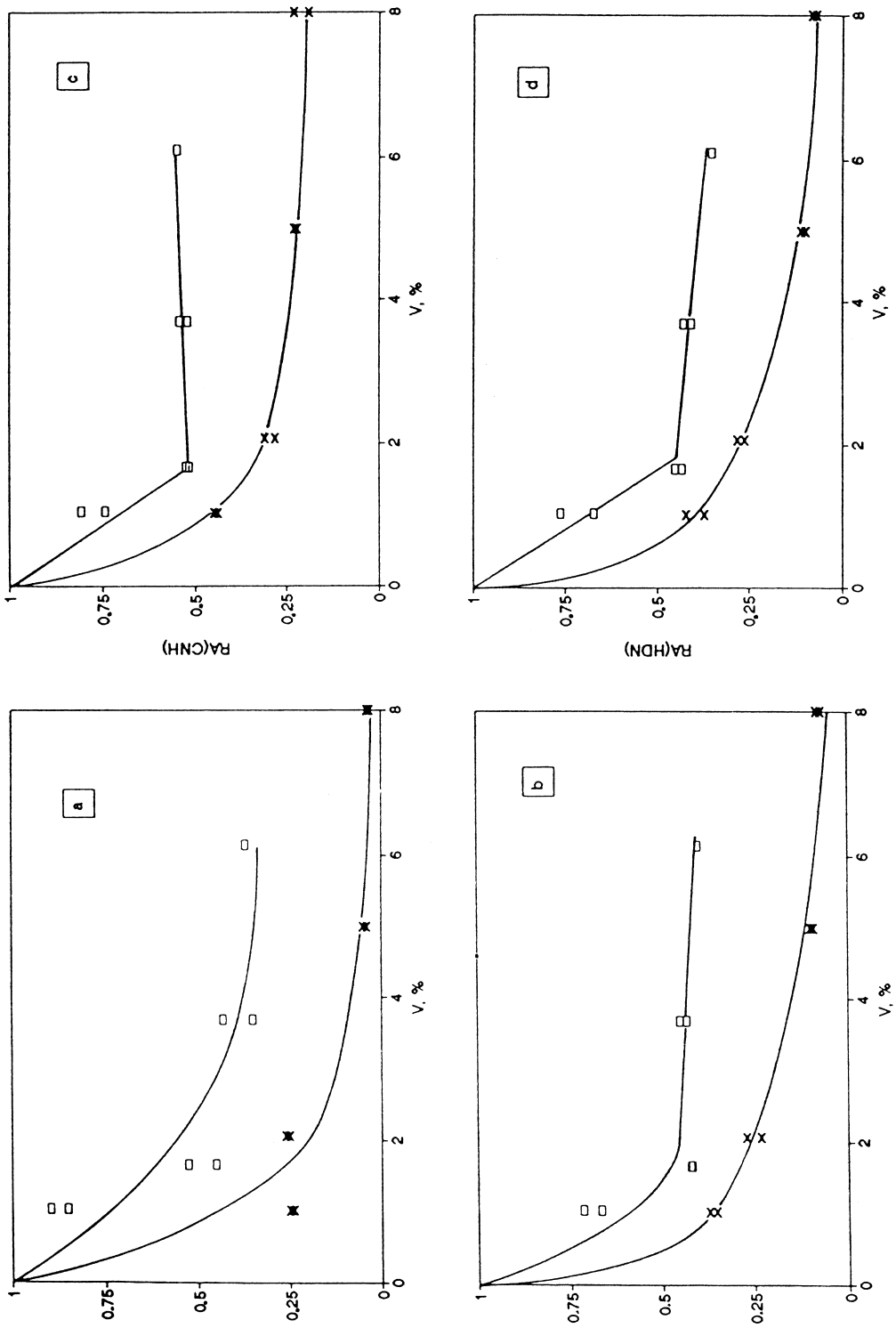


Fig. 108. Relative activity (RA) vs. vanadium content of catalysts for (a) HDS; (b) HYD; (c) CNH and (d) HDN: x – V-IMP, * – V-TTP (NiMo/Al₂O₃, 623 K, 3.5 MPa H₂) [266].

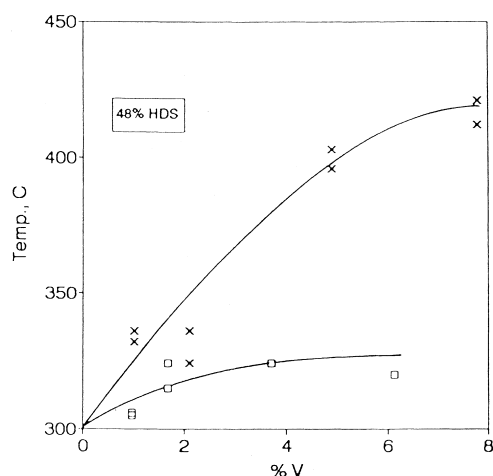


Fig. 109. Effect of vanadium content (V-IMP) of catalyst on temperature for 48% HDS conversion (conditions as in Fig. 108) [266].

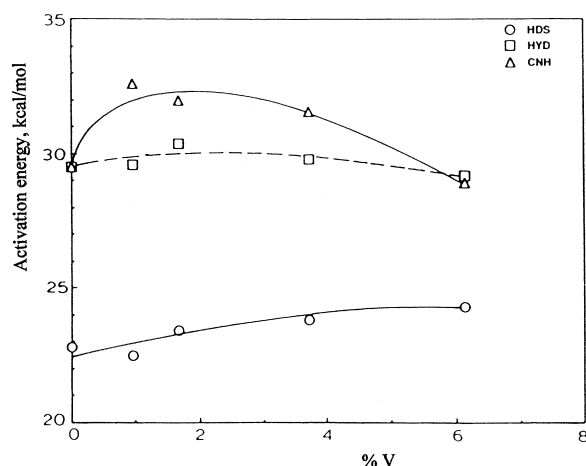


Fig. 110. Activation energies vs. vanadium content of (V-TPP) catalysts [266].

mainly due to the fact that less coke and metals were deposited. Supporting evidence for these observations was published by Wukasz and Rase [267].

Ammus et al. [161] also correlated relative HDS activities of CoMo/Al₂O₃ catalysts with the amount of coke and metal (V + Ni) deposits. As the results in Figs. 111 and 112 show, for the pulverized catalyst, 25 wt.% coke and 0.7 wt.% metal deposits, respectively, developed before a measurable activity loss was detected. Further increase in the deposits caused an almost linear activity loss. The more pronounced loss of activity observed for the extrudate samples is in line with the presence of diffusional phenomena. In a similar study, Koyama et al. [268] studied hydroprocessing of a vacuum residue in a reactor consisting of four beds in series. The samples of spent catalysts

were taken after 22 weeks, except for one sample taken from bed 3 after two weeks. Properties of the spent catalysts are shown in Table 26. The adverse effect of both coke and metal deposits is quite evident. The effect of metal deposits on relative activity obtained from these results is shown in Fig. 113. Subsequently, the catalysts were regenerated and compared with the spent catalysts for HDS, HDN and hydrogenation of model compounds. The summary of these experiments is shown in Fig. 114. Comparison of Fig. 114 with Table 27 suggests that the detrimental effect of metals increases with their content in the catalyst.

Inoguchi et al. [251] evaluated three catalysts after about 3000 h of operation during the hydroprocessing a Kuwait atmospheric residue containing 53 ppm V

Table 26
Effect of coke and metals on catalyst properties [161]

Time on stream (h)	Coke (CHN) (wt.%)	Metals (wt.%)		Surface area (m ² /g)	Pore volume (cm ³ /g)	Pore diam. (Å)
		V	Ni			
0 fresh				215	0.442	86
30 spent		0.532	0.178	146	0.219	36
Regenerated				221	0.465	74
70 spent	28.9	0.986	0.222	111	0.188	36
Regenerated				208	0.429	64
200 spent	31.6	2.028	0.884	26	0.047	36
Regenerated				141	0.323	56

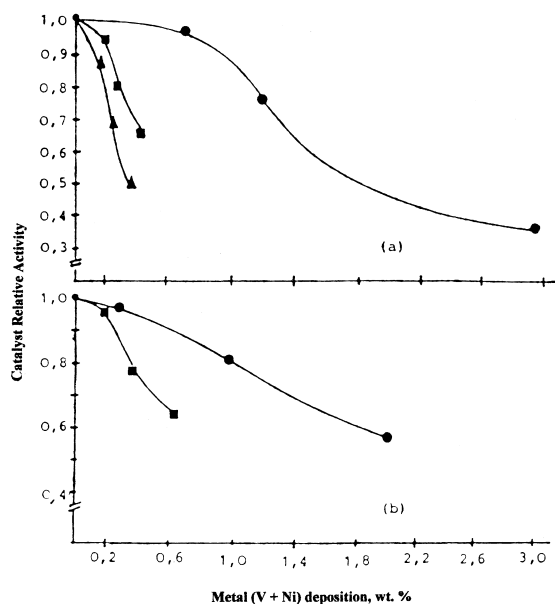


Fig. 111. Catalyst relative HDS activity vs. metal (V + Ni) deposit; (a) CoMo/Al₂O₃ of 0.414 bed void, (b) CoMo/Al₂O₃ of 0.472 bed void, ● – pulverize, ■ – extrudates 1/16-in., ▲ – extrudates 1/8-in. (623 K, near atm. H₂) [161].

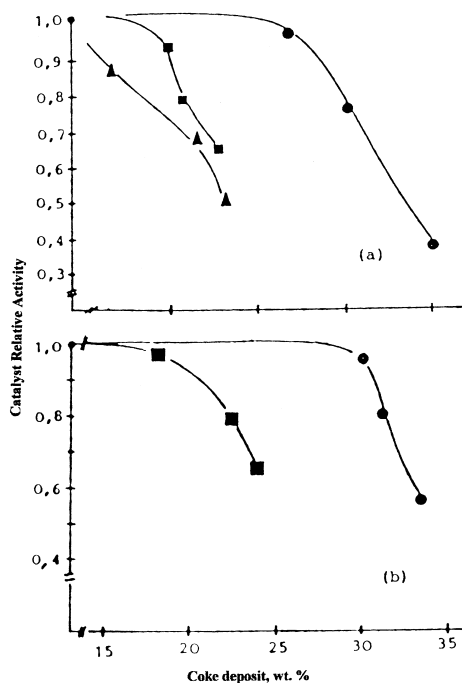


Fig. 112. Catalyst relative HDS activity vs. coke deposit (symbols and conditions as in Fig. 111) [161].

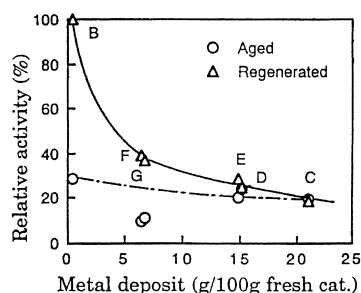


Fig. 113. Relative dibenzothiophene HDS activity vs. metal deposits (NiMo/Al₂O₃, 633 K, 12 MPa) [268].

and 13 ppm Ni. The catalysts were taken from the upper part and lower part of the bed. The catalysts were regenerated at 400°C in 2% O₂. Parameters such as surface area, pore volume and pore diameter were determined for the fresh, spent and regenerated catalysts. The results of these evaluations are shown in Table 28. The higher recovery of surface area and pore volume for the catalyst taken from the lower part (reactor exit) of the bed was attributed to lower content of V and Ni compared with that in the upper part. Little effect on the mean pore diameter was consistent with preferential filling of small pores. The difference in the parameters among the catalysts can be almost certainly attributed to the different properties of the catalysts, which were not given. Only a partial recovery of the activity could be achieved on regeneration, indicating a deactivating effect of metals. In a similar study published by Johnson et al. [222], three CoMo/Al₂O₃ extrudate (1/32-in.) catalysts were evaluated

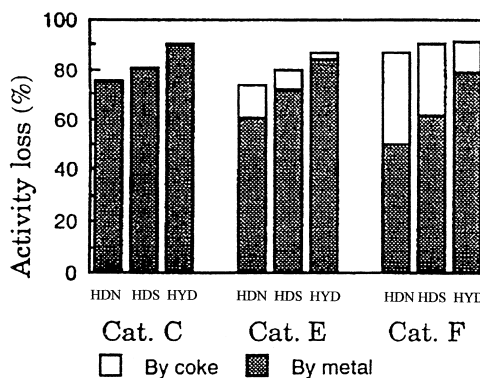


Fig. 114. Loss of HDS, HDN and HYD activities due to coke and metals (catalysts and conditions as in Fig. 113) [268].

Table 27
Properties of spent catalysts [268]

Age	Fresh	2 weeks	22 weeks		
Bed No.		3	2	3	4
Catalyst No.	A	B	C	D/E	F/G
Deposits, (wt.%)					
Carbon		16.8	12.1	15.7/13.0	25.1/22.2
V + Ni		0.5	21.2	15.2/14.8	6.5/ 6.8
Properties ^a					
Surface area, (m ² /g)	205	187	187	169/169	147/160
Pore volume (cm ³ /g)	0.57	0.40	0.38	0.35/0.35	0.32/0.34

^a Based on fresh catalyst.

after being used in a trickle bed reactor for the hydroprocessing of an atmospheric residue. Properties of the fresh and aged catalysts from this study are shown in Table 29. A marked decrease in the surface area and pore volume was quite evident. At the same time, little change was observed in the average pore diameter. The activity tests of these catalysts are summarized in Table 30. Interestingly enough, after regeneration of catalyst E, HYD and HDN activities

were partly recovered, whereas the HDS activity remained unchanged. Also, for all functionalities, no difference was observed between the extrudate and crushed samples, in contrast to large differences in diffusivities measured with coronene. Apparently, the test molecules were sufficiently small that diffusion did not influence their activities.

A significant loss in porosity, surface area and HDS activity of spent catalysts used in commercial operations was reported by Babcock et al. [269] and by Alvarez et al. [77]. In the former case, the activity could be recovered by leaching V and Ni from the catalyst, while the activity recovery on oxidative regeneration was much less. Almost complete recovery of the pore volume, average pore diameter and HDS activity was achieved after the leaching of a spent NiMo/Al₂O₃ catalyst with an acid by Hildebrandt et al. [270], while the catalyst still contained more than 50% of the deposited V and Ni. The catalyst was used in an ebullated bed for hydroprocessing of a vacuum residue.

Zeuthen et al. [271] published perhaps the most detailed results on the loss of surface area and porosity. They used a three-stage system for hydroprocessing of a Khafji vacuum residue containing 153 ppm V, 46 ppm Ni and traces of Fe with a CoMo/Al₂O₃ catalyst. At the beginning of the run, all three stages were filled with the fresh catalyst. Subsequently, samples were taken at various intervals from stage 1 and 3 reactors. The pore size distributions of the catalysts are shown in Fig. 115. Coke and metals deposited more rapidly on the first stage catalyst after 1 day on stream, whereas that on the third stage catalyst showed only a minor loss of pore

Table 28
Properties of fresh, spent and regenerated catalysts [251]

Catalyst No.	Surface area (BET m ² /g)	Pore volume (cm ³ /g)	Mean pore diameter (Å)
KC-28			
Fresh	239	0.458	76.5
Spent U	106	0.172	65.1
Spent L	102	0.187	73.6
Regenerated U	119	0.233	78.2
Regenerated L	170	0.343	80.9
KS-83			
Fresh	128	0.367	114.6
Spent U	55	0.144	105.4
Spent L	50	0.140	112.9
Regenerated U	69	0.197	114.9
Regenerated L	81	0.259	127.4
KS-97			
Fresh	106	0.401	151.3
Spent U	56	0.130	92.9
Spent L	54	0.134	99.3
Regenerated U	49	0.182	148.1
Regenerated L	83	0.302	145.8

U: Upper part of bed.

L: Lower part of bed.

Table 29
Properties of fresh and aged catalysts [222]

Catalyst	Carbon (wt.%)	Metals		Surf. area (m ² /g)	Pore vol. (cm ³ /g)	Avg. pore diam. (nm)	$D_e \times 10^{10}$, (m ² /s)
		V (wt.%)	Ni (wt.%)				
Fresh*							
E				219	0.57	11.4	4.3
A				194	0.60	12.3	5.1
F				125	0.54	17.3	5.1
Aged							
E	11.5	9.0	2.5	92	0.21	9.1	**
A	9.5	11.8	3.4	60	0.20	13.3	<0.01
F	4.3	13.7	4.1	57	0.20	14.0	<0.01

^a Fresh E 2.1 Co + 6.9 Mo; A 1.9 Co + 6.9 Mo; F 1.7 Co + 6.9 Mo.

^b Too slow to measure.

Table 30
Catalyst activities [222]

Catalyst	Rate constant $\times 10^3$ (Rel. activity ^a)		
	HDS	HYD	HDN
E			
Fresh extrudate	4.22 (1.00)	3.35 (1.00)	1.13 (1.00)
Aged extrudate	0.65 (0.15)	0.30 (0.09)	0.18 (0.16)
Aged crushed	0.65 (0.15)	0.30 (0.09)	0.18 (0.16)
Regen. extrudate	0.65 (0.15)	0.70 (0.21)	0.30 (0.26)
F			
Fresh extrudate	4.92 (1.00)	4.33 (1.00)	
Aged extrudate	0.13 (0.03)	0.02 (0.01)	

^a Activity relative to the fresh catalyst in terms of ratios of rate constants.

volume after the first day on stream. By Day 8, however, the third stage sample had lost significantly more pore volume than the first stage samples, i.e., by Day 8 the first-stage catalyst retained 71% of the initial surface area compared with only 50% retention in the third-stage catalyst. Average mesopore diameter decreased steadily over most of the run for both stages. Also, macropore volume in pores >1200 Å diameter decreased more rapidly in third-stage samples, indicating predominance of a lower density coke in the third-stage as compared to a higher density metal sulfide in the first-stage. The porosity data on samples taken at the end of the run clearly showed that the third stage sample had less pore volume in both mesopores and macropores as compared with that for the first stage spent catalyst. Further results showed that meso-

pores were almost completely filled with coke and/or metal deposits.

Zeuthen et al. [271] performed an extensive activity evaluation of the catalyst samples of Fig. 115. These results are shown in Fig. 116 using three dimensional plots of the relative activities (HDS, HDN and HYD) as a function of the carbon (normalized to 21 day samples) and V content (logarithmic scale). The activities were determined using model compounds. The deactivating effect of coke was not the same for all functionalities. This is seen most clearly from the third reactor samples, Days 0–8, which contained very small amounts of deposited metals. Thus, the HDN and HYD decreased rapidly, whereas HDS deactivated only slightly up to a coke level of 55%, suggesting that there are two different sites for these reactions [272]. Similar evaluation of the first reactor samples confirmed a more rapid deactivation for all functionalities. This was attributed to a higher content of metals compared with the third reactor samples. To distinguish between the deactivating effect of V and Ni, these authors impregnated the fresh catalyst with V and Ni and compared the activity of the resulting catalysts with that decoked after 21 days. These results are shown in Table 31 [271]. It is quite evident that V had a much more detrimental effect on all functionalities than Ni, particularly on HDS. This is in the agreement with the results published by Yoshimura et al. [273], confirming that among several metals, V had the largest deactivating effect on HYD.

Gualda and Kasztelan [274] used two sets of spent NiMo/Al₂O₃ catalysts during hydroprocessing of an

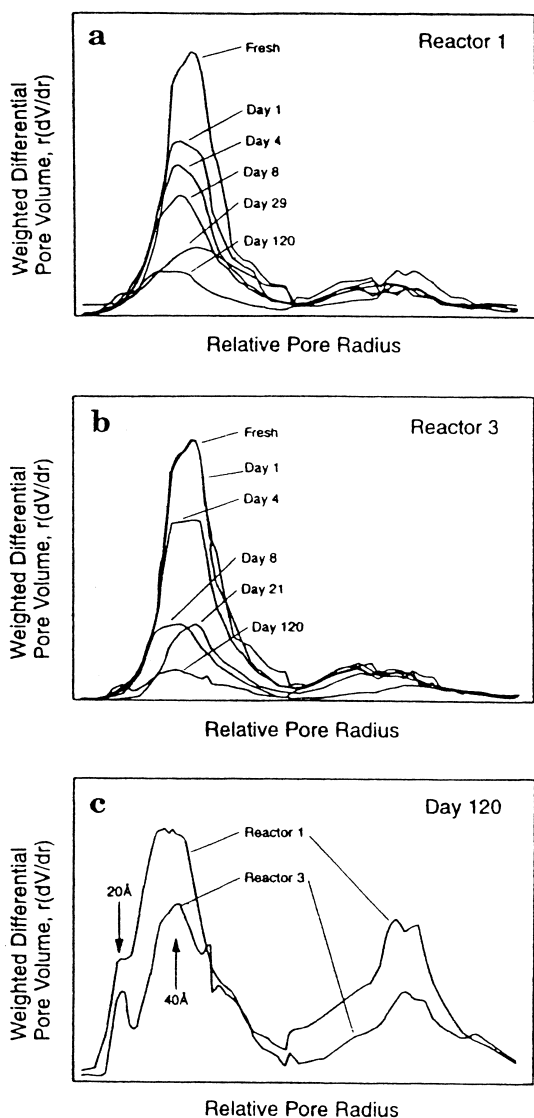


Fig. 115. Pore size distribution of (a) first-stage samples; (b) third-stage samples and (c) catalyst withdrawn after 120 days from both stages [271].

atmospheric residue, i.e., one in a batch reactor under varying pressure of H_2 (symbol P) and the other in a continuous fixed bed unit under typical hydroprocessing conditions (symbol TS). In the latter case, the samples of catalyst were withdrawn periodically. The results in Fig. 117 (from the TS series) show the deposition of metals and coke with time and their effect on HDS activity. The HYD and HDS activities

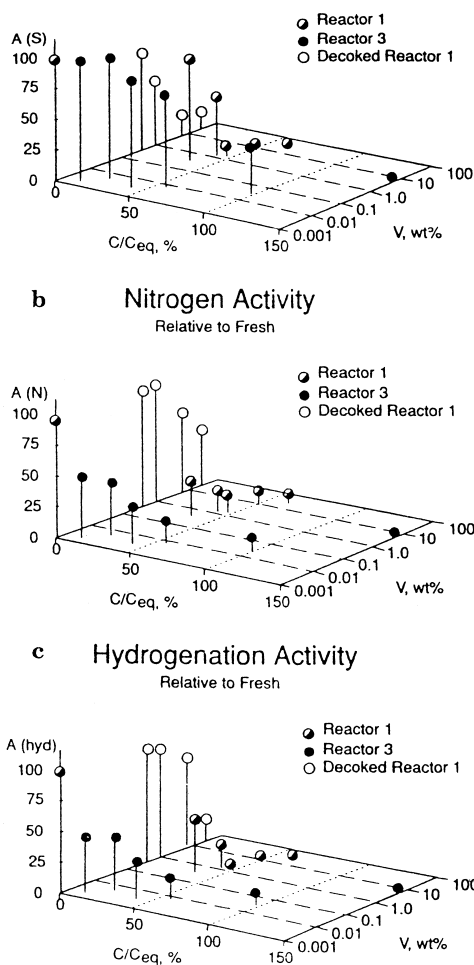


Fig. 116. Relative fresh catalyst activities with carbon content as normalized to 21 days of exposure and vanadium deposits (logarithmically) as (a) HDS activity; (b) HDN activity and (c) HYD activity [271].

of the spent catalysts were evaluated using toluene and thiophene, respectively, as model compounds. The effects of carbon and V content on the HYD and

Table 31

Activity data of aged catalysts relative to fresh catalysts [271]

	HDS	HDN	HYD
Fresh	100	100	100
Fresh + 1.5% Ni	193	154	152
Fresh + 6% V	9.8	80.7	53.6
Decoked 21 days (2.1% Ni and 7.1% V)	17.8	72.3	79.1

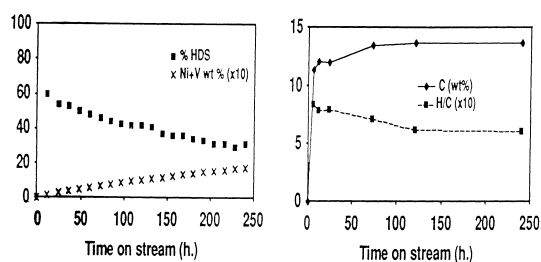


Fig. 117. Time on steam vs. (a) HDS conversion and metals (V + Ni) deposition and (b) carbon content and H/C ratio of coke [274].

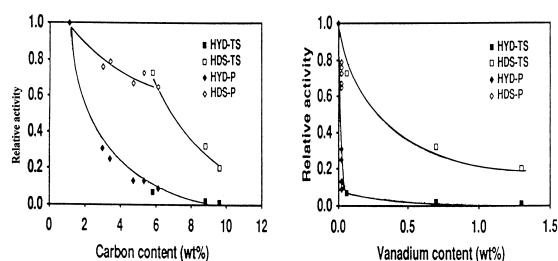


Fig. 118. Relative HYD and HDS activities vs. (a) carbon content and (b) vanadium content [274].

HDS activities are shown in Fig. 118. Small amounts of V had a dramatic effect on HYD activity regardless the origin of the spent catalysts, whereas the effect on the HDS activity was more gradual. At the same time, the effect of carbon on the HDS activity of the P samples was different than on that of the TS samples. The comparison of the carbon contents in Fig. 117 with that in Fig. 118 shows that the HDS activity refers to the very early stages of the test. Nevertheless, it is evident that the origin of coke influences the residual activity, suggesting that some differences in observations among different researchers may be traced to the conditions to which the spent catalysts are exposed.

Four NiMo/Al₂O₃ catalysts, having different unimodal and bimodal pore size distributions and different proportions of mesopores and macropores (Table 32) were compared by Absi-Halabi et al. [275]. The decline in the HDS activity with time on stream during the hydroprocessing of a Kuwait vacuum residue is shown in Fig. 119. The HDS activity of the PD-M1 catalyst was significantly higher than that of the PD-M2 catalyst; however, the former was much more active for HDM. For HDM and HDN, large pore

Table 32
Properties of catalysts [275]

	Catalysts			
	PD-M1	PD-M2	PD-B1	PD-B2
<i>Fresh catalysts</i>				
Bulk density (g/cm ³)	0.56	0.72	0.55	0.58
Surface area (m ² /g)	85	228	138	312
Pore volume (cm ³ /g)	0.60	0.53	0.73	0.76
<i>Mesopore distribution (%)</i>				
3–10 nm	4	38	7	55
10–25 nm	11	60.5	34	8
25–50 nm	27	1.5	19	8
<i>Macropore distribution (%)</i>				
50–100 nm	15	0	6	6
100–300 nm	43	0	16	21
>300 nm	0	0	18	2
<i>Spent catalysts</i>				
Carbon (wt.%)	15.5	15.8	19.7	21.2
Vanadium (wt.%)	11.0	6.8	9.6	8.7
Loss of surface area (%)	20.5	39.7	44.5	50.0
Loss of pore volume (%)	36.5	55.0	67.0	80.0

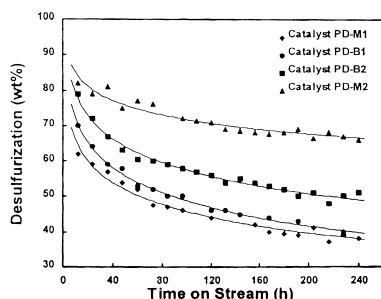


Fig. 119. HDS activities and deactivation of catalysts [275].

catalysts having a major proportion of the pore volume in 100–300 nm diameter exhibited the lowest deactivation rates. Bimodal pore catalysts with a large amount of narrow pores (PD-B1) showed higher rates of deactivation for HDS than unimodal pore catalysts (PD-B2) with a maximum amount of medium size mesopores. The results shown in Fig. 120 are in support these observations [276]. In this case, the feed contained Fe, V, Ni and Ti; therefore metals were the

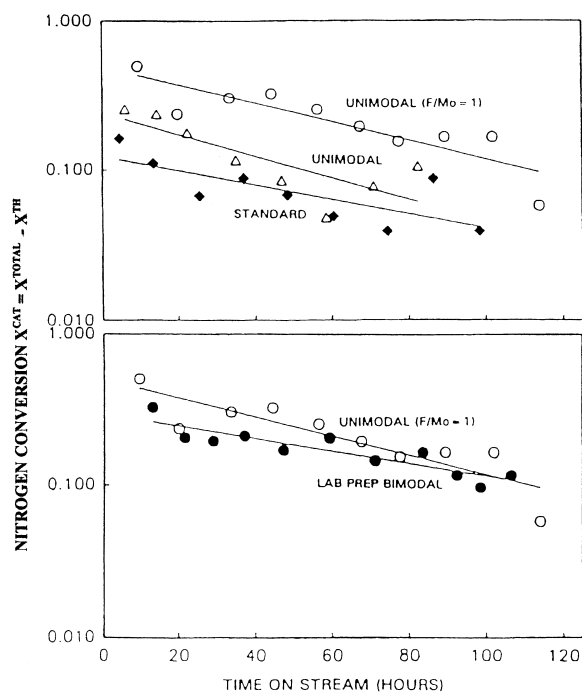


Fig. 120. Catalytic nitrogen conversion vs. time on stream; • – laboratory-prepared bimodal. ○ – Unimodal containing fluoride ions [276].

main cause of the deactivation. The HDN activity continued to decline after the steady-state level of coke was attained.

5.2. Formation of and Deactivation by Fe and Ti Deposits

Most of the studies on the deposition of Fe and Ti on catalysts deal either with the liquefaction of coal or with hydroprocessing of coal-derived liquids, and, to a lesser extent, with other feeds as well. Both single-stage and multi-stage liquefaction processes were investigated. Various forms of $NiMo/Al_2O_3$ catalysts were used in these studies. Most of the relevant information was published in the 1980s. In this regard, the evaluation studies on spent catalysts from the ebullated hydrotreater in the Wilsonville Coal Liquefaction Facility have received the most attention and represents perhaps the most significant contribution to the field.

5.2.1. Mechanism of deposit formation

The information on the formation of Fe and Ti deposits is much less documented compared with that for V and Ni. Similarly, as for the latter, deposition of Fe and Ti occurs simultaneously with that of coke. The results in Fig. 121 show that the formation of coke is faster than that of Fe and Ti deposits [277], but the difference seems to be less pronounced than in the

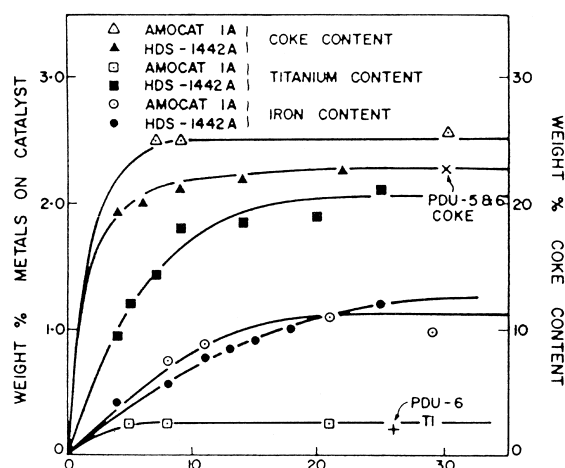


Fig. 121. Coke and metal contaminants as a function of catalyst age [277].

case of V and Ni [97]. The use of Fe- and Ti-containing model compounds did not attract much attention in elucidating the mechanism of deposit formation. Kovach et al. [278] impregnated a CoMo/Al₂O₃ catalyst with Fe₂O₃ and TiCl₄ in cyclopentane before hydroprocessing a coal-derived liquid, whereas Lynch [279] used Ti-porphyrin in a similar study. However, these compounds may not be representative of the Fe and Ti species in coal and coal-derived liquids.

The origin of the Fe and Ti deposits may be traced to the forms of Fe and Ti in the coal. Pyrite (FeS₂) is the main form of Fe in coal. A small amount of mixed structures of Fe sulfides with other elements, as well as Fe sulfates can also be present. The existence of an organically bound Fe in the coal cannot be excluded. There is an indication that part of the Ti can be organically bound, whereas the other occurs mostly as TiO₂ [280]. Under coal liquefaction conditions, pyrite will be gradually converted to FeS, in which case the H₂S/H₂ ratio is important [281]. However, this conversion may not be complete. Thus, according to the results published by Cable et al. [61], the Fe deposit on a spent catalyst from coal liquefaction comprised both FeS₂ and FeS. It is believed that some FeS was formed on the catalyst surface from the deposited FeS₂. It was suggested by Attar and Martin [282] that the conversion of FeS₂ to FeS results in a catalytic effect of the latter on liquefaction. Thus, during the first stage, Fe may play opposing roles, i.e., on one hand positively influence liquefaction, while at the same time decreasing liquefaction by covering catalyst sites. TiO₂ resists both reduction and sulfidation [283]. There are some suggestions that part of the Ti is of a porphyrin type [279]. Ti-porphyrins were assumed to be present in heavy oils derived from tar sands [284]. It is believed that during hydroprocessing, Ti-porphyrins will undergo similar reactions as those occurring during HDM of V and Ni, whereas FeS and especially FeS₂ will be mostly physically deposited on the catalyst exterior surface, with only a small portion of the FeS entering the pores.

It is evident that FeS and TiO₂ will be the predominant species in the primary metal-containing products from liquefaction and/or during the second liquefaction stage. During the first stage, the organometallic forms will release the metals, which subsequently will be converted either to sulfides (Fe) or oxides (Ti). The conversion of Ti to TiO₂ was con-

firmed by Lynch [279], who studied NiMo catalyst deposited with Ti-porphyrin. TiO₂ was indeed found on the catalyst surface after hydrogenation in creosote oil. Apparently, there is enough oxygen in the coal for oxidation of the Ti to occur. The species formed from the organometallics will be very finely dispersed in the primary deposits. Relatively deep penetration of TiO₂ into the catalyst interior observed by Stanulonis et al. [285] during the first and second coal liquefaction stage using a CoMo catalyst would be consistent with its presence in an organic form. On the other hand, most of the FeS was deposited on the external surface of the catalyst particles (Figs. 122 and 123), particularly during the first stage. In another study, Stohl et al. [286] observed that one portion of the Fe was deposited on the external surface, while another was evenly distributed, suggesting that the internal Fe deposit originated from a different precursor. Accumulation of coal mineral components on the catalyst surface resulted in substantial losses in catalyst surface area

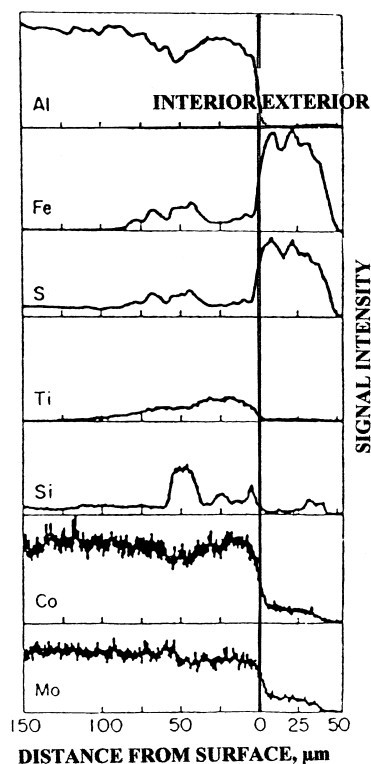


Fig. 122. Electron microprobe profiles of a catalyst particle from the upstream end of the reactor [285].

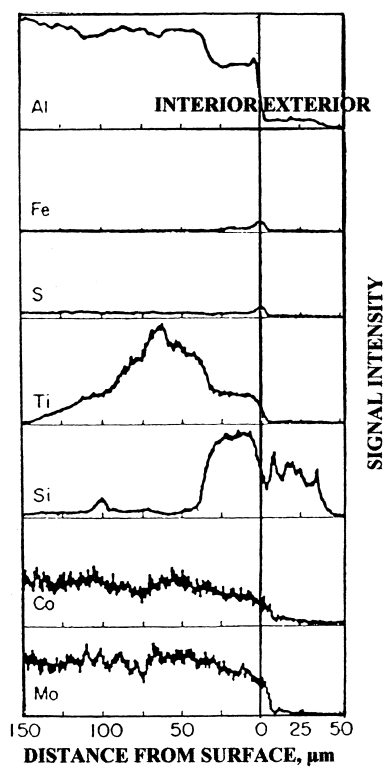


Fig. 123. Electron microprobe profiles of a catalyst particle from the downstream end of the reactor [285].

[287]. Because of the variability in the structure and composition of coal, different relative reactivities and diffusivities of the metal contaminants can be expected.

5.2.2. Kinetics of Fe and Ti deposition

Much less attention has been paid to the kinetics of the deposition of Fe and Ti compared with that of V and Ni. This applies both to diffusion controlled and intrinsic kinetics of deposition. The effective diffusivities of fresh, spent and regenerated coal liquefaction NiMo/Al₂O₃ catalysts were investigated by Stephens and Stohl [288]. For the spent catalysts, a significant decrease in effective diffusivity was observed.

The results shown in Figs. 124 and 125 demonstrate, a linear accumulation of Fe and Ti during hydroprocessing of several feeds obtained during a two-stage liquefaction of coal [88]. At the same time, the coke build-up was initially rapid and then reached a steady-state. The catalyst consisted of NiMo/Al₂O₃

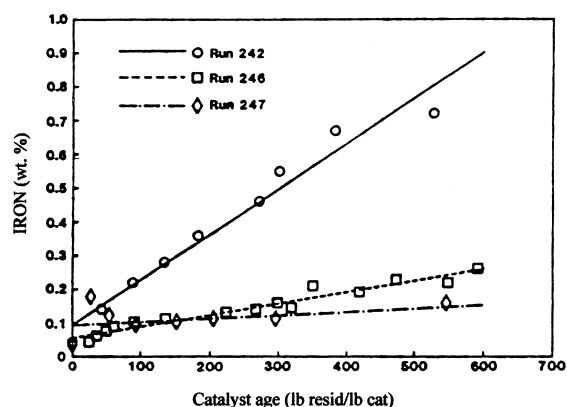


Fig. 124. Iron content of aged catalyst [88].

extrudates of 4 mm length and 0.8 mm diameter. The run numbers in these figures indicate different catalyst pretreatment and/or experimental conditions. Typical trends in Fe and Ti distributions in catalysts were observed, with the maxima of both Fe and Ti slightly displaced towards the interior of the particle. Depths of penetration of Fe and Ti appear to correlate with their bulk concentrations, i.e., the higher the concentration, the deeper the penetration. Thakur et al. [289] also showed that both Fe and Ti penetration increased with time on stream (Fig. 126).

Adkins et al. [290] developed a diffusion-limited model to predict deposition of Fe and Ti in 1/32-in. diameter NiMo/Al₂O₃ catalysts used in the Wilsonville pilot plant ebullated hydrotreater. The authors recognized the importance of the characterization of

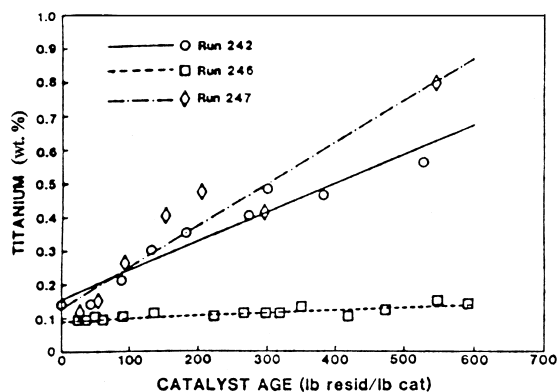


Fig. 125. Titanium content of aged catalyst [88].

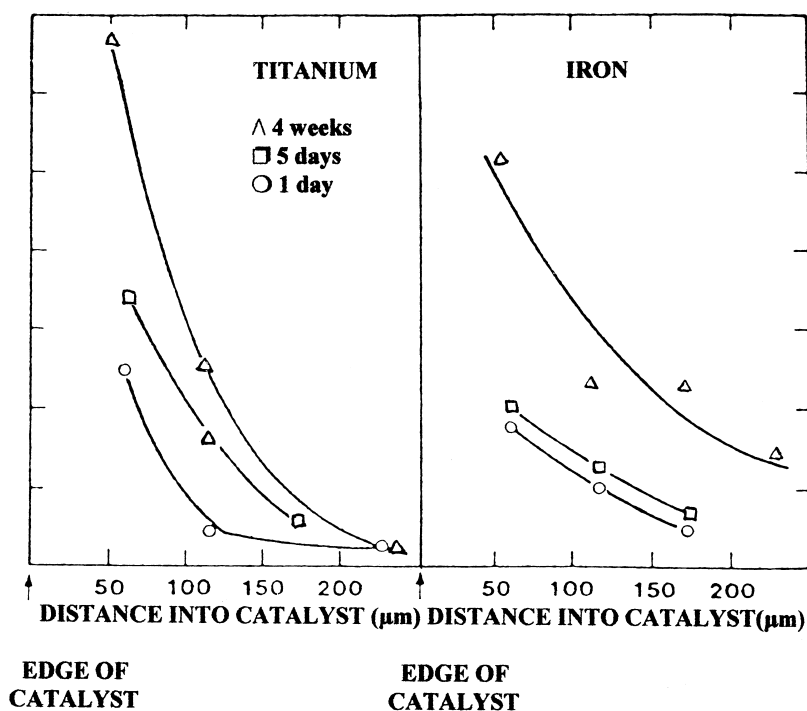


Fig. 126. Metal (Fe-Ti) concentration profiles for samples with different ages [289].

the catalyst, in particular the spatial distribution of the metals, as well as time trends in the distributions. The level of metal accumulation was much lower (no more than 1 to 2 wt.%) than that of coke (up to 14 wt.%). Initially, the coke deposition occurred rapidly, causing a significant change in pore size, and then remained constant during the metal deposition period. During the later period, the catalyst pore structure showed little change, supporting the view that the effective diffusivity remained constant during the entire metal accumulation period. The model used had the form of two ordinary differential equations and was based on a first-order adsorption of metal with linear site blocking and subsequent saturation, assuming one site deactivated per molecule of contaminant.

5.2.3. Effect of Fe and Ti on catalyst activities

Deactivation by Fe and Ti is a common phenomenon occurring during coal liquefaction and hydroprocessing of coal-derived feeds. Also in this case, deactivation by coke occurs simultaneously. The higher aromaticity of the coal derived feeds suggests a higher contribution of coke to the overall deactivation,

compared with the conventional feeds. In a single-stage coal liquefaction process, catalyst contacts both coal and solvent [291]. In the two-stage configuration, coal dissolution occurs in the first stage, while upgrading of the products occurs in the second stage [277]. It was shown by Stanulonis et al. [285], that catalyst deactivation in the first stage differs from that in the second stage. Deactivation by Fe and Ti may also occur during hydroprocessing of the other feeds. As was indicated earlier, most of the Fe and Ti are of inorganic origin, although organometallic forms may also be present. The difference between the cross-sectional distribution of Fe and Ti indicates different deactivating effects. In any case, the loss in porosity, accompanied by the decrease in the effective diffusivity, occurs similarly as for V and Ni. The ultimate result of Fe and Ti deposits is coverage of active sites.

An extensive evaluation of a CoMo/Al₂O₃ catalyst used for the processing of a coal was conducted by Cable et al. [292]. The properties of the aged catalysts are given in Table 33. It is quite evident that as coke and metals deposited, the pore volume and surface area decreased and the average pore diameter

Table 33
Properties of fresh and aged catalyst [292]

Sample	Coke (CHN) (wt.%)	Metals (wt.%)			Surface area (m ² /g)	Pore volume (cm ³ /g)	Average diameter (Å)
		Ti	Fe	B			
Fresh					308	0.69	45
Aged							
Day 1	0.48	0.16	0.12	160	0.38	48	
Day 4	17.4	0.96	0.48	0.47	37	0.15	81
Day 9	19.1	1.8	0.46	0.50	28	0.12	86
Day 18	21.1	1.9	0.98	0.55	17	0.08	94
Day 25	21.9	2.1	0.64	0.42	14	0.08	114

Table 34
Catalyst activities of aged catalysts expressed on fresh basis [292]

Sample	Extrudates			Crushed			
	k_T	k_H	k_C	k_T	k_H	k_C	k_O
Fresh	17.3	62.4	109	20.3	64.6	124	378
Aged Day 1 ^a	10.0	–	5	10.5	26.0	8	–
1	4.7	14.6	2	8.8	24.9	7	26
4	3.3	13.4	14	4.7	16.6	21	10
9	0.5	6.2	10	1.9	8.6	8	

^a Exposed to recycle oil only.

increased. Catalytic functions such as HDS, HYD and cracking (CKG) were evaluated for catalyst extrudate and crushed samples using model compounds. The results of the activity evaluations are presented in Table 34, where k_T , k_H and k_C are first-order rate constants for HDS, HYD and CKG, respectively. The catalysts in Table 33 were regenerated to determine recovery of the activity. As shown in Fig. 127, after regeneration of the catalyst exposed to coal for 1 day, almost all hydrogenation (HYD) activity was restored and CKG activity was higher than that of the fresh catalyst. However, both HDS and HDO activity showed permanent losses. The 4-day regenerated catalyst showed an additional increase in cracking activity and most of the hydrogenation activity was still restored, whereas only 60% of HDS and HDO activity was restored. After 25 days, all regenerated activities were considerably lower. To gain more insight into the deactivation, Cable et al. [292] impregnated the catalyst extrudates with solutions containing Fe, Ti, B, Si and Ca. Activities of the impregnated catalysts are given in Table 35. The composite catalyst (Fe, Ti, B) resulted in a large decrease in HDS activity

of the 9-day aged-regenerated catalyst, whereas the HDO activity was only decreased to 85%. In addition, the authors artificially coked the catalyst to attain

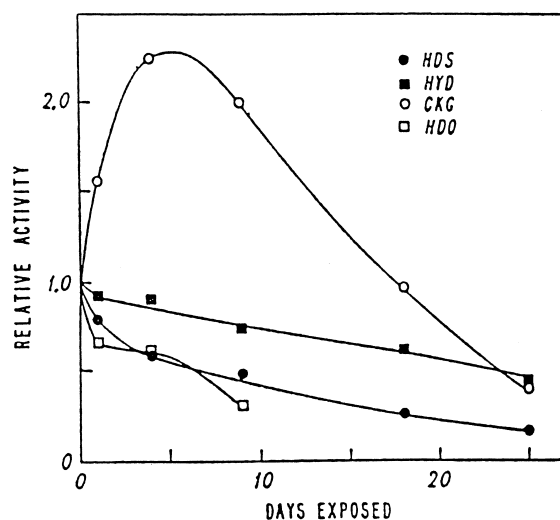


Fig. 127. Relative activities of regenerated extrudates [292].

Table 35

Catalyst activities of metal impregnated catalysts [292]

Metal	Content in catalyst (wt.%)	Catalyst activity			
		k_T	k_H	k_C	k_O
None	–	18.4	80.9	143	378
Ti	0.75	11.6	65.7	156	–
Ti	2.0	12.0	74.4	270	–
Fe	0.2	18.0	76.5	189	–
Fe	0.8	11.4	72.2	100	–
B	0.25	23.2	81.1	230	–
B	0.50	23.4	71.9	427	–
Ca	1.0	7.6	53.0	194	–
Si	1.0	18.1	66.8	396	–
Ti, Fe, B	2.0, 0.8, 0.5	8.4	61.8	341	313

Table 36

Catalyst activity of artificially coked catalyst^a [292]

Catalyst	Catalyst activity ^b			
	k_T	k_H	k_C	k_O
Fresh, calcined	25.7	70.8	204	430
Artificially coked ^c	0.2	8.7	6	6
Regenerated	24.7	104	267	416

^a Data for crushed catalysts.^b Calculated at 25% conversion.^c Coked with isooctene/He (about 24% coke).

about 24% of coke. As the results in Table 36 show, the coked catalyst was totally deactivated for HDS, CKG, and HDO, and hydrogenation was decreased to about 10%. On regeneration, nearly all HDS and HDO activities were restored and HYD and CKG increased.

In a similar study, Stephens and Stohl [288] investigated the effect of aging of an extrudate (0.8 mm) NiMo/Al₂O₃ catalyst on its activity for the hydrogenation of perylene. Both the aged and regenerated

catalysts were evaluated. Properties of the catalysts and rate constants from this study are shown in Tables 37 and 38, respectively. A steady loss of surface area and porosity on deposition of the contaminants was observed. The average pore diameter decreased as well, but, as seen in Fig. 128, it could be mostly restored by regeneration. In spite of restoring nearly all the pore volume, the activities of the regenerated catalysts were markedly lower than those of the fresh catalysts, indicating permanent deactivation by metals. Also, the activities of the crushed catalysts were significantly higher than those of the extrudates, indicating diffusional limitations caused by both the coke and metal deposits.

Another set of the activity data published by Stohl et al. [286] involved two spent NiMo/Al₂O₃ catalysts used for the upgrading of a mixture containing 70% solvent refined coal and 30% prehydrogenated creosote oil. The properties of the fresh, aged and regenerated catalysts from this study are shown in Table 39. The rather high level of recovery of surface area and

Table 37

Properties of fresh and aged catalysts [288]

Age of catalyst (lb of feed/lb of catalyst)	Major contaminants (wt.%)			Surface area (m ² /g)	Pore volume (cm ³ /g)
	C	Fe	Ti		
Fresh				150	0.49
43	8.2	0.14	0.14	125	0.32
88	9.3	0.22	0.21	113	0.29
133	9.6	0.28	0.30	108	0.28
381	9.2	0.67	0.46	102	0.27
527	9.4	0.72	0.56	100	0.27

Table 38

Rate constants for crushed and extrudate catalysts [288]

Age of catalysts (lb/lb)	Rate constants ($\text{s}^{-1} \text{g}^{-1} \times 10^2$)			
	Aged catalysts		Regenerated catalysts	
	Crushed	Extrudates	Crushed	Extrudates
Fresh	15.9	4.1	17.6	4.7
41	1.6	0.39	13.6	1.3
88	1.2	0.59	12.1	1.7
133	0.88	0.37	11.8	0.98
381	0.49	0.32	7.2	0.85
527	0.49	0.26	5.2	0.45

Table 39

Surface area and total pore volume of fresh, aged and regenerated catalysts [286]

	Surface area (m^2/g)		pore volume (cm^3/g)	
	Measured	Fresh basis	Measured	Fresh basis
Fresh	147	147	0.44	0.44
Aged 1	107	143	0.23	0.31
Aged 2	86	113	0.19	0.25
Regenerated 1	112	123	0.35	0.39
Regenerated 2	127	132	0.41	0.43

pore volume with regeneration should be noted. However, the activities of the regenerated catalysts (Table 40) were much lower than that of the fresh catalysts, confirming extensive deactivation by metals. Similar results obtained at near atmospheric pressure showed a marked difference between the activities of the extrudate and crushed catalyst, the latter being

much more active. At high pressure, the HDS and HYD activities for the extrudates and crushed catalyst were comparable, indicating the absence of diffusional limitations due to the outer barrier. The pore volume distribution for one of the investigated catalysts is shown in Fig. 129. In this case, a shift to lower

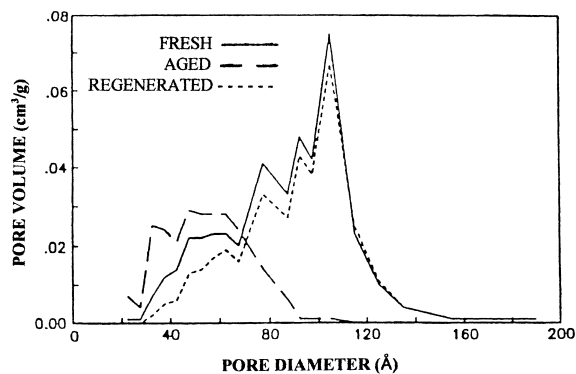


Fig. 128. Pore volume distribution for fresh, aged and regenerated catalysts [288].

Table 40

Activity testing in high pressure reactor [286]

Catalyst	Relative activity			
	HDS	HYD	HDO	HDN
<i>Extrudates</i>				
Fresh	1	1	1	1
Aged 2	0.21	0.03	0.11	0.14
Regeneated 1	0.10	0.02	0.06	0.11
Regenerated 2	0.25	0.16	0.18	0.25
<i>Crushed</i>				
Fresh	1	1	1	1
Aged 1	0.07	0.01	0.04	0.16
Aged 2	0.17	0.01	0.04	0.17
Regenerated 1	0.14	0.04	0.14	0.20
Regenerated 2	0.20	0.08	0.27	0.41

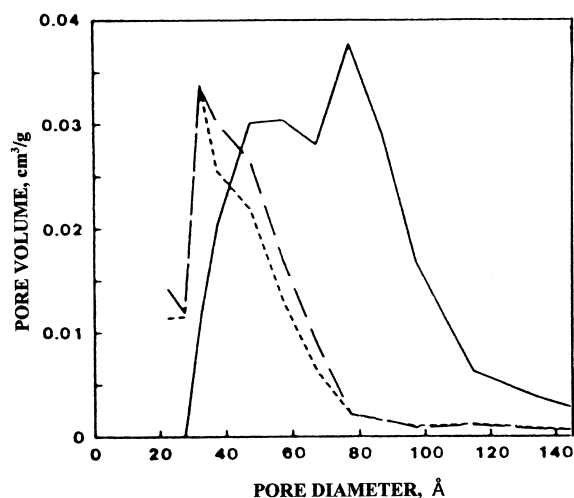


Fig. 129. Pore volume distribution for fresh (—), aged 1 (---) and aged 2 (-·-) catalysts [286].

pore diameter is seen, suggesting that larger pores were filled. On regeneration, the pore volume distribution was similar to that of the fresh catalyst. With respect to the change in pore diameter, properties of the catalyst are important. Thus, either an increase or a decrease in average pore diameter is possible. This was confirmed by Ihnatowicz and Worsztynowicz [293], who tested 11 catalysts of different structure used for upgrading a coal derived feed. In this study, the loss of surface area and pore volume were consistent for all catalysts, whereas both increases and decreases in pore diameter were observed.

Thakur et al. [289] studied the deactivation of a CoMo/Al₂O₃ catalyst (1.5 mm extrudate) during the hydroprocessing of a coal-derived feed lasting 30 days. The focus was on the HDO activity determined from the content of phenolic -OH, as well as on the hydrogenation activity measured by the ratio of aromatic to aliphatic protons determined by NMR. Fig. 130A presents the dependence of the activities on surface area; while Fig. 130B presents plots of the composition of residue (coke, metal contents and H/C ratio) against surface area and time on stream. In the first region, corresponding to the initial 4 days of the run, the surface area decreased by a factor of 8, indicative of filling of micropores. In this region, the phenolic -OH concentration curve shows a parallel behavior with the Fe content and the H/C ratio of the coke.

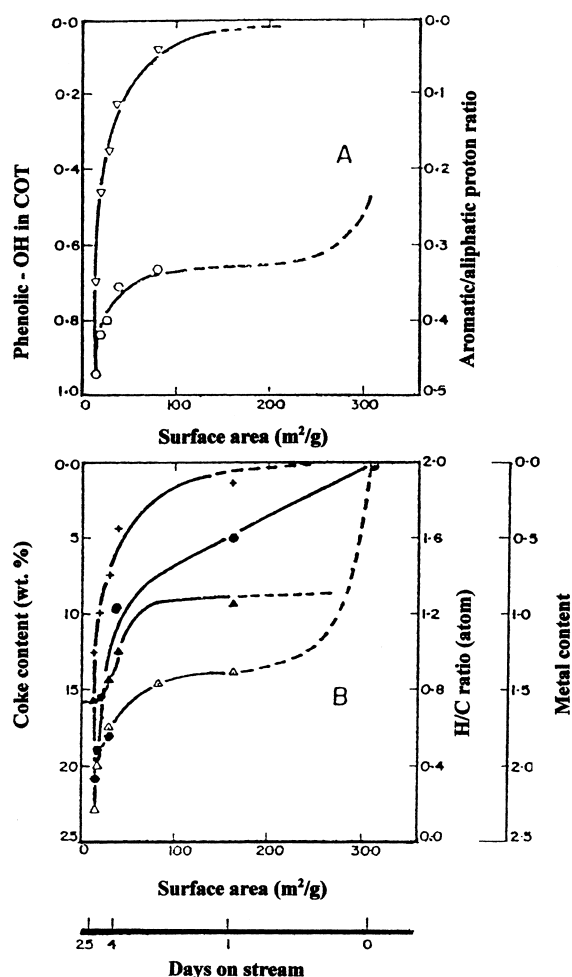


Fig. 130. Variation of HDO and HYD activities with surface area (A) and composition of catalyst residue against surface area; ∇ – phenolic-OH content, \circ – aromatic/aliphatic proton ratio, + – Fe content, \bullet – Ti content, \blacktriangle – H/C ratio, \triangle – coke content [289].

Surprisingly, the decrease in the surface area from 308 to 37 m²/g did not have a significant influence on HDO. On the other hand, the aromatic/aliphatic proton ratio and coke concentration curve exhibited a parallel trend. This suggests that the HDO activity does not greatly depend on the surface area, whereas the hydrogenation activity appears to be related to the surface area. The second region corresponds to the period of 4 days to 24 days on stream. In this region, activities and chemical composition of the catalyst deposit exhibit a parallel behavior. Thus, the catalytic activities are closely related to the coke and metal contents and

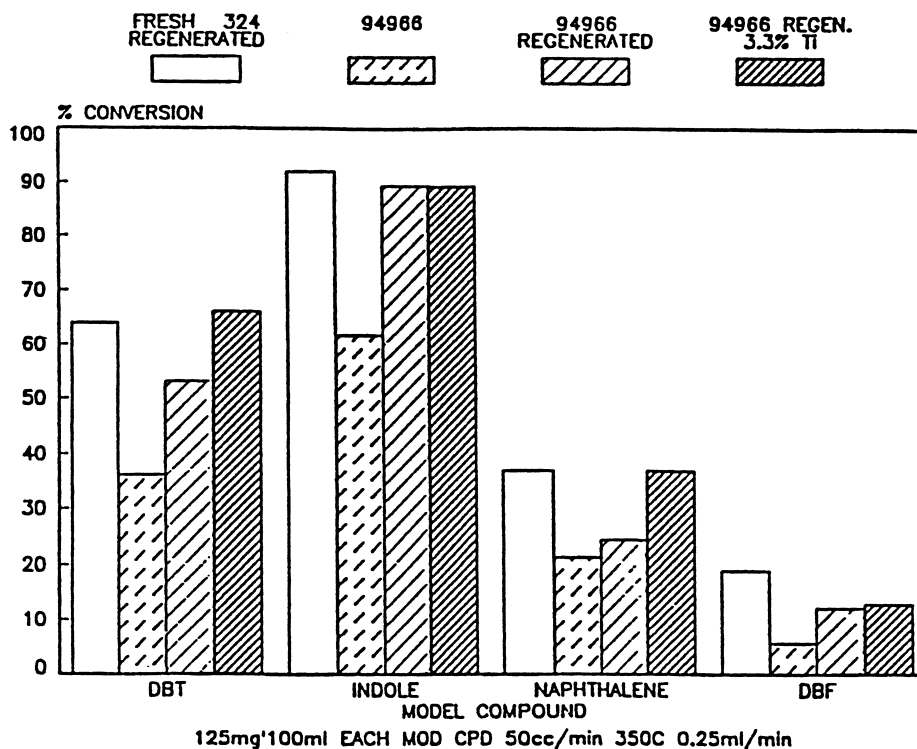


Fig. 131. Model compounds conversion on fresh regenerated, spent (#94966), regenerated and Ti doped catalysts [279].

the H/C ratio. It is noted that in this region, a small change in surface area and/or pore volume is accompanied by a sharp decline in activity.

Information on the deactivating effect of Ti is limited. According to the results published by Lynch [279], Ti when added to the NiMo/Al₂O₃ catalyst from hydrogenated creosote oil had only a minor adverse effect on the activity compared with the same catalyst which was deactivated in creosote oil without Ti present (Fig. 131). In this case, coke was mainly responsible for the loss of activity. However, surface area and pore volume were lower for the Ti deposited catalyst. Results in Table 35[292] suggest that at about 0.8% of metals, Ti and Fe had a similar deactivating effect on HDS, but Fe was less detrimental to HYD activity. A significant difference was observed in cracking activities, where Ti increased while Fe decreased the activity. Kovach et al. [278] impregnated a CoMo/Al₂O₃ catalyst with water soluble salts, such as chlorides and nitrates to different levels of various metals, which were then roasted to obtain the

corresponding oxides, and subsequently presulfided prior to their use in hydroprocessing a coal-derived feed. The effect of metal loading on relative activities is shown in Fig. 132. These results suggest no deactivating effect of Ti, whereas Fe decreased activity with metal loading. In addition, these authors exposed the catalyst to several minerals by suspending them in a hydrogen donor solvent before the hydroprocessing experiments. These results are shown in Fig. 133. Initially, Ti-containing species had little effect; however, after a certain time on stream, the activity decreased rapidly. In the case of Fe, a rapid decrease in the relative activity began at the start of the experiment before reaching a steady state at about 30% of the original activity. An interesting observation was made by Bogdanor and Rase [294]. These authors attrited outer layers of a spent NiMo/Al₂O₃ catalyst and performed activity tests on both spent catalyst and attrited material. The activity of the latter was significantly lower, presumably because of the presence of large quantities of Fe. It was further concluded that

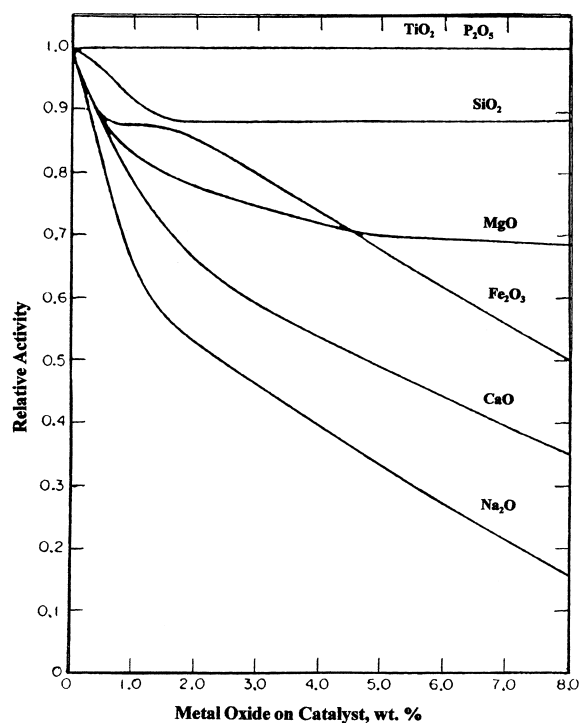


Fig. 132. Relative HYD activity vs. metal oxides on catalyst [278].

Fe was associated with the part of the coke which was the most difficult to oxidize during regeneration.

5.3. Deactivation by other deposits

Analyses of spent catalysts from various hydroprocessing operations indicate the presence of other metals in the deposits. The content and type of metals vary from feed to feed. The feeds derived from conventional crudes may be contaminated by alkalis if the crude was not properly desalted prior to its processing. This might be case for the spent CoMo/Al₂O₃ catalyst from HDS of an atmospheric residue having a high content of NaCl [222]. Relatively high content of Na was found in spent catalysts used for upgrading coal-derived feeds [295]. Cable et al. [61] have determined the depth profile in an aged catalyst used for upgrading a coal-derived feed. As the results in Fig. 134 show, the presence of Ca and Mg was confirmed. Compared with Fe and Ti, Ca and Mg accumulated on the exterior of the particles. The high content of Ti resulted from its higher content in the feed compared

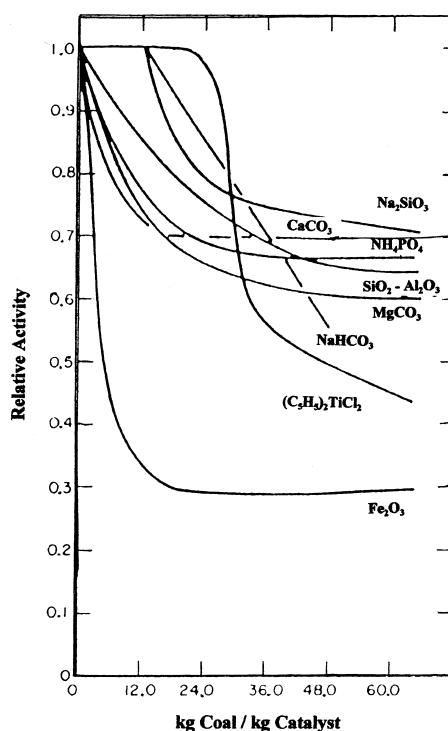


Fig. 133. Relative HYD activities vs. content of minerals on catalyst [278].

with Fe. The coal ash could be the only source of Ca and Mg. The presence of Ca and Mg, in addition to Fe, Ti and Na in the spent catalyst from hydroprocessing of a coal-derived feed, was also confirmed by Kovach

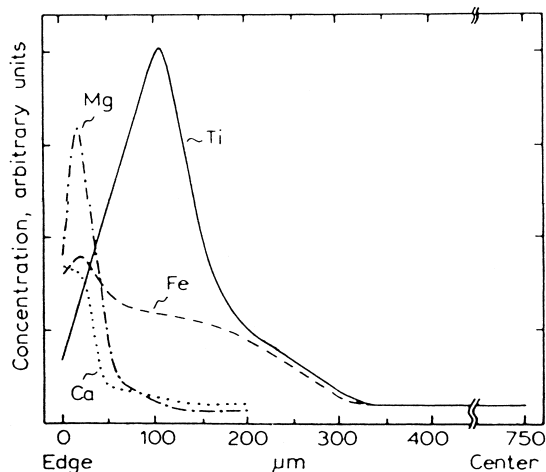


Fig. 134. Depth profile for aged catalyst [61].

et al. [278] and Stanulonis et al. [285]. Holloway et al. [296] reported a spatial correlation between alkali metals and Si, indicating the presence of alkali silicates. One report indicates the presence of Cr and Zn in the spent catalyst from coal liquefaction [285]. Berebi et al. [297] have analyzed a series of spent catalysts from hydroprocessing light feeds and confirmed the presence of arsenic, whereas Thakur et al. [289] found boron.

The amount of metals which end up in the deposit on the catalyst can be influenced by the feed preparation. In the case of coal, the level of its de-ashing is important. Heavy crudes derived from tar sands are usually contaminated by clay-like species originating from the sand. Also, a caustic agent is added during the separation of the tar from the sand. Part of this agent enters the organic phase. Both clay-like species and Na from the caustic agent affect the catalyst performance during upgrading, in addition to adverse effects caused by metals in the organic phase. In some cases, silicon type antifoaming agents are added to the crude before distillation [298]. Part of this agent may end up in the distillate and affect catalyst performance during subsequent upgrading. Feeds derived from oil shale may also be contaminated by metal elements originating from the shale.

5.3.1. Effect of other metals on catalyst activity

The alkalis are the most common metals found on spent hydroprocessing catalysts, aside from the major metals such as V, Ni, Ti and Fe. Their deactivating effect has been studied to a much lesser extent than that of the major metals. As the results in Fig. 134 show, Ca and Mg tend to accumulate on the external surfaces. Similar information on the other alkalis is not available. Nevertheless, the presence of alkalis in the feeds should not be underestimated. Yoshimura et al. [273,299] have established the order of deactivation as follows:

$V > Fe > Na > Mg > Ni$ for hydrogenation

$Na \gg Mg > Ni > Fe$ for hydrocracking

The detrimental effect of alkalis on hydrocracking is not surprising in view of the importance of acidic sites on the catalyst. Thermodynamic analyses conducted by these authors suggested a possibility of the formation of double oxides between the oxides of Mo and Na, and Mg and Ca upon regeneration. This may

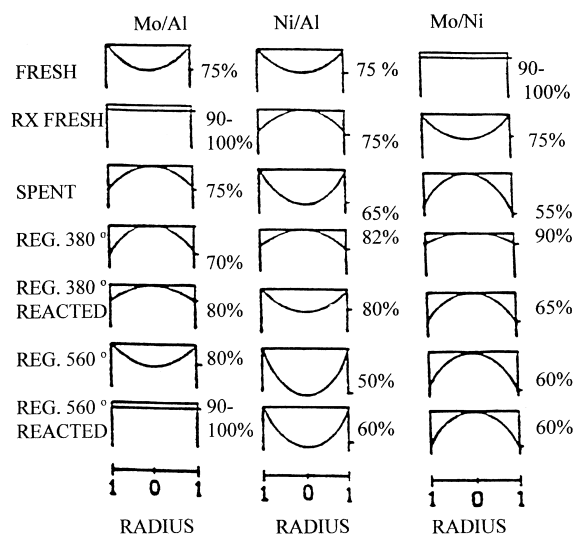


Fig. 135. Summary of trends for intraparticle Mo/Al; Ni/Al and Mo/Ni profiles (in Ni(Mo)/Al max.) for different catalyst treatments [294].

lead to irreversible structural changes in the catalyst and lowering of the activity. The results in Table 35[292] suggest that Ca enhanced cracking activity but had a significant deactivating effect on HDS, HDO and hydrogenation activities. Based on the results in Fig. 135 [278], the following order in catalyst deactivation was established at about 5% metal loading:

$Na > Ca > Mg = Fe$

However, when the minerals were impregnated on the catalyst, this order was changed (Fig. 133).

Other possible mineral species in the feeds are clays, such as silicates and aluminosilicates, usually present in heavy feeds derived from tar sands. Figs. 132 and 133 [278] show a loss in hydrogenation activity when such species are present in the feed. This is in an agreement with the results in Table 35, which indicate loss of hydrogenation activity on the deposition of SiO_2 on the catalyst. At the same time, cracking activity was significantly enhanced and HDS activity remained unaffected. Clay-like materials are expected to deposit on the front of the fixed bed of the catalyst. This may lead to the formation of a crust and ultimately to the malfunctioning of the bed due to increasing the pressure drop. Boron is a common element in coals and is expected in coal-derived feeds. As the

results of Table 35 show, boron at certain levels affected hydrogenation activity but enhanced the HDS and cracking activities.

A rather unique case represents catalyst deactivation by silica gel, which is formed from silicone oil used during hydroprocessing of a coker naphtha [300]. Part of the silicone oil, which is added to the coker unit to suppress foaming, ends up in the naphtha. During hydroprocessing of the naphtha, silicone oil transforms into modified silica gels, which adsorb on the catalyst surface. This leads to an irreversible loss of activity. In another case, caustic is added to the water during the hot water separation of bitumen from tar sands. Part of the caustic ends up in the bitumen and causes catalyst deactivation during the subsequent upgrading step [298].

It was suggested by Rase [301] that several other elements, notably lead and arsenic can poison hydroprocessing catalysts. Apparently, poisoning with these elements is irreversible and the contaminated catalyst cannot be regenerated for reuse.

6. Deactivation due to change in catalyst structure

The stability of the active phase is essential for maintaining desirable lifetime of the catalyst. In this regard, temperature appears to be the most important parameter. Changes in catalyst structure are very slow at temperatures used during hydroprocessing operations. However, in some cases, the catalyst remains in operation for a long period of time, sometimes as much as several years. Although temperatures may be relatively low, prolonged exposure can lead to structural changes, which have an adverse effect on the catalyst activity. These changes are for the most part irreversible, causing permanent loss of the activity. This may include segregation of the active phase, followed by the diffusion of active metals to the support and/or recrystallization. When metals are present in the feed, they can interact with the promoters in the active phase, in addition to the deactivating effects discussed earlier.

The deactivation of $\text{CoMo/Al}_2\text{O}_3$ and $\text{NiMo/Al}_2\text{O}_3$ catalysts from upgrading of coal liquids was attributed to the gradual conversion of a more active type II Co(Ni)MoS phase into the type I Co(Ni)MoS phase

[147]. The former consists of multilayer slabs of MoS_2 with Co/Ni at its edges, while type I phase consists predominantly of the monolayer slabs. The higher activity of the type II phase was attributed to the decreasing interaction between the support and MoS_2 in multilayer slabs compared with that between the support and monolayer slabs. This increases the amount of edges in the MoS_2 crystallites, which are believed to be the active sites. The lack of the multilayer slabs on spent catalysts was attributed to the preferential removal of sulfur from the multilayers by hydrogenation [147]. Yueqin et al. [302] measured the stack density (number of MoS_2 sheets per 1000 nm^2), length and number of slabs in fresh and spent $\text{NiMo/Al}_2\text{O}_3$ catalysts by TEM. Compared to the fresh catalyst, the spent catalyst showed a decrease in the stack density and an increase in the average slab length, while the layer thickness increased only slightly.

Cable et al. [292] used ESCA to determine the state of the active metals in aged catalysts which were regenerated. The technique can determine the ratio of the active metal to Al in the fresh and aged-regenerated catalysts. In the case of Mo, the Mo/Al ratio is an indication of the MoS_2 dispersion. The values of the experimental Mo/Al ratios are compared in Table 41 with the theoretical monolayer values [303]. The relative ratio of 0.85 for the fresh catalyst compared with the theoretical 0.92 indicates a high dispersion of MoS_2 . The relative values for the aged-regenerated catalysts declined to 0.74 after 25 days. This is a rather small change to account for the loss of activity (Fig. 127). Because a significant three-dimensional growth of the Mo phase has not occurred, the deactivation may be ascribed to lateral growth of the Mo phase with attendant loss of active edge sites, in agreement with other studies [304,305]. The ESCA

Table 41
ESCA results on aged-regenerated catalysts^a [301]

Ratio	Fresh catalyst	Aged-regenerated catalyst		
		1 day	9 days	25 days
Mo/Al	0.78 (0.92)	0.87 (0.94)	0.77 (1.02)	0.87 (1.17)
Co/Al	0.19	0.11	0.07	0.10
Co/Mo	0.24	0.13	0.07	0.10

^a Values in parenthesis are calculated for monolayer dispersion of Mo.

results showed that the Co/Mo ratio decreased sharply after one day and then more gradually with time on stream. This can affect the activity of the catalyst, since it is the Co associated with Mo phase, which facilitates the activity. The Co/Mo ratio for the fresh catalyst was less than one-half of the theoretical value of 0.58 Table 41. This means that part of the Co is not in the Co–Mo–S phase, but is most likely residing in the support. A similar decrease in the Ni/W ratio accompanied by a lateral growth of the WS₂ crystallites was ascribed to the cause of deactivation in a study published by Makishima et al. [305].

Aged NiMo/Al₂O₃ catalysts used for the upgrading of coal-derived feeds containing different amounts of preasphaltenes were evaluated by Matsubayashi et al. [306] using EXAFS and XPS. Catalyst samples were taken from the inlet, middle and exit of the fixed bed. The decomposition of the catalytically active Ni–Mo–S phase was observed in the samples taken from the inlet of the bed. This decomposition was enhanced when high preasphaltene feeds were hydroprocessed. Apparently, polar groups in the preasphaltene, i.e., –OH or –NH₂, occupied some of the sulfur vacancies at the edge of the MoS₂ slabs.

Such decomposition was not observed in the samples taken from the exit of the bed, because at this point all the preasphaltenes in the feed were already converted. However, at the exit of the bed, the catalyst was deactivated due to agglomeration of MoS₂ crystallites. This was attributed to higher temperatures caused by exothermic hydrogenation reactions.

Yoshimura et al. [299,307] evaluated an aged CoMo/Al₂O₃ catalyst used in a commercial operation for about one year and the corresponding fresh catalyst by EXAFS. They observed a significant enhancement of Mo–S and Mo–Mo coordinations, indicating an increase in the size of the basal plane of the MoS₂ crystallites. This would be consistent with the lateral growth of the MoS₂ crystals reported by Cable et al. [292]. On regeneration and subsequent sulfidation, the MoS₂ crystallites were redispersed, but the original dispersion was not achieved. This was attributed to the segregation of Co from the active phase, resulting in the agglomeration of Co₉S₈ crystallites during hydroprocessing. Kure et al. [308] have also reported lateral growth of WS₂ crystallites as the cause of deactivation. However, on regeneration and subsequent sulfidation of the spent NiW/Al₂O₃ catalyst, the

Table 42
Surface composition of catalysts [307]

	Al	S	Co	Mo	Co/Mo
CoMo/Al ₂ O ₃ fresh	100	14.6	3.6	6.5	0.55
Regenerated	100	2.2	3.8	7.9	0.48
Regenerated sulfur	100	15.0	3.6	7.3	0.49
	Al	S	Ni	W	Ni/W
NiW/Al ₂ O ₃ fresh	100	21.6	5.0	10.8	0.46
Regenerated	100	3.4	4.3	10.9	0.39
Regenerated sulfur	100	22.5	4.6	11.6	0.40

redispersion of the WS₂ slabs approached that of the fresh catalyst. Eijbouts and Inoue [309] noted a loss in homogeneity of an aged NiMo/Al₂O₃ catalyst due to a similar segregation of Ni₂S₃, resulting in a decrease in activity of the catalyst. Yoshimura et al. [299,307] observed an increase in the basal plane size of WS₂, similar to that of MoS₂. However, on regeneration and subsequent sulfidation, WS₂ was redispersed to the level of the fresh catalyst. The data obtained by EXFAS was complemented by the XPS data shown in Table 42. It is seen that after regeneration of the aged catalysts followed by resulfidation, the Co/Mo and Ni/W ratio did not return to the original values. This suggests that the amount of Co/Ni located around the MoS₂/WS₂ crystals was less than that of the fresh sulfided catalysts. The redispersion of Co relative to Mo was similar to the redispersion of Ni relative to W, suggesting that the degree of recovery of the active phase was similar for both catalysts, inspite of the higher redispersion of WS₂ compared with MoS₂. The sulfur remaining after regeneration is most likely in the form of Co and Ni sulfates and small amounts of unoxidized sulfides.

Catalyst samples from the Wilsonville coal liquefaction facility were characterized by Stohl and Stephens employing ESCA [88]. The results of this study are shown in Table 43. The catalysts are from two runs identified as 242 and 246. The other numbers indicate the amount of the processed feed in lb/lb of catalyst. Prior to the analysis, the aged catalysts were regenerated. The fresh catalyst was subjected to the same treatment as applied during the regeneration. In addition, the fresh catalyst was sulfided and regenerated (242-PS regenerated). The results of the fresh, regenerated fresh, 242-PS and 242-43 catalysts gave the

Table 43
ESCA results of fresh and regenerated catalysts [88]

Catalysts	Ni/Al	Mo/Al
Fresh	1.0	1.0
Fresh regenerated	1.1	0.9
242-PS regenerated	0.9	1.0
242-43 regenerated	1.0	1.0
242-527 regenerated	0.5	0.8
246-592 regenerated	0.9	0.7

same Mo/Al and Ni/Al ratios. This suggests that there were no measurable changes in the active metals due to either regeneration procedure or early stages of processing. However, sample 242–527 showed a decrease in the Mo/Al ratio and especially in the Ni/Al ratio. The decrease in the ratios was attributed to sintering because the quantitative bulk analysis of Mo and Ni, corrected to a catalyst fresh basis, indicated no loss of metals. Stohl et al. [286] showed that Fe and Ti deposits on the catalysts did not cause decreases in either the Mo/Al or Ni/Al ratio. Sample 246–592 showed a Mo/Al ratio comparable to 242–527, but did not show any sintering of the Ni. Run 246 sample was exposed to significantly lower temperature (335°C) than run 242 (about 400°C). Moreover, during the latter, a temperature excursion up to about 470°C, lasting about 50 min, occurred. This indicates that sintering of the Ni species is enhanced at higher temperatures. An ultimate result of the Ni sintering is the significant decrease in the ratio of Ni/Mo, suggesting some loss of active phase during the operation. Stanislaus et al. [310] observed that a NiMo/Al₂O₃ catalyst is more sensitive to temperature compared with a CoMo/Al₂O₃ catalyst. Using diffuse reflection spectroscopy, Gellerman et al. [311] proposed that Ni may be in the form of an aluminum-nickel spinel type (NiAl₂O₄). In this case, the aged NiMo/Al₂O₃ catalyst was used in the operation for about one year. A spinel form of Ni was observed in a heat-treated sample of a NiMo/Al₂O₃ catalyst [310].

Rase et al. [294,301] conducted a detailed study of the migration of the active metals in 1/16-in. extrudates of a NiMo/Al₂O₃ catalyst aged in a hydroprocessing operation. The unit, consisting of four fixed beds in series, was operated for one year on a blend of heavy coker and virgin gas oils. The fresh and aged

catalysts were subjected to the same laboratory treatment, involving sulfiding and activity tests which lasted between 10 and 15 h. A mixture of cyclohexene and thiophene was used for the activity testing. The catalysts were subjected to extensive evaluations using scanning electron microscopy (SEM) and XPS. A summary of the SEM results is displayed in Fig. 135 [294]. It is evident that for the fresh catalyst, the concentration of both Mo and Ni increased towards the exterior of the extrudate, giving a flat Mo/Ni ratio. After sulfiding and reacting with the test feed, the profiles of Mo and Ni exhibited dramatic changes, giving a concave Mo/Ni ratio. In the spent catalyst, the Mo concentration slightly increased towards the interior and that of Ni showed a pronounced decrease, giving a convex profile for the Mo/Ni ratio. Regeneration at 380°C again changed the Mo and Ni profiles. Subsequent exposure to the reaction mixture resulted in profiles which approached those of the spent catalyst. The profiles were further changed by increasing the temperature of regeneration. These observations have some implications for the activity of the catalyst. Thus, it is evident that the optimal Mo/Ni ratio, which might have been attained in the fresh catalyst, no longer existed in the aged and/or regenerated catalysts. However, the temperature used for the sulfidation of the regenerated catalysts had a significant impact on the metals profiles. Apparently, if a proper temperature is chosen, an optimal metal distribution across the extrudate can be achieved. V and Fe were also present in the aged catalysts. The concentrations of these metals increased significantly towards the exterior. The results of the SEM analysis complemented the XPS analysis, which confirmed agglomeration of Mo components as another cause of deactivation.

Migration of active metals during hydroprocessing of coal-derived liquids was reported by Yoshimura et al. [312]. These authors studied extrudate and powdered forms of NiMo/Al₂O₃ and CoMo/Al₂O₃ catalysts having similar contents of Mo and Ni/Co and similar surface area and pore size distribution. The XPS results of these catalysts are shown in Table 44. The migration of the metals in the spent catalysts to the catalyst exterior is quite evident. The migration of Mo was more pronounced than that of Ni and Co. The higher concentrations of S and O on the exterior result, almost certainly, from the higher content of coke on the particle exterior.

Table 44

Surface composition of fresh and spent catalysts (relative intensities of atomic ratio to Al) [312]

Catalyst	Al	C	O	S	Ni	Co	Mo	Ni/Mo	Co/Mo
NiMo/Al₂O₃									
Fresh, pw	1	0.32	2.49	0.20	0.06	–	0.09	0.73	–
Spent, pw	1	0.84	2.40	0.17	0.06	–	0.08	0.71	–
Spent, ex		4.46	5.02	0.71	0.11	–	0.27	0.40	–
CoMo/Al₂O₃									
Fresh, pw	1	0.38	2.38	0.20	–	0.06	0.08	–	0.70
Spent, pw	1	1.01	2.39	0.18	–	0.06	0.09	–	0.68
Spent, ex	1	4.10	3.08	0.41	–	0.09	0.20	–	0.42

pw: Powder form; ex: Extrudate.

An extensive modification of the active phase, leading to decrease in activity, may occur after metals from the feed are deposited on the catalyst. For example, according to Ledoux and Hantzer [263], V atoms can compete with Ni and/or Co on the MoS₂ edges and interfere with their promoting effect by diminishing the electronic transfer from the promoters to Mo, which according to Harris and Chianelli [313,314] is the origin of the high activity. A potential formation of the topotatic structures on the basal planes of MoS₂, leading to a structure resembling V₅S₈ and VMo₄S₈ phases, was proposed as well [263]. This could block bonding of the Ni atoms around the small MoS₂ crystallites, thus allowing the growth of larger, less active MoS₂ crystallites. It is not expected that Ni, after deposition on the catalyst from the feed, will have similar negative effects as V when a certain level of the deposited Ni is exceeded. Thus, it was shown earlier that to a certain extent, Ni, which always accompanies V in the feed, may have beneficial effects on the activity. In fact, it was suggested that both V and Ni sulfides are catalytically active before a critical V + Ni concentration is reached [245,315]. After this point, Ni and V form relatively inactive mixed sulfides, such as NiV₂S₄ and NiV₃S₄. Gualda and Kasztelan [274] made a theoretical estimate of the amount of V required for a complete contamination and/or promoter ion substitution in the MoS₂ slabs. They assumed two sizes of slabs, i.e., 2 and 5 nm. Assuming a 100% dispersion of V, a complete contamination of MoS₂ would be reached at about 1% loading of V. Yoshimura et al. [316] observed a significant decrease in the Mo/Al ratio on the addition of alkalis to Ni(Co)/Al₂O₃ catalysts due to the growth of the MoS₂ crystallites.

The results shown in Fig. 91 represent an extreme example of catalyst deactivation by metals and coke [239]. Thus, the amount of deposited metals (V + Ni + Fe) ranged from about 15% at the exit to almost 110% of the fresh catalyst at the entrance of the catalyst bed. The ESCA results confirmed the presence of Mo in all samples, suggesting that even in the most heavily deposited catalyst some Mo is still available for reaction. The presence of mixed metal sulfides such as (V_x(Fe,Ni))_{3–x}S₄ was suggested, where *x* represents a small deviation from ideality resulting from structural defects. Besides MoS₂, other Mo containing species were proposed, i.e., MoO₂, NiMoO₄ and MoVS₄. Ni was detected as Ni₃S₂, NiSO₄, NiAl₂O₄ and NiO.

Thermodynamics indicate the possibility of formation of several compounds, if other metals deposit on the catalyst from the feed [299,307]. Significant modifications of the catalyst surface are predicted, especially after regeneration of aged catalysts. If Fe is present, thermodynamics predict the possible formation of several species, e.g., FeMoO₄, FeWO₄, CoFe₂O₄, NiFe₂O₄, FeAl₂O₄ and CoFeO₄. The presence of FeMoO₄ in an aged-regenerated catalyst was indeed experimentally confirmed by Kim et al. [317]. A probability for the formation of several compounds was indicated in the presence of alkalis, e.g., Na₂MoO₄, Na₂Mo₂O₇, Na₂WO₄, Na₂W₄O₁₃, Na₂W₆O₁₉, NaAlO₂, Na₂Al₂₂O₃₄, CaMoO₄, CaWO₄, CaAl₄O₇, MgAl₂O₄, MgWO₄ and MgMoO₄. Arsenic is a possible contaminant in the feeds. If deposited on the catalyst, the following compounds can be formed: AsMoO₄, Co₃As₂O₈ and AlAsO₄. There is virtually no information on the stability, activity and behavior of these compounds under hydroprocessing conditions.

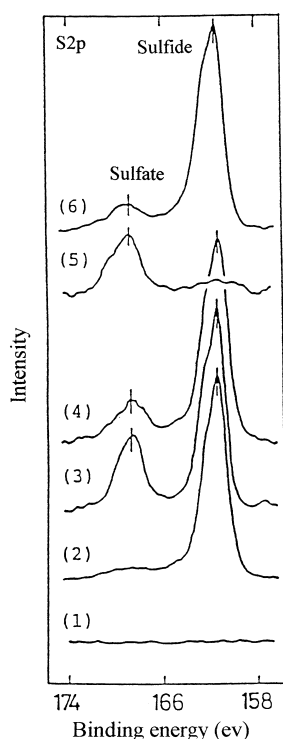


Fig. 136. XPS spectra of S2p for the fresh and spent catalysts: (1) oxidic; (2) presulfided; (3) spent; (4) spent-degassed; (5) spent-degassed-regenerated; (6) spent-degassed-regenerated-presulfided [318].

Of particular importance is the release of Mo/W and/or Co/Ni from these compounds during sulfiding. The amount of active phase would be decreased if these metals remain bound in the compounds having either low or no activity.

Residual sulfur as sulfates in the aged-regenerated catalysts can also modify the activity. The most probable sulfates include NiSO_4 , CoSO_4 and $\text{Al}_2(\text{SO}_4)_3$. Fig. 136 shows sulfate formation during regeneration [318]. The sulfate survives during the subsequent utilization in the operation. The sulfate ion was also detected in a spent catalyst withdrawn from the reactor. However, its formation during the operation is not possible. Therefore, most likely, the sulfate was formed on the exposure of the spent catalyst to air while still hot [319,320]. The effect of sulfate on the performance of the aged-regenerated catalyst is not well understood. Ramaswamy et al. [321] have observed a significant increase in the surface acidity

in the aged-regenerated catalyst as determined by NH_3 adsorption, when compared with the fresh catalyst. These authors attributed this observation to the presence of sulfate. Little difference between the acidity of the fresh and aged-regenerated catalysts was observed when the adsorption was performed with 2,6 dimethyl pyridine, suggesting that the Lewis acidity on the catalyst was affected, whereas the Brønsted acidity was not. A potential effect of the increased acidity on coke formation during operation had not been investigated until the study by Yoshimura et al. [318] was published. These authors showed that surface acidity can also be modified by some metals in the feed. Thus, alkalis reduced acidity of the catalysts. This resulted in a decrease in coke formation. On the other hand, Fe, Ti and V increased the catalyst acidity, presumably through the formation of acidic double oxides with Mo and/or Al. This resulted in an increase in hydrocracking activity. However, a decrease in hydrogenation activity enhanced coke formation.

Hydroprocessing of bio-derived feeds is accompanied by the formation of relatively large amounts of H_2O . The effect of H_2O on the properties of catalysts has attracted little attention except for the work by Laurent and Delmon [55–57]. In an investigation of a $\text{NiMo}/\text{Al}_2\text{O}_3$ catalyst, these authors observed that in the presence of H_2O , the $\gamma\text{-Al}_2\text{O}_3$ was transformed into boehmite, resulting in a loss of catalyst surface area. However, the surface area loss was not large enough to account for all the loss in catalyst activity. XPS evaluation of catalysts after parallel treatments with and without H_2O confirmed that in the former case, part of the Ni was in the form of an oxide and/or sulfate, whereas the MoS_2 phase remained unchanged. This is consistent with loss of promotor activity. In particular, it is believed that part of the Ni which decorates the MoS_2 is particularly sensitive to oxidation. The Ni oxide formed will be converted to Ni aluminate and become unavailable for promotion. It was proposed that Ni sulfate may form a protective layer above the sulfide phase [322,323]. It may be more difficult to maintain the required level of sulfidation of the active phase in the presence of large quantities of H_2O . The initial loss of sulfur during the HDO of THF in the presence of a $\text{CoMo}/\text{Al}_2\text{O}_3$ catalyst (Fig. 137) was attributed to the loss of incompletely coordinated sulfur in the CoMoS phase [79]. The loss of sulfur coincided with a rapid initial

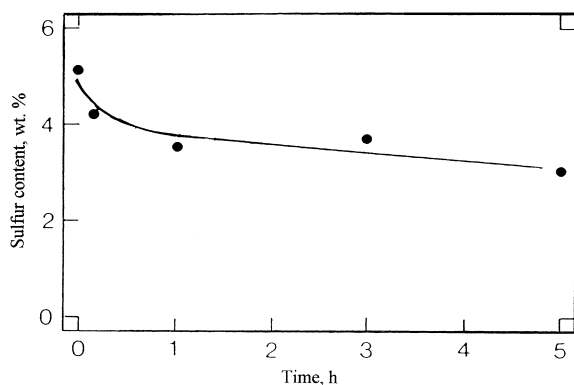


Fig. 137. Sulfur content of catalyst vs. time on stream [79].

decrease in the conversion, as well as a rapid coke build up.

7. Remedies

The impact of catalyst deactivation during hydroprocessing can be minimized by an optimal combination of catalyst properties, feed properties and type of reactor. In the case of light feeds derived from conventional crudes, the choice of processing conditions is quite straightforward. However, this becomes more complex with increasing average molecular weight or boiling range of the feed. For this purposes, a new generation of catalysts has been developed. Also, several different types of reactors available commercially enable processing high-asphaltenes and high-metals feeds. A modification of the catalyst may be needed to process non-traditional feeds. Changes in fuel specifications to comply with new environmental regulations require continuous attention to development of new catalysts possessing higher activity and selectivity, as well as resistance to deactivation.

7.1. Selection of catalysts

As was indicated in the previous chapters, catalysts of varying properties exhibit different deactivation patterns. The traditional HDS catalysts are not suitable for processing heavier feeds. In this regard, physical properties, such as pore volume and size distribution, shape and size of catalyst particles, become perhaps more important than chemical composition, provided

adequate activity is available. The selection of catalysts and reactors suitable for hydroprocessing various feeds was recently reviewed in detail by Furimsky [324].

Fig. 138 shows significant differences in pore size distribution required for processing a light feed compared with that for processing a heavy feed [325]. In the latter case, the presence of meso- and macroporosity is essential to offset the effects of restrictive diffusion and to increase the metal storage capacity of the catalysts, i.e., to increase the catalyst utilization. In this regard, an important study published by Absi-Halabi and Stanislaus [326] is noted. It is believed that for a given feed to a given process, there is an optimal pore size distribution. Fig. 139 illustrates, that there is an optimal combination of the catalyst activity, surface area and pore diameter for a particular feed, giving the highest activity [92]. This assumes the catalytic activity (or number of active sites) is proportional to the surface area, which is not always true for hydroprocessing catalysts. An optimal presulfiding procedure can result in further increase in the activity of hydroprocessing catalysts, as well as an improved metal foulant distribution throughout the catalyst particle [327,328]. Moyse et al. [178] investigated a series of catalysts of a similar chemical composition but varying in pore size distribution, during hydroprocessing of two heavy vacuum gas oils and one light gas oil. The trends shown in Fig. 58 for the heavy feeds differ markedly from those for the light feed. A macroporous bimodal catalyst performed better than a microporous unimodal catalyst, with the former accumulating much more coke but at the same time maintaining its activity for a much longer period of time than the unimodal catalyst [329,330]. These results show that a universal multifunctional catalyst possessing a high activity for all functionalities (e.g., HDS, HDN, HDM and asphaltene conversion), suitable for hydroprocessing of a wide range of feeds, still needs to be developed. Thus, the design of the most suitable physical properties of the catalyst for a particular feed requires expert advice from those involved in catalyst development.

In the case of heavy feeds, special attention has to be paid to the shape and size of the catalyst particles. This can be crucial for achieving an efficient catalyst utilization and a smooth reactor performance. The operation may be affected if the size and shape of

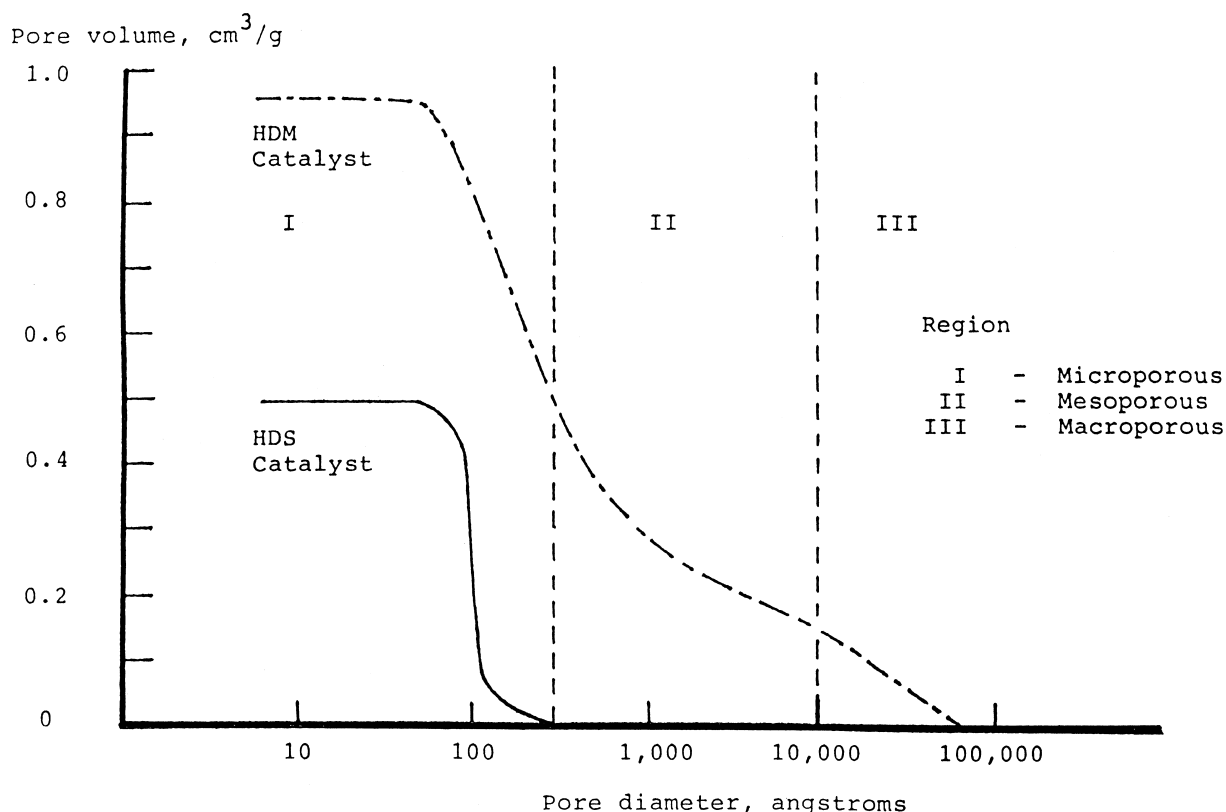


Fig. 138. Effect of catalyst pore size distribution on hydroprocessing [325].

the catalyst particles are not matched properly with the feed properties and reactor. Various shaped hydroprocessing catalysts discussed in the literature were

REACTION RATE CONSTANT.

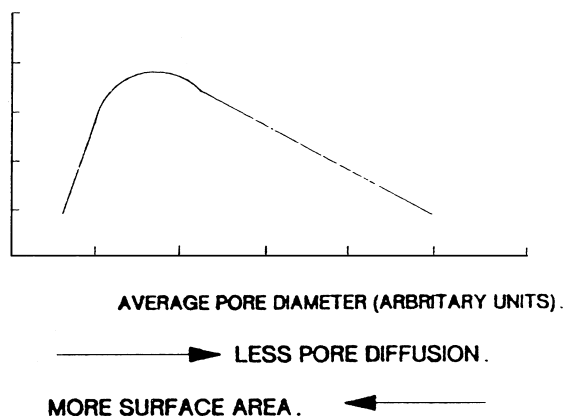


Fig. 139. Effect of pore diameter on reaction rate [92].

reviewed by Pereira et al. [331]. Traditional shapes, such as pellets and cylinders are suitable for hydroprocessing light feeds; however, for heavy feeds, the selection of the size and shape is more complex. In this case, small particles are more suitable because they present a shorter path to the catalyst interior. This ensures a more efficient utilization of the active surface. However, if used in fixed beds, small particles may affect the operation due to the occurrence of unwanted pressure drops. Ring-shaped particles are used when an increased voidage in the catalyst bed is required. Polylobe and minilith particles were developed with the aim of improving the accessibility to the catalyst interior [331].

Cooper et al. [332] compared relative HDS activities of the different sizes and shapes of catalysts. In this case, the catalyst particle size (L_p) was defined as

$$L_p = \frac{V_p}{S_p} \quad (7.1)$$

Table 45
Effect of particle size and shape on HDS activity [332]

Shape	Code	Dimensions (mm)	V_p/S_p (mm)	Activity ^a
Cylinder	1/32	0.83 OD \times 3.7 length	0.189	9.7
Cylinder	1/20	1.2 OD \times 5.0	0.268	7.9
Cylinder	1/16	1.55 OD \times 5.0	0.345	5.7
Ring	1/16	1.62 OD \times 0.64 ID \times 4.8	0.233	8.7
Ellipse	1/16	1.9 \times 1.0 \times 5.0	0.262	8.4
3-lobe	1/12	Diameter = 1.0; length = 5.0	0.295	8.2
Crushed	–	0.25–0.45	–0.04	14.0

^a HDS activity on catalyst weight basis (heavy gas oil, 622 K, 7 MPa)

where V_p and S_p are the particle volume and external surface area, respectively. The results of these measurements are shown in Table 45. The trend of increasing activities correlates well with decreasing V_p/S_p . The authors developed a computer model to calculate the effect of the size and shape on the pressure drop. For these calculations, particle size (D_p) was defined by

$$D_p = 6 \frac{V_p/S_p}{\phi_s} \quad (7.2)$$

where ϕ_s is the shape factor defined as the ratio of the surface area of a sphere of equal volume to the surface area of the particle. DeBruijn et al. [333] found that L_p correlated with the Thiele modulus (ϕ_L) defined as:

$$\phi_L = L_p \left(\frac{k_i C^{n-1}}{D_{\text{eff}}} \right)^{0.5} \quad (7.3)$$

where k_i is the intrinsic rate constant, C the concentration of the reactant, n the reaction order and D_{eff} is the effective diffusivity.

7.2. Selection of reactors

Three types of hydroprocessing reactors are available commercially, i.e., fixed bed, moving bed and ebullated bed. It is unlikely that a smooth and continuous performance can be achieved with the same catalyst in any of these reactors. In this regard, physical properties of the catalyst particles are the determining factor in finding the most optimal match of the catalyst with the reactor.

Fixed bed reactors have been traditionally used for hydroprocessing light feeds. Performance of these

reactors can be increased by loading more catalyst per unit volume of reactor, so called dense loading [334,335]. For example, the relative HDS activity of a fixed bed prepared by dense loading of spheres, cylinders and quadrolobe particles was increased from 5 to 8%, 10 to 15% and 20 to 25%, respectively, compared with sock loading. In the case of sock loading, particles lay against one another, form bridges and maintain random patterns as the result of the faster addition of the catalyst to the reactor compared to the dense loading. This leads to creation of oversized voids. If some forces are created on such a bed, e.g., pressure drop, the bridges may collapse, resulting in the shrinkage of the catalyst bed. This increases the danger of channeling and malperformance of the bed. A negative effect of dense loading is an increased pressure drop at start of run. For a given fixed bed, there is a limit to the maximum pressure drop at which the reactor can operate. Thus, an optimal combination of bed void and activity per reactor volume is needed, for which the pressure drop is within acceptable limits. Fig. 140 shows that the pressure drop can be controlled by selecting the proper size and shape of the catalyst particles [336]. An example of the effect of the shape and size of the particles on the fraction of bed void and catalyst surface area per reactor volume is given in Table 46 [337]. It is important that a comparison of the bed performance, including catalyst activity, for different shapes and sizes is made on an equal pressure drop basis.

The occurrence of pressure drop can be diminished by pretreatment of the feed. Conventional crudes have been traditionally desalted to remove water soluble alkalis. Sikonia et al. [338] reported the use of auto-

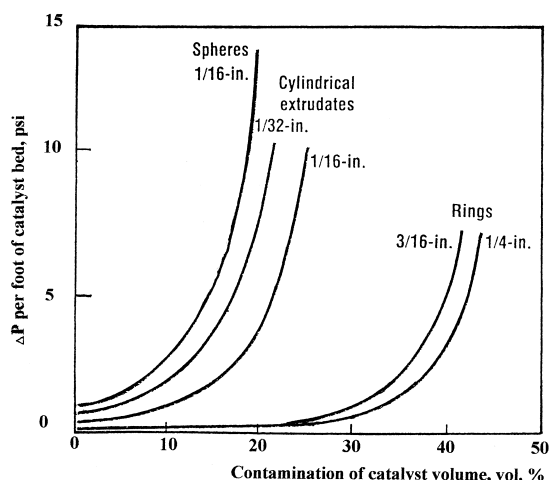


Fig. 140. Effect of particle shape and size on pressure drop [336].

matic back-wash filters to remove atmospheric residues. In any case, metals and clays present in feeds are the main cause of pressure drop occurring during the operation. It is apparent that little of the organically bound metals can be removed during desalting and/or filtering. This problem can be partly overcome by using guard reactors containing macroporous material having a high metal storage capacity. In this case, HDM of the feed would be the primary objective. The study published by van Zijl Langhout et al. [156,339] suggests that feeds containing less than 100 ppm of metals can be processed by a fixed-bed reactor. They suggested that a narrow pore catalyst can be used for a feed containing less than 25 ppm of metals. For feeds containing between 25 and 50 ppm of metals, a dual catalyst system may be required, i.e., the front end catalyst should possess a high metals tolerance, whereas the tail-end a high catalytic activity. For metals content between 50 and 100 ppm, a triple

catalyst system with the front end HDM catalyst having a high metal storage capacity may be needed. The features of the quick catalyst replacement reactor (QCR) designed for this purpose enable quick and complete catalyst unloading.

Beaton et al. [340] concluded that the history of commercial fixed-bed units with vacuum residues was not sufficient to confirm good operability; whereas, for atmospheric residues and light feeds the units operate reliably. A major concern was the excessive number of catalyst replacements required and tight schedules involved when using multiple reactor trains, especially for poor quality feeds. These problems were overcome by developing moving bed and ebullated bed reactors. In this case, the addition and withdrawal of catalyst is carried out during the operation avoiding any interruption.

The 'bunker reactor' developed by Shell [339] is the best known moving-bed reactor. In this trickle-flow system, the catalyst moves downwards; however, its movement is slow compared with the linear velocity of the feed. Catalyst addition and withdrawal are performed via sluice systems at the top and at the bottom of the reactor. The advantage of the bunker reactor is that the top layer of the moving bed consists of fresh catalyst. Thus, metals and salts deposited on the top of the bed move downwards with the catalyst and are removed at the bottom. The tolerance to metals and other contaminants is, therefore, much greater than in a fixed-bed reactor. One commercial unit was designed for 4000 tons/day of a straight run vacuum residue containing about 760 ppm metals [341]. The unit consists of two parallel strings of five reactors each. The first three reactors of each string are bunker reactors filled with HDM catalysts. The last two reactors of each string are of a fixed-bed type, containing HDS and hydrocracking catalysts. This plant

Table 46
Packed-bed properties of catalyst particles [337]

Description of particles ^a	Bed void fraction	Geometric surface area per reactor volume (cm ⁻¹)
Minilith ($D = 2.54$ mm, $L/D = 1$)	0.52	23
Trilobe (1.3 mm size, $L/D = 3$)	0.41	30
Cylindrical ($D = 1.6$ mm, $L/D = 3$)	0.41	18
Cylindrical ($D = 1.3$ mm, $L/D = 3$)	0.43	23

^a L: Length; D: diameter.

demonstrates the potential of combining fixed-bed reactors with moving bed reactors to achieve a high performance on feeds difficult to process.

The ebullated-bed reactor represents the culmination in the development of hydroprocessing reactors. It was successfully tested on vacuum residues and heavy oils as well as for coprocessing mixtures of coals and heavy feeds. These reactors have a provision for periodic addition and withdrawal of catalyst without interrupting the operation. The bed design ensures ample free space between particles, allowing entrained solids to pass through the bed without accumulation, plugging or increased pressure drop. Thus, the feed and H_2 enter at the bottom and move upwards through a distributor plate at sufficient velocity to expand the catalyst above the grid into a random and turbulent motion. This is achieved by controlling the speed of the recycle oil pump. These conditions are ideal for utilization of catalyst particles having a diameter less than 1 mm (e.g., 1/32-in. extrudates), and results in a considerable increase in reaction rate due to significantly diminished diffusion limitations. The process is flexible and can operate either in a high conversion or low conversion mode, i.e., for hydrocracking and HDS, respectively. The most established processes employing ebullated bed reactors include the LC-Fining process licensed by Lummus [340,341], the H-Oil process licensed by Hydrocarbon Research Inc. (HRI) [342,343] and the Texaco process [344,345]. Dozens of commercial ebullated-bed reactors have been operated in various parts of the world. Both LC-Fining and H-Oil reactors can be used in a multistage mode. Usually, three reactors are used in series. The first is for HDM, whereas the second and third are for HDS and/or hydrocracking.

7.3. Multiple catalyst beds

Trends in refining industry indicate on a growing use of the graded catalyst systems consisting of multiple beds [346,347]. In this case, the first bed provides HDM activity, the second some HDM but significant HDS and the third is responsible for hydrocracking as well as HDS and HDN. It is obvious that pore size of the catalyst will decrease towards the second and third bed. Also, each bed may require different chemical composition of the catalyst. Thus, selection of the

catalyst has to consider change in the feed composition from bed to bed. Koyama et al. [348] reported the results from hydroprocessing of a residue using two reactors in series, containing two catalyst beds each. The first bed consisted of an HDM catalyst and accounted for about 30% of the total catalyst volume. The remaining three beds consisted of HDS catalysts. A multiple-catalyst bed system may be required also for a metal free feed if a high hydrocracking conversion is the primary objective [339]. In this case, a catalyst on top of a zeolite-based hydroprocessing catalyst furnishes the necessary HDS and HDN activities. The latter is required to reduce the level of N-containing compounds to prevent poisoning of cracking sites.

The production of low aromatic fuels requires multiple-bed systems. The flowsheet of the process developed by Haldor Topsoe A/S [349] is shown in Fig. 141. In this case, hydrotreating is provided in the first bed comprising a high activity base metal catalyst. H_2S and NH_3 produced in the first stage are removed by stripping. Hydrogenation of aromatics is completed in the second stage using a sulfur-tolerant noble metal catalyst. The aromatic hydrogenation topic was reviewed in detail by Stanislaus and Cooper [350].

7.4. Next generation catalysts

Attempts have been made to develop new hydroprocessing catalysts to improve the performance of the currently used commercial catalysts. In this regard, at least two approaches have been used. In one, research has concentrated on modification of $\gamma-Al_2O_3$ supports or use of other oxides as the support, while using the same active metals (Co/Ni and Mo/W). In the other approach, focus has been on modification of the active phase by adding other metals, such as the platinum group metals. Hydrogenation catalysts used for the production of reformulated fuels may require a chemical composition which differs significantly from that of the typical hydroprocessing catalysts. Because this area of catalyst research is not a primary objective of this review, only a brief summary of some relevant studies will be given.

It was shown by Breyse et al. [351] that performance of hydroprocessing catalysts can be influenced by the support. They concluded that a modification of the support could be one of the approaches for

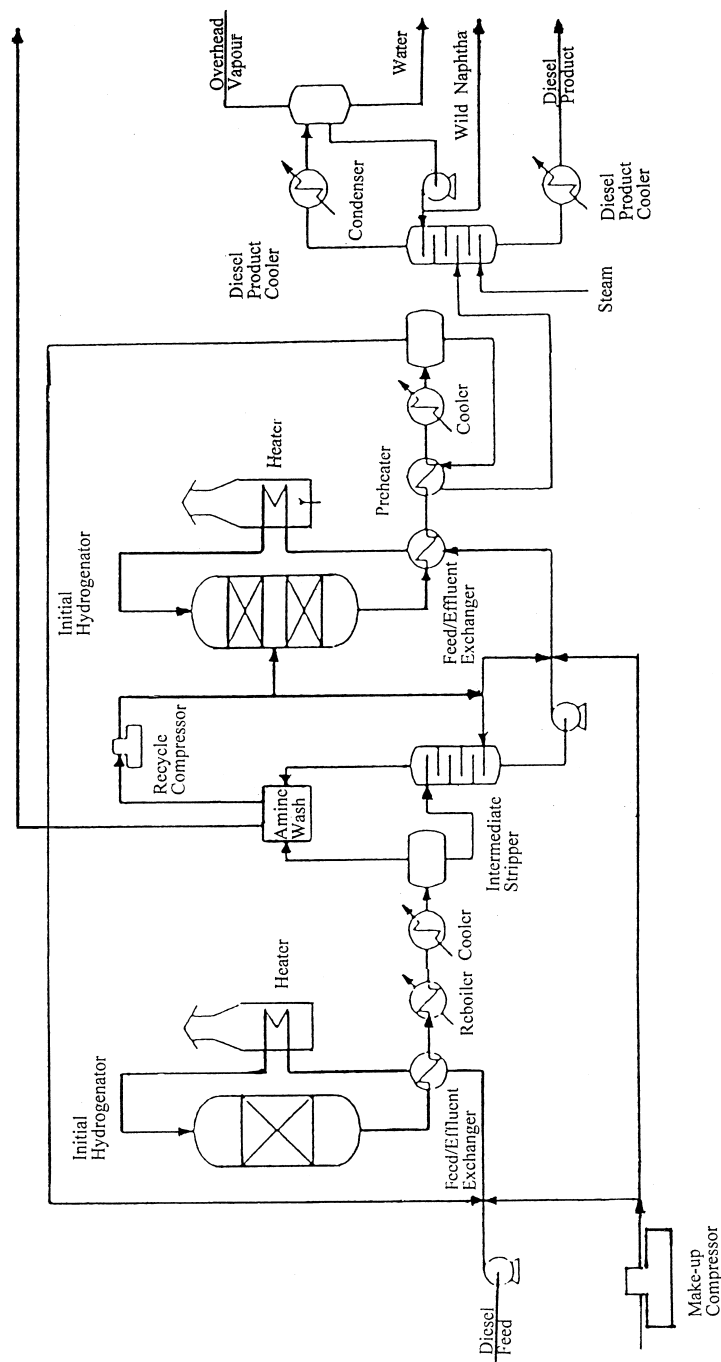


Fig. 141. Two-stage process for diesel dearomatization [349].

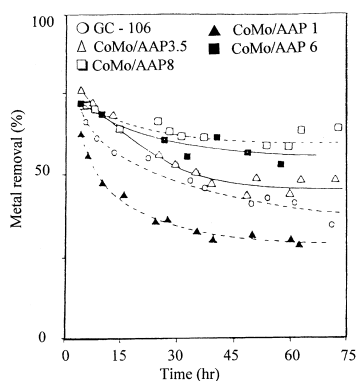


Fig. 142. Effect of Al/P ratio on metal removal [355].

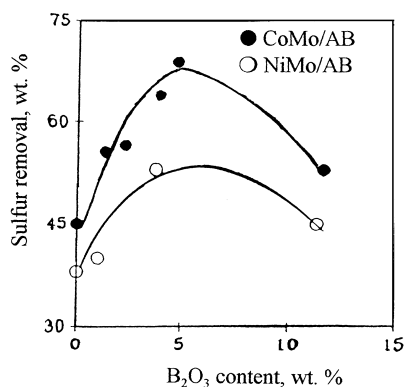


Fig. 143. Effect of boron content on sulfur removal [357].

developing better catalysts. In recent years, this avenue of research has been explored by several researchers. Reardon et al. [352] showed that the γ - Al_2O_3 surface can be tailored for efficient use of supported MoS_2 . Phosphorus is among potential modifiers of the γ - Al_2O_3 support that have been investigated. Halachev et al. [353] showed that the addition of 0.6 wt.% P_2O_5 increased hydrogenation activity of a $\text{NiW}/\text{Al}_2\text{O}_3$ catalyst. These authors stressed the importance of the conditions used during the preparation of the catalysts. Chen et al. [354,355] reported an improvement in activity of phosphorus doped $\text{CoMo}/\text{Al}_2\text{O}_3$ catalysts for HDS and HDM of an atmospheric gas oil. As Fig. 142 shows, the HDM rate depends on the Al/P ratio, i.e., the highest HDM was observed at an Al/P ratio of about 8. Kemp and Adams showed [356] that highly efficient Co/Mo and Ni/Mo hydroprocessing catalysts can be prepared in a simple synthesis using alumina hydrogel or phosphated alumina hydrogel. The final catalysts had extremely high surface area. Also, various pore structures could be attained. Chen and Tsai [357,358] investigated effects of the addition of boron to $\text{CoMo}/\text{Al}_2\text{O}_3$ and $\text{NiMo}/\text{Al}_2\text{O}_3$ catalysts. As the results in Fig. 143 show, the addition of boron significantly improved HDS activity. The HDS optimum was achieved at a B_2O_3 content of about 4 wt.%, which corresponds to an Al/B ratio of about 10. Hydrogenation activity of the same catalysts was improved as well. The addition of fluoride to an $\text{NiW}/\text{Al}_2\text{O}_3$ catalyst resulted in a marked improvement in HDN activity [359,360]. Ramos-Galvan et al. [361] compared the NiMo catalysts supported on Al- and Ti-pillared clays with a conventional $\text{NiMo}/\text{Al}_2\text{O}_3$

catalyst during the hydroprocessing of residual oils. The activity (HDS and hydrocracking) of the NiMo/Ti -pillared clay was significantly higher than that of the $\text{NiMo}/\text{Al}_2\text{O}_3$ catalyst. An $\text{NiMo}/\text{Al}_2\text{O}_3$ catalyst supported on fibrillar alumina showed both high activity for HDM and much longer lifetime compared with a commercial $\text{NiMo}/\text{Al}_2\text{O}_3$ catalyst [362]. Other potential supports include silica-ceria [363] and silicon-amine intercalated titanates [364]. Zeolites and silica-alumina supports were also evaluated [365,366]. In this regard, the method of the addition of the active metals to the support can be crucial. Thus, zeolite-supported catalysts prepared by an ion exchange with the Mo and Mo-Ni sulfide clusters were much more active for HDS than a conventional $\text{NiMo}/\text{Al}_2\text{O}_3$ catalyst [367]. Nomura et al. [368] showed that the activity and crushing strength of catalysts can be improved by blending γ - Al_2O_3 with a sepiolite support. This is significant for HDM catalysts which need to possess a sufficient macroporosity.

Another approach to develop novel hydroprocessing catalysts is based on the study published by Pecoraro and Chianelli [369] who showed that some unsupported noble metal sulfides exhibit significantly higher HDS activity than MoS_2 . Recent developments in this field, including supported transition metal sulfides, as well as their combination with Mo, were reviewed in detail by Vasudevan and Fierro [370] and Topsoe et al. [14]. More recently, Raje et al. [371] observed that RuS_2 and RhS_2 were more active than MoS_2 during simultaneous HDS, HDN and HDO of a coal-derived naphtha. However, to be cost competitive with the commercial $\text{Co}(\text{Ni})/\text{Mo}(\text{W})$ catalysts, the

content of the noble metal in the catalyst would have to be less than 1%. Also, to achieve a desirable sulfur tolerance, supports having a higher acidity than γ - Al_2O_3 are required [372]. Raje et al. [373] have compared a Ru/zeolite catalyst containing 0.77% Ru with a commercial CoMo/ Al_2O_3 catalyst during hydroprocessing of a coal-derived naphtha between 275 and 400°C. The former was much more active for HDN, whereas the commercial catalyst exhibited better HDS activity. A platinum (0.95%) supported on an amorphous SiO_2 - Al_2O_3 and a zeolite exhibited higher HDS and HYD activities than commercial CoMo/ Al_2O_3 and NiMo/ Al_2O_3 catalysts during hydroprocessing of a diesel fuel and HDS of dibenzothiophene [374,375]. A strong dependence of the catalyst activity on the type of support was reported by Song and Schmitz [376]. In this case, Pd and Pt supported on zeolites were compared with the corresponding catalysts supported on γ - Al_2O_3 during low temperature (200°C) hydrogenation of naphthalene. The former were more active and more sulfur tolerant. Similar observation was made by Corma et al. [377] during low temperature hydrogenation of a gas oil. In view of these results, the potential for further improvement in the performance of commercial hydroprocessing catalysts consisting of noble metals and acidic supports is believed to be promising. In fact, noble metal-based catalysts have been used commercially for producing low-aromatic diesel fuels. In this case, the operation at low temperatures, where thermodynamic limitations are not severe, is advantageous [378]. Deep HDS of the feed is necessary to achieve good catalyst performance. It is, however, apparent that progress is being made in developing sulfur tolerant catalysts enabling processing the feeds containing up to 1000 ppm of sulfur [379,380]. Nevertheless, a two stage process comprising deep HDS in the presence of a suitable conventional catalyst, followed by a low temperature hydrogenation in the presence of a noble metal based catalyst has been widely adapted for these purposes [381].

It is anticipated that new metal compounds possessing a high catalytic activity for hydroprocessing reactions will be identified. In this regard, metal-containing carbides, nitrides, oxynitrides and oxycarbonitrides have attracted attention [382–386]. It was shown by Oyama et al. [382,383] that Mo_2C , WC and Mo_2N were comparable in their activity for HDN of

quinoline to a commercial sulfided NiMo/ Al_2O_3 , whereas the latter was more active for the HDS of dibenzothiophene. A VN catalyst exhibited a good activity for the HDO of benzofuran. An examination of the spent catalysts confirmed their resistance to sulfur, as the content of sulfur was well below that required for the presence of MoS_2 . Subsequently, Sajkowski and Oyama [387] compared unsupported Mo_2N and $\text{Mo}_2\text{C}/\text{Al}_2\text{O}_3$ catalysts with commercial $\text{MoS}_2/\text{Al}_2\text{O}_3$ and NiMo/ Al_2O_3 catalysts during hydroprocessing of a coal derived gas oil and residue. The HDN results obtained for the gas oil are shown in Fig. 144. The Mo_2N catalyst was particularly active for hydroprocessing of the residue. The resistance of both Mo_2C and Mo_2N to sulfidation was also confirmed. Mo_2C and Mo_2N supported on γ - Al_2O_3 were more hydrogen efficient than the corresponding MoS_2/γ - Al_2O_3 catalyst [388]. McCrea et al. [389] observed that Mo_2N and Mo_2C supported on Al_2O_3 were more active for HDS of thiophene than the corresponding $\text{MoS}_2/\text{Al}_2\text{O}_3$. Relative HDS activities from this study, shown in Table 47 were complemented by O_2 and CO chemisorption data. Park et al. [390] made an attempt to promote Mo_2N with Co and Ni.

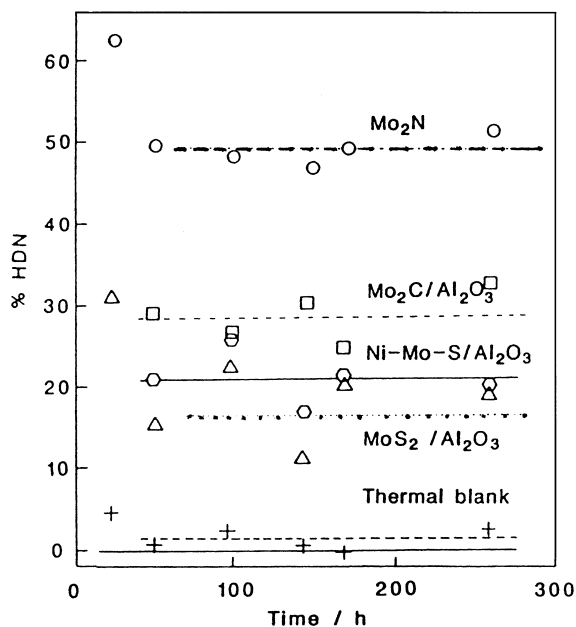


Fig. 144. Change of HDN activity of novel catalysts with time on stream [387].

Table 47
Relative HDS activities [389]

Catalyst	RA
MoS ₂ /Al ₂ O ₃	1.00
Mo ₂ C/Al ₂ O ₃	1.41
MoC _(1-x) /Al ₂ O ₃	1.04
Mo ₂ N/Al ₂ O ₃	1.22

However, the addition of Ni and Co to Mo₂N had little promoting effect in contrast with MoS₂. Djega-Mariadassou et al. [391] observed an Mo-oxynitride to be catalytically active during hydrogenation of propyl benzene with its activity progressively increasing during the run. At the end of the run, the composition of the catalyst approached that of an Mo-oxycarbonitride, suggesting that the new structure is more active than the oxynitride. It is apparent that commercial catalysts based on metal nitrides and carbides still need to be developed and their long term performance under commercial operating conditions has to be demonstrated.

8. US patent literature on remedies

The patent literature on various aspects of hydroprocessing catalysts is rather extensive. The book published by Satriana [392] gives descriptive information on 225 US patents issued between 1974 and 1981. Preparation of hydroprocessing catalysts varying in chemical and physical properties is the predominant part of this collection. Remedies are addressed in some 15 of these patents. More than 70 additional patents relevant to remedies were identified by a thorough examination of patents issued by US Patent office between 1980 and 1997. This may not be a complete list of patents issued on these aspects of hydroprocessing catalysts in the world. Nevertheless, as Satriana [392] states, the US patent literature is the largest and most comprehensive collection of technical information in the world. An important part of this collection are patents disclosed in other parts of the world. Therefore, it is an adequate and perhaps the best source for identifying trends in the development of more efficient catalytic systems to be applied for hydroprocessing of various feeds.

Guard beds are among several options used to alleviate problems with catalyst deactivation. Single beds of mixed catalysts and/or consisting of several layers of different catalysts can also be used successfully for particular feeds. Multi-bed systems consisting of several beds in the same reactor account for a large number of patents. For more difficult feeds, two or more reactors in a series can be used to slow down deactivation and to extent the operation cycle. Novel reactors, ensuring an improved operation, have been developed. The development of novel catalysts has been continuing and in this regard, the patent literature is quite extensive. However, this topic will not be included in this patent summary.

8.1. Guard beds

In this case, a guard bed of a suitable solid is employed above one or more individual beds of catalyst particles in the same reactor. A separate guard reactor placed before the catalyst reactor can also be used. Porous solids, such as activated bauxite or alumina, are used in the systems disclosed by Wolk et al. [393,394]. In one case, a significant improvement in hydrocracking conversion of an atmospheric residue containing 100 ppm of metals is achieved by passing the feed and H₂-rich gas upward through the first bed of alumina having pore diameter in excess of 125 Å. Both guard bed and catalyst bed are maintained under the same processing conditions. Alumina is employed as the guard material in the processes patented by Hilbert et al. [395] and Howell [396]. A number of other low cost solids suitable for this purpose may be available. In the system disclosed by Hutchings [397], the feed stream is divided into a number of portions, each of which passes through a different annular guard bed. After exiting through the bottom of the guard bed, the feed stream passes through a lower and much larger catalyst bed. The guard bed developed by Jones [398] has a provision for sensing the differential pressure across the bed. In this system, vapor components are withdrawn from the reactor chamber above the guard bed at a rate proportional to the differential pressure. The withdrawn vapor components are reintroduced into a particle-free void volume below the guard bed and above the bed of catalyst particles. Fukui et al. [399] disclosed a two-step process, in which the first bed (guard bed)

of the process consists of magnesium silicate as a major component and/or supported on one or more catalytic metal components selected from the metals of Groups V-A, VI-A and VIII. With this arrangement, a significant improvement in the performance of the second bed (catalyst bed) is achieved. Several patents cite adsorption process for removal of arsine [400,401].

8.2. *Mixed and layer beds*

In the case of mixed beds, the bed consists of a mixture of two or more catalysts. The invention disclosed by Habib et al. [402] comprises a mixture of two distinctly different catalyst particles in the same bed. The first catalyst has a high HDN and HDS activity, whereas the second catalyst is active for hydrocracking. Both catalysts have the same size and shape. This arrangement provides surprisingly good selectivity for liquid products and resistance to catalyst deactivation. Wolk and Rovesti [393] reported an improved performance of the bed, metal removal from the feed in particular, by mixing the catalyst particles with the activated bauxite and alumina. Another example of a mixed bed comprising two catalysts of different chemical composition is the invention disclosed by Ho [403]. An enhanced hydroprocessing conversion is achieved using a fixed bed of nonuniformly sized grade of catalyst particles of a similar chemical composition [404]. In this case, the graded particles are arranged with the largest particles in either the upstream or downstream portion of the bed. In either case, the performance of the graded bed is better than that of the convectional bed consisting of the same size particles. The process disclosed by Bartholdy [405] comprises a physical mixture of high void and low void catalyst particles mixed in different amounts and different layers of the fixed bed of catalyst.

The system developed by Kukes et al. [406–409] employs a single bed consisting of a layer of spherical alumina on the top of the catalyst layer. The former is pretreated to improve crush strength retention by impregnating the alumina with either ammonium or magnesium salts followed by heating at about 450°C. The alumina layer removes V and Ni from the feed. The performance of the bed is better compared with that without the alumina layer. The

two-layer system patented by Winslow and Sullivan [410] was developed for hydrocracking of vacuum gas oil to produce various fuels. The first layer consists of Ni(Co)MoP/Al₂O₃ catalysts possessing a high HDN activity, while the second layer consists of NiW(Mo)/SiO₂-Al₂O₃-zeolite catalysts. The first layer catalyst has a relatively large pore size, i.e., more than 60 Å. The inventors claim that the layered system increased the catalyst life and had other advantages.

8.3. *Multiple bed systems*

The patent literature on multiple beds in the same reactor is rather extensive. In this case, processing conditions such as temperature and pressure in the beds are similar. A dual-bed system patented by Banta [411] consists of a first large-pore catalyst bed and a second small-pore catalyst bed of CoMo/Al₂O₃. In a similar process, a heavy feed is mixed with a recycle oil before being contacted with the first bed containing a large-pore catalyst [412]. Preferably both catalysts have a quadrilobal shape. The system disclosed by Gillespie [413] employs two beds of which the second bed contains the catalyst having, on a gram equivalent weight basis, 1.5 times or more of catalytically active metals and the average effective diameter of 0.75 times or less than that of the first bed catalyst. A large number of other patents on two-bed systems were issued [414–420]. The main difference among these systems are different chemical compositions and physical properties of the catalysts employed. It is apparent that these reactors were developed to suit hydroprocessing of the particular feeds. The multi-bed process patented by Cash [421] has a provision for withdrawal of vapor between the stages and replacing it with H₂. Such withdrawal and replacement reduces the partial pressure of NH₃ and H₂S in the reaction mixture entering the bed succeeding each interspace, thereby increasing the rate of hydroprocessing reactions. An improvement in the operation was achieved by removing lighter fractions which were not heavily hydroprocessed in the first bed to be hydroprocessed in the second bed in the absence of heavy components [422]. The process for converting a gas oil feed to lighter hydrocarbon fractions comprises two fixed beds of a hydrocracking catalyst in one reactor [423]. The product

from the first bed is fractionated to obtain a heavy fraction which is hydrocracked in the second bed. A heavy fraction after the fractionation of the second bed product is recycled to the first bed. For more difficult feeds, three beds are needed to meet the final product specifications [424,425].

8.4. Multi stage systems

In this case, processing conditions and types of catalysts used in the different stages are significantly different. Thus, the operation cannot be conducted in the same reactor. An example of a multi-stage process is the dewaxing of feeds to decrease the pour point of the final products. This usually requires two steps, where in the first step the feed is dewaxed and subsequently hydrotreated. If nitrogen and sulfur are present in the feed, a hydrotreating step precedes the dewaxing step to prevent poisoning of the dewaxing catalyst, which is usually zeolite based. An example of this approach is the patent awarded to Albinson et al. [426]. Several patents were disclosed on processes in which the dewaxing step precedes the hydrotreating step [427–429]. It is evident that properties of the feeds are the determining factor in selecting a suitable combination. In one case, the feed is extracted by *N*-methyl-2-pyrrolidone to remove aromatics and heterorings [430]. The raffinate is then passed through a hydrotreating reactor followed by the dewaxing reactor. The process described by Chen and Degnan [431] comprises two trickle bed reactors in series containing a dewaxing catalyst and a hydroprocessing catalyst in the first and the second reactor, respectively. The dewaxing catalyst is supported on vertically tiered and staggered trays while H_2 is concurrently injected into the catalyst on each of the trays. A similar arrangement of trays in the second reactor allows trickling of the liquid while H_2 introduced into each tray flows upwardly together with the light fractions stripped from the liquid stream.

A combination of several reactors is required to produce ultra clean fuels. A three-stage process invented by Trachte et al. [432] employs a conventional hydrotreater to remove sulfur and nitrogen in the first step, followed by further hydrotreating in the second stage over a noble metal zeolite catalyst. The ultimate product quality is determined in the last hydrocracking step. A three-stage process for conver-

sion of a residue to a higher cetane number fuel was invented by Angevine [433]. In this case, the feed is demetallized and desulfurized in the first stage in the presence of a conventional catalyst, followed by hydrocracking in the second stage over a zeolite based catalyst. The required specifications of the fuel are attained in the last stage. A three-stage process to produce low sulfur and low aromatic fuels, disclosed by Haun et al. [434], employs a conventional HDS catalyst in the first stage, followed by H_2S stripping from the reactor effluent before the latter enters the second and third reactors containing sulfur sensitive noble metal catalysts. Three fixed-bed reactors in series are part of the process patented by Melconian [435]. The operating temperature of each bed is higher than that of the preceding bed. Once a predetermined temperature is reached, the third bed is removed from the system, reactivated or replaced by a fresh catalyst, and then used as the first bed.

Several dual fixed-bed reactor processes for conversion of heavy feeds to products, which require additional hydrotreating, were disclosed. For example, the process patented by Wolk et al. [436] has a provision for removing light fractions from the effluent of the first stage to minimize naphtha concentration and potentially avoid precipitation of heavy components in the second reactor. Various modifications of the two-reactors upgrading process were patented by Nelson and Wray [437] and Hamner et al. [438–440]. In the former case, a gas oil fraction is removed from the effluent of the first stage. A two-reactor and dual-component process [440] employs a large pore and a small pore catalyst. The feed is divided into a $+550^\circ C$ and $-550^\circ C$ fractions which are processed in the separate reactors. A fixed-bed hydrotreating reactor which precedes an expanded bed reactor, are part of the process described by Hagashi [441]. The process described by Henke and McKinney [442] is suitable for upgrading heavy oils and residues. In this case, three fixed-bed reactors in series are used. A macroporous $NiMo/Al_2O_3$ catalyst used in the first reactor contains a relatively small amount of active metals. The amount of active metals increases and H_2 pressure decreases towards the third reactor.

It was indicated earlier that problematic feeds cannot be successfully processed in a fixed-bed system. For this purpose, several patents were disclosed employing more than one ebullated bed reactors in

a series [443,444], or one ebullated bed reactor in a series with one or more fixed bed reactors [445]. The latter approach is the basis of the process described by Kunesh [446]. In this case, shale oil is hydrocracked in the ebullated-bed reactor, followed by hydrotreating in a fixed bed reactor under more severe conditions. After the phase separation, the resulting product has properties of jet fuels and diesel fuels. In the process described by Beret et al. [447], a thermal hydrocracking step, performed in the presence of a coke suppressing agent, precedes hydrocracking step performed in the ebullated bed reactor.

8.5. *Novel systems and reactors*

The performance of hydroprocessing units can be improved by maintaining and/or attaining an efficient contact of the feed with H_2 and catalyst. For this purpose, several ideas were put forward and were identified among US Patents. For example, Trimble et al. [448] described a system comprising a packed bed of a catalyst whose entire volume is filled during a continuous flow of uniformly distributed H_2 and feed. In addition, part of the feed, stripped of the light fractions, is injected into the bed to increase penetration in and contact time of the feed with the catalyst. In the dewaxing process disclosed by Kyan and Oswald [449], the feed is divided into a lower-boiling stream and a heavier-boiling stream. The latter is hydrocracked in the top bed. The effluent from the top bed enters an interbed redistributor, where it is combined with the lighter fraction before entering the dewaxing bed at the bottom. Goebel et al. [450] patented an apparatus for mixing fluids flowing downward concurrently. The apparatus can be placed between two fixed beds in the same reactor. The system is suitable particularly for containing temperature within the acceptable limits by admixing H_2 . An improved operation of the reactor can be achieved by an efficient supply of H_2 . In the multi-bed reactor described by Harrison et al. [451], the make up H_2 is supplied to the second bed, whereas H_2 -containing gas from this bed is used in the first bed. The H_2 -containing gas recovered from the first bed is purged and introduced into the third bed. Temperature control across the reactor is important to ensure a smooth operation. In the reactor described by Pool [452], the feed is split into two streams, one of which is intro-

duced into the first bed and the other into the second bed to cool the effluent from the first bed. In another system [453], the H_2 quench is introduced concurrently into the effluent from dewaxing beds to control temperature during the hydrotreating step in the last fixed bed.

Uniform distribution of the feed and H_2 is an important requirement to achieve smooth operation of catalyst beds. This issue is addressed by a number of US Patents. For example, the reactor described by Chou [454] employs a packed bed with redistribution screens spaced in the bed to prevent channeling. Plugging can be prevented by placing removable partition forms and/or permanent interbed baskets in the bed [455]. This creates gradual transition zones between the layers of catalyst and increases the open area available for flow at the interface of such zones. An upright multi-bed reactor patented by Wijffels et al. [456] contains a permeable filter between the beds to prevent carryover of catalyst particles to the next bed. Den Hartog and Van Vliet [457] developed a chamber which can be placed between the adjacent catalyst beds of a multi-bed downflow reactor. This chamber includes a device for injecting additional liquid and/or gas for controlling temperature, a tray for receiving liquid and compartments for receiving gas, a distribution tray comprising passages allowing liquid and gas to pass downwardly over an adjacent bed, and guiding channels to direct liquid into a mixing zone before entering the other bed. A special feed distributor, comprising an octagonal manifold with tangential outlet openings, was designed by McDaniel et al. [458]. It is claimed that the operation of an expanded bed is improved with this distributor employed. The separator-distributor system designed by Smith [459] comprises an upper foraminous wall allowing gaseous components to escape outwardly into an upper reactor portion, and a lower distribution means for receiving liquid and dividing it into several streams towards the catalyst bed. This device can be placed between the reactor inlet and catalyst bed.

Systems incorporating multiple-fixed beds in a vertical stripping tower were described by several inventors. Such systems are suitable for hydroprocessing light feeds, e.g., naphtha. The stripping tower designed by Harandi [460] has an upper catalytic contact zone and lower catalytic contact zone. The light gas stream containing H_2 , stripped from the feed

at the top, is introduced into the lower contact zone, whereas the liquid portion of the feed is introduced to the upper contact zone. Hydroprocessing occurs in the upper contact zone by flowing the liquid stream and gas stream countercurrently. A column described by Yeoman et al. [461] includes distillation trays which allow accumulation of liquid from a liquid stream and passage of a vapor stream through the liquid. The catalyst beds, housed in perforated containers, extend downwardly from the trays. A portion of the liquid can bypass the catalyst bed and be directed to the adjacent catalyst bed, so that higher volumetric flows are achieved. The tower described by Al-Saigh [462] employs catalyst beds in the form of removable baskets with a grid at the bottom allowing downwardly flow of the liquid.

For hydroprocessing heavy feeds, continuous moving multiple-bed systems attracted attention of several inventors [463–466]. In this case, the catalyst is disposed in an annular-form bed, moving downwardly through the reaction zone. H₂ can be added separately into the beds so that different H₂/liquid ratios can be attained. Catalyst addition (at the top) and withdrawal (at the bottom) can be carried out during the operation.

Monticelli [467] disclosed a process which employs two HDS reactors. The first reactor is suitable for HDS of the reactive sulfur-containing compounds. In the second reactor, the feed is subjected to biocatalytic desulfurization in the presence of the biocatalyst such as a culture of *Rhodococcus rhodocrous* bacteria or its active lysate, extract, fraction or subfraction. The bacteria is capable of catalyzing cleavage of thiophenic rings.

References

- [1] P.W. Tamm, H.P. Harnsberger, A.G. Bridge, *Ind. Eng. Chem. Proc. Des. Dev.* 20 (1981) 262.
- [2] C.H. Bartholomew, *Chem. Eng.* 12 (1984) 96.
- [3] D.S. Thakur, M.G. Thomas, *Appl. Catal.* 15 (1985) 197.
- [4] D.S. Thakur, M.G. Thomas, *Ind. Eng. Chem. Prod. Res. Dev.* 23 (1984) 349.
- [5] P.G. Menon, *J. Mol. Catal.* 59 (1990) 207.
- [6] M. Absi-Halabi, A. Stanislaus, D.L. Trimm, *Appl. Catal.* 72 (1991) 193.
- [7] G. Gualda, H. Toulhoat, *Rev. Inst. Fr. du Petrol.* 43 (1988) 567.
- [8] F.M. Dautzenberg, M. Frits, J.C. de Deken, *ACS Symp. Series 344*, ACS, Washington, DC, p. 233.
- [9] J. Wei, in: C.H. Bartholomew, J.B. Butt (Eds.), *Catalyst Deactivation*, Elsevier, Amsterdam, 1991.
- [10] C.H. Bartholomew, in: M.C. Oballa, S.S. Shih (Eds.), *Catalytic Hydroprocessing of Petroleum and Distillates*, Marcel Dekker, New York, 1994.
- [11] P. Grange, *Catal. Rev. -Sci. Eng.* 21 (1980) 135.
- [12] F.E. Massoth, G. Muralidhar, in: H.F. Barry, P.C. Mitchell (Eds.), *Fourth Climax Int. Conf. Chemistry and Uses of Molybdenum*, Climax Molybdenum Co., Ann Arbor, MI, 1982, p. 343.
- [13] P. Ratnasamy, S. Sivashanker, *Catal. Rev. -Sci. Eng.* 22 (1980) 401.
- [14] H. Topsøe, B.S. Clausen, F.E. Massoth, in: J. Anderson, M. Boudart (Eds.), *Catalysis, Science and Technology*, vol. 11, Springer, 1996, p. 1.
- [15] H. Topsøe, B.S. Clausen, E. Pedersen, *Ind. Eng. Chem. Fund.* 25 (1986) 25.
- [16] D.L. Trimm, *Design of Industrial Catalysts*, Elsevier, Amsterdam, 1980.
- [17] G. Poncelet, P. Grange, P. Jacobs (Eds.), *Preparation of Catalysts III*, Elsevier, Amsterdam, 1983.
- [18] V.J. Lostaglio, J.D. Carruthers, *Chem. Eng. Progr. March* 1986, p. 46.
- [19] D.L. Trimm, A. Stanislaus, *Appl. Catal.* 21 (1986) 215.
- [20] M.J. Girgis, B.C. Gates, *Ind. Eng. Chem. Res.* 30 (1991) 2021.
- [21] E. Furimsky, *Erdoel und Kohle* 36 (1983) 518.
- [22] L.C. Gutberlet, R.J. Bertolacini, *Ind. Eng. Chem. Prod. Res. Dev.* 22 (1983) 246.
- [23] P. Desikan, C.H. Amberg, *Can. J. Chem.* 42 (1964) 843.
- [24] F.E. Massoth, C.L. Kibby, *J. Catal.* 47 (1977) 300.
- [25] J.M.J.G. Lipsch, G.C.A. Schuit, *J. Catal.* 15 (1969) 179.
- [26] H.C. Lee, J.B. Butt, *J. Catal.* 49 (1977) 320.
- [27] C.N. Satterfield, M. Modell, J.A. Wilkens, *Ind. Eng. Chem. Proc. Des. Dev.* 19 (1980) 154.
- [28] C.N. Satterfield, M. Model, J.F. Mayer, *AIChE J.* 21 (1975) 1100.
- [29] N. Topsøe, H. Topsøe, F.E. Massoth, *J. Catal.* 119 (1989) 252.
- [30] M. Lacroix, C. Dumonteil, M. Breyse, *Am. Chem. Soc. Div. Petrol. Chem. (Preprints)* 43 (1998) 35.
- [31] V. LaVopa, C.N. Satterfield, *J. Catal.* 110 (1988) 375.
- [32] M. Nagai, T. Sato, A. Aiba, *J. Catal.* 97 (1986) 52.
- [33] J. Miciukiewicz, W. Zmierczak, F.E. Massoth, in: *Proc. 8th Int. Congr. on Catalysis*, Berlin, 1984, vol. 2, p. 671.
- [34] T.C. Ho, A.A. Montagna, J.J. Steger, in: *Proc. 8th Int. Congr. on Catalysis*, Berlin, 1984, vol. 2, p. 257.
- [35] J. Yang, F.E. Massoth, *Appl. Catal.* 34 (1987) 215.
- [36] M. Nagai, T. Kabe, *J. Catal.* 81 (1983) 440.
- [37] E.O. Odegunmi, D.F. Ollis, *J. Catal.* 80 (1983) 76.
- [38] R. Ramachandran, F.E. Massoth, *Chem. Eng. Commun.* 18 (1982) 239.
- [39] D. Dong, S. Jeong, F.E. Massoth, *Catal. Today* 37 (1997) 267.
- [40] B. Muegge, F.E. Massoth, in: C.H. Bartholomew, J.B. Butt (Eds.), *Catalyst Deactivation*, Elsevier, Amsterdam, 1991, p. 297.

- [41] S.H. Yang, C.N. Satterfield, *Ind. Eng. Chem. Proc. Des. Dev.* 23 (1984) 20.
- [42] S.C. Kim, F.E. Massoth, unpublished data.
- [43] F.E. Massoth, J. Miciukiewicz, *J. Catal.* 101 (1986) 505.
- [44] S. Gültekin, S.A. Ali, C.N. Satterfield, *Ind. Eng. Chem. Proc. Des. Dev.* 23 (1984) 179.
- [45] M.J. Girgis, B.C. Gates, *Ind. Eng. Chem. Res.* 33 (1994) 2301.
- [46] R. Hughes, G.J. Hutchings, C.L. Koon, B. McGhee, C.E. Snape, in: B. Delmon, G.F. Froment (Eds.), *Catalyst Deactivation*, Elsevier, Amsterdam, 1994, p. 377.
- [47] R. Hughes, G.J. Hutchings, C.L. Koon, B. McGhee, C.E. Snape, D. Yu, *Appl. Catal.* 144 (1996) 269.
- [48] R.A. Ware, J. Wei, *J. Catal.* 93 (1985) 122.
- [49] J.M. Jones, R.A. Kydd, P.M. Boorman, P.H. van Rhyen, *Fuel* 74 (1995) 1875.
- [50] M.W. Vogelzang, C.-L. Lee, G.C.A. Schuit, B.C. Gates, L. Petrakis, *J. Catal.* 84 (1983) 170.
- [51] S. Krishnamurthy, Y.T. Shah, *Chem. Eng. Commun.* 16 (1982) 109.
- [52] E.O. Odebunmi, D.F. Ollis, *J. Catal.* 80 (1983) 65.
- [53] C.N. Satterfield, S.H. Yang, *J. Catal.* 81 (1983) 335.
- [54] C.N. Satterfield, C.M. Smith, M. Ingalls, *Ind. Eng. Chem. Proc. Des. Dev.* 24 (1985) 1000.
- [55] E. Laurent, B. Delmon, *Ind. Eng. Chem. Res.* 32 (1993) 2516.
- [56] E. Laurent, B. Delmon, *Appl. Catal.* 109 (1994) 31.
- [57] E. Laurent, B. Delmon, in: B. Delmon, G.F. Froment (Eds.), *Catalyst Deactivation*, Elsevier, Amsterdam, 1994, p. 459.
- [58] A. Fonseca, P. Zeuthen, J.B. Nagy, *Fuel* 75 (1996) 1363.
- [59] M. Marafi, A. Stanislaus, *Appl. Catal.* 159 (1997) 259.
- [60] D.A. Netzel, F.P. Miknis, J.M. Mitzel, T. Zhang, P.D. Jacobs, H.W. Haynes Jr., *Fuel* 75 (1996) 1397.
- [61] T.L. Cable, F.E. Massoth, M.G. Thomas, *Fuel Process. Technol.* 4 (1981) 265.
- [62] E. Furimsky, *Fuel Process. Technol.* 6 (1982) 1.
- [63] E. Furimsky, *Ind. Eng. Chem. Prod. Res. Dev.* 18 (1979) 206.
- [64] E. Furimsky, *Ind. Eng. Chem. Prod. Res. Dev.* 17 (1978) 329.
- [65] P. Wiwel, P. Zeuthen, A.C. Jacobsen, in: C.H. Bartholomew, J.B. Butt (Eds.), *Catalyst Deactivation*, Elsevier, Amsterdam, 1991, p. 257.
- [66] E. Furimsky, *AIChE J.* 25 (1979) 306.
- [67] P. Magnoux, C. Canaff, F. Machado, M. Guisnet, *J. Catal.* 134 (1992) 286.
- [68] P. Zeuthen, J. Bartholdy, P. Wiwel, B.H. Cooper, in: B. Delmon, G.F. Froment (Eds.), *Catalyst Deactivation*, Elsevier, Amsterdam, 1994, p. 199.
- [69] I. Mochida, X.Z. Zhao, K. Sakanishi, S. Yamamoto, H. Takashira, S. Vemura, *Ind. Eng. Chem. Res.* 28 (1989) 418.
- [70] H. Beuther, B.K. Schmidt, in: *Proc. 6th World Petroleum Congr. 1963*, Section 3, p. 297.
- [71] F.M. Dautzemberg, J.C. de Deken, *Am. Chem. Soc. Div. Petrol. Chem. (Preprints)* 30 (1985) 8.
- [72] D.K. Banerjee, K.J. Laidler, B.N. Nandi, D.J. Patmore, *Fuel* 65 (1986) 480.
- [73] H. Nagaishi, E.W. Chan, E.C. Sanford, M.R. Gray, *Energy Fuels* 11 (1997) 402.
- [74] S. Eser, R.G. Jenkins, F. Derbyshire, M. Malladi, *Carbon* 24 (1986) 77.
- [75] E. Furimsky, *Ind. Eng. Chem. Prod. Res. Dev.* 22 (1983) 641.
- [76] T. Suzuki, M. Itoh, Y. Takegami, Y. Watanabe, *Fuel* 61 (1982) 402.
- [77] D. Alvarez, R. Galiasso, P. Andreu, *J. Japan Petr. Inst.* 22 (1979) 234.
- [78] E. Laurent, A. Centeno, B. Delmon, in: B. Delmon, G.F. Froment (Eds.), *Catalyst Deactivation*, Elsevier, Amsterdam, 1994, p. 573.
- [79] E. Furimsky, *Ind. Eng. Chem. Prod. Res. Dev.* 22 (1983) 34.
- [80] W.G. Appleby, J.W. Gibson, G.M. Good, *Ind. Eng. Chem. Proc. Des. Dev.* 2 (1962) 102.
- [81] E. Furimsky, *Erdöl und Kohle* 35 (1982) 455.
- [82] A.W. Scaroni, R.G. Jenkins, J.R. Utrilla, P.L. Walker Jr., *Fuel Process. Technol.* 9 (1983) 103.
- [83] G.M.K. Abotsi, A.W. Scaroni, *Fuel Process. Technol.* 22 (1989) 107.
- [84] T.C. Ho, *Catal. Rev. -Sci. Eng.* 30 (1988) 117.
- [85] A.W. Scaroni, R.G. Jenkins, P.L. Walker Jr., *Appl. Catal.* 14 (1985) 173.
- [86] K.P. de Jong, D. Reinalda, C.A. Emeis, in: B. Delmon, G.F. Froment (Eds.), *Catalyst Deactivation*, Elsevier, Amsterdam, 1994, p. 155.
- [87] M. Ternan, E. Furimsky, B.I. Parsons, *Fuel Process. Technol.* 2 (1979) 45.
- [88] F.V. Stohl, H.P. Stephens, *Ind. Eng. Chem. Res.* 26 (1987) 2466.
- [89] I. Mochida, X.-Z. Zhao, K. Sakanishi, *Fuel* 67 (1988) 1101.
- [90] J. van Dorn, J.L. Bosch, R.J. Bakkun, J.A. Moulijn, in: B. Delmon, G.F. Froment (Eds.), *Catalyst Deactivation*, Elsevier, Amsterdam, 1987.
- [91] S.M. Richardson, H. Nagaishi, M.R. Gray, *Ind. Eng. Chem. Res.* 35 (1996) 3940.
- [92] J.M. Oelderik, S.T. Sie, D. Bode, *Appl. Catal.* 47 (1989) 1.
- [93] G. Gualda, S. Kasztelan, *J. Catal.* 161 (1996) 319.
- [94] R.A. Bakulin, M.E. Levinter, F.G. Unger, *Int. Chem. Eng.* 18 (1978) 89.
- [95] F. Beguin, R. Setton, *Carbon* 10 (1972) 539.
- [96] P. Kovacic, J. Oziomek, *J. Org. Chem.* 29 (1964) 100.
- [97] M. Meot-Ner, *J. Phys. Chem.* 88 (1980) 2724.
- [98] B.D. Flockart, I.M. Sesay, R.C. Pink, *J. Chem. Soc. Chem. Comm.* 10 (1980) 439.
- [99] B.C. Gates, J.R. Katz, G.C.A. Schuit, *Chemistry of Catalytic Processes*, McGraw Hill, New York, 1979.
- [100] A.W. Scaroni, R.G. Jenkins, *Am. Chem. Soc. Div. Petrol. Chem. (Preprints)* 30 (1985) 544.
- [101] I.C. Lewis, L.S. Singer, *Am. Chem. Soc. Div. Petrol. Chem. (Preprints)* 31 (1986) 834.
- [102] I.C. Lewis, *Carbon* 20 (1981) 519.
- [103] J.W. Bunger, *Am. Chem. Soc. Div. Petrol. Chem. (Preprints)* 30 (1985) 549.
- [104] D. Nohara, T. Sakai, *Ind. Eng. Chem. Res.* 31 (1992) 14.

- [105] F. Diez, B.C. Gates, J.T. Miller, D.J. Sajkowski, S.G. Kukes, *Ind. Eng. Chem. Res.* 29 (1990) 1999.
- [106] D.J. Sajkowski, M.A. Pacheco, T.H. Fleisch, B.L. Meyers, in: *Proc. 9th Int. Congr. on Catalysis*, 1998, vol. 1, p. 223.
- [107] N.O. Egiebor, M.R. Gray, C. Natsuko, *Appl. Catal.* 55 (1989) 81.
- [108] A. Fonseca, P. Zeuthen, J.B. Nagy, *Fuel* 75 (1996) 1413.
- [109] T.E. Myers, F.S. Lee, B.L. Meyers, T.H. Fleisch, G.W. Zajac, *AIChE Symp. Series No. 273*, vol. 85, 1989, p. 21.
- [110] J.G. Weissman, J.C. Edwards, *Appl. Catal.* 142 (1996) 289.
- [111] M. Marafi, A. Stanislaus, *Am. Chem. Soc. Div. Petr. Chem. (Preprints)* 42 (1997) 573.
- [112] C.N. Satterfield, *Mass Transfer in Heterogeneous Catalysis*, Kreiger, Melbourne, FL, 1981.
- [113] C.N. Satterfield, C.K. Colton, W.H. Pitcher Jr., *AIChE J.* 19 (1973) 628.
- [114] A. Chantong, F.E. Massoth, *AIChE J.* 29 (1983) 725.
- [115] R.E. Beck, J.S. Schultz, *Science* 170 (1970) 1302.
- [116] C.-H. Tsai, F.E. Massoth, S.Y. Lee, J.D. Seader, *Ind. Eng. Chem. Res.* 30 (1991) 22.
- [117] G. Seo, F.E. Massoth, *AIChE J.* 31 (1985) 494.
- [118] S.Y. Lee, J.D. Seader, C.-H. Tsai, F.E. Massoth, *Ind. Eng. Chem. Res.* 30 (1991) 1683.
- [119] J.M. Smith, *Chemical Engineering Kinetics*, 3rd ed., McGraw-Hill, New York, 1981.
- [120] E. Ruckenstein, A.S. Vaidyanathan, G.Y. Youngquist, *Chem. Eng. Sci.* 26 (1971) 1305.
- [121] C.R. Wilke, P. Chang, *AIChE J.* 1 (1995) 264.
- [122] S.Y. Lee, J.D. Seader, C.-H. Tsai, F.E. Massoth, *Ind. Eng. Chem. Res.* 30 (1991) 29.
- [123] B.D. Prasher, G.A. Gabriel, Y.H. Ma, *Ind. Eng. Chem. Proc. Des. Dev.* 17 (1978) 266.
- [124] B.D. Prasher, G.A. Gabriel, Y.H. Ma, *AIChE J.* 24 (1978) 1118.
- [125] B.D. Prasher, Y.H. Ma, *AIChE J.* 23 (1977) 303.
- [126] C.N. Satterfield, C.K. Colton, W.H. Pitcher, *AIChE J.* 19 (1973) 628.
- [127] D.M. Malone, J.L. Anderson, *Chem. Eng. Sci.* 33 (1978) 1429.
- [128] S.Y. Lee, J.D. Seader, C.-H. Tsai, F.E. Massoth, *Ind. Eng. Chem. Res.* 30 (1991) 607.
- [129] C.H. Tsai, F.E. Massoth, S.Y. Lee, J.D. Seader, *Fuel Process. Technol.* 29 (1991) 153.
- [130] R. Hughes, *Deactivation of Catalysts*, Academic Press, New York, 1984.
- [131] A.S. Krishna, *Catal. Rev. -Eng. Sci.* 32 (1990) 279.
- [132] A. Voorhies Jr., *Ind. Eng. Chem.* 37 (1945) 318.
- [133] J.B. Butt, *Adv. Chem. Series* 109 (1972) 259.
- [134] E.E. Wolf, F. Alfani, *Cat. Rev. -Sci. Eng.* 24 (1982) 329.
- [135] J.W. Beekman, F. Gilbert, *Ind. Eng. Chem. Fund.* 18 (1979) 245.
- [136] E. Newson, *Ind. Eng. Chem. Proc. Des. Dev.* 14 (1975) 27.
- [137] S. Masamune, J.M. Smith, *AIChE J.* 12 (1966) 384.
- [138] K.P. deJong, *Ind. Eng. Chem. Res.* 33 (1994) 821.
- [139] K.P. deJong, *Ind. Eng. Chem. Res.* 33 (1994) 3141.
- [140] H.W. Haynes Jr., K. Leung, *Chem. Eng. Commun.* 23 (1983) 161.
- [141] K. Leung, H.W. Haynes jr., *Chem. Eng. Commun.* 31 (1984) 1.
- [142] J. van Dorn, J.A. Moulijn, *Fuel Process. Technol.* 35 (1993) 275.
- [143] K.-S. Chu, D. Dong, F.V. Hanson, F.E. Massoth, *Ind. Eng. Chem. Res.* 35 (1996) 4012.
- [144] R.G. Haldeman, M.C. Botty, *J. Phys. Chem.* 63 (1959) 489.
- [145] J.V. Sanders, J.A. Spink, S.S. Polack, *Appl. Catal.* 5 (1983) 66.
- [146] J.R. Fryer, *Carbon* 19 (1981) 431.
- [147] J. van Dorn, J.A. Moulijn, G. Djega-Mariadassou, *Appl. Catal.* 63 (1990) 77.
- [148] T.H. Fleisch, B.L. Meyers, J.B. Hall, G.L. Ott, *J. Catal.* 86 (1984) 147.
- [149] J. van Dorn, H.A.A. Barbolina, J.A. Moulijn, *Ind. Eng. Chem. Res.* 31 (1992) 101.
- [150] A.E. Hughes, K.C. Pratt, P. Tsai, *Appl. Catal.* 90 (1992) 117.
- [151] K.-S. Chu, F.V. Hanson, F.E. Massoth, *Fuel Process. Technol.* 40 (1994) 79.
- [152] B.D. Muegge, F.E. Massoth, *Fuel Process. Technol.* 29 (1991) 19.
- [153] C.H. Tsai, M.D. Deo, F.V. Hanson, A.G. Oblad, *Fuel Sci. Technol. Int.* 10 (1992) 1437.
- [154] A.W. Aldag, *AIChE Symp. Series* 273, vol. 85, 1989, p. 32.
- [155] K.P. de Jong, H.P.C.E. Kuipers, J.A.R. van Veen, in: C.H. Bartholomew, J.B. Butt (Eds.), *Catalyst Deactivation*, Elsevier, Amsterdam, 1991 p. 28.
- [156] A.D. van Langeveld, E.L.J. Ariëns, J.A. Moulijn, *Am. Chem. Soc. Div. Petrol. Chem. (Preprints)* 42 (1998) 55.
- [157] Y. Yoshimura, T. Sato, H. Shimada, A. Nishijima, *Fuel Sci. Technol. Int.* 4 (1986) 621.
- [158] W.C. van Zijl Langhout, C. Ouwerkerk, K.M. Pronk, *Oil Gas J.* 1 (1980) 120.
- [159] X. Yang, J.A. Guin, *Appl. Catal.* 141 (1996) 153.
- [160] F.V. Stohl, H.P. Stephens, *Am. Chem. Soc. Div. Fuel Chem. (Preprints)* 30 (1985) 148.
- [161] J.M. Ammus, G.P. Androustopoulos, A.H. Tsetseku, *Ind. Eng. Chem. Res.* 26 (1986) 1323.
- [162] Y. Yamamoto, F. Kumata, F.E. Massoth, *Fuel Proc. Technol.* 19 (1988) 253.
- [163] G.F. Froment, K.B. Bischoff, *Chemical Reactor Analysis and Design*, Wiley, New York, 1979, Chap. 3.
- [164] E.K. Reif, J.R. Kittrell, *Ind. Eng. Chem. Fund.* 19 (1980) 126.
- [165] I.-S. Nam, J.W. Eldridge, J.R. Kittrell, *Chem. Eng. Commun.* 31 (1984) 121.
- [166] J.R. Kittrell, P.S. Tam, J.W. Eldridge, *Hydroc. Proc.* 8 (1985) 63.
- [167] A. Artega, J.L.G. Fierro, F. Delannay, B. Delmon, *Appl. Catal.* 26 (1986) 227.
- [168] A. Artega, J.L.G. Fierro, P. Grange, B. Delmon, in: B. Delmon, G.F. Froment (Eds.), *Catalyst Deactivation*, Elsevier, Amsterdam, 1987, p. 59.
- [169] F.V. Stohl, H.P. Stephens, *Am. Chem. Soc. Div. Fuel Chem. (Preprints)* 30 (1985) 251.
- [170] S.M.A.M. Bouwens, D.C. Koningsberger, V.H.J. de Beer, R. Prins, *Catal. Lett.* 1 (1988) 55.

- [171] B.S. Clausen, H. Topsøe, R. Candia, J. Villadsen, B. Lengeler, J. Als-Nielsen, F. Christensen, *J. Phys. Chem.* 85 (1981) 3868.
- [172] T.F. Hayden, J.A. Dumesic, *J. Catal.* 103 (1987) 366.
- [173] H.P. Stephens, H.P. Stohl, *Am. Chem. Soc. Div. Fuel Chem. (Preprints)* 30 (1985) 465.
- [174] C.W. Curtis, J.A. Guin, R. Nalitham, A. Mohain, A.R. Tarrer, *Am. Chem. Soc. Div. Fuel Chem. (Preprints)* 26 (1981) 164.
- [175] P.A. Hertan, F.P. Larkins, W.R. Jackson, *Fuel Proc. Technol.* 10 (1985) 121.
- [176] F.E. Massoth, in: C. Bartholomew, G. Fuentes (Eds.), *Proc. Symp. on Catalysis Deactivation*, Elsevier, New York, 1997, p. 275.
- [177] C.T. Adams, A.A. Del Paggio, H. Schaper, W.H.J. Stork, W.K. Shiflett, *Hydroc. Proc.* 9 (1989) 57.
- [178] B.M. Moyse, B.H. Cooper, A. Albjerg, in: *NPRA Annual Meeting*, Paper AM-84-59, San Antonio, TX, March 1984.
- [179] Y. Yoshimura, K. Mayamizu, T. Sato, H. Shimada, A. Nishijima, *Fuel Process. Technol.* 16 (1987) 55.
- [180] A. Ocampo, J.T. Schrodt, S.M. Kovach, *Ind. Eng. Chem. Prod. Res. Dev.* 17 (1978) 56.
- [181] S. Kobayashi, S. Kushiya, R. Aizawa, Y. Koinuma, K. Imoue, Y. Shimizu, K. Egi, *Ind. Eng. Chem. Res.* 26 (1987) 2245.
- [182] T.E. Myers, F.S. Le, B.L. Myers, T.H. Fleisch, G.E. Zajac, *AIChE Symposium Series* 273, vol. 85, 1989, p. 32.
- [183] A.C. Jacobsen, B.H. Cooper, P.N. Hannerup, in: *12th Petrol World Congr.*, vol. 4, 1987, 97.
- [184] J. Goulon, A. Retournard, P. Friant, C. Ginet-Goulon, C. Berthe, J.F. Muller, J.L. Poncet, R. Guillard, J.C. Escalier, B. Neff, *J. Chem. Soc. Dalton Trans.* 6 (1984) 1095.
- [185] T.F. Yen (Ed.), *Chemical aspects of metals in native petroleum*, Ann Arbor Science, Ann Arbor, MI, 1975, p. 221.
- [186] R.H. Filby, D. Strong, in: S.S. Shih, M.C. Oballa, (Eds.), *Tar Sand and Oil Upgrading Technology*, *AIChE Symp. Series* 282, vol. 87, 1991, p. 1.
- [187] J.P. Janssens, G. Elst, E.G. Schrikkema, A.D. van Langeveld, S.T. Sie, J.A. Moulijn, *Recl. Trav. Chim. Pays Bas* 115 (1996) 465.
- [188] W.I. Beaton, R.J. Bertolacini, *Catal. Rev. -Sci. Eng.* 33 (1991) 281.
- [189] P.C.H. Mitchell, *Catal. Today* 7 (1990) 439.
- [190] R.D. Grigsby, J.B. Green, *Energy Fuels* 11 (1997) 602.
- [191] K. Sakanishi, N. Yamashita, D.D. Witehurst, I. Mochida, *Am. Chem. Soc. Div. Petr. Chem. (Preprints)* 42(2) (1997) 373.
- [192] M. Loos, I. Ascone, P. Friant, M.F. Ruiz-Lopez, J. Goulon, J.M. Barbe, N. Seglet, R. Guillard, D. Faure, T. des Courieres, *Catal. Today* 7 (1990) 497.
- [193] M. Loos, I. Ascone, C. Goulon-Ginet, J. Goulon, C. Guillard, M. Lacroix, M. Breysse, D. Faureand, T. des Courieres, *Catal. Today* 7 (1990) 515.
- [194] P.C.H. Mitchell, C.E. Scott, *Catal. Today* 7 (1990) 467.
- [195] B. Vielhaber, H. Knozinger, *Appl. Catal.* 26 (1986) 375.
- [196] H. Knozinger, D. Cordischi, B. Vielhaber, *Catal. Today* 7 (1990) 447.
- [197] C.-W. Huang, J. Wei, *Ind. Eng. Chem. Proc. Des. Dev.* 19 (1980) 250.
- [198] C.-W. Huang, J. Wei, *Ind. Eng. Chem. Process. Des. Dev.* 19 (1980) 257.
- [199] R. Agrawal, J. Wei, *Ind. Eng. Chem. Process. Des. Dev.* 23 (1984) 505.
- [200] R.A. Ware, J. Wei, *J. Catal.* 93 (1985) 100.
- [201] F. Vandeneeckhoutte, R. Hubaut, S. Pietrzyk, T. Des Courieres, J. Grimlot, *Reac. Kinet. Catal. Lett.* 45 (1991) 191.
- [202] H.-J. Chen, F.E. Massoth, *Ind. Eng. Chem. Res.* 27 (1988) 1629.
- [203] Y. Kamiya, S. Nagae, *Fuel* 64 (1985) 1242.
- [204] B.R. Utz, H.R. Appell, B.D. Blaustein, *Fuel* 65 (1986) 1085.
- [205] J. Weitkamp, W. Gerhardt, D. Scholl, in: *Proc. 8th Int. Congr. on Catalysis*, vol. II, 1984, p. 269.
- [206] L.A. Rinkel, *Am. Chem. Soc. Div. Petr. Chem. (Preprints)* 2 (1981) 689.
- [207] C.W. Hung, Ph.D Thesis, MIT, Cambridge, MA, 1979.
- [208] E. Furimsky, P.J. Champagne, *Fuel Process. Technol.* 6 (1982) 269.
- [209] E.L. Sughrue, D.W. Hausler, P.C. Liao, D.J. Strobe, *Ind. Eng. Chem. Res.* 27 (1988) 397.
- [210] J.C. Plumail, R. Marseu, G. Martino, H. Toulhoat, in: *Proc. Symp. on Recent Development and Challenges in Hydrotr. Catalysts*, Toronto, 6–10 June 1988.
- [211] O.A. Larson, H. Beuther, *Am. Chem. Soc. Div. Petrol. Chem. (Preprints)* 11 (1966) B95.
- [212] K.L. Riley, *Am. Chem. Soc. Div. Petrol. Chem. (Preprints)* 23 (1978) 1104.
- [213] J.M. Pazos, L. Aquino, J. Pachano, *Am. Chem. Soc. Div. Petrol. Chem. (Preprints)* 26 (1981) 456.
- [214] J.F. Mosby, G.B. Heokstra, T.A. Kleinhertz, J.M. Sroka, *Hydroc. Process.* 52 (1973) 93.
- [215] S.M. Oleck, H.S. Sherry, *Ind. Eng. Chem. Process. Des. Dev.* 16 (1977) 525.
- [216] S.M. Oleck, S.H. Sherry, *Ind. Eng. Chem. Process. Des. Dev.* 16 (1977) 263.
- [217] C.D. Chang, A.J. Silvestri, *Ind. Eng. Chem. Process. Des. Dev.* 13 (1974) 315.
- [218] C.D. Chang, A.J. Silvestri, *Ind. Eng. Chem. Process. Des. Dev.* 15 (1976) 161.
- [219] K. Rajagopalan, D. Luss, *Ind. Eng. Chem. Process. Des. Dev.* 18 (1979) 459.
- [220] E.L. Sughrue, R. Adarme, M.M. Johnson, C.J. Lord, M.D. Phillips, in: C.H. Bartholomew, J.B. Butt (Eds.), *Catalyst Deactivation*, Elsevier, Amsterdam, 1991, p. 281.
- [221] J.J. Yu, J.B. Butt, in: *Catalyst Deactivation*, Elsevier, Amsterdam, 1991, p. 343.
- [222] B.G. Johnson, F.E. Massoth, J. Bartholdy, *AIChE J.* 32 (1986) 1980.
- [223] J. Bartholdy, P.N. Hannerup, *Am. Chem. Soc. Div. Petrol. Chem (Preprints)* 35 (1990) 619.
- [224] P. Bourseau, G. Muratet, C. Saillour, H. Toulhoat, *Rev. Inst. Fr. Petr.* 40 (1985) 595.

- [225] S. Kobayashi, S. Kushiya, R. Aizawa, Y. Koinuma, K. Inoue, Y. Shimizu, K. Egri, *Ind. Eng. Chem. Res.* 26 (1987) 2241.
- [226] L. Reyes, C. Zerpa, J.H. Krasuk, in: B. Delmon, G.F. Froment (Eds.), *Catalyst Deactivation*, Elsevier, Amsterdam, p. 85.
- [227] C. Takeuchi, Y. Fukui, Y. Shioto, M. Nakamura, in: *Proc. 11th World Petroleum Congr.*, London, UK, 1993, vol. 4, p. 87.
- [228] C.J. Pereira, J. W. Beeckman, *Ind. Eng. Chem. Res.* 28 (1989) 422.
- [229] C.J. Pereira, R.G. Donnelly, L.L. Hegedus, in: E.E. Petersen, A.T. Bell (Eds.), *Catalyst Deactivation*, Marcel Dekker, New York, 1987, p. 315.
- [230] J.C. Spry, W.H. Sawyer, in: *Proc. 68th AIChE Annual Meeting*, Los Angeles, 1975, paper 30C.
- [231] Y.T. Shah, J.A. Paraskos, *Ind. Eng. Chem. Process. Des. Dev.* 14 (1975) 266.
- [232] N. Midoux, J.C. Charpentier, *Chem. Eng. Sci.* 28 (1973) 2108.
- [233] J.W. Beeckman, G.F. Froment, *Ind. Eng. Chem. Fund.* 18 (1979) 245.
- [234] J.W. Beeckman, G.F. Froment, *Chem. Eng. Sci.* 35 (1980) 805.
- [235] A. Wheeler, A.J. Robell, *J. Catal.* 13 (1969) 299.
- [236] P.B. Weisz, *Chem. Eng. Prog.* 25 (1954) 55.
- [237] O. Macé, J. Wei, *Ind. Eng. Chem. Res.* 30 (1991) 909.
- [238] T. Takatsu, Y. Wada, S. Inoue, in: P. O'Connor, T. Takatsu, G.L. Woolery (Eds.), *Deactivation and Testing of Hydrocarbon-Processing Catalysts*, ACS Symp. Series, 634, 1996, p. 414.
- [239] H.D. Simpson, in: C.H. Bartholomew, J.B. Butt (Eds.), *Catalyst Deactivation*, Elsevier, Amsterdam, 1991, p. 265.
- [240] J. Wei, in: C.H. Bartholomew, J.B. Butt (Eds.), *Catalyst Deactivation*, Elsevier, Amsterdam, 1991, p. 333.
- [241] B.J. Smith, J. Wei, *J. Catal.* 132 (1991) 1.
- [242] N. Nourbakhsh, B.J. Smith, I.A. Webster, J. Wei, T.T. Tsotsis, *J. Catal.* 132 (1991) 178.
- [243] J.P. Janssens, A.D. van Langeveld, S.T. Sie, J.A. Moulijn, in: P. O'Connor, T. Takatsuka, G.L. Woolery (Eds.), *Deactivation and Testing of Hydrocarbon-Processing Catalysts*, ACS Symp. Series 634, 1996, p. 238.
- [244] H. Toulhoat, J.C. Plumail, G. Martino, *Am. Chem. Soc. Div. Petrol. Chem. (Preprints)* 27 (1985) 85.
- [245] H. Toulhoat, R. Szymanski, J.C. Plumail, *Catal. Today* 7 (1990) 531.
- [246] C. Hung, R.L. Howell, D.R. Johnson, *Chem. Eng. Prog.*, March 1986, p. 57.
- [247] R. Agrawal, J. Wei, *Ind. Eng. Chem. Process. Res. Dev.* 23 (1984) 515.
- [248] R.A. Ware, J. Wei, *Ind. Eng. Chem. Res.* 93 (1985) 135.
- [249] F. Audibert, P. Duhaut, in: *Proc. 35th Meeting of American Petroleum Institute*, 13–15 May 1970, Houston, TX.
- [250] A.H. Hardin, R.H. Packwood, M. Ternan, *Am. Chem. Soc. Div. Petrol. Chem. (Preprints)* 23 (1978) 1450.
- [251] M. Inoguchi, S. Sakurada, Y. Satomi, K. Inaba, H. Kagaya, K. Tate, T. Mizutori, R. Nishiyama, T. Nagai, S. Onishi, *Bull. Jap. Petrol. Inst.* 14 (1972) 153.
- [252] W.F. Arey, N.E. Blackwell, A.D. Reichle, in: *7th World Petroleum Congr.* vol. 4, Mexico, 1967, p. 167.
- [253] T. Kwan, M. Sato, *Nippon Kagaku Zasshi* 91 (1970) 1103.
- [254] M. Sato, N. Takayama, S. Kurita, T. Kwan, *Nippon Kagaku Zasshi* 92 (1971) 834.
- [255] L.O. Oyekunle, R. Hughes, *Ind. Eng. Chem. Res.* 62 (1984) 339.
- [256] N. Todo, T. Kabe, K. Ogawa, M. Kurita, T. Sato, K. Shimada, Y. Kuriki, T. Oshima, T. Takemats, Y. Kotera, *Kogyo Kagaku Zasshi* 74 (1971) 563.
- [257] B. Ahn, J. Smith, *AIChE J.* 30 (1984) 739.
- [258] M. Sahimi, T.T. Tsotsis, *J. Catal.* 96 (1985) 552.
- [259] J.M. Pazos, J.C. Gonzales, A.J. Salazar, *Ind. Eng. Chem. Process. Des. Dev.* 25 (1983) 653.
- [260] R.R. Melkote, K.F. Jensen, *Chem. Eng. Sci.* 44 (1989) 649.
- [261] J.P. Janssens, B.J. Bezemer, A.D. van Langeveld, S.T. Sie, J.A. Moulijn, in: B. Delmon, G.F. Froment (Eds.), *Catalyst Deactivation*, Elsevier, Amsterdam, 1994, p. 335.
- [262] M. Sahimi, G.R. Gavels, T.T. Tsotsis, *Chem. Eng. Sci.* 45 (1990) 1443.
- [263] M.J. Ledoux, S. Hantzler, *Catal. Today* 7 (1990) 479.
- [264] S. Dejonghe, R. Hubaut, J. Grimblot, J.P. Bonelle, T. des Courieres, *Catal. Today* 7 (1990) 569.
- [265] C. Guillard, M. Lacroix, M. Vrinat, M. Breyse, B. Mocaer, J. Grimblot, T. des Courieres, D. Faure, *Catal. Today* 7 (1990) 587.
- [266] C.-S. Kim, F.E. Massoth, *Fuel Process. Technol.* 35 (1993) 289.
- [267] J.E. Wukasch, H.F. Rase, *Ind. Eng. Chem. Prod. Res. Dev.* 21 (1982) 558.
- [268] H. Koyama, E. Nagai, H. Kumagai, *Am. Chem. Soc. Div. Petrol. Chem. (Preprints)* 40 (1995) 446.
- [269] K.W. Babcock, L. Hiltzik, W.R. Ernst, J.D. Carruthers, *Appl. Catal.* 51 (1989) 295.
- [270] S.J. Hildebrandt, R.O. Koseoglu, J.E. Duddy, D.E. Sherwood, *Am. Chem. Soc. Div. Petrol. Chem. (Preprints)* 38 (1993) 40.
- [271] P. Zeuthen, B.H. Cooper, F.T. Clark, D. Arters, *Ind. Eng. Chem. Res.* 34 (1995) 755.
- [272] G. Muralidhar, F.E. Massoth, J. Shabtai, *J. Catal.* 85 (1984) 44.
- [273] Y. Yoshimura, T. Sato, H. Shimada, N. Matsubayashi, M. Imamura, A. Nishijima, S. Yoshitoni, *Am. Chem. Soc. Div. Petrol. Chem. (Preprints)* 38 (1993) 32.
- [274] G. Gualda, S. Kasztelan, in: B. Delmon, F.G. Froment (Eds.), *Catalyst Deactivation*, Elsevier, Amsterdam, 1994, p. 145.
- [275] M. Absi-Halabi, A. Stanislaus, T. Al-Mughni, S. Khan, A. Qamra, *Fuel* 74 (1995) 1211.
- [276] D.-S. Yang, R. Dureau, J.-P. Charland, M. Ternan, *Fuel* 75 (1996) 1199.
- [277] D.S. Thakur, M.G. Thomas, *Ind. Eng. Chem. Prod. Res. Dev.* 23 (1984) 349.
- [278] S.M. Kovach, L.J. Castle, J.V. Bennett, *Ind. Eng. Chem. Prod. Res. Dev.* 17 (1978) 62.
- [279] A.W. Lynch, *Appl. Catal.* 24 (1986) 227.

- [280] L.B. Clarke, Trace elements-emissions from coal, IEA Coal Research Report IEACR/49, July 1992.
- [281] R.A. Davidson, IEA Coal Research Report ICTIS/TR22, 1983.
- [282] A. Attar, J.B. Martin, Am. Chem. Soc. Div. Fuel Chem. (Preprints) 26 (1981) 73.
- [283] I. Barin, O. Knacke, Thermochemical Properties of Inorganic Substances, Springer, Dusseldorf, 1973.
- [284] J.B. Speight, The Chemistry and Technology of Petroleum, Marcel Dekker, New York, 1980.
- [285] J.J. Stanulonis, B.C. Gates, J.H. Olson, AIChE J. 22 (1976) 576.
- [286] F.V. Stohl, Q.A. Qader, F.E. Massoth, D.S. Thakur, Ind. Eng. Chem. Res. 26 (1987) 846.
- [287] F. Diez, D.J. Sajkowski, B.C. Gates, Fuel Process. Technol. 31 (1992) 43.
- [288] H.P. Stephens, F.V. Stohl, Am. Chem. Soc. Div. Fuel Chem. (Preprints) 29 (1989) 79.
- [289] D.S. Thakur, F.E. Massoth, M.G. Thomas, in: Proc. 4th Int. Conf. on Chemistry and Uses of Molybdenum, Climax Molybdenum Company, 1982, p. 48.
- [290] B.D. Adkins, D.R. Milburn, B.H. Davis, Ind. Eng. Chem. Res. 27 (1988) 796.
- [291] M.B. Neuworth, F.C. Moroni, Fuel Process. Technol. 8 (1984) 231.
- [292] T.L. Cable, F.E. Massoth, M.G. Thomas, Fuel Process. Technol. 10 (1985) 105.
- [293] M. Ihnatowicz, A. Worstynowicz, Przegl. Gorn. 37 (1981) 459.
- [294] J.M. Bogdanor, H.F. Rase, Ind. Eng. Chem. Prod. Res. Dev. 25 (1986) 220.
- [295] J.P. Goodman, B.D. Adkins, D.R. Milburn, B.H. Davis, Fuel Process. Technol. 22 (1989) 65.
- [296] P.H. Holloway, B. Granoff, E.J. Nowak, A.W. Mullendore, M.L. Liberman, Chemical studies in synthoil process, Report. No. SAND76-0644 to ERDA, 1976.
- [297] G. Berebi, P. Dufresne, Y. Jacquier, Environ. Progr. 12 (1993) 97.
- [298] L. Kellberg, P. Zeuthen, H.J. Jackobsen, J. Catal. 143 (1993) 45.
- [299] Y. Yoshimura, T. Sato, H. Shimada, N. Matsubayashi, M. Imamura, A. Nishijima, S. Yoshitomi, T. Kameoka, H. Yanase, Energy Fuels 8 (1994) 435.
- [300] Q. Dai, K.H. Chung, J. Can. Petr. Technol. 35 (1996) 57.
- [301] H.F. Rase, Chemical Reactor Design for Process Plants, Wiley, New York, 1977.
- [302] N. Yueqin, Z. Jingling, Z. Yan, W. Jifeng, in: B. Delmon, G.F. Froment (Eds.), Catalyst Deactivation, Elsevier, Amsterdam, 1994.
- [303] F.E. Massoth, G. MuraliDhar, J. Shabtai, J. Catal. 85 (1984) 53.
- [304] Y. Yokoyama, N. Ishikawa, K. Nakanishi, K. Satoh, A. Nishijima, H. Shimada, N. Matsubayashi, M. Nomura, Catal. Today 29 (1996) 261.
- [305] H. Makishima, Y. Tanaka, Y. Kato, S. Kure, H. Shimada, N. Matsubayashi, A. Nishijima, M. Nomura, Catal. Today 29 (1996) 267.
- [306] N. Matsubayashi, H. Shimada, T. Sato, Y. Yoshimura, M. Imamura, A. Nishijima, Fuel Process. Technol. 41 (1995) 261.
- [307] Y. Yoshimura, T. Sato, H. Shimada, N. Matsubayashi, M. Imamura, A. Nishijima, S. Yoshitomi, Am. Chem. Soc. Div. Petr. Chem. (Preprints) 38 (1993) 32.
- [308] S. Kure, Y. Yokoyama, H. Makishima, H. Shimada, N. Matsubayashi, A. Nishijima, M. Nomura, J. de Physique III C2-929, April 1997.
- [309] E. Eijssbouts, Y. Inoue, Science and Technology in Catalysis 1994, 76 (1995) 429.
- [310] A. Stanislaus, M. Absi-Halabi, K. Al-Dolama, A. Katrib, M. Ismail, Appl. Catal. 41 (1988) 109.
- [311] N.M. Gellerman, R.R. Aliev, V.G. Sidelkovskaya, Chem. Process. Fuels 10 (1994) 391 (in Russian).
- [312] Y. Yoshimura, H. Shimada, T. Sato, M. Kubota, A. Nishijima, Appl. Catal. 29 (1987) 25.
- [313] S. Harris, R.R. Chianelli, J. Catal. 86 (1984) 400.
- [314] S. Harris, R.R. Chianelli, J. Catal. 98 (1986) 17.
- [315] C. Takeuchi, S. Asaoka, S.I. Nakata, Y. Shioto, Am. Chem. Soc. Div. Petr. Chem. (Preprints) 30 (1985) 96.
- [316] Y. Yoshimura, S. Endo, S. Yoshitomi, T. Sato, H. Shimada, N. Matsubayashi, A. Nishijima, Fuel 70 (1991) 733.
- [317] C.-S. Kim, F.E. Massoth, E. Furimsky, Fuel Process. Technol. 32 (1992) 39.
- [318] Y. Yoshimura, E. Furimsky, T. Sato, H. Shimada, N. Matsubayashi, A. Nishijima, in: Proc. 9th Int. Congr. on Catalysis, Calgary, 1988.
- [319] J.S. Brinen, W.D. Armstrong, J. Catal. 54 (1978) 57.
- [320] T.G. Parham, R.P. Merrill, J. Catal. 85 (1984) 295.
- [321] A.V. Ramaswamy, L.D. Sharma, A. Singh, M.L. Singhal, L. Sivasanker, Appl. Catal. 13 (1985) 311.
- [322] Y. Yoshimura, H. Yakokawa, T. Sato, N. Shimada, N. Matsubayashi, A. Nishijima, Appl. Catal. 73 (1991) 39.
- [323] M. Montes, M. Genet, D.K. Hodnett, W.E. Stone, B. Delmon, Bull. Soc. Chim. Belg. 95 (1986) 1.
- [324] E. Furimsky, Appl. Catal. 171 (1998) 177.
- [325] J.P. Peries, A. Billon, A. Hennico, E. Morrison, F. Morel, Inst. Fr. Petr. Rapport IFP #34 297, June 1986.
- [326] M. Absi-Halabi, A. Stanislaus, in: P. O'Connor, T. Takatsuba, G.L. Woolery (Eds.), Deactivation and Testing of Hydrocarbon-Processing Catalysts, ACS Symp. Series 634, 1996, p. 229.
- [327] P. Dufresne, N. Brahma, F. Labruyère, M. Lacroix, M. Breyse, Catal. Today 29 (1996) 251.
- [328] W.-P. Wang, J.A. Guin, Fuel Process. Technol. 28 (1991) 149.
- [329] A. Stanislaus, M. Absi-Halabi, Z. Khanin, in: M. Absi Halabi (Ed.), Catalysts in Petroleum Refining and Petrochemical Industries, Elsevier, Amsterdam, 1995, p. 189.
- [330] C.J. Pereira, R.G. Donnelly, L.L. Hegedus, in: E.E. Petersen, A.T. Bell (Eds.), Catalyst Deactivation, Marcel Dekker, 1987, p. 315.
- [331] C.J. Pereira, L.L. Hegedus, US Patent 4510263 (1985).
- [332] B.H. Cooper, B.B.L. Donis, B.M. Moyse, Oil Gas J. 8 (1986) 39.

- [333] A. de Bruijn, I. Naka, J.W.M. Sonnemans, *Ind. Eng. Chem. Process. Des. Dev.* 20 (1981) 40.
- [334] F.M. Nooy, *Oil Gas J.* 12 (1984) 152.
- [335] J.T. Wooten, S.R. Kauffman, *Oil Gas J.* 28 (1986) 81.
- [336] B.M. Moyse, *Oil Gas J.* 15 (1986) 108.
- [337] C.J. Pereira, W.-C. Chang, J.W. Beeckman, W. Suarez, *Appl. Catal.* 42 (1988) 47.
- [338] J.G. Sikonia, F. Stolf, L.E. Hutchings, W.L. Jacobs, V.P. Burton, *Oil Gas J.* 5 (1981) 141.
- [339] W.C. van Zijl Langhout, P.B. Kwant, G.J. Lambert, in: *Proc. Symp. on Oil Refining*, October 1985, La Plata, Argentina.
- [340] W.I. Beaton, N.K. McDaniel, W.E. McWhirter, R.D. Petersen, R.P. Van Driesen, *Oil Gas J.* 7 (1986) 47.
- [341] K.W. Röbschläger, W.J. Deelen, J.E. Naber, in: *4th UNITAR/UNDP Int. Conf. on Heavy Crudes and Tar Sands*, August 1988, Edmonton, Canada, vol. 5, p. 249.
- [342] R.P. Van Driesen, J. Caspers, A.R. Campbell, G. Lunin, *Hydroc. Process.* 5 (1975) 107.
- [343] R.E. Boening, N.K. McDaniel, R.D. Petersen, R.P. van Driesen, *Hydroc. Process.* 9 (1987) 59.
- [344] R. M Eccles, A.M. Gray, W.B. Livingstone, *Oil Gas J.* 12 (1982) 121.
- [345] T.E. Johnson, J.R. Murphy, K.G. Tasker, *Oil Gas J.* 1 (1985) 50.
- [346] R.L. Howell, C. Hung, K.R. Gibson, H.C. Chen, *Oil Gas J.* 29 (1985) 121.
- [347] C.T. Adams, A.A. Del Paggio, H. Schaper, W.H.J. Stork, W.K. Shiflett, *Hydroc. Process.* 9 (1989) 57.
- [348] H. Koyama, E. Nagaiana, H. Kumagai, in: P. O'Connor, T. Takatsu, G.L. Woolery (Eds.), *Deactivation and Testing Hydrocarbon Processing Catalysts*, ACS Symp. Series 634, 1996, p. 208.
- [349] B.H. Cooper, P. Sogaard-Andersen, P. Nielsen-Hannerup, in: M.C. Oballa, S.S. Shih (Eds.), *Catalytic Hydroprocessing of Petroleum and Distillates*, Marcel Dekker, New York, 1994, p. 279.
- [350] A. Stanislaus, B.H. Cooper, *Catal. Rev. -Sci. Eng.* 36 (1994) 75.
- [351] M. Breyse, J.L. Portefaix, M. Vrinat, *Catal. Today* 10 (1991) 489.
- [352] J. Reardon, A.K. Datye, A.G. Sault, *J. Catal.* 173 (1998) 145.
- [353] T. Halachev, P. Atanasova, A. Lopez-Agudo, M.G. Arias, J. Ramirez, *Appl. Catal.* 136 (1996) 161.
- [354] Y.W. Chen, W.C. Hsu, C.S. Lin, B.C. Kang, S.T. Wu, L.J. Leu, J.C. Wu, *Ind. Eng. Chem. Res.* 29 (1990) 1830.
- [355] Y.W. Chen, W. C Hsu, *Ind. Eng. Chem. Res.* 36 (1997) 2526.
- [356] R.A. Kemp, C.T. Adams, *Appl. Catal.* 134 (1996) 299.
- [357] Y.W. Chen, M.C. Tsai, *Ind. Eng. Chem. Res.* 36 (1997) 2521.
- [358] Y.W. Chen, M.C. Tsai, *Am. Chem. Soc. Div. Petrol. Chem. (Preprints)* 42 (1997) 577.
- [359] J. Yang, F.E. Massoth, *Appl. Catal.* 34 (1987) 215.
- [360] J.M. Jones, R.A. Kydd, P.M. Boorman, P.H. van Rhy, *Fuel* 74 (1995) 1875.
- [361] C.E. Rmos-Galvan, G. Sandoval-Robles, A. Castillo-Mares, J.M. Dominguez, *Appl. Catal.* 150 (1997) 37.
- [362] Z.-S. Ying, B. Gevert, J.-A. Otterstedt, J. Sterte, *Appl. Catal.* 153 (1997) 69.
- [363] Z. Vit, *Appl. Catal.* 125 (1995) 61.
- [364] R.G. Anthony, S. Udomsak, S.E. Lott, *Appl. Catal.* 122 (1995) 111.
- [365] I.S. Sambhi, R.S. Mann, *Can. J. Chem. Eng.* 67 (1989) 337.
- [366] R. Cid, F. Orellana, A. Lopez-Agudo, *Appl. Catal.* 32 (1987) 327.
- [367] T. Tatsumi, M. Taniguchi, S. Yasuda, Y. Ishii, T. Murata, M. Hidai, *Appl. Catal.* 139 (1996) 5.
- [368] S. Inoue, T. Takatsu, Y. Wada, T. Ono, *Am. Chem. Soc. Div. Petrol. Chem. (Preprints)* 42 (1997) 351.
- [369] T.A. Pecoraro, R.R. Chianelli, *J. Catal.* 67 (1981) 430.
- [370] P.T. Vasudevan, J.L.G. Fierro, *Catal. Rev. -Sci. Eng.* 38 (1996) 161.
- [371] A.P. Raje, S.-J. Liaw, R. Srinivansan, B.H. Davis, *Appl. Catal.* 150 (1997) 297.
- [372] P. Gallezot, *Catal. Rev. -Sci. Eng.* 20 (1979) 21.
- [373] S.-J. Liaw, R. Lin, A. Raje, B.H. Davis, *Appl. Catal.* 151 (1997) 423.
- [374] R. Navarro, B. Pawelec, J.L.G. Fierro, P.T. Vasudevan, J.F. Cambra, P.L. Arias, *Appl. Catal.* 137 (1996) 269.
- [375] R. Navarro, B. Pawelec, J.L.G. Fierro, P.T. Vasudevan, *Appl. Catal.* 148 (1996) 23.
- [376] C. Song, A.D. Schmitz, *Energy Fuels* 11 (1997) 656.
- [377] A. Corma, A. Martínez, V. Martínez-Soria, *J. Catal.* 169 (1997) 480.
- [378] S. Kasztelan, N. Marchal, S. Kresmann, A. Billon, in: *14th World Petroleum Congr. on Catalysis*, Section 9, Paper 3, 1994.
- [379] N. Marchal, S. Kasztelan, S. Mignard, *Catalyst Hydroprocessing of Petroleum Distillates*, Marcel Dekker, New York, 1995, p. 315.
- [380] J.P. Lucien, G. van den Berg, H.M.J.H. van Hooijdonk, M. Gijers, G.L.B. Thielemans, *Catalyst Hydroprocessing of Petroleum Distillates*, Marcel Dekker, New York, 1994, p. 291.
- [381] B.H. Cooper, B.B.L. Donis, *Appl. Catal.* 137 (1996) 203.
- [382] J.C. Schlatter, S.T. Oyama, J.E. Metcalfe, J.M. Lambert Jr., *Ind. Eng. Chem. Res.* 27 (1988) 1648.
- [383] S. Ramanathan, S.T. Oyama, *J. Phys. Chem.* 99 (1995) 16365.
- [384] S. Li, J.S. Lee, *J. Catal.* 173 (1998) 134.
- [385] C.C. Yu, S. Ramanathan, S.T. Oyama, *J. Catal.* 173 (1998) 1.
- [386] S. Ramanathan, C.C. Yu, S.T. Oyama, *J. Catal.* 173 (1998) 10.
- [387] D.J. Sajkowski, S.T. Oyama, *Appl. Catal.* 134 (1996) 339.
- [388] G.M. Dolce, P.E. Savage, L.T. Thompson, *Energy Fuels* 11 (1997) 668.
- [389] K.R. McCrea, J.W. Logan, T.L. Tarbuck, J.L. Heiser, M.E. Bussel, *J. Catal.* 171 (1997) 255.
- [390] H.K. Park, J.K. Lee, J.K. Yoo, E.S. Ko, D.S. Kim, K.L. Kim, *Appl. Catal.* 150 (1997) 21.
- [391] G. Djéga-Mariadassou, M. Boudart, G. Bugli, C. Sayag, *Catal. Lett.* 31 (1995) 411.

- [392] M.J. Satriana, Hydroprocessing Catalysts for Heavy Oil and Coal, Noyes Data, Park Ridge, NJ, 1982.
- [393] R.H. Wolk, W.C. Rovesti, US Patent 3,819,509, June 25, 1974.
- [394] R.H. Wolk, G. Noglobri, W.C. Rovesti, US Patent 3,901,792, 26 August 1975.
- [395] T.T. Hilbert, N.D. Mazzone, M.S. Sarli, US Patent 5,510,016, 23 April 1996.
- [396] J.A. Howell, US Patent 4,659,452, 21 April 1987.
- [397] L.E. Hutchings, US Patent 4,239,614, 16 December 1980.
- [398] E.A. Jones, US Patent 4,234,314, 18 November 1980.
- [399] Y. Fukui, Y. Shiota, M. Ando, Y. Homma, US Patent 4,166,026, 28 August 1979.
- [400] N.L. Carr, F.E. Massoth, D.L. Stahlfeld, J.E. Young, Jr., US Patent 3,782,076, January 1974.
- [401] F.E. Massoth, J.E. Young, US Patent 3,812,653, May 1974.
- [402] M.M. Habib, P.L. Winslow, R.O. Moore Jr., US Patents 5,593,570, 14 January 1997 and 5,439,860, 8 August 1995.
- [403] T.C. Ho, US Patent 4,973,397, 27 November 1990.
- [404] T.-S. Chou, C.R. Kennedy, S.S. Shih, US Patent 4,997,544, March 1991.
- [405] J. Bartholdy, US Patent 5,368,722, November 29, 1994.
- [406] L.E. Gardner, S.G. Kukes, US Patent 4,828,683, 9 May 1989.
- [407] S.G. Kukes, K.K. Brandes, US Patent 4,767,523, 30 August 1988.
- [408] S.G. Kukes, T. Davis, K.K. Brandes, US Patent 4,778,587, 18 October 1988.
- [409] K.K. Brandes, S.G. Kukes, T. Davis, US Patent 4,778,588, October 18, 1988.
- [410] P.L. Winslow, R.F. Sullivan, US Patent 5,071,805, 10 December 1991.
- [411] F. Banta, US Patent 4,447,314, 8 May 1984.
- [412] S.S. Shih, D. Milstein, US Patent 4,421,633, 20 December 1983.
- [413] W.D. Gillespie, US Patent 5,232,578, 1 August 1993.
- [414] J.W. Ward, US Patent 4,572,778, 25 February 1986.
- [415] J.W. Myers, S.L. Parrott, E.L. Sughrue, US Patent 4,619,759, October 28 1986.
- [416] H.D. Simpson, D.P. McArthur, US Patent 4,431,526, 14 February 1984.
- [417] H. Higashi, K. Shirono, Y. Arima, Y. Nishimura, S. Yoshida, US Patent 4,613,425, 23 September 1986.
- [418] G. Sato, H. Higashi, K. Shirono, Y. Eto, US Patent 4,925,554, 15 May 1990.
- [419] M. Daage, T.C. Ho, K.L. Riley, US Patent 5,474,670, 12 December, 1995.
- [420] T.C. Ho, US Patent 4,902,404, 20 February 1990.
- [421] R.D. Cash, US Patent 4,430,203, 7 February 1984.
- [422] A.G. Bridge, B.E. Stangeland, US Patent 4,615,789, 7 October 1986.
- [423] A.J. MacLean, R.L. Holloway, V.A. Lawson, J.W. Cronen, US Patent 4,902,405, 20 February 1990.
- [424] L.E. Gardner, R.J. Hogan, E.L. Sughrue, J.W. Myers, US Patent 4,657,663, 14 April 1987.
- [425] A.L. Hensley Jr., L.M. Quick, US Patent 4,431,525, February 14, 1984.
- [426] K.R. Albinson, S. Mizrahi, D.J. Neuman, US Patent 4,913,797, 3 April 1990.
- [427] J.F. Grootjans, P.J. Bredael, US Patent 4,810,356, 7 March 1989.
- [428] S.M. Oleck, R.C. Wilson Jr., US Patent 4,437,976, 20 March 1984.
- [429] S.M. Oleck, R.C. Wilson Jr., US Patent 4,490,242, 25 December, 1984.
- [430] E.E. Unmuth, J.A. Mahoney, R.J. Bertolacini, US Patent 4,636,299, 13 January 1987.
- [431] N.Y. Chen, T.F. Degnan, US Patent 4,604,261, 5 August 1986.
- [432] K.L. Trachte, W. Lasko, E. Effron, G.F. Stuntz, K.D. Chomyn, US Patent 5,198,099, 30 March 1993.
- [433] P.J. Angevine, US Patent 4,415,436, 15 November 1983.
- [434] E.C. Haun, G.J. Thompson, J.K. Gorawara, US Patent 5,110,444, 5 May 1992.
- [435] M.G. Melconian, US Patent 4,406,777, 27 September 1983.
- [436] R.H. Wolk, M.C. Chervenak, S.B. Alpert, US Patent 3,788,973, 29 January 1973.
- [437] G.V. Nelso, G.C. Wray, US Patent 3,891,539, 24 June 1975.
- [438] G.P. Hamner, US Patents 3,977,961, August 31, 1976 and 4,014,821, 29 March 1977.
- [439] W.F. Arey Jr., G.P. Hamner, W.H. Sawyer, US Patent 3,977,962, 31 August 1976.
- [440] G.P. Hamner, US Patent 4,073,718, February 14, 1978.
- [441] H. Higashi, US Patent 5,591,325, 7 January 1997.
- [442] A.M. Henke, J.D. McKinney, US Patent 3,936,370, 3 February 1976.
- [443] W. Mounce, US Patent 3,830,728, 20 August 1974.
- [444] R.H. Wolk, M.C. Chervenak, S.B. Alpert, US Patent 3,788,973, 29 January 1974.
- [445] G.P. Hamner, K.R. Clem, US Patent 3,887,455, 3 June 1975.
- [446] J.G. Kunesch, US Patent 4,344,840, 17 August 1982.
- [447] S. Beret, S.G. Yu, C.R. Hsie, US Patent 4,761,220, 2 August 1988.
- [448] H.J. Trimble, B.E. Reynolds, R.W. Bachtel, R.J. Klett, D.N. Brossard, D.E. Earls, US Patent 5,660,715, 26 August 1997.
- [449] C.P. Kyan, P.J. Oswald, US Patent 5,603,824, February 18, 1997.
- [450] K.W. Goebel, V.A. Patel, E.L. Whittington, Jr., US Patent, 5,232,283, 3 August 1993.
- [451] G.E. Harrison, D.H. McKinley, A.J. Dennis, US Patent, 5,292,428, 8 March 1994.
- [452] J.V. Pool, US Patent 4,272,823, 9 June 1981.
- [453] T.R. Forbus, US Patent 5,246,568, September 21, 1993.
- [454] T.-S. Chou, US Patent 4,481,105, 6 November 1984.
- [455] F.A. Aly, P.W. Snyder, US Patent 4,896,704, 30 January 1990.
- [456] J.B. Wijffels, A.A. Pegels, A. Wezenberg, US Patent 4,228,418, 21 October 1980.
- [457] A.P. Den Hartog, W. Van Vliet, US Patent 5,635,145, June 3, 1997.
- [458] N.K. McDaniel, P.E. Stelly, R.E. Boening, W.E. McWhirter Jr., D.E. Atkinson, R.D. Petersen, US Patent, 4,753,721, 28 June 1988.

- [459] F.A. Smith, US Patents 4,579,647, 1 April 1986 and 4,743,433, 10 May 1988.
- [460] M.N. Harandi, US Patent 5,554,275, 10 September 1996.
- [461] N. Yeoman, R. Pinaire, M.A. Ulowitz, T.P. Nace, D.A. Furse, US Patent 5,593,548, 14 January 1997.
- [462] A. Al-Saigh, US Patent 4,642,223, 10 February 1987.
- [463] K.D. Peters, US Patents 4,250,018 and 4,250,019, 10 February, 1981.
- [464] G.L. Scheuerman, D.R. Johnson, D.C. Kramer, US Patent 5,472,928, December 1995.
- [465] B.E. Stangeland, D.C. Kramer, D.S. Smith, J.T. McCall, G.L. Scheuerman, R.W. Bachtel, D.R. Johnson, US Patent 5,599,440, 4 February 1997.
- [466] B.P. Vora, N.H. Scott, US Patent 4,869,808, 26 September 1989.
- [467] D.J. Monticello, US Patent 5,387,523, 7 February 1995.